

Monday Morning, October 29, 2012

Actinides and Rare Earths Focus Topic
Room: 6 - Session AC+MI+SS+TF-MoM

Electronic Structure and Spectroscopy of Actinides

Moderator: A.J. Nelson, Lawrence Livermore National Laboratory

9:00am **AC+MI+SS+TF-MoM3 Strong Correlations and the Electronic Structure of the Actinide Dioxides, R.L. Martin**, Los Alamos National Laboratory **INVITED**

The series of actinide dioxides (AnO_2 , $An=Pa, \dots Cm$) are difficult challenges for electronic structure theory. The early members of the series are Mott insulators, the band gap corresponding to f_7^2 transitions, while the later members, beginning with PuO_2 , are $O2p \rightarrow An5f$ charge transfer insulators. I will review recent experimental results (X-ray absorption, photoemission and optical band gaps) which now allow us to distinguish among several many-body approximations to their electronic structure, including the SIC, DFT+U, DMFT+U and hybrid DFT (HSE) approaches.

9:40am **AC+MI+SS+TF-MoM5 Synchrotron Radiation Studies of Actinide Compounds, S.M. Butorin**, Uppsala University, Sweden **INVITED**

Core-to-core resonant inelastic x-ray scattering (RIXS) and valence-to-core RIXS techniques are two complimentary ways for probing the electronic structure in actinide systems. Specific cuts of the core-to-core RIXS maps around $M\beta$ and L lines of actinides represent remarkably improved high-resolution x-ray absorption spectra of actinide $3d$ and $2p$ edges, respectively, as a result of limited lifetime broadening of core holes present in shallower levels in the final state of the spectroscopic process. That allows for more detailed studies of unoccupied states and better oxidation states assignments. In turn, the valence-to-core RIXS spectra are only limited by the instrumental resolution and provide information about actinide chemical bonding and interactions between valence electrons.

A comparison of experimental data with results of model calculations shows that the resonant spectra of actinide systems recorded at the actinide $M(3d)$ and $O(5d)$ thresholds which probe the $5f$ states can be interpreted using the many-body theory, such as the Anderson impurity model, while the data obtained at the $L3$ threshold and representing the $6d$ states of actinides can be described within a single-particle approach, such as LDA+ U (local density approximation with supplemented Coulomb interaction U) framework.

In course of discussion of the above statements, we present the RIXS data for a number of actinide systems with emphasis on the results contributing to understanding of the U-O and Pu-O phase diagrams, in particular data for UO_{2+x} , U_4O_9 , U_3O_8 and PuO_{2+x} . The influence of the Coulomb interaction between $5f$ electrons on the electronic structure of actinides is also discussed.

10:40am **AC+MI+SS+TF-MoM8 Quasiparticle Dynamics in Uranium Systems from Ultrafast Spectroscopies, T. Durakiewicz**, Los Alamos National Laboratory

Every time we add a new dimension to an experimental method, we open a window to novel, unexpected and fascinating phenomena. Here we show the results of our focused effort of adding time-domain to the powerful experimental techniques of Angle Resolved Photoelectron Spectroscopy (ARPES) and reflectivity. The novel tools are applied to actinides and help us understand the details of the electronic structure of the correlated f -electron materials.

In the hidden order system URu_2Si_2 we investigate the massive renormalization of the Fermi surface at specific k values. The application of time-resolved ARPES allowed a direct measurement of the momentum-resolved quasiparticle lifetime which was shown to increase by an order of magnitude at the hidden order transition. Time-resolved ARPES together with the ultrafast reflectivity results provided evidence for forming a multiple gap structure, including the hybridization gap, pseudogap and HO gap [1, 2].

Another actinide system of interest is a Mott insulator UO_2 , where we have investigated the complex dynamics of the Hubbard excitons. We have found that the dynamics can be divided into four distinct processes: instantaneous hop, picosecond lattice deformation, phonon emission and relaxation, and the slow relaxation related to the propagation of Hubbard excitons [3]. We

have also obtained the first direct measurement of Hubbard gap in $5f$ system [4].

The novel femtosecond pump-probe methods provide unique information about the dynamics of $5f$ quasiparticles, and open novel possibilities in addressing the long-standing questions about the role of near-Fermi level band renormalization in establishing the physical properties of correlated materials.

References

- [1] Physical Review B 84, 161101(Rapid Comm.) (2011)
- [2] Physical Review B 84, 161103(Rapid Comm.) (2011)
- [3] Physical Review Letters 106, 207402 (2011)
- [4] manuscript in preparation

11:00am **AC+MI+SS+TF-MoM9 Comparison of Spectroscopic Data with Cluster Calculations of Plutonium, Plutonium Dioxide and Uranium Dioxide, J.G. Tobin, S.W. Yu, B.W. Chung**, Lawrence Livermore National Laboratory, *M.V. Ryzhkov*, Russian Academy of Science-Ekaterinburg, *A. Mirmelstein*, Russian Federation Nuclear Center-Snezhinsk

Using spectroscopic data produced in the experimental investigations of bulk systems, including X-Ray Absorption Spectroscopy (XAS), Photoelectron Spectroscopy (PES) and Bremsstrahlung Isochromat Spectroscopy (BIS) [1-5], the theoretical results within for UO_2 [6], PuO_2 [6] and Pu [7] clusters have been evaluated. The calculations of the electronic structure of the clusters have been performed within the framework of the Relativistic Discrete-Variational Method (RDV). [6,7] The comparisons between the LLNL experimental data and the Russian calculations are quite favorable. The cluster calculations may represent a new and useful avenue to address unresolved questions within the field of actinide electron structure, particularly that of Pu . Observation of the changes in the Pu electronic structure as a function of size suggests interesting implications for bulk Pu electronic structure.

Acknowledgements

Lawrence Livermore National Laboratory is operated by Lawrence Livermore National Security, LLC, for the U.S. Department of Energy, National Nuclear Security Administration under Contract No. DE-AC52-07NA27344. JGT and SWY were supported by the DOE Office of Science, Office of Basic Energy Science, Division of Materials Science and Engineering. Work at the RAS and VNIITF was supported in part by Contract B590089 between LLNL and VNIITF. The Advanced Light Source (ALS) in Berkeley and the Stanford Synchrotron Radiation Laboratory are supported by the DOE Office of Science, Office of Basic Energy Science.

References

1. J.G. Tobin and S.-W. Yu, Phys. Rev. Lett, **107**, 167406 (2011).
2. S.-W. Yu, J. G. Tobin, J. C. Crowhurst, S. Sharma, J. K. Dewhurst, P. Olalde-Velasco, W. L. Yang, and W. J. Siekhaus, Phys. Rev. B **83**, 165102 (2011).
3. J.G. Tobin, B.W. Chung, R. K. Schulze, J. Terry, J. D. Farr, D. K. Shuh, K. Heinzelman, E. Rotenberg, G.D. Waddill, and G. Van der Laan, Phys. Rev. B **68**, 155109 (2003).
4. J.G. Tobin, P. Söderlind, A. Landa, K.T. Moore, A.J. Schwartz, B.W. Chung, M.A. Wall, J.M. Wills, R.G. Haire, and A.L. Kutepov, J. Phys. Cond. Matter **20**, 125204 (2008).
5. S.-W. Yu, J. G. Tobin, P. Olalde-Velasco, W. L. Yang, and W. J. Siekhaus, J. Vac. Sci. Tech. A. **30**, 011402 (2012).
6. M.V. Ryzhkov and A.Ya. Kupryazhkin, J. Nucl. Materials **384**, 226 (2009).
7. M.V. Ryzhkov, A. Mirmelstein, S.-W. Yu and J.G. Tobin, "Probing Actinide Electronic Structure through Pu Cluster Calculations," submitted to Phys. Rev. B, Feb 2012.

Spectroscopic Ellipsometry Focus Topic

Room: 19 - Session EL+TF+AS+EM+SS+PS+EN+NM-MoM

Spectroscopic Ellipsometry for Photovoltaics and Semiconductor Manufacturing

Moderator: M. Creatore, Eindhoven University of Technology, the Netherlands, H. Wormeester, MESA+ Institute for Nanotechnology, University of Twente, Enschede, The Netherlands

8:20am **EL+TF+AS+EM+SS+PS+EN+NM-MoM1 Multichannel Spectroscopic Ellipsometry: Applications in I-III-VI₂ Thin Film Photovoltaics**, *R.W. Collins, D. Attygalle, P. Aryal, P. Pradhan, N.J. Podraza*, University of Toledo, *V. Ranjan, S. Marsillac*, Old Dominion University **INVITED**

Multichannel spectroscopic ellipsometry (SE) has been applied successfully as an in situ, real time tool for optimizing, monitoring, and controlling multi-stage deposition processes in various thin film photovoltaics (PV) technologies. A particularly challenging process optimization problem involves the thermal co-evaporation of individual elements of Cu, In, Ga, and Se in a three-stage process, which has proven to produce high quality Cu(In_{1-x}Ga_x)Se₂ (CIGS) materials and high performance PV devices. This three-stage process provides a high level of flexibility in determining the phase, composition, and microstructure of the film, but also generates greater challenges in run-to-run reproducibility of the optimized process. Information extracted from real time SE measurements includes the evolution of the bulk layer and one or more surface layer thicknesses, as well as layer dielectric functions. The layer dielectric functions can be analyzed further to extract the phase and alloy compositions and the defect density or grain size, which can assist in understanding the fabrication process, in optimizing solar cells, and ultimately in monitoring and controlling the optimized process for improved reproducibility. In this study, the focus is on analysis of ellipsometric (ψ , Δ) spectra acquired by real time SE in order to characterize (i) the structural and compositional evolution in (In,Ga)₂Se₃ film growth from In, Ga, and Se fluxes in the first stage, (ii) the transition from Cu-poor to Cu-rich CIGS at the end of the second stage, which occurs under Cu and Se fluxes, and (iii) the transition from Cu-rich to the desired Cu-poor CIGS, which defines the end of the third and final stage, and occurs under a second application of In, Ga, and Se fluxes. After the transition from Cu-poor to Cu-rich material in the second stage, a Cu_{2-x}Se phase near the surface of the bulk layer is tracked. In the Cu-rich to Cu-poor transition, this Cu_{2-x}Se phase has fully reacted with In, Ga, and Se to form CIGS. Studies using a standard Mo substrate and 2 μ m thick CIGS for solar cells have also revealed features in the (ψ , Δ) spectra characteristic of the anticipated changes in the near surface phase composition as established by detailed modeling on thinner and smoother films. Although careful analysis of real time SE is expected to provide quantitative information on the surface properties and their evolution in this case of solar cells, control of the deposition has been successful simply by monitoring real time changes in the ellipsometric (ψ , Δ) spectra.

9:00am **EL+TF+AS+EM+SS+PS+EN+NM-MoM3 Contribution of Plasma Generated Nanoparticles to the Growth of Microcrystalline Silicon Deposited from SiF₄/H₂/Argon Gas Mixtures**, *J.-C. Dornstetter, S. Kasouit, J.-F. Besnier*, Total S.a, France, *P. Roca i Cabarrocas*, LPICM-CNRS, Ecole Polytechnique, France

Despite the low fabrication cost of thin film silicon solar modules, this type of technology remains non competitive in main stream markets because of the high BOS costs, due to the low energy conversion efficiency of this type of modules (~10%). We have recently shown that microcrystalline silicon films deposited using SiF₄/H₂/Argon RF capacitive plasmas have excellent structural and transport properties, compared to films deposited using conventional SiH₄/H₂ mixtures, allowing for a very good carrier collection, even for thick cells, and Voc values of 0.55 V, without device optimization, thus opening up the path for the realization of high performance solar cells. However, little is known so far about the growth mechanism of this type of materials and the reason for such interesting properties. Studies of silicon thin films deposition from SiF₄/H₂ mixes, under conditions different from ours, suggested that the growth is due to the deposition of SiF₂ radicals, followed by the abstraction of fluorine by hydrogen. Previous work within our group has also shown that deposition occurs only when particles are present in the plasma, and that growth starts from crystallites without any amorphous phase. We present here a systematic study of the growth of microcrystalline films, together with the composition of nanoparticles attracted by thermophoresis to cold traps located both on the walls of the plasma chamber and in the fore line as a function of deposition conditions.

The composition of the deposit on the traps is found to be amorphous at low power/ low hydrogen conditions and becomes crystalline when either of them increases. This correlates well with an increase in atomic hydrogen concentration in the plasma, as estimated by actinometry. The crystalline fraction of the deposited film was measured using in-situ ellipsometry and was found to correlate with the composition of the deposit on the cold traps. Deposition rate is drastically reduced when a water cooled trap is installed on the walls of the plasma chamber, and switches off at high H₂ flow rates. Under these conditions, TEM and AFM images, show that at the initial stages of the growth the film is constituted of sparse, hexagonal crystalline particles, having sizes on the order of few tens of nanometers. We interpret the data above as a result of plasma-generated nanocrystals being a significant contribution to the deposited film. This may explain the excellent electronic properties of the films, as the particles are formed in the bulk of the plasma region, free from energetic ions bombardment. We will correlate the structural properties and the film growth mechanisms to the properties of solar cells.

9:20am **EL+TF+AS+EM+SS+PS+EN+NM-MoM4 Multichannel Spectroscopic Ellipsometry for CdTe Photovoltaics: from Materials and Interfaces to Full-Scale Modules**, *P. Koirala, J. Chen, X. Tan, N.J. Podraza*, The University of Toledo, *S. Marsillac*, Old Dominion University, *R.W. Collins*, The University of Toledo

Real time spectroscopic ellipsometry (RTSE) has been implemented in studies of the evolution of the semiconductor structural and optical properties during sputter deposition of thin film polycrystalline CdS/CdTe solar cells on transparent conducting oxide (TCO) coated glass substrates. Analysis of the real time optical spectra collected during CdS/CdTe deposition requires an optical property database as a function of measurement temperature for all substrate components. These include not only soda lime glass, but also an SiO₂ layer and three different SnO₂ layers. We report optical functions parameterized versus temperature for the glass substrate and its overlayers starting from room temperature and ending at elevated temperature above which the semiconductor layers are deposited. In fact, such a database has additional applications for on-line, through-the-glass monitoring applications of coated glass at elevated temperature. In the RTSE studies, knowledge of the temperature dependent optical functions of the substrate components enables an accurate substrate temperature determination before the onset of deposition and is critical for accurate extraction of the semiconductor layer optical properties. We implement RTSE to study the filling process of the surface roughness modulations on the top-most SnO₂ substrate layer and modification of the optical properties of this layer. This modification is further studied post-deposition by infrared spectroscopic ellipsometry. In addition to providing information on interface formation to the substrate during film growth, RTSE also provides information on the bulk layer CdS growth, its surface roughness evolution, as well as overlying CdTe interface formation and bulk layer growth. Information from RTSE at a single point during solar cell stack deposition assists in the development of a model that can be used for mapping the completed cell stack properties, which can then be correlated with device performance. Independent non-uniformities in the layers over the full area of the cell stack enable optimization of cell performance combinatorially.

9:40am **EL+TF+AS+EM+SS+PS+EN+NM-MoM5 Determination of Electronic Band Gaps from Optical Spectra**, *R.A. Synowicki*, J.A. Woollam Co., Inc.

The band gap of a material E_g is defined theoretically as the lowest energy for electronic transition from the valence to conduction bands in a solid. For an ideal material free of defects this is the photon energy or wavelength where the optical properties change from transparent to absorbing. However, real materials contain defects which cause absorption to begin below the band gap (i.e. the Urbach Tail) making determination of the true band gap position difficult. For example, in a solar cell the measured absorption edge represents the onset of transitions first due to defects, then from band to band. Empirical methods used to determine the band gap in real materials with defects include the Tauc plot and the Mott-Davis plot. More theoretical mathematical dispersion models such as the Tauc-Lorentz, Cody-Lorentz, and Herzinger-Johs models have been developed which include an adjustable band gap parameter. The various plots and dispersion model methods will be discussed and applied to different materials measured optically via spectroscopic ellipsometry, intensity transmission, reflection, absorption, or a combination of these methods.

10:00am **EL+TF+AS+EM+SS+PS+EN+NM-MoM6 Optical Modeling of Plasma-Deposited ZnO: Extended Drude and its Physical Interpretation**, *H.C.M. Knoops, M.V. Ponomarev, J.W. Weber, N. Leick, B.W.H. van de Loo, Y.G. Melese, W.M.M. Kessels, M. Creatore*, Eindhoven University of Technology, the Netherlands

High-quality transparent conductive oxides such as ZnO are important due to their electrical and optical properties. To improve these properties the

responsible physical processes have to be understood. Traditionally, charge-carrier-scattering processes are investigated by combining morphology data and Hall measurements. This contribution discusses the extensive optical modeling of plasma-deposited ZnO and how its interpretation directly provides insight into the relevant charge-carrier-scattering processes at different length scales. The interpretation is generalized to the concept of frequency-dependent resistivity, which is used to explain the applicability of different Drude models.

Thin films (50-1000 nm) of Al-doped and undoped ZnO were deposited using an expanding thermal plasma MOCVD process.¹ Conditions of high pressure and high diethyl zinc flow allowed for dense films with low electrical resistivities (e.g., $4 \times 10^{-4} \Omega \text{ cm}$ at 300 nm). The films were analyzed with variable-angle spectroscopic ellipsometry (SE) (0.75 – 5.0 eV), FTIR reflection spectroscopy (0.04 – 0.86 eV), Four-point-probe (FPP), and Hall measurements.

The SE and FTIR data were combined and fitted with classical and extended Drude² models. The high intensity of the Drude in the FTIR range resulted in a high sensitivity with which the carrier concentration and mobility could even be determined for thin (~40 nm) undoped ZnO films. An extended Drude model was needed to correctly model the SE energy range, which was explained by the dominance of ionized impurity scattering and a reduction of this scattering for higher photon energies. The grain-boundary-scattering mobility could be determined by the difference between optical and Hall mobilities.³ When combined with FPP results, the effective mobility can be determined from these optical techniques without the use of Hall measurements. The optical response above the band gap was modeled by a PSEMI or Tauc-Lorentz oscillator model, where a broadening and shift of the transition was seen for increasing carrier concentration.⁴

These insights and a generalized view of electron scattering in ZnO at different length scales will be presented.

1. Ponomarev et al., *J. Appl. Phys.* **Submitted** (2012)
2. Ehrmann and Reineke-Koch, *Thin Solid Films* **519**, 1475 (2010)
3. Steinhauser et al., *Appl. Phys. Lett.* **90**, 142107 (2007)
4. Fujiwara and Kondo, *Phys. Rev. B* **71**, 075109 (2005)

10:40am **EL+TF+AS+EM+SS+PS+EN+NM-MoM8 The Ellipsometric Response of Single-Crystal Silicon to Doping**, *H.G. Tompkins*, Consultant

The current wisdom is that for ellipsometry in the UV-vis-NIR spectral range, doping of single-crystal silicon can be ignored. We study the ellipsometric response of silicon doped with arsenic at various levels. We also studied the response after implant (before activation) and after the activation (anneal). We find that for samples implanted with $1E18 \text{ atoms/cm}^3$, the single-crystal silicon was not amorphized. Implants of $2E19 \text{ atoms/cm}^3$ and higher left an amorphous layer on the surface of the wafer the thickness of which was about the depth of the implant. Activation of the sample implanted with $2E19 \text{ atoms/cm}^3$ returned the sample to single-crystal silicon and the ellipsometric response in the UV-vis-near IR is essentially that of undoped silicon. However, the response in the mid-IR is that the extinction coefficient is no longer zero. For samples implanted with $2.5E20 \text{ atoms/cm}^3$ and greater, annealing did not return the UV-vis-near IR ellipsometric response to that of single-crystal silicon. Although this amount of other material (arsenic) is still less than about one tenth of one percent, our conjecture is that the microstructure simply could not be returned to that of a single crystal. As with the lower doped sample, the mid-IR spectral region showed significant increase in the extinction coefficient.

11:00am **EL+TF+AS+EM+SS+PS+EN+NM-MoM9 The Effect of Stress on the Optical Properties Semiconductor Films**, *A.C. Diebold, G.R. Muthinti, M. Medikonda, T.N. Adam*, College of Nanoscale Science and Engineering, University at Albany, *A. Reznicek, B. Doris*, IBM Research at Albany Nanotech

Here we review the impact of stress on the complex dielectric function of semiconductor films measured using spectroscopic ellipsometry. Two relevant examples of stressed semiconductor layers are pseudomorphic epitaxial layers fabricated during semiconductor manufacturing and strained silicon on insulator (sSOI) wafers. Stress is known to shift the energies of direct gap critical point transitions in semiconductors. The biaxial stress in pseudomorphic films grown on silicon wafers can be as high as that used during opto-elastic studies of bulk semiconductors. The amount of stress in un-relaxed, pseudomorphic films of $\text{Si}_{1-x}\text{Ge}_x$ on Si (100) reaches 1 GPa for alloys with 20% Ge and is more than 3 GPa for films with > 50% Ge. The bi-axial stress in sSOI is typically ~1 GPa. An elastic theory approach for the effect of strain on the k^*p determined band structure and optical transition energy is well known. Both low shear stress and high shear stress approximations can apply to the shift in transition energy depending on the magnitude of the spin orbit splitting energy vs the magnitude of the shear

stress. Until recently it was difficult to obtain sets of samples that test both approximations. Here we discuss results from our recent study of pseudomorphic films of $\text{Si}_{1-x}\text{Ge}_x$ on Si (100) from $x=0.05$ to 0.75 which covers both low and high shear regimes. We also present our recent study of the dielectric function of thinned sSOI which illustrates the impact of stress on the optical transitions for the Si layer on sSOI. All of these samples are examples of new materials being used in semiconductor research. The results of this study are directly transferred into cleanroom spectroscopic ellipsometry systems used for process control during manufacturing.

11:20am **EL+TF+AS+EM+SS+PS+EN+NM-MoM10 Numerical Ellipsometry: Spectroscopic n-k Plane Analysis of Thin Films Growing on Unknown Layered Substrates**, *F.K. Urban, D. Barton*, Florida International University

Spectroscopic ellipsometry measurements on thin films commonly make use of prior knowledge of the structure and optical properties of the underlying substrate. However, imprecision in substrate statistics propagates into the solution for the film of interest. Thus it is more accurate to have a method for solving for film properties which simultaneously obtains whatever is needed about the substrate. And it makes solutions possible whether or not book data or previous substrate solutions are available. In this work we apply Complex Analysis in the $n-k$ plane to achieve solutions employing the well-know reflection equations. The method is carried out at each measured wavelength and does not necessitate an *a-priori* assumption of optical property dependencies on wavelength. The mean square error has been improved by many orders of magnitude, a selected limit of 10^{-14} as opposed to 1 to 30 or so for least squares. Thus the full accuracy of the ellipsometer is now available for more accurate measurements of film thickness and optical properties. The method requires six measurements during growth. The first is used to determine the relationship between R_p and R_s at the film-substrate interface. The following four are used to uniquely determine the values of R_p , R_s , and film n , k , and d . The final measurement confirms the unique solution. Suitability of the model is tested by comparing measurements at two of more wavelengths for self consistency. Results for n and k of the growing film are examined across the measurement spectrum in comparison with parameterizations in common use.

Electronic Materials and Processing
Room: 9 - Session EM+TF+OX+GR-MoM

High-k Dielectrics for MOSFETs I
Moderator: A.C. Kummel, University of California San Diego

8:20am **EM+TF+OX+GR-MoM1 Surface Preparation and Dielectric Growth for Graphene-based Devices**, *R.M. Wallace*, University of Texas at Dallas **INVITED**

In addition to interesting physics, numerous device applications are under investigation for graphene. Many of these devices require an interaction of graphene with dielectrics, and require a thorough understanding of the graphene/dielectric interface. As practical device applications require large area graphene, CVD methods have been employed to synthesize graphene and typically involve a wet chemical transfer process, which can leave residues that impact device behavior. This talk will review recent progress in the investigation of CVD graphene growth, transfer and dielectric growth processes with an emphasis on in-situ studies of the surfaces produced by these processes and the resultant electrical behavior. This work is supported by the NRI SWAN Center.

9:00am **EM+TF+OX+GR-MoM3 Antimonide-Based P-Channel MOSFET: Progress and Challenges**, *S. Oktyabrsky, A. Greene, S. Madiseti, P. Nagaiah, M. Yakimov, R. Moore, S. Novak, H. Bakhr, V. Tokranov*, University at Albany-SUNY **INVITED**

Development of p-type MOSFETs using new materials is an important goal to provide a further scaling of CMOS circuits. Although Ge is still considered as a main candidate for novel p-channels due to its superior bulk transport properties, recent progress in strained III-Sb channels and MOS technologies makes it a good competitor in particular for deeply scaled devices. The materials parameters affecting MOSFET's figures-of-merit are reviewed with the emphasis on strain in quantum wells (QWs), effective mass, density of states and mobility.

Progress in development of materials for III-Sb channels is reported. Optimization of MBE growth of metamorphic buffers and GaSb on lattice-mismatched GaAs substrates has resulted in "step-flow" growth mode of GaSb with monolayer-high steps on the surface, $\sim 10^8 \text{ cm}^{-2}$ dislocation

density and bulk hole mobility $860\text{cm}^2/\text{Vs}$. Optimization of strain in QWs provided the highest Hall mobility of $1020\text{cm}^2/\text{Vs}$ at sheet hole density of $1.3 \times 10^{12}/\text{cm}^2$ obtained for $\text{In}_{0.36}\text{Ga}_{0.64}\text{Sb}$ with compressive strain of 1.8%. Hole mobility in QW channel was benchmarked against the thickness of top semiconductor AlGaSb barrier. The effect of interface-related scattering hole mobility in the channel was found to be significantly less than e.g. for n-InGaAs, that might be due to stronger localization of holes in QWs.

Two approaches to fabricate high-quality III-Sb/high-k interface were studied: all *in-situ* Al_2O_3 or HfO_2 gate oxides, and *ex-situ* atomic layer deposited (ALD) Al_2O_3 with InAs top semiconductor capping layer. Interface with *in-situ* MBE gate oxides was found to improve with *in-situ* deposited a-Si interface passivation layer (IPL). Interfaces with better thermal stability, reduced interface trap density and hysteresis were observed on both n- and p- type GaSb MOSCaps with the IPL. P-type MOSFETs with HfO_2 showed a maximum drain current of 23 mA/mm for a $3\mu\text{m}$ gate length. Use of a-Si IPL has also resulted in a significant (over an order of magnitude) reduction of the hole density in QWs and corresponding negative flat band voltage shift and drop of mobility which becomes remote Coulomb scattering-limited. An interface with ALD Al_2O_3 was improved by a thin 2nm interface layer of InAs which was treated with HCl or $(\text{NH}_4)_2\text{S}$ immediately prior to ALD process. Optimized annealing further improved the C-V characteristics, reduced interface trap density down to $10^{12}\text{cm}^{-2}\text{eV}^{-1}$, leakage current and MOSFET subthreshold slope down to 200 mV/dec. Increasing annealing temperature to and above 450°C drastically degraded C-V characteristics due to low thermal budget of antimonides.

9:40am **EM+TF+OX+GR-MoM5 Interface Study of the Atomic Layer Deposited Al_2O_3 on $\text{Al}_{0.25}\text{Ga}_{0.75}\text{N}$** , X. Qin, B. Brennan, H. Dong, R.M. Wallace, The University of Texas at Dallas

Due to the high two-dimensional electron gas (2-DEG) density, AlGaIn/GaN high electron mobility transistors (HEMTs) are recognized as key devices for high power and low noise applications. However, the associated large gate leakage current degrades the performance of AlGaIn HEMTs. In order to solve this problem, MOS-HEMTs have been developed, in which the incorporation of a high-k gate dielectric layer can overcome the drawbacks.

In this work, the native and treated $\text{Al}_{0.25}\text{Ga}_{0.75}\text{N}$ surface chemical states and structure of were studied by x-ray photoelectron spectroscopy (XPS), ion scattering spectroscopy (ISS) and low energy electron diffraction. Different chemical treatment processes including $(\text{NH}_4)\text{OH}$, $(\text{NH}_4)_2\text{S}$ and HF were studied, followed by atomic layer deposition (ALD) Al_2O_3 layers on $\text{Al}_{0.25}\text{Ga}_{0.75}\text{N}$. The oxidation states of the $\text{Al}_{0.25}\text{Ga}_{0.75}\text{N}$ interface and Al_2O_3 deposition process were studied by *in-situ* XPS analysis. In addition, *ex-situ* atomic force microscopy (AFM) was used to observe the surface topography before and after the Al_2O_3 deposition. According to the XPS results, it is found that chemical treatments could remove the native Al_2O_3 but were not effective to eliminate the Ga oxide, and the growth rate of Al_2O_3 is low on the native and treated $\text{Al}_{0.25}\text{Ga}_{0.75}\text{N}$ samples. The AFM images show that there are many pin holes in the surface of $\text{Al}_{0.25}\text{Ga}_{0.75}\text{N}$. Studies of HfO_2 deposition will also be presented.

This work is supported by the AOARD under AFOSR Grant No. FA2386-11-1-4077

10:00am **EM+TF+OX+GR-MoM6 Ideal Monolayer Nitridation of Semiconductors using a Nitrogen Radical Generator**, A.T. Lucero, J. Kim, University of Texas at Dallas

Thin silicon nitride films have long been desirable for various applications. Suggested uses range from surface and interface passivation to ultra-thin dielectric layers. Traditional deposition techniques are low pressure chemical vapor deposition (LPCVD) and plasma enhanced chemical vapor deposition (PECVD). High quality LPCVD films require high processing temperatures, and PECVD exposes the substrate to damaging plasma and electric potentials. While both techniques are suitable for many applications, there are some instances where both processes are too harsh.

In this paper, we report the growth of silicon nitride using a remote nitrogen radical generator system. Growth temperatures range from room temperature to 400°C , and growth time is varied from two minutes to one hour. Film composition is analyzed using x-ray photoelectron spectroscopy (XPS) and morphology is checked using atomic force microscopy. Results indicate that surface nitrogen saturation can be reached at both low temperatures and short exposure times, and that the reaction is self limiting, terminating at one monolayer. Film thickness is approximately one Angstrom, as determined by XPS. Results for silicon and III-V passivation will be discussed.

We would like to thank Toshiba Mitsubishi-Electric Industrial Systems Corporation for providing the nitridation system used in this study.

11:00am **EM+TF+OX+GR-MoM9 Characterization of ALD Laminated Gate Dielectrics on GaN MOSCAPs**, D. Wei, T. Hossain, Kansas State University, N. Nepal, N.Y. Garces, Naval Research Laboratory, H.M. Meyer III, Oak Ridge National Laboratory, C.R. Eddy, Jr., Naval Research Laboratory, J.H. Edgar, Kansas State University

To improve the efficiency of GaN based power electronic devices there is tremendous and growing interest in employing metal-insulator-semiconductor (MIS) transistors. As with all compound semiconductors, there is a significant challenge in forming an electronic quality dielectric-semiconductor interface. Thus, there is a need to better understand and improve the dielectric-semiconductor interface quality in order to improve the overall performance of the device.

This research focuses on the benefits and properties of Al_2O_3 , TiO_2 and $\text{TiO}_2\text{-Al}_2\text{O}_3$ nanolaminate thin films deposited on GaN and GaOx/GaN by plasma-assisted atomic layer deposition (PA-ALD) for gate dielectric development. Correlations were sought between the films' structure, composition, and electrical properties. The gate dielectrics were approximately 15nm thick as determined by spectroscopic ellipsometry. The interface carbon concentration, as measured by x-ray photoelectron spectroscopy (XPS) depth profile, was lower for $\text{Al}_2\text{O}_3/\text{GaN}$ than TiO_2/GaN , and the nanolaminate structure did not decrease the carbon concentration. However, carbon was not detected at the interface for the GaN samples pretreated by annealing in O_2 for 30 minutes at 800°C . Also, according to XPS, the Al_2O_3 films had a better coverage than TiO_2 . The RMS roughness of TiO_2 and Al_2O_3 top layers were $\sim 0.53\text{nm}$ and $\sim 0.20\text{nm}$ respectively, as determined by atomic force microscopy. The dielectric constant of Al_2O_3 on GaOx/GaN was greatly increased compared to that of the $\text{TiO}_2\text{-Al}_2\text{O}_3$ and pure Al_2O_3 on GaN substrate. In addition, the Al_2O_3 deposited on the GaOx/GaN showing no hysteresis in capacitance-voltage (C-V) characteristics, which is corresponding with a negligible carbon concentration from the XPS depth profile. These results indicate the promising potential of plasma ALD deposited Al_2O_3 serving as the gate oxide on GaOx/GaN based MOS devices.

11:20am **EM+TF+OX+GR-MoM10 Passivation of Interfacial Defects in GaAs and Other III-Vs**, J. Robertson, Cambridge University, UK
INVITED

It has always been harder to make FETs from GaAs than Si, because of 'Fermi level pinning' and the difficulty of passivating its surfaces. These issues were discussed by Spicer et al [1] in the 'unified defect model' and Hasegawa [2] is his 'Disorder Induced Gap states' model. Since 1997 it was possible to make inverted GaAs MOSFETs using the epitaxial Gadolinium gallium oxide [3]. The main impetus now is to use atomic layer deposition (ALD) to make scalable FETs [4], as recently achieved by Intel [5]. The obvious question is why (In)GaAs is much harder to passivate than Si. The early answer was its poor native oxide. But since the advent of good ALD HfO_2 or Al_2O_3 oxides on Si, this answer is deficient, as they should also work on GaAs [6]. The underlying reason for defects is not stress, it must be chemical. I show that it arises from the polar bonding of GaAs [7], and a driving force to keep the surface Fermi level in a gap. The electron counting rule of Pashley [8] that describes surface reconstructions is shown to be a variant of auto-compensation, and it works more generally [9]. It leads to a continuous generation of defects if it is not satisfied. So the answer is to deposit oxide layers that meet this rule, and also to break any surface reconstructions that may lead to As-As dimers [9]. Diffusion barriers are also crucial to a good passivant, on GaAs or on Ge.

1. W E Spicer, et al, J Vac Sci Technol 16 1422 (1979); Phys Rev Lett 44 420 (1980)
2. H Hasegawa, et al, J Vac Sci Technol B 5 1097 (1987)
3. M Hong et al, Science 283 1897 (1997)
4. P D Ye et al, App Phys Lett 83 180 (2003)
5. M Radosavljevic, et al, Tech Digest IEDM (2009) p13.1
6. C Hinkle, et al, Curr Opin Solid State Mat Sci 15 188 (2011)
7. W Harrison, J Vac Sci Technol 16 1492 (1979)
8. M D Pashley, Phys Rev B 40 10481 (1989)
9. J Robertson, L Lin, App Phys Letts 99 222906 (2011); 98 082903 (2011)

Graphene Growth

Moderator: M. Spencer, Cornell University, V.D. Wheeler, U.S. Naval Research Laboratory

8:20am **GR+EM+NS+PS+SS+TF-MoM1 Synthesis Ingredients Enabling Low Noise Epitaxial Graphene Applications, D.K. Gaskill, L.O. Nyakiti, V.D. Wheeler, U.S. Naval Research Lab, A. Nath, George Mason Univ., V.K. Nagareddy, Newcastle University, UK, R.L. Myers-Ward, N.Y. Garces, S.C. Hernandez, S.G. Walton, U.S. Naval Research Lab, M.V. Rao, George Mason Univ., A.B. Horsfall, Newcastle Univ., UK, C.R. Eddy, Jr., U.S. Naval Research Lab, J.S. Moon, HRL Labs LLC**

Sensors made from graphene flakes have demonstrated single molecule detection [Schedin *et al.*, Nat Mat 6, 652 (2007)]; this ultra-sensitivity is likely due to the high crystalline quality of the graphene and the associated relative lack of defects that give rise to noise. The low noise nature of high quality graphene should also facilitate other applications, e.g., low-noise amplifiers. Combined with the unique ambipolar property of graphene field effect transistors (FETs), the low noise character of graphene would significantly advance the performance of frequency multipliers, mixers and high-speed radiometers. To exploit these applications, high quality, reproducible wafer-scale epitaxial graphene (EG) with minimal thickness variations and defects are essential requirements. Here, crucial graphene synthesis elements required to achieve the wafer-scale quality goal are described. Understanding the effect of substrate misorientation as well as hydrogen etch and Si sublimation conditions for graphene synthesis on the (0001) SiC surface is essential to achieve improved and reproducible wafer-scale graphene quality. For example, the impact of processing factors such as temperature control, laminar gas flow and substrate rotation on large area EG uniformity are described using examples created in an Aixtron SiC epitaxy reactor. In addition, managing SiC step formation on the nominal (0001) orientation is significant for achieving uniform EG thickness on terraces and to minimize additional growth at the step edges; this is illustrated using data from atomic force microscopy and scanning electron microscopy images in combination with Raman spectroscopy maps and x-ray photoelectron spectroscopy analysis. Managing step formation combined with optimal growth leads to the suppression of the Raman defect "D" band confirming minimal grain boundaries and defects, which are additional sources of electronic noise. Lastly, contactless Leighton resistivity maps of 75 mm wafers are used to illustrate the overall uniformity of optimally synthesized graphene as well as to show the resistance state-of-the-art, with individual wafers exhibiting about a $\pm 3\%$ relative variation. Examples of the impact of this synthesis approach on chemical sensors devices and FETs will be shown, each exhibiting 1/f noise behavior down to 1 Hz and possessing noise spectral densities similar to reports from exfoliated graphene. Hence, careful control of EG formation across the wafer results in improved quality which subsequently leads to the reduction or elimination of additional noise sources from graphene defects that would then adversely affect device performance.

8:40am **GR+EM+NS+PS+SS+TF-MoM2 Growth of Graphene by Catalytic Decomposition of Ethylene on Cu(100) and Cu(111) With and Without Oxygen Predosing, Z.R. Robinson, P. Tyagi, T. Mowll, C.A. Ventrice, Jr., University at Albany- SUNY, K. Clark, A.-P. Li, Oak Ridge National Laboratory**

Graphene growth on Cu substrates has become one of the most promising techniques for the mass production of graphene, and therefore significant effort has been put into developing growth conditions that lead to large area, defect and grain boundary free graphene films. One key consideration is the influence that the underlying copper substrate has on the growth of the graphene. In order to study this, graphene growth on Cu(100) and Cu(111) was carried out in a UHV system. The samples were heated using an oxygen series button heater. The hydrocarbon pressure was measured using a capacitive manometer instead of an ion gauge, which could cause dissociation of the hydrocarbon molecules. Initially, it was found that annealing the crystals to 900 °C resulted in impurity segregation at the surface. Several cycles of sputtering at 600 °C were required to remove all bulk impurities so that the surface remained clean even after annealing to 900 °C. Initial attempts to grow graphene by annealing each crystal to temperatures as high as 900 °C in UHV, followed by backfilling the chamber with up to 5×10^{-3} torr of C_2H_4 did not result in graphene formation. It was found that by first backfilling the chamber with C_2H_4 and then raising the temperature from 25 °C to 800 °C, graphene growth could be achieved. A four-domain epitaxial overlayer is observed for the Cu(100) surface. Pre-dosing the Cu(100) with oxygen at 300 °C, which forms a saturation coverage of chemisorbed oxygen, was found to result in a 2-

domain graphene overlayer using similar growth conditions. A study of the effect of oxygen pre-dosing on the growth of graphene on Cu(111) has been initiated.

9:00am **GR+EM+NS+PS+SS+TF-MoM3 Impact of Growth Parameters on Uniformity of Epitaxial Graphene, L.O. Nyakiti, V.D. Wheeler, R.L. Myers-Ward, J.C. Culbertson, U.S. Naval Research Laboratory, A. Nath, George Mason University, N.Y. Garces, U.S. Naval Research Laboratory, J. Howe, Oak Ridge National Laboratory, C.R. Eddy, Jr., D.K. Gaskill, U.S. Naval Research Laboratory**

Epitaxial graphene (EG) offers a facile method for attaining large area graphene for device applications. Since wafer uniformity and thickness control is vital, a systematic study of the parameters affecting the EG growth process was performed and the optimal conditions for obtaining uniform morphology and high electronic quality were determined. EG was synthesized in a low pressure Ar flowing ambient on $8 \times 8 \text{ mm}^2$ 6H-SiC(0001) substrates that were offcut 0.8° from the basal plane, using an Aixtron VP508 reactor. The samples were placed on a rotating ~ 100 mm diameter susceptor and excellent EG layer uniformity and run-to-run reproducibility were obtained. The investigation focused upon the critical synthesis parameters of temperature (T) (1520-1660°C) and time (t) (15-60 min), an *in-situ* H_2 etch conditions (1520-1600°C for 10-30min). Morphology, layer thickness, chemical analysis, and strain variations across the samples were characterized using electron microscopy, AFM, XPS and μ -Raman spectroscopy. Large-area van der Pauw Hall effect was performed to quantify the graphene mobility (μ), and carrier density. Results show that growth T and t had the most significant impact on EG electronic and morphological properties. For example, synthesis at 1660°C for 30min resulted in 4-8 monolayers (ML) and a step-bunched morphology with high concentration of wrinkles originating from the step-edge and pinned at the nearest terrace edge. Other morphological features were pits primarily located at the step edges having a depth ~ 20 nm and density $6.4 \times 10^6 \text{ cm}^{-2}$. In contrast, EG synthesis at 1520°C for 30min results in uniform ML coverage along the terrace width that is devoid of pits and wrinkles. Mobility was found to have a drastic dependence on graphene thickness. Under optimal conditions, 1-2 ML were obtained and μ as high as $1240 \text{ cm}^2 \text{ V}^{-1} \text{ s}^{-1}$ was achieved; in contrast, for EG with >2 ML $\mu \sim 550 \text{ cm}^2 \text{ V}^{-1} \text{ s}^{-1}$, presumably due to interlayer interaction and electronic screening. XPS C1s and Raman 2D spectra of EG grown on substrates after undergoing *in-situ* H_2 etch at different times did not show shifts in peak position/intensity suggesting lack of etch time dependence on EG electronic or structural quality. Yet etch conditions affect the final morphology, as EG synthesis performed after an *in-situ* H_2 etch at 1600°C resulted in step-bunched morphology with step heights 5-10nm, whereas, substrates etched at 1520°C had EG with step-heights 10-15nm. In addition other growth parameters investigated were found to be of secondary importance, including: Ar pressure, flow rates, and sample cool down conditions.

9:20am **GR+EM+NS+PS+SS+TF-MoM4 Uniform Epitaxial Growth of Charge Neutral Quasi-Free-Standing Monolayer Graphene on a 6H-SiC(0001) Surface by Combination of Metal Silicidation and Intercalation, H. Shin, I. Song, C.-Y. Park, J.R. Ahn, Sungkyunkwan University, Republic of Korea**

Intrinsic high mobility of graphene are much reduced in graphene devices by various factors. Two critical factors degrading mobility are uniformity in an atomic structure such as number of a layer and an interaction with a substrate. Recently Shuai-Hua Ji *et al.* reported quantitatively that conductivity is much reduced by one sixth when electrons pass through a boundary between monolayer and bilayer graphene at a step edge in comparison to conductivity of monolayer graphene. This suggests that uniformity of number of graphene layer is a more crucial factor than expected. In particular, in epitaxial graphene on SiC, the uniformity of number of layer is an intrinsic and serious problem because Si is more rapidly sublimated near a step edge in the formation of epitaxial graphene by thermal evaporation of Si and, subsequently, epitaxial graphene with different layers coexists intrinsically on a terrace. Another factor degrading mobility is an interaction between graphene and a substrate. In epitaxial graphene, the interaction was reduced by intercalation of metal or molecule such as H, F, and Au between graphene and a substrate, which results in quasi freestanding graphene. Various charge neutral quasi freestanding graphene has been reported, but the charge neutrality was found at an optimal coverage of an intercalated element and annealing temperature. This makes it difficult to achieve spatially homogeneous charge neutrality of quasi freestanding graphene, and a method with a broad range of coverage and temperature is demanded. We demonstrate that charge neutral quasi freestanding monolayer graphene can be grown uniformly without coexistence of a buffer layer and a bilayer graphene which limit mobility of epitaxial monolayer graphene. Because coexistence of two different phases is inevitable on a SiC surface, uniform monolayer graphene was produced based on two different phases, a Si-rich phase and a C-rich phase called a

buffer. Pd was deposited on both the Si-rich and C-rich phases and annealed up to 900°C. The Si-rich phase produced Pd silicide and charge neutral quasi freestanding monolayer graphene was produced on the Pd silicide while, on the C-rich phase, Pd was intercalated between the buffer layer and SiC resulting in charge neutral quasi freestanding monolayer graphene, where the quasi freestanding monolayer graphene on two different regions was connected atomically. The combination of Si silicidation and intercalation result in uniform charge neutral quasi freestanding uniform monolayer on a SiC surface, where the electronic and atomic structures were observed using angle-resolved photoemission spectroscopy and scanning tunneling microscopy.

9:40am **GR+EM+NS+PS+SS+TF-MoM5 Epitaxial Graphene on Ir(111) - A Playground for the Fabrication of Graphene Hybrid Materials**, *T.W. Michely*, Universität zu Köln, Germany **INVITED**

Carefully optimizing the growth of graphene on Ir(111) yields a virtually defect free, weakly bound epitaxial monolayer ranging from quantum dot sizes to macroscopic extension. In the talk I will show how this system can be used to construct new types of graphene based materials. Specifically, patterned adsorption of transition metals results in dense cluster arrays with exciting magnetic and catalytic properties. Intercalation underneath the graphene allows one to manipulate the properties of graphene itself, e.g. its ability to adsorb atoms and molecules as well as its magnetism.

10:40am **GR+EM+NS+PS+SS+TF-MoM8 Graphene Growth Studied with LEEM, PEEM, EELS, ARPES, MEIS, and STM**, *R.M. Tromp, J.B. Hannon, M.W. Copel, S.-H. Ji, F.M. Ross*, IBM T.J. Watson Research Center **INVITED**

We have studied the growth of graphene on a variety of substrates, including SiC (both Si and C terminated), polycrystalline Cu and Ni foils, as well as single-crystal Ni foils. Low Energy Electron Microscopy (LEEM) and Photo Electron Emission Microscopy (PEEM) offer the unique opportunity to follow the growth in real time, as it proceeds at high temperature, and in the presence of processing gases such as disilane (for growth on SiC) or ethylene (for growth on the metal substrates). Low Energy Electron Diffraction (LEED) allows us to determine crystallographic orientations as well as atomic structure of areas well below a micrometer in extent. Information on electronic structure can be obtained from the plasmon loss features using Electron Energy Loss Spectroscopy (EELS), or from Angle Resolved Photo Electron Spectroscopy (ARPES). These spectroscopic experiments are carried out in the LEEM/PEEM microscope using an in-line energy filter with which energy and angle resolved analysis of the electrons can be performed on selected areas. Finally, to obtain information on the layer-by-layer evolution of the graphene films, particularly on SiC, we have used isotope sensitive Medium Energy Ion Scattering (MEIS), to follow the growth by thermal decomposition of ¹²C vs ¹³C graphene monolayers from a three-bilayer thick Si¹³C homoepitaxial film grown on a SiC substrate. Taken together, these results provide a comprehensive view of the growth of graphene films. In this talk, we will review the most salient results of these studies, and their relevance to the use of graphene films for electronic applications. To address the latter, we will discuss the results of three-probe STM experiments in which we measured the excess resistivity of a graphene sheet as it crosses an atomic step of the underlying substrate.

11:20am **GR+EM+NS+PS+SS+TF-MoM10 Spatial Confinement of Epitaxy of Graphene on Microfabricated SiC to Suppress Thickness Variation**, *H. Fukidome, T. Ide, H. Handa*, RIEC, Tohoku Univ., Japan, *Y. Kawai*, Tohoku Univ., Japan, *F. Fromm*, Univ. Erlange-Nürnberg, Germany, *M. Kotsugi, T. Ohkouchi*, JASRI/SPring-8, Japan, *H. Miyashita*, Tohoku Univ., Japan, *Y. Enta*, Hirotsaki Univ., Japan, *T. Kinoshita*, JASRI/SPring-8, Japan, *Th. Seyller*, Univ. Erlange-Nürnberg, Germany, *M. Suemitsu*, RIEC, Tohoku Univ., Japan

Epitaxial graphene on SiC (EG) is promising owing to a capability to produce high-quality film on a wafer scale [1]. One of the remaining issues is microscopic thickness variation of EG near surface steps, which induces variations in its electronic properties and device characteristics. To suppress the variation, spatial confinement of surface reactions is effective. The spatial confinement using substrate microfabrication, for instance homoepitaxy and sublimation on microfabricated Si substrates, can induce self-ordering of steps, and even produce step-free surfaces [2]. The spatial confinement is therefore anticipated effective to obtain EG without the thickness variation.

We have for this reason applied the spatial confinement to the epitaxy of graphene on 6H-SiC(0001). For the spatial confinement, 6H-SiC(0001) substrates were microfabricated by using electron beam lithography and fast atomic beam etching using sulfur hexafluoride [3, 4]. Epitaxial graphene on the microfabricated 6H-SiC(0001) substrates was obtained by annealing at 1923 K in Ar ambience [2]. It is verified by using low energy electron

microscopy (LEEM) and photoemission electron microscopy (PEEM) that step-free SiC surface and EG without thickness variation can be formed on smaller patterns [4]. This result clearly demonstrates that the spatial confinement is effective for the epitaxy of graphene on SiC. Furthermore, Raman spectroscopy and LEEM reveals that the spatial confinement can suppress the fluctuations of the electronic properties, e.g. (unintentional) doping in EG [4].

In conclusion, we have demonstrated that the spatial confinement of EG is effective to control both structural and electronic properties. This novel technique can boost the development of electronic devices based on EG.

[References]

- [1] K. V. Emstev et al., Nature Mater. 8 (2009) 203.
- [2] Y. Homma et al., Jpn. J. Appl. Phys. 35 (1996) L241.
- [3] T. Ide et al., accepted for the publication in Jpn. J. Appl. Phys.
- [4] H. Fukidome et al., submitted.

11:40am **GR+EM+NS+PS+SS+TF-MoM11 Three-Dimensional Graphene Architecture Growth and Its Facile Transfer to Three-Dimensional Substrates**, *J.-H. Park*, Sungkyunkwan University, Republic of Korea, *H.-J. Shin, J.Y. Choi*, Samsung Advanced Institute of Technology, Republic of Korea, *J.R. Ahn*, Sungkyunkwan University, Republic of Korea

Recent development of large area graphene synthesis on metal layer by chemical vapor deposition (CVD) or epitaxial growth on silicon carbide (SiC) opened the possibility for applications such as transparent electrodes for ITO replacement. For instance, graphene has been demonstrated for use in a liquid crystal display (LCD) and/or organic light emitting diode (OLED) test cell as a bottom electrode. However, the actual device, e.g., an active-matrix (AM) LCD, operates by switching individual elements of a display, using a thin-film transistor (TFT) for each pixel. Here, the pixel electrode of a display should extend down to the transistor's source or drain, thereby making contact with a via hole, which demands that a three-dimensional (3D) architecture electrode be deposited on a flat surface as well as its side walls. Although large-area graphene growth can be applied for a wide range of applications, 3D graphene architecture growth has not been realized for actual devices due to the original limitation of planar graphene growth. Herein, we demonstrate for the first time 3D graphene architecture growth and its facile transfer to a planar and/or 3D substrate. To prevent agglomeration of nano-scale metal catalyst by the CVD process, we chose a SiC system. Graphene, a few layers thick, was epitaxially grown on a pre-patterned SiC substrate with nano-size thickness which was produced by photolithography and dry etching. Graphene on a vertical facet of the SiC pattern with a few-hundred nanometers in height was perfectly prepared using this approach, contrary to the CVD method. Furthermore, we suggest the use of a facile transfer method of graphene on SiC to a SiO₂ substrate using thermal release tape after hydrogen intercalation. In spite of the troublesome transfer issue of SiC, the geometry of the 3D graphene was perfectly transferred onto the planar SiO₂ as well as the 3D SiO₂ structure. In other words, the 3D graphene architecture was maintained as a floating cap structure on planar SiO₂ and the vertical facet of the 3D SiO₂ structure was well covered. Moreover, the graphene bottom layer without a 3D cap and the inverted bowl structure in the 3D graphene architecture were selectively transferred by controlling intercalation and pressure. These approaches could provide a beneficial method for preparing a 3D graphene architecture as well as for modifying the ordered structure to be utilized in real devices.

Oxide Heterostructures-Interface Form & Function
Focus Topic

Room: 7 - Session OX+EM+MI+NS+TF-MoM

Structure-Property Relationships in Epitaxial Oxide Interfaces

Moderator: E.I. Altman, Yale University

8:20am **OX+EM+MI+NS+TF-MoM1 Role of Dual-laser Ablation in Controlling Mn Oxide Precipitation during the Epitaxial Growth of Mn Doped ZnO Thin Films with Higher Doping Concentrations**, *D. Mukherjee, M. Hordagoda, R.H. Hyde, N. Bingham, H. Srikanth, P. Mukherjee, S. Witanachchi*, University of South Florida

The low solubility of Mn (equilibrium limit of 13 %) and precipitation of Mn oxides at slightly higher Mn doping (> 4 %) have remained major obstacles in the growth of Mn doped ZnO (ZnO:Mn) thin films for potential spintronic applications. In this work, epitaxial ZnO:Mn thin films were deposited on c-cut Al₂O₃ (0001) substrates, with increasing Mn

concentrations from 2 to 12 %, using the dual-laser ablation process. In this process, an excimer (KrF) laser and a CO₂ laser pulses are spatially and temporally overlapped onto the target surface. Initially the target is heated by the CO₂ laser to produce a transient molten layer, from which the slightly time-delayed KrF laser initiates the ablation. Ablation for a momentary liquid target not only results in a drastic reduction of particulates in the deposited films but also overcomes the problem of non-congruent ablation of the ZnO:Mn target, leading to stoichiometric film deposition. Moreover, the optimum coupling of the laser energies produces an ablation plume that has a broader angular distribution, compared to the plume generated by KrF pulse alone, as observed from the intensified-charge-coupled-detector (ICCD) images of the ablated plumes. This allows the deposition of uniform films over larger area. Further, the higher ionization of the ablated species as seen in the optical emission spectra (OES) of the dual-laser ablated plumes leads to enhanced gas phase reaction and better film morphology and crystallinity. X-ray diffraction studies revealed that the dual-laser deposited ZnO:Mn films were single crystalline with no secondary phase formation even at 12 % doping while single-laser deposited ZnO:Mn films showed secondary Mn oxide phases. Room temperature magnetic measurements showed ferromagnetism (FM) with enhanced saturation magnetization (M_s) values from 1.3 emu/cm³ for 2 % ZnO:Mn films to 2.9 emu/cm³ for 12 % ZnO:Mn films. In- and out-of-plane magnetization revealed absence of magnetic anisotropy. Further, temperature dependent Hall measurements showed a strong correlation between the effective carrier densities and the observed FM. All these measurements suggested a carrier mediated mechanism of FM in ZnO:Mn thin films. Using both the experimental data and theoretical analysis the FM in less conducting ZnO:Mn films was described by a bound magnetic polaron model whereas that in highly conducting films was consistent with a carrier mediated interaction via RKKY exchange mechanism.

8:40am **OX+EM+MI+NS+TF-MoM2 Structural Characterization of Heterojunction *n*-ZnO/*p*-NiO Thin Films Epitaxially Deposited on (0002)Al₂O₃ Substrates**, *Y.H. Kwon*, Sungkyunkwan University, Republic of Korea, *J.H. Lee*, KAIST, Republic of Korea, *S.H. Chun*, Sungkyunkwan University, Republic of Korea, *J.Y. Lee*, KAIST, Republic of Korea, *H.K. Cho*, Sungkyunkwan University, Republic of Korea

Recently, oxide semiconductors with superior electrical properties have been considered as candidates to replace Si based electronics. Furthermore, their thermally and chemically stable characteristic is preferable for devices. Especially, among a lot of oxides, ZnO based semiconductors have been extensively investigated to apply in wide application such as thin film transistor and light emitting diode. ZnO is an intrinsic *n*-type semiconductor which characteristic comes from Zn interstitials and O vacancies. And band-gap and exciton binding energy are 3.37 eV and 60 meV, respectively, which is suitable for optical application operating in ultra-violet region. Therefore, *p-n* homojunction diode structure combined with *n*-ZnO and *p*-ZnO having well matched interface had been studied by a lot of researchers.[1] However, it was not reliable since *p*-type ZnO synthesized by doping of group V elements is unstable and return to the *n*-type by self-compensation.[2]

Therefore, *p-n* heterojunction diode composed of *n*-ZnO and stable *p*-type oxide such as Cu₂O and NiO was alternatively studied.[3] Among the *p*-type oxides, NiO with wide direct band-gap (3.7 eV) have been expected to apply in optical applications. And conductivity of NiO could be significantly controlled by Li⁺ doping. Furthermore, according to T. Dutta et. al., (111) plane of NiO could well matched with (0002) of ZnO by domain match epitaxy.[4]

In this study, heterojunction diode structure was fabricated with *n*-type ZnO and *p*-type NiO on [0002] oriented Al₂O₃ substrates. RF magnetron sputtering method was used for deposition of NiO and ZnO films. After the deposition of NiO films at 400°C in O₂ atmosphere, ZnO films were grown at 600°C and in Ar and O₂ mixed gas atmosphere. XRD result showed the NiO films were fabricated with high crystallinity and preferred orientation of [111]_{NiO}. And sixfold symmetry of (100)_{NiO} plane obtained by phi-scan indicates that the NiO films were bi-epitaxially grown on Al₂O₃ substrates. In addition, electrical properties of NiO showed relatively low resistivity (1.648 Ωcm) and high mobility (14.52 cm²/Vs) due to Li⁺ doping. Sixfold symmetry of (1-102)_{ZnO} observed at phi-scan result indicates that ZnO films were also epitaxially grown on [111] oriented NiO films.

REFERENCES

- [1] F. Zhuge, L. Zhu, Z. Ye, D. Ma, J. Lu, J. Huang, F. Wang, Z. Ji, S. Zhang, Applied Physics Letters, 87 (2005) 092103.
- [2] C. Park, S. Zhang, S.H. Wei, Physical Review B, 66 (2002) 073202.
- [3] H. Kawazoe, H. Yanagi, K. Ueda, H. Hosono, MRS Bulletin, 25 (2000) 28.
- [4] T. Dutta, P. Gupta, A. Gupta, J. Narayan, Journal of Applied Physics, 108 (2010) 083715.

9:00am **OX+EM+MI+NS+TF-MoM3 Manipulating the Electrostatic Boundary Conditions of Polar Interfaces**, *Y. Hikita*, SLAC National Accelerator Laboratory

INVITED

Transition metal oxides (TMO) offer various functionalities ranging from electronic devices to environmental catalysts [1, 2]. Often, the central part of such devices is the interface between different materials. In order to improve their device performance, control of charge transport across these interfaces is essential. Originally developed in semiconductor heterostructures, interface band alignment control is based on the interface electrostatic boundary conditions and is one of the most fundamental methods to tune the carrier transport across interfaces [3]. Given their strongly ionic nature and their accessibility to multiple valence states, the TMO interface should be more suitable than covalent semiconductors for manipulating interface band alignments. Here we focus on epitaxial metal-semiconductor Schottky interfaces between perovskite oxides to demonstrate the effectiveness of this technique. I will present two SrTiO₃ based perovskite Schottky junctions in which the interface energy barriers were modulated by interface dipoles controlled on the atomic scale [4]. Further, I will present the application of this technique in the form of an all-oxide hot electron transistor [5].

1. R. Ramesh and D. G. Schlom, MRS Bull. **33**, 1006 (2008).
2. J. Suntivich *et al.*, Science **334**, 1383 (2011).
3. F. Capasso *et al.*, Appl. Phys. Lett. **46**, 664 (1985).
4. Y. Hikita *et al.*, Phys. Rev. B **79**, 073101 (2009).
5. T. Yajima *et al.*, Nature Mater. **10**, 198 (2011).

11:20am **OX+EM+MI+NS+TF-MoM10 Strain-induced Oxygen Vacancy Ordering at SrTiO₃/La_{0.5}Sr_{0.5}CoO₃ Interfaces, and its Impact on Magnetic "Dead" Layers**, *S. Bose*, *M. Sharma*, *M. Torija*, University of Minnesota, *J. Gazquez*, *M. Varela*, Oak Ridge National Laboratory, *J. Schmitt*, *C. He*, University of Minnesota, *S. El-Khatib*, American University of Sharjah, United Arab Emirates, *M. Laver*, *J. Borchers*, NIST Center for Neutron Research, *C. Leighton*, University of Minnesota

The remarkable functionality and epitaxial compatibility of complex oxides provides many opportunities for new physics and applications in oxide heterostructures. Perovskite cobaltites provide an excellent example, being of interest for solid oxide fuel cells, oxygen separation membranes, catalysis, ferroelectric RAM, resistive switching memory, and oxide spintronics. However, the same delicate balance between phases that provides this diverse functionality also leads to a serious problem - the difficulty of maintaining desired properties close to the interface with other oxides. Although this problem is widespread, manifests itself in several ways, and could present a significant roadblock to the development of heterostructured devices for oxide electronics, there is no consensus as to its origin. In our work, using SrTiO₃(001)/La_{1-x}Sr_xCoO₃ as a model system, we have combined epitaxial growth via high pressure oxygen sputtering [1] with high resolution x-ray diffraction, atomic resolution scanning transmission electron microscopy (STEM) and electron energy loss spectroscopy (EELS), and detailed magnetic, transport, and neutron scattering measurements to determine the fundamental origin of the deterioration in interfacial transport and magnetism [2,3]. The effect is found to be due to nanoscopic magnetic phase separation in the near-interface region driven by a significant depletion in interfacial hole doping due to accumulation of O vacancies. This occurs due to a novel mechanism for accommodation of lattice mismatch with the substrate based on formation and long-range ordering of O vacancies [4]. This fundamental link between strain state and O vacancy formation and ordering is explored in detail in this presentation. We demonstrate that the O vacancy density, depth profile, and ordering vector can all be controlled via strain, leading to a potential mechanism to substantially improve interfacial properties.

UMN support from NSF and DOE (neutron scattering). ORNL support from DoE; UCM support from the European Research Council.

- [1] Torija *et al.*, J. Appl. Phys. **104** 023901 (2008); Sharma *et al.*, J. Vac. Sci. Technol. **29** 051511 (2011).
- [2] Torija *et al.*, Adv. Mater. **23** 2711 (2011).
- [3] Sharma *et al.*, Phys. Rev. B., **84** 024417 (2011). [4] Gazquez *et al.*, Nano. Lett. **11** 973 (2011).

11:40am **OX+EM+MI+NS+TF-MoM11 Fabrication and Characterization of Titanium Oxide Films with Tunable Stiffness**, *K. Gotlib-Vainshtein*, *O. Girshevit*, *C.N. Suenik*, Bar Ilan University, Israel, *D. Barlam*, Ben Gurion University, Israel, *E. Kalfon-Cohen*, *S.R. Cohen*, Weizmann Institute of Science, Israel

The design of surfaces with controlled stiffness is attractive for a variety of applications ranging from controlling cell growth to mechanical and electrical engineering design. Here, the creation of layered composites with tunable surface stiffness has been achieved by coating a soft PDMS

polymer with a stiff film of amorphous titanium oxide with thickness varying from 2 to 50 nm. The oxide layer is smooth (6 nm rms roughness at 2 μm^2 image size), and crack-free. Air plasma treatment was used to form a silica surface layer on the soft polymer base to promote of adhesion of the titania overlayer. To gain insight into the mechanics of the layered structure, nanomechanical quantification has been performed using different experimental approaches, as well as modeling studies. The surface mechanical properties of the samples have been probed using both instrumented nanoindentation and atomic force microscopy—based nanomechanical characterization. These results have been compared to finite element analysis (FEA) simulations.

By fitting the FEA simulations with experimental curves it is shown that the hard titania film and softer PDMS substrate individually maintain their characteristic elastic moduli, while the stiffness of the vertical nanocomposite can be controllably modified by changing the thickness of the stiff layer. Liquid phase deposition of the oxide allows control of its thickness at the nm level. During an indentation cycle, the stiff layer transmits the stress to the underlying PDMS base by deformation of its overall shape, but only negligible compression of the film thickness.

This synthetic approach can be quite versatile, and can, in principle, be extended to different oxides and a wide range of thicknesses. It allows control of surface properties while maintaining bulk material properties. This exploratory work is a first step towards defining the range of surface stiffnesses that can be achieved in this way, as well as developing general methodologies for their characterization.

Thin Film

Room: 11 - Session TF-MoM

ALD Enabled Applications

Moderator: W.M.M. Kessels, Eindhoven University of Technology, the Netherlands

9:00am **TF-MoM3 Atomic Layer Deposition Films as Diffusion Barriers for Silver Artifacts**, *A.E. Marquardt*, University of Maryland, *E. Breitung*, E-Squared Art Conservation Science, *G. Gates*, *T. Drayman-Weisser*, The Walters Art Museum, *G.W. Rubloff*, *R.J. Phaneuf*, University of Maryland

In this work we investigate atomic layer deposition (ALD) to create transparent oxide diffusion barrier coatings to reduce the rate of tarnishing for silver objects in museum collections. Elevated heating and H_2S pressure tests determined the effect of various thicknesses of Al_2O_3 ALD thin films, ranging from 5 to 100nm thick, and the effect of annealing temperature on the thickness of the tarnish layer (Ag_2S) created at the interface of the ALD coating and the silver substrate. Reflectance spectroscopy and an integrated sphere spectrophotometer were used to measure the thickness of the tarnish layer and indicate the effectiveness of the Al_2O_3 ALD thin films in reducing the tarnishing rate of silver while minimally affecting the visual appearance of the silver. X-ray photoelectric spectroscopy (XPS), and time of flight secondary ion mass spectroscopy (TOF-SIMS) analysis determined the concentration profile of sulfur through the ALD oxide film. A model for predicting the tarnishing kinetics of sulfur diffusion through ALD oxide films is established, influenced by the composition of the alloy, phase of sulfide at the interface, and non-uniformity of diffusion due to pinhole and concentration dependence. Evidence was found for the slow diffusion of sulfur through the bulk of the films and faster diffusion through pinholes in the ALD oxide films.

9:20am **TF-MoM4 Quasi-ALD for Deposition of a Water Resistive Barrier Layer and Prevent Electronic Devices from Water Shock**, *V. Gupta*, *M.R. Linford*, Brigham Young University

Water resistant surfaces and devices have an ever increasing importance in various areas of technology, including electronics (e.g., cell phones), fabrics, shoes, chemical handling equipment, and hearing aids to name only a few. However, while important and effective against splashes, ultrathin hydrophobic films are not always sufficient for water proofing devices. Herein we describe the development of a water resistant barrier layer, deposited by a method similar to atomic layer deposition, which can also be made hydrophobic by deposition of fluorosilanes, for imparting improved protection against water to underlying surfaces and devices. The resulting barrier has been found effective in resisting the infiltration of water and preventing underlying surfaces such as electronic circuits from water shock. The precursors we use appear to have low toxicity in their molecular and (especially) deposited form, are inexpensive, have good vapor pressures so they can be deposited at low temperature, and can be deposited in a straightforward manner because of their high reactivity. Different plasma

pre-treatments of substrates have been studied, although good uniformity in the deposition takes place on substrates, such as Si/SiO₂ and nylon, that have not been primed in any way. Film growth on Si/SiO₂ and nylon spin coated onto Si/SiO₂ has been monitored by spectroscopic ellipsometry, which shows consistent increases in film thickness with deposition cycles, contact angle goniometry, which shows similar wetting properties for all layers of the films and is consistent with deposition of a constant surface chemistry, XPS, which shows the expected elements in the film, AFM, which provides surface roughness, and ToF-SIMS, which is also a probe of the surface chemistry. This barrier layer has been tested on model circuit boards and results are consistent with both the number of layers deposited and their mode of deposition. That is, water damage shows a proportional decrease with an increase in the number of the above mentioned layers. This process appears to be applicable on multiple substrates ranging from inorganic to organic surfaces. Presently we are working on increasing the number of layers and more effective crosslinking of the films. Additional film characterization will also be done by RBS and NRA.

9:40am **TF-MoM5 Atomic Layer Deposition for Astronomy and Space Applications**, *F. Greer*, Jet Propulsion Laboratory/California Institute of Technology **INVITED**

Future UV, X-ray, infrared, and sub-millimeter telescopes and spectrometers have the potential to revolutionize our understanding of the formation and habitability of the modern universe. Star formation, dark energy, and the composition of the intergalactic medium are only some of the key scientific topics that can be addressed by UV astronomy and astrophysics. Infrared astronomy enables the hunt for new planets and stars, even through clouds of interstellar dust, while sub-millimeter astronomy can probe the fine structure of the cosmic microwave background, giving glimpses into the early universe immediately following the Big Bang. While existing technology has allowed us to probe deep into the universe, materials or fabrication challenges still limit the sensitivity and capability of the detectors and instruments used in these applications. In this talk, we will first discuss, in general, how the precision and control afforded by atomic layer deposition can be used to substantially increase the capability of astronomers to make new discoveries. Then, we will focus on specific cases to show the impact of ALD films on the coating, passivation, and fabrication of UV, infrared, and submillimeter detectors, respectively. For example, atomic layer deposition coatings utilized in UV instruments, once fully optimized, can yield as much as a 100X increase in signal to noise ratio over conventional technology. Here, we will demonstrate how small changes in nucleation and growth conditions of ALD fluorides, oxides, and transition metal nitrides have a significant effect on the performance of these detectors and other instrument components, even for films with comparable indices of refraction and resistivity. We will also discuss the novel ALD chemistries that we have pursued, e.g. for MgF_2 deposition, in order to achieve reliable processes. Finally, this presentation will detail the unique surface engineering approaches such as the combination of atomic layer deposition and MBE, demonstrating the advantages that are obtained by achieving atomic level precision at key steps in detector fabrication processes.

10:40am **TF-MoM8 ALD-Enabled Pt/HfO₂/Ti and Pt/TiO₂/Ti Tunneling Diodes with Enhanced Tunneling Characteristic**, *O. Ajayi*, *G. Mumcu*, *J. Wang*, University of South Florida

Due to its unique resistive switching capability, Metal-Insulator-Metal (MIM) diodes have attracted substantial interests ever since 1960's. The early generation of MIM device (point-contact diode) is composed of a sharp metal tip placed right on top of a planar metal electrode coated with an ultra-thin layer of insulator. It has been envisioned that MIM diodes hold great promise for detecting and mixing high frequency signals up to Terahertz (THz) range. Particularly, several prior works have suggested for operation at THz frequencies, the MIM diodes are anticipated to outperform heterojunction diodes, which have limited cutoff frequency (<3THz). Hence, the MIM devices are well-suited for a wide range of applications in security, imaging and energy scavenging. In lieu of this, microfabricated MIM diodes with low zero-bias impedance have been actively pursued in this work for a strategically-designed antenna-coupled detector with high responsivity.

With introduction of ultra-thin tunneling layer sandwiched between two planar metal electrodes, the microfabricated MIM diodes are amenable for direct integration with ICs. In particular, we have devoted most of our efforts on developing techniques to improve the overall diode characteristics through tuning its tunneling properties. The effective junction capacitance and resistance limit the operation frequency range of tunneling diode. The key factors that affect the frequency range of tunneling diodes are the junction area, defect density, permittivity and thickness of the tunneling layer. For the MIM diode, a small deviation in tunneling barrier thickness can cause a significant change in the junction resistance and its I-V responses. Hence, atomic layer deposition (ALD) process was employed

which offer superb uniformity, low defect density, and precise thickness control of the tunneling layer. In this work, MIM diodes with a variety of junction areas ranging from $3\mu\text{m} \times 3\mu\text{m}$ to $100\mu\text{m} \times 100\mu\text{m}$ have been fabricated with different ALD thin films (e.g., TiO_2 and HfO_2) of varied thicknesses. By systematic investigation of the measured I-V characteristics for MIM devices with a variety of junction materials, junction thickness and junction area, it is evident that the performance of the MIM tunneling diodes can be greatly enhanced through optimizing junction properties (material, thickness, area, etc.). As compared to similar devices reported previously, we have successfully demonstrated high-yield MIM diodes with 1.5nm-thick tunneling junction with unprecedented low junction resistance in the range of 500Ω or even less, thus resulting in greatly enhanced responsivity.

11:00am TF-MoM9 Uniform Adsorption of Ligand Free Ag Nanoparticles onto TiO_2 Thin Films Deposited by Atomic Layer Deposition, J.C. Halbur, J.S. Jur, North Carolina State University

Nanoparticle modification of inorganic thin films, such as TiO_2 or Al_2O_3 , represents a method to enhance or alter the catalytic, antimicrobial, or responsive behaviors of a material. The use of nanoparticle inks for application is challenging, as the nanoparticles tend to be stabilized using surfactants or other molecules during the synthesis process, and these ligands can interfere with or prevent nanoparticle adsorption onto the oxide. This work shows the efficacy to attach ligand-free Ag nanoparticles onto TiO_2 surfaces formed by atomic layer deposition (ALD). Sonochemical synthesis is used to create Ag NPs of 14-20 nm diameter in an aqueous solution at room temperature without the need for additives such as stabilizing agents. After ALD of TiO_2 thin films onto polymer substrates, a facile dip coating process at ambient conditions results in the uniform decoration of the ligand free Ag nanoparticles on the TiO_2 surface. The efficiency of nanoparticle adsorption is examined by TEM and EDS. Finally, the photocatalytic degradation of methylene blue is used to assess the photocatalytic efficiency of the fiber based composite.

11:20am TF-MoM10 Alloy Films Grown Using Al_2O_3 ALD and Alucone MLD: Critical Tensile Strains, Water Vapor Transmission Rates and Compliant Interlayers, S.H. Jen, B.H. Lee, S.M. George, University of Colorado, Boulder, P.F. Carcia, R.S. McLean, DuPont Central Research and Development

Hybrid organic-inorganic alloy films can be grown using Al_2O_3 ALD and alucone MLD. These alloy films may display the excellent gas diffusion barriers properties of Al_2O_3 ALD films and also may be more flexible than Al_2O_3 ALD films. Critical tensile strains (CTSs) and water vapor transmission rates (WVTRs) were measured for the ALD:MLD alloy films using trimethylaluminum, ethylene glycol and H_2O as the reactants. The alloy composition was controlled by varying the ratio of ALD: MLD cycles during film growth. The CTS reached its highest values of $\sim 1.0\%$ for the 3:1 alloy. The WVTR decreased 4 orders of magnitude versus alloy composition. The 7:2, 5:1 and 6:1 alloys had the lowest WVTRs of $\sim 1 \times 10^{-4} \text{ g/m}^2/\text{day}$ at the sensitivity limit. These alloys are more flexible than Al_2O_3 ALD and may serve as gas diffusion barriers for flexible thin film devices. The alucone MLD film was also used as a compliant interlayer to minimize stress caused by thermal expansion mismatch between Al_2O_3 ALD films and Teflon FEP substrates. Without the alucone MLD interlayer, the Al_2O_3 ALD films are susceptible to cracking resulting from the high coefficient of thermal expansion mismatch between Al_2O_3 ALD and Teflon FEP. With an alucone compliant interlayer, the Al_2O_3 ALD film has a crack density that is reduced progressively versus alucone interlayer thickness.

Monday Afternoon, October 29, 2012

Actinides and Rare Earths Focus Topic
Room: 6 - Session AC+TF+SS+MI-MoA

Actinides and Rare Earths: Thin Films and Surface Science

Moderator: R.K. Schulze, Los Alamos National Laboratory

2:00pm **AC+TF+SS+MI-MoA1 Rare Earth 4f Hybridization in Gallium Nitride**, *J.W. McClory, S.R. McHale*, Air Force Institute of Technology, *L. Wang, W.N. Mei*, University of Nebraska-Lincoln, *J.C. Petrosky*, Air Force Institute of Technology, *J. Wu, R. Palai*, University of Puerto Rico – San Juan, *Ya.B. Losovyj*, Louisiana State University, *P.A. Dowben*, University of Nebraska-Lincoln **INVITED**

The location of the Gd, Er and Yb 4f states within the GaN valence band has been explored both experimentally and theoretically. The 4d – 4f photoemission resonances for various rare earth doped GaN thin films (RE = Gd, Er, Yb) provide an accurate depiction of the occupied 4f state placement within the GaN valence band. The resonant photoemission show that the major Er and Gd rare earth 4f weight is at about 5-6 eV below the valence band maximum, similar to the 4f weights in the valence band of many other rare earth doped semiconductors. For Yb, there is very little resonant enhancement of the valence band of Yb doped GaN, consistent with a largely 4f^{14-d} occupancy. The placement of the rare earth 4f levels is in qualitative agreement with theoretical expectations.

2:40pm **AC+TF+SS+MI-MoA3 Revisiting the Yb Electronic Structure with Low-Energy Photoemission Spectroscopy**, *F. Offi*, CNISM and Univ. Roma Tre, Italy, *P. Vilmercati, L. Petaccia, S. Gorovikov*, ELETTRA Sincrotrone Trieste, Italy, *A. Ruocco*, CNISM and Univ. Roma Tre, Italy, *M.I. Trioni*, CNR-ISTM, Milano, Italy, *A. Rizzo*, CNISM and Univ. Roma Tre, Italy, *A. Goldoni*, ELETTRA Sincrotrone Trieste, Italy, *G. Stefani*, CNISM and Univ. Roma Tre, Italy, *G. Panaccione*, CNR-IOM, Basovizza-Trieste, Italy, *S. Iacobucci*, CNI-IFN, Rome, Italy

The peculiar electronic structure of rare-earth elements and compounds is mostly defined by the partially filled 4f band. Of particular interest is the investigation of the valence states, which is linked to the degree of hybridization of f electrons with delocalized s-d bands. In the simple case of Yb, the 4f states are fully occupied with a Fermi level of 6s character and a 2+ valency. However, the occupation of the Yb valence band has been the subject of several investigations over the years, intended in particular to separate the contribution of 5d states. Early experimental photoelectron emission (PES) spectra at very low excitation energy ($h\nu < 10$ eV) have reported a spectral modulation in the region close to the Fermi level that was attributed to the emission from a 5d band. The poor energy resolution did not allow however a detailed investigation of such spectral features. In recent years this low energy photoemission spectroscopy (LEPES) encountered a renewed interest, under the stimulus of the extremely high energy resolution obtainable with laser excited LEPES and given the expectation of a large increase of the bulk sensitivity at these low energies. We monitored the 4f spectral intensity in polycrystalline Yb films in the LEPES regime (between 5.5 and 21 eV photon energy, with experiments at the BaDELPH beamline of the ELETTRA synchrotron radiation facility), observing a moderate increase of the electron attenuation length and, thus, a moderate increase of the information depth when we reach the lowest energies. By lowering the photon energy below about 11 eV a prominent peak at the Fermi level is observed. The analysis of its intensity variation versus photon energy and the comparison of the experimental spectra with *ab initio* density of states (DOS) calculations allow to attribute this structure to a p band crossing the Fermi level, enhanced at selected photon energies due to the influence of the empty DOS, probably amplified by a photoionization cross section effect and by the general increase of the photoelectron yield at low photon energy. In this respect LEPES may thus be considered as a probe of the joint DOS.

3:00pm **AC+TF+SS+MI-MoA4 Erbium Rare Earth Thin Film Hydride Stress Studies as a Function of Processing Techniques**, *J.L. Provo*, J.L. Provo Consulting

An important part of understanding the behavior of rare earth, Group 3A and 4A thin film hydrides is the determination of indirect effects such as stress in the film lattice which can lead to film flaking. In this study, special vacuum sample containers were prepared to observe and record basal-plane film stress levels, and film flaking (optical observations).

The special vacuum sample containers contained erbium deuteride (ErD₂) and erbium tritide (ErT₂) films on AT and BT quartz resonator substrates with chromium underlays in pairs prepared by air-exposure, (in-situ)

evaporate-load and reactive evaporation hydriding techniques. The erbium deuteride samples were prepared as controls for aging studies. All samples were processed with PVD Electron Beam deposition techniques, hydriding techniques mentioned above and a 450°C temperature bakeout and exhaust in consideration of the $\alpha \rightarrow \beta$ crystal phase transformation in crystalline quartz at 573°C.

Samples for the measurement of initial film deposition stress as a function of hydride processing and for the determination of stress produced in ErT₂ films due to the generation of helium-3 with time (i.e., tritium decay) were designed to utilize the double-resonator technique developed by EerNisse(1). Measurements of mass change and induced film stress were determined by frequency measurement changes obtained with a precision frequency counter, data being taken from the output of a one transistor Colpitts type driving oscillator circuit in which the crystal is an integral part.

A summary of initial film deposition stress (tensile) and film aging accumulative stress (compressive) for the erbium films from the different deposition and hydriding techniques is given. Reactively evaporated erbium occluder films were seen to have an initial film deposition tensile stress approximately 5 times less than (in-situ) evaporate-load films and 11 times less than air-exposed loaded films. Accumulative aging compressive stress for erbium occluder films were shown to be more variable but data indicate that reactively evaporated film aging stress is less than that of (in-situ) evaporate-load and air-exposed tritided films.

(1)-J. Appl. Phys. 43, 1330 (1972)

3:40pm **AC+TF+SS+MI-MoA6 Splat Cooling Technique Contributing to Understanding of Uranium Systems**, *L. Havela*, Charles University, Czech Republic, *A. Gonçalves, J.-C. Waerenbogh, L. Pereira*, ITN Sacavém, Portugal, *I. Tkach*, Charles University, Czech Republic, *N.-T. Kim-Ngan*, Pedagogical University Cracow, Poland, *T.B. Scott*, University of Bristol, UK

The splat cooling technique is one of the methods of ultrafast cooling of a melt, particularly suitable for small amounts of material. In particular cases it can help to overcome constraints imposed by thermodynamics. One of them was the issue of magnetic properties of non-stoichiometric Laves phase UFe₂. This compound has a ferromagnetic ground state (with both U and Fe magnetic moments). An excess of U, achieved by quenching, led to the decrease of T_c from 162 K for pure compound to 112 K for UFe_{1.7} [1]. Quenching was, however, unable to provide Fe-rich material, with expected increase of T_c. Using splat cooling of a series of materials with various off-stoichiometry from UFe₂ to UFe₆ we found that the cubic Laves phase structure (with sub-micron grains) can absorb excessive Fe up to the stoichiometry UFe_{2.3}. Additional excess leads to the segregation of α -Fe [2]. The increase of T_c up to 230-240 K was the impact on magnetic properties. The spontaneous magnetization also increases from 1.0 μ_B /f.u. in UFe₂ to 1.9 μ_B /f.u. in UFe_{2.3}. ⁵⁷Fe Mössbauer spectroscopy reveals that the excessive Fe atoms enter the U sublattice and develop higher magnetic moments (approx. 1.0 μ_B /Fe).

Applying the splat cooling technique on pure and doped U metal had the aim to stabilize the high temperature bcc phase (γ -U) to low temperatures, to be able to establish its basic electronic properties. In particular, changes in magnetic characteristics and electronic specific heat can be expected due to the modest volume expansion comparing to orthorhombic α -U. We found that splat cooling reduces the necessary concentration of dopants and U with 12 at.% Mo has no traces of α -U. The Sommerfeld coefficient $\gamma = 19$ mJ/mol K² estimated for pure γ -U is enhanced comparing to 11 mJ/mol K² for pure U splat, which is close to values given in literature [3] for the U metal. The splats exhibit a superconducting ground state with T_c ranging from 1.24 K for pure U to 2.11 K for 15 % Mo. The γ -U superconductivity is characterized by a large critical field exceeding 6 T and a sharp λ -type anomaly in specific heat C_p(T) with the size corresponding to the BCS theory. The superconductivity of a pure U splat, which contains only traces of γ -U, has much lower critical field (0.33 T) and the weak anomaly in C_p(T) does not convince about the bulk character of superconductivity.

This work was supported by Grant Agency of the Czech Republic under the grant No. P204/10/0330.

[1] A.T. Aldred, J.Magn.Magn.Mater. 10, 42 (1979).

[2] L. Havela et al., Intermetallics 19, 113 (2011).

[3] J.C. Lashley et al., Phys. Rev. B 63, 224510 (2001).

4:00pm **AC+TF+SS+MI-MoA7 Investigation of Rare Earth Doped Lithium Tetraborate Glasses with XAFS and Emission and Excitation Spectroscopy.** *T.D. Kelly, J.W. McClory, D.A. Buchanan, A.T. Brant, J.C. Petrosky*, Air Force Institute of Technology, *Ya.B. Losovyj*, Louisiana State University, *V.T. Adamiv, Ya.V. Burak*, Institute of Physical Optics, *P.A. Dowben*, University of Nebraska-Lincoln

The local structure of rare earth doped lithium tetraborate ($\text{Li}_2\text{B}_4\text{O}_7$) glasses has been studied by extended x ray absorption fine structure (EXAFS) at the rare earth L shells and by optical emission and excitation spectroscopies. The samples investigated were 1% rare earth doped by weight with Gd and Nd. The EXAFS signal was recorded in fluorescence mode with the energies calibrated for Nd L1 and L3 edges and Gd L3 edge. X rays were applied to the samples to activate emission and excitation centers in the glasses. The spectra were analyzed to determine rare earth occupation sites in the lithium tetraborate crystal structure and the emission and excitation lines due to rare earth doping.

4:40pm **AC+TF+SS+MI-MoA9 Eu-implanted p-type GaN: Charge-Driven Luminescence Hysteresis and Identification of a Possible Charge-State-Alternation Resonance of the Mg Acceptor.** *K.P. O'Donnell, P.R. Edwards, R.W. Martin*, Strathclyde University, Scotland, UK, *K. Lorenz, E. Alves, V. Darakchieva*, ITN Sacavém, Portugal, *M. Bockowski*, Unipress, Poland

Europium-doped p-type GaN shows *spectral switching* and *luminescence hysteresis* when samples are temperature-cycled between room temperature and 20 K (*K.P. O'Donnell et al, Late News paper at ICPS2012, Zurich*). An explanation of this unusual behaviour may be found in the charge-state dependence of the local structure of the Mg acceptor in GaN, recently modelled by J.L. Lyons et al., (*Phys. Rev. Lett.* 108, 156403 (2012)). Eu ions, sensitive to their local environment, may act as 'spectators' of the charge-induced local distortions. The dominant impurity-induced luminescence spectrum at RT (hereafter, Eu0) *switches completely* to another spectrum (Eu1) when samples are cooled below 25 K. Upon subsequent warming of the sample, Eu1 fades with increasing temperature, as expected, but Eu0 *does not reappear* until the temperature exceeds 150 K; its recovery is complete only above 210 K. The noted temperature extremes correspond to hole localisation (carrier freeze-out) and delocalisation, respectively. Here, we extend Lyons' model to consider the possibility of observing the resonance in which the acceptor alternates rapidly between neutral and negative charge states, leading to a spatial oscillation of the associated defect between Eu0 and Eu1 forms, and describe the possible spectral identification of this resonance.

Spectroscopic Ellipsometry Focus Topic

Room: 19 - Session EL+TF+BI+AS+EM+SS-MoA

Spectroscopic Ellipsometry: From Organic and Biological Systems to Inorganic Thin Films

Moderator: M.S. Wagner, The Procter & Gamble Company

2:00pm **EL+TF+BI+AS+EM+SS-MoA1 Biochemical Optical Sensors Based on Highly-Ordered Slanted Columnar Thin Films.** *D. Schmidt, K.B. Rodenhausen*, University of Nebraska-Lincoln, *J. VanDerslice, T.E. Tiwald, J.A. Woollam Co., Inc., E. Schubert, M. Schubert*, University of Nebraska-Lincoln

Highly-ordered three-dimensional nanostructure thin films offer substantially increased surface area for attachment of organic layers, and in addition, new detection principles due to the physical properties of the nanostructures. For example, upon material attachment the optical birefringence of the nanostructures changes due to screening of polarization charges. Because of these advantages, highly-ordered three-dimensional nanostructure thin films lend themselves as suitable candidates for studying of organic attachments as well as for low-cost humidity sensing, for example.

We utilize glancing angle electron-beam deposition for fabrication of highly spatially coherent metal slanted columnar thin films. Subsequently, the nanostructures may be further functionalized with thin conformal coatings by means of atomic layer deposition. The ellipsometry model analysis and resulting anisotropic optical properties of hybrid metal slanted columnar thin films determined by generalized spectroscopic ellipsometry in the visible and near-infrared spectral region will be discussed. We will be reviewing research in this area and report in particular on in-situ monitoring of organic attachments using ellipsometry combined with quartz crystal microbalance with dissipation. Exemplarily, we discuss studies of fibronectin protein adsorption, octanethiol chemisorption (self-assembled monolayer growth) on platinum coated titanium slanted columnar thin films as well as relative humidity sensing.

2:20pm **EL+TF+BI+AS+EM+SS-MoA2 Studies of Optical Properties of Hybrid J-aggregates and Nanocrystal Quantum Dots Layers for Photonic Applications.** *K. Roodenko, H.M. Nguyen, L. Caillard, A. Radja, O. Seitz, Yu.N. Gartstein, A.V. Malko, Y.J. Chabal*, The University of Texas at Dallas

The integration of organic materials and inorganic nanocrystal quantum dots (NQDs) on the nanoscale offers the possibility of developing new photonic devices that utilize the concept of resonant energy transfer between an organic material and NQDs. Electromagnetic coupling that takes place between excitons—bound electron-hole pairs—at the interfaces of the hybrid composite can be utilized for light-emitting, photovoltaic and sensor applications.

As the key ingredients for the nanocomposite material system reported in this work are the J-aggregates (JA, dye self-assembled molecules) that have exceptional optical absorption due to their strong oscillator strength. NQDs on the other hand combine a variety of important properties, such as high quantum yields, excellent photo- and chemical stability, and size dependent, tunable absorption and emission. Excitation energy transfer in NQDs / J-aggregate hybrids is characterized by their strong excitonic transitions at room temperature with spectrally well-defined absorption and emission.

In order to understand the energy transfer mechanisms in such complex systems, optical properties of JA and NQDs/JA hybrid systems were characterized by means of spectroscopic ellipsometry and polarized IR spectroscopy.

Spectroscopic ellipsometry in 0.6-5 eV spectral range was employed to study optical properties of J-aggregates drop-casted on silicon surfaces. Thin JA films were found to exhibit strong optical anisotropy due to the specific molecular orientation of thin layers on Si substrates. Variation of optical properties due to the deposition of nanocrystal quantum dots (NQDs) was systematically studied for applications in new photonic devices that utilize excitonic energy transfer from NQDs to JA layer. Ellipsometric results were cross-referenced with atomic force microscopy (AFM) data to derive a quantitative understanding of the distribution of NQDs upon deposition on JA layer. Integration of hybrid colloidal NQD/JA structures could be potentially attractive for a range of optoelectronic applications.

2:40pm **EL+TF+BI+AS+EM+SS-MoA3 Love and Death, the Story of Most Proteins and Most Surfaces as Told by Spectroscopic Ellipsometry.** *T. Benavidez, K. Chumbuni-Torres, J.L. Felhofer, C.D. Garcia*, The University of Texas at San Antonio

INVITED

Biosensors are analytical platforms that integrate a biological recognition element with a signal transducer. Because they have the potential to provide rapid, real-time, and accurate results, biosensors have become powerful tools in clinical and biochemical settings. Our group is particularly interested in the development of electrochemical biosensors based on enzymes adsorbed to nanomaterials. When integrated to microfluidic devices, these sensors offer sensitivity, portability, low cost, and the possibility of analyzing turbid samples. Adsorption was selected to immobilize the biorecognition element because it is one of the simplest and most benign methods, avoiding cross-linking reactions or additional components (such as entrapping polymers). Most importantly, as adsorption is a required (and sometimes limiting) step for any immobilization mechanism, the identification of key variables influencing this process can be applied to a variety of strategies. Although several techniques have been used to study the adsorption of proteins to nanomaterials,¹ only a few of them provide information about the kinetics of the process in real time. This is a critical aspect, as most of the post-adsorption conformational changes occur within a few minutes after the interaction.² Among those, reflectometry was used by our group to perform the first kinetic study related to the interaction of proteins with carbon nanotubes.³ These kinetic studies have been recently extended to the interaction of enzymes (D-amino acid oxidase,⁴ catalase,⁵ and glucose oxidase⁶) by variable angle spectroscopic ellipsometry, which enabled a more thorough analysis of the interaction process with a much more versatile experimental design.^{7,8} The use of VASE demonstrated that a number of variables, (being the amount of enzyme only one of them) can influence the biological activity of proteins adsorbed to the substrate. Furthermore, our results indicate that the activity of enzymes adsorbed to nanomaterials can be directly related to the kinetics of the adsorption process (dG/dt).⁵

Please see supplemental document for figures and footnotes.

3:40pm **EL+TF+BI+AS+EM+SS-MoA6 Detailed Photoresist and Photoresist Processing Studies using Spectroscopic Ellipsometry.** *C. Henderson*, Georgia Institute of Technology

INVITED

Spectroscopic ellipsometry has become an invaluable tool for the study of a wide variety of thin film systems. In particular, it has become extremely valuable in the development and study of advanced photoresists and of lithographic processes used in the production of integrated circuits and other related semiconductor devices. In our work, we have used

spectroscopic ellipsometry to study a variety of problems related to photoresists including swelling phenomena, exposure induced refractive index changes, and ultra-fast dissolution phenomena. We have combined spectroscopic ellipsometry with quartz crystal microbalance techniques to simultaneously study thin film optical properties, thickness, film mass, and film modulus. Such techniques have been particularly useful in understanding the dissolution properties of polymeric photoresists developed for 193 nm lithography. This talk will review some of the applications for spectroscopic ellipsometry in this field and in particular will highlight some of the results of our work made possible using spectroscopic ellipsometry.

4:20pm **EL+TF+BI+AS+EM+SS-MoA8 Ellipsometric Characterization of a Thin Titaniumoxide Nanosheets Layer.** *H. Wormeester, G. Maidecchi, S. Kumar, A. Kumar, A. ten Elshof, H.J.W. Zandvliet*, MESA+ Institute for Nanotechnology, University of Twente, The Netherlands

The photochemical properties of titaniumoxide make this a widely studied material. Of special interest is a thin nanostructured layer of such a material. A variety of a nanostructured material is the single sheet titaniumoxide that can be obtained by delaminating a layered titanate, with stoichiometry $Ti_{1-x}O_{2-4x}$ ($x=0.0875$). The slight titanium deficiency leads to a negatively charged nanosheet that can be used as a building block in a layer by layer assembled composite film [1]. In this work we used Langmuir Blodgett to deposit successive thin layers of nanosheets. The electronic properties of these layers were investigated with ellipsometry and Scanning Tunneling Microscopy (STM). The optical spectra show the well known absorption peak at 4.6 eV for titaniumoxide nanosheets. The optical spectra can be well modeled with a Cody-Lorentz dielectric function profile providing a bandgap of ... eV, a value also found from STM IV spectroscopy. The Cody-Lorentz profile also indicates a slight below band gap light absorption by the nanosheet material.

[1] T. Sasaki, Y. Ebina, T. Tanaka, M. Harada, M. Watanabe and G. Decher, Chem. Mater. 2001, 13, 4661

4:40pm **EL+TF+BI+AS+EM+SS-MoA9 Preparation of Abrupt LaAlO₃ Surfaces Monitored by Spectroscopic Ellipsometry.** *C.M. Nelson, M. Spies, L.S. Abdallah, S. Zollner, Y. Xu, H. Luo*, New Mexico State University

LaAlO₃ is a polar perovskite oxide, used as a single-crystal substrate in oxide epitaxy. It has created much interest for novel electronic applications, because a two-dimensional electron gas is formed at LaAlO₃/SrTiO₃ heterostructures. The purpose of our work is twofold: First, we are interested in an accurate determination of the complex refractive index of LaAlO₃ at room temperature. Second, we studied the impact of various cleaning methods on the abruptness of the LaAlO₃ surface.

We obtained a commercial single-side polished LaAlO₃ substrate with 2-inch diameter and a (100) pseudo-cubic surface orientation. The surface was polished with an rms roughness below 0.8 nm. We determined the ellipsometric angles ψ and Δ for LaAlO₃ at 300 K from 0.7 to 6.5 eV. For a bulk insulator with a clean smooth surface, the phase change Δ should be zero or π below the band gap. In practice, this never happens, because surfaces are covered with overlayers (adsorbed organic or water vapors). Surface roughness has a similar effect on the ellipsometric spectra as a surface overlayer. Even for an abrupt bulk/air interface, there is a thin (~0.5nm) transition region where the electron wave functions leak from the crystal into the ambient. For the as-received sample, the data were described with a Tauc-Lorentz model for LaAlO₃, plus 2.1 nm of surface layer thickness (described as an effective medium with 50% density of the bulk). After ultrasonic cleaning in acetone, the overlayer thickness decreased to 1.8nm. Next, we mounted the wafer in a UHV cryostat, pumped down to below 10⁻⁸Torr, and acquired an ellipsometric spectrum at 70°. The surface layer thickness was reduced to 1.2 nm, presumably because a part of the adsorbed surface layer (especially water) desorbed under vacuum.

So far, everything worked as expected, but here it gets interesting: We heated the sample to 700 K for about an hour to desorb the remaining surface overlayer. After cooling down to 300 K, we measured the ellipsometric angles again at 70° angle of incidence from 0.7 to 6.5 eV. The ellipsometric angle Δ at 2 eV was reduced to below 0.2°, consistent with a surface layer thickness of less than 1 Å, much less than the surface roughness specified by the supplier (8 Å).

In conclusion, a macroscopically smooth and clean LaAlO₃ surface was prepared by ultrasonic cleaning of the wafer in acetone, followed by heating in UHV to 700 K. The resulting surface layer thickness was below 1 Å, as measured by spectroscopic ellipsometry. We will report Tauc Lorentz parameters. We will also describe the temperature dependence of the LaAlO₃ dielectric function from 77 to 700 K. This work was supported by NSF (DMR-11104934).

5:00pm **EL+TF+BI+AS+EM+SS-MoA10 Determination of the Refractive Index of a Gold-Oxide Thin Film Using X-Ray Photoelectron Spectroscopy and Spectroscopic Ellipsometry.** *K. Cook, G.S. Ferguson*, Lehigh University

A two-step procedure will be presented for measuring the complex refractive index of an electrochemically produced oxide film on a gold surface. In the first step, the composition and the thickness of the oxide film were determined using angle-resolved X-ray photoelectron spectroscopy. The experimental composition defined the system, thereby avoiding assumptions about the film stoichiometry that would otherwise be required. The value of thickness derived from these measurements was then used to calculate n and k from ellipsometric data collected across the visible spectrum (350 - 800 nm).

Electronic Materials and Processing

Room: 9 - Session EM+TF+OX+GR-MoA

High-k Dielectrics for MOSFETS II

Moderator: C.L. Hinkle, University of Texas at Dallas, H.J.

Kim, National Institute of Aerospace (NIA)

2:00pm **EM+TF+OX+GR-MoA1 "6.1" Family: The Next Generation of III-V Semiconductors for Advanced CMOS: Epitaxial Growth and Passivation Challenges.** *C. Merckling, A. Alian, A. Firrincelli, S. Jiang, M. Cantoro, J. Dekoster, M. Caymax, M. Heyns*, IMEC, Belgium **INVITED**

The integration of high carrier mobility materials into future CMOS generations is presently being studied in order to increase drive current capability and to decrease power consumption in future generation CMOS devices. If III-V materials are the candidates of choice for n-type channel devices, antimonide-based III-V semiconductors present the unique property of owning both high electrons (InSb) and holes (GaSb) mobilities, which triggered much of the interest in these III-Sb compounds for advanced CMOS. Moreover recent simulations have demonstrated that higher hole mobility could be found in strained III-antimonides compounds, suggesting the possibility of an all III-antimonide solution for full III-V based CMOS. In this work we studied the heteroepitaxy of 6.1 family semiconductors (GaSb, AlSb & InAs) on various III-V and Si substrates as well as the passivation of such semiconductors.

The relatively large lattice parameter of "6.1" semiconductors makes the growth and the integration on standard surfaces difficult. But is it possible to grow such semiconductors fully relaxed with low defect density due to the formation of a highly periodic array of 90° misfit dislocations at the III-Sb/substrate interface. In this contribution both MBE and MOVPE growth techniques have been studied in order to propose novel integration scheme on Si substrate.

In a second part, we will focus on the passivation of these III-V semiconductors. Because III-V surfaces are very sensitive to oxygen compounds, this will generate the formation of native oxide. This undesirable interlayer will contribute aggressively to the high density of surface states within the energy band gap, resulting in Fermi level pinning which disturbs the basic III-V MOSFET-operation. In this context both ex-situ and in-situ Al₂O₃ high-k gate dielectric deposition by standard ALD or MBD processes is reported. The interface is abrupt without any substantial interfacial layer, and is characterized by high conduction and valence band offsets. Finally, MOS capacitors showed well-behaved C-V with relatively low D_{it} along the band gap. Such a D_{it} profile is promising for the future devices and suggests possibility to attain a low subthreshold swing.

2:40pm **EM+TF+OX+GR-MoA3 Improving Nucleation and Passivation of Ge(100) via H₂O and H₂O₂ Dosing.** *T. Kaufman-Osborn, K. Kiantaj, J.S. Lee, A.C. Kummel*, University of California San Diego

Germanium is a promising candidate for potential channel materials due to its higher hole and electron mobility. To minimize the oxide-semiconductor interfacial defect density, a proper passivation layer must be used before the oxide layer is deposited. In this study, a monolayer of H₂O chemisorbrates is shown to activate TMA chemisorption due to the Ge-OH bonds catalyzing the formation of an ultrathin passivation layer which can serve as an ideal ALD nucleation template on a Ge surface. However, since H₂O chemisorption results in equal density of Ge-H and Ge-OH sites on the Ge(100), H₂O can only provide a maximum of 0.5 monolayer of Ge-OH sites, limiting the TMA nucleation density. By using H₂O₂ dosing, the density of Ge-OH sites can be doubled thereby increasing the potential TMA nucleation density. This study compares the passivation of the Ge(100) surface via H₂O and H₂O₂, for the application of nucleating ALD growth on the surface, using scanning tunneling microscopy (STM) and scanning tunneling spectroscopy (STS).

A saturation H₂O dose onto Ge(100) resulted in 0.85 ML coverage of –OH and –H species chemisorbed on the surface. The remaining unreacted atoms on the surface have half filled dangling bond states causing a large local amount of conduction band edge states in the bandgap. The Ge–OH and Ge–H sites on the surface have limited thermal stability. Annealing the H₂O/Ge(100) sample to 100°C significantly reduces the H₂O coverage due to the recombinative desorption of H₂ or H₂O.

A saturation dose of H₂O₂ on Ge(100) at 250°C results in a coverage of 0.95 ML of Ge–OH species chemisorbed on the surface with very few unreacted sites. Compared to a H₂O dose, H₂O₂ provides more than double the number of reactive Ge–OH sites thereby increasing the number of potential ALD nucleation sites. In contrast to the H₂O passivated surface, annealing the H₂O₂/Ge surface to 100°C generates no additional dangling bond sites and even eliminates the dangling bonds present from the 250°C dose and forms a highly ordered surface of Ge–OH bonds. The improved coverage of Ge–OH sites allows for increased nucleation density of O–Al bonds and also minimizes the dangling bonds which are considered as the major source of interfacial trap states (Dit). The improved thermal stability allows for an increased thermal budget during ALD cycles. STS measurements show that TMA nucleation on the H₂O₂ functionalized Ge(100) surface unpins the Fermi level and has a wide bandgap with no band edge states demonstrating very good interface quality.

3:00pm **EM+TF+OX+GR-MoA4 Electrical and Physical Characteristics of High-k/Metal Gate MOS Devices on MBE-Grown Germanium on Silicon Using Aspect Ratio Trapping.** S.R.M. Anwar, C. Buie, N. Lu, M.J. Kim, C.L. Hinkle, University of Texas at Dallas

Due to its high hole mobility and relative compatibility with Si CMOS processing, Ge has long been considered as a replacement channel material for PMOS devices. Selective area growth of Ge channels on bulk Si substrates would be ideal for minimizing fabrication costs and allowing the co-implementation of other materials (III-Vs for NMOS). However, due to the 4.2% lattice mismatch between Ge and Si, unacceptably high dislocation densities (~10⁹ cm⁻²) are created during this heteroepitaxy.

In this work, we investigate the fabrication of MOS gate stacks on MBE-grown Ge on Si using Aspect Ratio Trapping (ART)^{1,2} to reduce Ge defect density. ART is a growth technique that allows for the reduction of defects for lattice mismatched materials by trapping the threading dislocations into the sidewalls of patterned nanoscale trenches in which the epitaxial growth takes place. This technique has the added benefit of producing the necessary geometric structure required for highly scaled tri-gate devices while reducing defect density simultaneously. Surface roughness and defect density dependence on growth temperature and growth rate will be discussed as will be the effect of varying the trench geometry. RHEED, XRD, XPS, TEM, EPD, AFM, SEM, and IPE data are correlated with growth conditions to produce high quality heteroepitaxial growth. Data will be presented demonstrating the use of low-temperature buffer layers in conjunction with low-growth rate bulk Ge results in a reduction in threading dislocations of 2-3 orders of magnitude.

MOS devices were fabricated on the MBE-grown Ge on Si samples. A high-quality interface was obtained using a DI-H₂O surface functionalization by pre-pulsing the H₂O 50 times in the atomic layer deposition (ALD) chamber at 250 °C.³ A thin interfacial Al₂O₃ film was deposited by ALD at 250 °C followed by forming gas anneal (FGA) performed for 30 minutes at 350 °C. This FGA step converts the surface functionalized oxide to a thin layer of GeO₂ resulting in improved electrical performance. 2.5 nm of HfO₂ was then deposited by ALD. 10 nm of RF sputtered TiN was deposited as the gate metal followed by low-temperature anneals in various ambients to tune the effective work function of the HfO₂/TiN gate stack.⁴ A final FGA for 30 minutes at 350 °C completed device processing. These devices show excellent PMOS characteristics and will be discussed.

This work is supported by the SRC Global Research Corporation.

1 J.-S. Park, *et al.*, *Appl. Phys. Lett.* **90**, 052113 (2007).

2 J. Bai, *et al.*, *Appl. Phys. Lett.* **90**, 101902 (2007).

3 S. Swaminathan, *et al.*, *J. Appl. Phys.* **110**, 094105 (2011).

4 C. L. Hinkle, *et al.*, *Appl. Phys. Lett.* **100**, 153501, (2012).

3:40pm **EM+TF+OX+GR-MoA6 In Situ Infrared Spectroscopy Study on the Temperature Dependence on the Growth Mechanism of Atomic Layer Deposition of Al₂O₃ on InP(100).** W. Cabrera, The University of Texas at Dallas, I.M. Povey, Tyndall National Institute, Y.J. Chabal, The University of Texas at Dallas

One of the current challenges in fabricating III-V-based electronics is the growth of an interfacial layer during the atomic layer deposition (ALD) of high-k dielectrics on III-V substrates, which has led to poor quality electrical properties. A process that can mitigate this problem is the “clean-up” effect that occurs when trimethylaluminum (TMA) is deposited by

atomic layer deposition during the formation of Al₂O₃. A recent theoretical study suggests that the principal pathway in the “clean-up” effect of TMA on the native oxides of GaAs and InGaAs involves oxygen getting¹. In this work, *in-situ* infrared absorption spectroscopy has been used to investigate the temperature dependence of the native oxide and the interface formation during Al₂O₃ deposition using TMA and deuterium oxide (D₂O) on chemically-treated InP(100) surfaces. Upon annealing a degreased sample to 300°C, compositional changes are observed, as evidenced by new absorption features in the region of 900-1250 cm⁻¹ of the infrared spectrum prior to TMA exposure. The initial native oxide, comprised in part of In(PO₃)₃ is transformed into an InPO₄-rich surface. Upon TMA exposure at 300°C, there is a clear loss of In(PO₃)₃ and gain of InPO₄ (at 1007 and 1145 cm⁻¹, respectively) along with the formation of Al-O bonds (absorption band at 800 cm⁻¹)². These observations are consistent with the “clean up” effect observed on GaAs₃ and InGaAs₄, and on InP(100)₅ where TMA preferentially withdraws oxygen from the native oxide forming Al-O bonds. However, the TMA reduces In(PO₃)₃ and fosters the formation of InPO₄. Furthermore, TMA exposure of the native oxide at lower deposition temperatures (150°C) gives rise to methoxy (CH₃) formation as evidenced by the appearance of a band centered at 1475 cm⁻¹. This indicates that TMA not only withdraws oxygen from the native oxide but also transfers a methyl group to the surface oxygen, which may lead to carbon contamination at the interface. Al₂O₃ oxide films are formed after 10 TMA and D₂O cycles on both degreased native oxide and chemically treated (HF and (NH₄)₂S) InP(100) substrates, although the quality is higher on the (HF and (NH₄)₂S)-treated surface. A more clearly defined LO phonon mode is detected for that surface, suggesting that a denser oxide is formed.

1 S. Klejna et al, *J. Phys. Chem. C*, **116**, (2012) 643-654

2 M. M. Frank et al, *Appl. Phys. Lett.* **82** (2003) 4758

3 C. L. Hinkle et al, *Appl. Phys. Lett.*, **92** (2008) 071901

4 M. Milojevic, et al *Appl. Phys. Lett.*, **93**, (2008) 202902

5 B. Brennan et al, *Appl. Phys. Exp.*, **4** (2011) 125701

4:00pm **EM+TF+OX+GR-MoA7 Ultimate Scaling of High-k Gate Dielectrics: Current Status and Challenges.** T. Ando, M.M. Frank, E.A. Cartier, B.P. Linder, J. Rozen, IBM T.J. Watson Research Center, K. Choi, GLOBALFOUNDRIES, V. Narayanan, IBM T.J. Watson Research Center

INVITED

Current status and challenges of aggressive equivalent-oxide-thickness (EOT) scaling of high-k gate dielectrics via higher-k (>20) materials and interfacial layer (IL) scavenging techniques are reviewed [1]. La-based higher-k materials [2, 3] and La-silicate IL with HfO₂ [4] showed aggressive EOT values (0.5–0.8 nm), but with large effective workfunction (EWF) shifts toward the Si conduction band edge, limiting their application to nFET. Further exploration for pFET-compatible higher-k materials is needed. Meanwhile, IL scavenging is a promising approach to extend Hf-based high-k dielectrics to future nodes [4, 5]. Remote-scavenging techniques enable EOT scaling below 0.5 nm. We will review IL scavenging techniques from the viewpoints of (1) IL growth condition; (2) Choice of scavenging element; (3) Location of scavenging element; (4) Choice of high-k material and (5) Maximum process temperature. Careful choice of materials and processes based on these considerations is indispensable. Mobility-EOT trends in the literature suggest that short-channel performance improvement is attainable with aggressive EOT scaling via IL scavenging or La-silicate formation. However, extreme IL scaling is accompanied with loss of EWF control [6] and with severe penalty in reliability [7]. Therefore, highly precise IL thickness control in an ultra-thin IL regime (<0.5 nm) will be the key technology to satisfy both performance and reliability requirements for future CMOS devices.

This work was performed by the Research alliance Teams at various IBM Research and Development Facilities.

[1] T. Ando, *Materials* **2012**, *5*, 478-500 [2] H. Arimura et al., *Electron Device Lett.* **2011**, *32*, 288–290 [3] L. F. Edge et al., *Appl. Phys. Lett.* **2011**, *98*, 122905 [4] T. Ando et al., *IEDM* 2009, 423-426 [5] L. Å. Ragnarsson et al., *IEDM* 2009, 663-666 [6] T. Ando et al., as discussed at *SISC* 2011 [7] E. A. Cartier et al., *IEDM* 2011, 18.4.1-18.4.4

4:40pm **EM+TF+OX+GR-MoA9 AR-XPS Study of Al₂O₃/In-based III-V Interfaces after Annealing under Vacuum at Low Temperature.** E. Martinez, H. Grampeix, O. Desplats, CEA, LETI, MINATEC Campus, France, A. Herrera-Gomez, O. Ceballos-Sanchez, CINVESTAV-Unidad Queretaro, Mexico, J. Guerrero, K. Yekache, F. Martin, CEA, LETI, MINATEC Campus, France

III-V semiconductor substrates are a potential solution for MOSTETs down scaling below the 16 nm technological node. Indium based semiconductors, such as InGaAs, InAs and InP are promising compounds to improve the speed of operation. The quality of the interface between these high mobility

substrates and the gate oxide is of crucial importance to preserve the devices electrical properties. Aluminium oxide is used to remove the As oxide ("self-cleaning" effect). The gate-last scheme is preferred to control of the high- k /III-V since it involves low temperature post deposition annealing [1]. State-of-the-art control of this interface has been obtained with annealing at 400°C under vacuum [2]. In this work we focus on the impact of low temperature annealing under vacuum on the quality of the Al₂O₃/In-based III-V interfaces. We have studied the interfacial oxides formed between alumina and III-V substrates such as InGaAs, InAs and InP. Annealing at 600°C under ultra high vacuum (UHV) is first performed and compared to thermal treatments at 600°C and 400°C at 3 × 10⁻⁴ mbar. Substrate passivation is done with NH₄OH (4 %). The 3-nm thick alumina is deposited by Atomic Layer Deposition (ALD) using TMA and H₂O as precursor and oxidant. Angle-resolved photoelectron spectroscopy (AR-XPS) has been carried out to investigate the interfacial chemical bonding states. Consistent and robust analysis of the As 3d, P 2p, Ga 3d and In 3d core levels was carried out through the simultaneous fitting method [3]. At 600°C, we show that, on InGaAs, no interfacial oxides are created after annealing under UHV, whereas a thin interfacial InGaO_x is observed under secondary vacuum. A clear difference between the three substrates is observed after annealing at 400°C under 3 × 10⁻⁴ mbar. In particular, the indium oxidation and the relative stability of interfacial oxides are substrate dependant. On InAs, indium hydroxide is formed after annealing, by OH release from TMA/H₂O deposited alumina. This is not the case with additional elements such as Ga and P, which react with residual species to create their respective oxides. On InGaAs, a regrowth of InGaO_x is observed after anneal, as a result of preferential oxidation of Ga. On InP, the InPO_x interfacial oxide seems to decrease after anneal. **Acknowledgements** This work was performed with financial support from the MOS35 project funded by the French National Research Agency. Measurements were carried out at the NanoCharacterization Centre (NCC) of MINATEC. [1] H. Zhao et al., Appl. Phys. Let. 95, 253501 (2009)[2] Y. Urabe et al., Appl. Phys. Let. 97, 253502 (2010)[3] J. Muñoz-Flores et al., J. Electron. Spec. Rel. Phen. 182, 81 (2011)

5:00pm **EM+TF+OX+GR-MoA10 Effect of a H₂ Plasma Pre-treatment on the Reduction of Native Oxides at the PEALD Al₂O₃/InAs Interface.** *E. Cleveland, L. Ruppalt, J.B. Boos, B. Bennett, J. Champlain, S.M. Prokes, Naval Research Laboratory*

The integration of high- k dielectrics with high mobility III-V semiconductor materials has attracted extensive interest recently as an alternative to Si-based complementary metal-oxide semiconductor (CMOS) applications at the 16 nm node and beyond. Among the III-V semiconductors, InAs is a promising material as the channel material in metal-oxide-semiconductor field-effect transistors (MOSFETs) due to its extremely high electron mobility and high saturation velocity. However, problems arise in the fabrication of high performance channel MOSFETs due to the poor quality of the gate oxide/InAs interface. InAs has a highly reactive surface and on exposure to air will form a native oxide layer composed of In₂O₃ and As₂O₃. The complexity of these native oxides leads to the formation of a relatively high density of interface states which in turn act as charge traps thus pinning the Fermi level and degrading device performance. Wet-chemical treatments based on HCl and (NH₄)₂S have been found to be an effective means of removing these oxides, however, due to the rapid re-oxidation and lack of reproducibility a better means of interface cleaning is needed. Recently, there has been much interest in the field of surface cleaning combined with atomic layer deposition (ALD) in order to deposit high quality dielectrics on III-V semiconductor materials, such as InAs and GaSb. Therefore, we examined the use of a H₂ plasma as a means to obtain an oxide-free InAs interface prior to the deposition of high- k Al₂O₃ via plasma enhanced atomic layer deposition (PEALD). Ex-situ XPS, AFM, and C-V measurements were performed to establish the effect of the plasma exposure time, temperature and rf power on the removal of the native oxide. It will be demonstrated that by removing or reducing the native oxides on the InAs surface that the density of interface defects at the Al₂O₃/InAs interface can be reduced and enhance the electrical performance. Similar work done on GaSb will be discussed, where XPS spectra revealed a significant reduction in Sb-O features for longer H₂ plasma exposures as the peaks associated with Ga-O increased. C-V measurements of fabricated MOSCAPS also found that samples treated with longer H₂ plasma exposures exhibited better C-V characteristics.

Energy Frontiers Focus Topic
Room: 15 - Session EN+TF-MoA

Chalcogenide Solar Cells I
Moderator: J. Luther, NREL

2:00pm **EN+TF-MoA1 Research Strategies and Results Toward Improving Thin Film CdTe Photovoltaic Devices Beyond 20% Conversion Efficiency.** *T.A. Gessert, National Renewable Energy Laboratory* **INVITED**

Recent studies of thin-film CdS/CdTe photovoltaic (PV) devices have suggested that significantly higher device performance will not be achieved unless recombination in the CdTe is reduced. Specifically, unless high recombination in the CdTe quasi-neutral region is reduced, benefits of increasing CdTe net-acceptor doping cannot be realized—because resulting higher open-circuit voltage will be accompanied by lower fill factor. Although some control of CdTe recombination has been achieved historically through the careful incorporation of oxygen, chlorine, and copper, many technologists believe a more promising avenue to higher device performance is by understanding and controlling the defects in the as-deposited CdTe. This is supported by theoretical studies that suggest much of the improvement associated with oxygen, chlorine, and copper is due to the interaction of these species with intrinsic defects related cadmium and tellurium (i.e., vacancies, interstitial, and anti-site defects). Although CdTe is a relatively simple semiconducting material that exists only near its 50%/50% composition, even at thermodynamic equilibrium, the material can sustain a small stoichiometric deficiency (~0.01%). Even this small extent of stoichiometry variation can produce intrinsic defects at a sufficient concentration to significantly alter device performance. Further, the typical techniques used in PV film deposition are not equilibrium processes, and so the extent of non-stoichiometry could be greater. Several research projects at NREL are currently focused on altering CdTe deposition and post-deposition processes to allow for an enhanced control of the as-deposited intrinsic defects. Related defect changes are being assessed using a combination of device analysis, time-resolved photoluminescence, low-temperature photoluminescence, and microscopic techniques. The presentation will discuss initial results where process changes expected to alter the as-deposited defects also affect junction evolution and device functionality. *This abstract is subject to government rights.*

2:40pm **EN+TF-MoA3 Nanocrystal-Ink and Soluble-Precursor Routes to Earth Abundant Element Kesterite Solar Cells.** *H.W. Hillhouse, University of Washington* **INVITED**

Given the terawatt scale of future energy needs, the most promising future photovoltaic materials should be Earth abundant with their primary mineral resources distributed across several geographic regions and their supply chains robust to reduce concerns of price volatility. In addition, the process of forming the solar cell should be scalable, low-cost, and not utilize dangerous or toxic materials. The strongest initial candidate appears to be kesterite structures of Cu₂ZnSnS₄ (CZTS) and similar materials. The presentation will review the progress in developing photovoltaics devices based on these materials and our group's recent experimental and modeling results.

CZTS thin film solar cells have historically been synthesized by evaporating or sputtering metals (Cu, Zn, & Sn) followed by sulfurization or selenization. More recently, two potentially low-cost high-throughput approaches have been demonstrated that form the quaternary or pentenary chalcogenide directly from solution-phase processes. One is based on first synthesizing multinary sulfide nanocrystals and then sintering them to form a dense layer. The other approach utilizes molecular precursors dissolved in hydrazine. Both new approaches reach their highest device efficiencies by incorporating Se to form Cu₂ZnSn(S_xSe_{1-x})₄ devices, and each has yielded substantially higher efficiency devices than the best vacuum deposited absorbers. The hydrazine route has yielded the most efficient CZTS-based devices thus far. The presentation will highlight our recent progress in CZTS-based nanocrystal-ink devices. In particular, we have shown that germanium may be alloyed with CTZS (at least up to Ge/(Sn+Ge) ratios of 0.7) to form Cu₂Zn(Sn,Ge)S₄ nanocrystals that have an increased bandgap. The defect chemistry is serendipitous, and yields devices at with greater than 8% power conversion efficiency. This exciting prospect may be used to create a back surface field and direct carriers in a similar manner to how gallium is used in high efficiency CIGS devices. In addition, we will report recent results from high throughput experiments focused on identifying doping and passivation agents.

3:40pm **EN+TF-MoA6 Developing Earth Abundant and Quantum Dot Materials for Thin-Film Photovoltaics**, *M. Law*, University of California Irvine **INVITED**

This talk describes projects in our group to develop thin-film photovoltaics based on earth-abundant iron pyrite (FeS_2) active layers and PbSe quantum dot (QD) solids. I will first introduce the promise and challenge of pyrite, describe solution- and gas-phase syntheses of pyrite films, and present preliminary electrical characterization of pyrite layers and device stacks. Then I will switch gears to highlight several projects focused on the chemistry/physics of QD solids, including our use of atomic layer deposition to produce environmentally-robust PbSe QD films with long carrier diffusion lengths for next-generation solar cells.

4:20pm **EN+TF-MoA8 Synthesis of Photovoltaic $\text{Cu}_2\text{ZnSnS}_4$ via Ex Situ Sulfidation of Co-Sputtered Cu-Zn-Sn Thin Films**, *M. Johnson, M. Manno, X. Zhang, C. Leighton, E.S. Aydil*, University of Minnesota

$\text{Cu}_2\text{ZnSnS}_4$ (CZTS) is an emerging low-cost solar absorber for thin film photovoltaics based on non-toxic, high earth-abundance elements. While *ex situ* sulfidation of Cu-Zn-Sn precursor films in S vapor is a popular synthesis route for CZTS, much remains to be understood with regard to the sulfidation mechanisms, microstructural control, and structure-property relationships. In this work, DC magnetron co-sputtered Cu-Zn-Sn films, of varying composition, were sealed with 1.0 mg of S in evacuated (10^{-6} Torr) quartz ampoules, and then isothermally heat treated at sulfidation temperatures in the range $100^\circ\text{C} \leq T_S \leq 700^\circ\text{C}$. The films were then characterized structurally by scanning electron microscopy, Raman spectroscopy, and X-ray diffraction, and electrically via resistivity measurements between 4.2 K and 300 K. We find that the phase purity of the resultant films depends strongly on T_S , with complete conversion of the precursor film to CZTS occurring only at $T_S \geq 550^\circ\text{C}$. The final phase purity of *ex situ* sulfidized CZTS films is however remarkably insensitive to modest amounts of excess Zn and Sn in the Cu-Zn-Sn precursor film. Excess Zn or Sn in the precursor is readily ejected during sulfidation, via elemental or binary sulfide evaporation, respectively, while Sn-deficiency can also be corrected by introducing elemental Sn to the sealed quartz ampoule. However, due to the low melting point of Sn, and the absence of appropriate Sn-Zn alloys, the precursor composition *does* play a significant role in defining the final CZTS film microstructure, and the lateral homogeneity. In addition to detailed discussion of the physics and chemistry underlying the above observations we will also provide data on the transport properties of such films, including observations of hopping conduction.

Work supported by NSF (CBET-0931145) and IREE (RL-0004-11)

4:40pm **EN+TF-MoA9 Crossover from Intergranular Hopping to Conventional Charge Transport in Pyrite FeS_2 Thin Films**, *X. Zhang, M. Manno, A. Baruth, M. Johnson, E.S. Aydil, C. Leighton*, University of Minnesota

Pyrite FeS_2 is undergoing a tremendous resurgence of interest as a candidate thin-film solar absorber based on abundant, low-cost, non-toxic elements. Historically, FeS_2 -based Schottky solar cells have suffered from low open circuit voltages (~ 100 mV), and thus low efficiency, although the origins of this behavior are not entirely clear. In fact, even the electronic properties of FeS_2 are not well understood, including the conduction mechanisms and doping behavior. Understanding these issues could contribute significantly to improvements in FeS_2 -based solar cells, particularly if doping can be understood and controlled. In this work, we present a comprehensive study of the conduction mechanism in FeS_2 thin films synthesized via the *ex situ* sulfidation of Fe films in a S vapor at sulfidation temperatures in the range $100^\circ\text{C} \leq T_S \leq 700^\circ\text{C}$. The resultant films were characterized structurally, using X-ray diffraction, scanning electron microscopy, energy dispersive spectroscopy, and confocal Raman microscopy; electrically, via transport and magnetoresistance measurements between 4.5 and 300 K; and magnetically with high-sensitivity dc magnetometry. At T_S around 500°C we observe a crossover in the conduction mechanism from some form of hopping conduction to a more conventional band transport-type mechanism. Through detailed analysis of the hopping parameters, measurement of the Fe spin-state, and simple calculations based on S diffusion in Fe, we demonstrate that intergranular hopping occurs via highly conductive, S-deficient, nanoscopic grain cores separated by nominally stoichiometric FeS_2 shells. We find that the approach towards more conventional band transport as T_S is increased above 500°C is due to an increase of S diffusion into the FeS_2 grains. Moreover, this conduction mechanism crossover is found to be accompanied by a sign reversal of the Hall coefficient, from hole-like (in the hopping regime) to electron-like. In addition to placing hard constraints on the conditions under which useful properties can be obtained from FeS_2 synthesized under diffusion-limited conditions, these results also highlight potential problems with prior conclusions on the dominance of *p*-type behavior.

The work was supported by the Initiative for Renewable Energy & the Environment, IREE (RL-0004-11). Part of this work was carried out in the University of Minnesota Characterization Facility, a member of the NSF-supported Material Research Facilities Network.

5:00pm **EN+TF-MoA10 Plasma Assisted Synthesis of Pyrite Absorbers**, *R. Morrish, R. Silverstein, C.A. Wolden*, Colorado School of Mines

Pyrite (FeS_2) is a non-toxic, earth abundant chalcogenide with desirable characteristics for application as a photovoltaic absorber including a modest band gap of 0.95 eV and a large optical absorption coefficient ($>10^5 \text{ cm}^{-1}$). Although theoretically capable of $>20\%$ efficiency, to date pyrite devices have displayed poor performance. One key challenge has been the production of stoichiometric material that is free of impurity phases. Conventional approaches employ thermal sulfurization of iron-based films or precursors. These routes inherently produce contaminate phases (troilite, pyrrhotite, marcasite), that once formed, are difficult to completely remove. Thermodynamics suggests that hematite ($\alpha\text{-Fe}_2\text{O}_3$) may be directly converted to pyrite in the presence of sufficiently high sulfur activity. In this work, we demonstrate pyrite synthesis using a H_2S plasma to sulfurize hematite nanorods produced using chemical bath deposition. Conversion to pyrite was achieved by exposure to a 90% Ar-10% H_2S plasma at moderate temperature ($350 - 450^\circ\text{C}$). The application of plasma dramatically enhances both the rate of conversion and the quality of the resulting material. Composition analysis using both Raman and X-ray photoelectron spectroscopy confirm that the resulting pyrite is free of common impurity phases. The degrees of sulfur incorporation could be precisely controlled by plasma exposure, and the apparent optical band gap could be systematically reduced from 2.2 to 1.0 eV. Electron microscopy images showed the surface maintained a nanostructured architecture following sulfurization, and a 150 nm thick film was sufficient to absorb 99% of incident visible light. In this presentation we discuss the kinetics of this solid state transformation, as well as report on the optoelectronic properties of these materials.

Graphene and Related Materials Focus Topic

Room: 13 - Session GR+EM+ET+NS+TF-MoA

Electronic Properties and Charge Transport

Moderator: T.W. Michely, Universität zu Köln, Germany

2:00pm **GR+EM+ET+NS+TF-MoA1 Influence of Substrate Offcut on Electrical and Morphological Properties of Epitaxial Graphene**, *R.L. Myers-Ward, V.D. Wheeler, L.O. Nyakiti, T.J. Anderson, F.J. Bezares, J.D. Caldwell, A. Nath, N. Nepal, C.R. Eddy, Jr., D.K. Gaskill*, U.S. Naval Research Laboratory

The promise of graphene-based device technologies is critically dependent on uniform wafer-scale graphene films and is most directly met through epitaxial graphene (EG) growth on silicon carbide (SiC) substrates. An essential parameter which influences this uniformity is the substrate offcut, as any deviation will result in a local change in the terrace width, impacting the growth rate and step-bunched heights observed after EG formation. For nominally on-axis SiC substrates, typical offcuts can range from $\sim 0^\circ$ to $\sim 1^\circ$ off-axis toward the [11-20] direction. Offcuts approaching 0° produce wide terraces with short step-bunched heights which offers the possibility of reduced anisotropy of transport properties [M. Yakes, *et al.*, Nano Lett. **10**(5), 1559 (2010)] and improved EG layer uniformity. Thus, it is of interest to understand the influence of substrate offcut on carrier mobility, surface morphology, step heights, and graphene growth rate. This study investigates EG grown on a unique single 3-inch substrate possessing a large variation in offcut, from $+0.1$ to -1° toward the [11-20] direction, enhancing the information obtained on offcut influence while eliminating other substrate influences. X-ray diffraction rocking curve and peak position maps of the (0012) reflection were performed prior to growth to evaluate the crystalline quality and local offcut, respectively. Electron mobilities of EG films were determined by van der Pauw Hall measurements. Surface morphology of the EG was investigated with scanning electron microscopy, while the step heights and terrace widths were measured using atomic force microscopy.

For a given set of conditions (1620°C for 30 min in 10 slm Ar), the EG morphology is dominated by straight steps that become wavy in character as the offcut decreases to zero degrees. Close to zero degrees, the step direction rotates from [11-20] to the [1-100] direction and the steps become further distorted. The step bunch heights generally decreased (from 8 to 3 nm) as the offcut decreased and the terrace widths increased (from 0.3 to ~ 3 μm); however, for the latter, the trend is interrupted near zero degrees offcut. In addition to such morphological assessments, the impact of growth

parameters, where the growth temperatures investigated were 1540, 1580 and 1620 °C and growth times were 15, 30 and 45 min, on the electrical and structural properties of EG grown on this unique substrate will be reported. For example, samples grown at 1540 °C for 30 min on witness substrates with offcuts ranging from ~ 0.4 to 0.9° had large area mobilities ranging from 780 to 1100 cm²/Vs, where larger offcuts led to lower mobilities.

2:20pm **GR+EM+ET+NS+TF-MoA2 Direct Determination of Dominant Scatterer in Graphene on SiO₂**, *J. Katoch, D. Le, T.S. Rahman, M. Ishigami*, University of Central Florida

Freely suspended graphene sheets display high-field effect mobility, reaching 2'105 cm²/V s. Yet, suspended graphene sheets are fragile and impractical for most experiments and applications. Graphene sheets on SiO₂ are easier to handle but possess low-carrier mobilities, which can vary by an order of magnitude from sample to sample. Poor and unpredictable transport properties reduce the utility of SiO₂-bound graphene sheets for both fundamental and applied sciences. Therefore, understanding the impact of substrates is crucial for graphene science and technology.

We have measured the impact of atomic hydrogen with kinetic energy less than 250 meV on the transport property of graphene sheets as a function of hydrogen coverage and initial, pre-hydrogenation field-effect mobility. The saturation coverages for different devices are found to be proportional to their initial mobility, indicating that the number of native scatterers is proportional to the saturation coverage of hydrogen. In order to understand this correlation between the field effect mobility and the apparent affinity of atomic hydrogen to graphene, we have performed a detailed temperature programmed desorption study on hydrogen-dosed graphene sheets. Atomic hydrogen is found to physisorb on graphene with activation energy for desorption of 60 ± 10 meV, consistent with our theoretical calculations. The associated charge transfer expected for such small desorption energy indicates that atomic-scale defects and ripples are not responsible for determining the mobility of graphene on SiO₂ and that charged impurities in substrates define the transport property of graphene on SiO₂.

1. J. Katoch, J.H. Chen, R. Tsuchikawa, C. W. Smith, E. R. Mucciolo, and M. Ishigami, *Physical Review B Rapid Communications*, 82, 081417 (2010).

2:40pm **GR+EM+ET+NS+TF-MoA3 Tuning Electronic Properties of Graphene by Controlling its Environment**, *K.I. Bolotin*, Vanderbilt University **INVITED**

Every atom of graphene, a monolayer of graphite, belongs to the surface. Therefore, the environment of graphene -- the substrate onto which graphene is deposited and any coating on top of graphene -- intimately affects the properties of graphene. In this talk, we demonstrate that both the mechanical and electrical properties of graphene can be tuned by varying its environment.

First, we discuss the dependence of electrical transport in graphene on the dielectric constant (*k*) of graphene's environment. For graphene in vacuum (*k*=1) we observe very strong electron-electron interactions leading to robust fractional quantum Hall effect at temperatures up to 15K. By suspending graphene in liquids, we explore the regime of dielectric constants between ~1.5 and ~30. We observe the dependence of carrier scattering in graphene on *k* and demonstrate large values for room temperature mobility (>60,000 cm²/Vs) in ion-free liquids with high *k*. We also explore the rich interplay between the motion of ions inside liquids and transport of electrons in graphene. We observe signatures due to streaming potentials and Coulomb drag between ions in the liquid and electrons in graphene.

We also briefly address the mechanical properties of graphene and their dependence on graphene's environment. We demonstrate that the built-in strain, the substrate adhesion force and even the thermal expansion coefficient of graphene depend on the substrate supporting graphene.

3:40pm **GR+EM+ET+NS+TF-MoA6 Study of Impurity-Induced Inelastic Scattering on Suspended Graphene by Scanning Confocal Micro-Raman Spectroscopy**, *L.W. Huang, C.S. Chang*, Academia Sinica, Taiwan, Republic of China

We utilized a polymer-based procedure to transfer the CVD-grown graphene onto a TEM copper grid. The heat treatment was performed on the graphene membrane in an argon/ hydrogen (Ar/H₂) atmosphere at 400 °C. After the transfer and heat treatment, TEM images, acquired by an ultra-high-vacuum transmission electron microscopy (UHV-TEM), demonstrated

areas with distinguishable impurity distribution on the suspended graphene membrane. These areal impurity distributions can also be mapped by the scanning Raman spectroscopy correspondingly, indicating the influence of impurity-induced inelastic scattering. The results of this experiment show that the intensity ratio of Raman spectra 2D band over G band (*I*_{2D}/*I*_G) is proportional to minus fourth power of the inelastic scattering rate.

4:00pm **GR+EM+ET+NS+TF-MoA7 The Adsorption of Molecules with Large Intrinsic Electrostatic Dipoles on Graphene**, *L. Kong*, Univ. of Nebraska-Lincoln, *G.J. Perez Medina*, Univ. of Nebraska-Lincoln, Univ. of Puerto Rico, *J. Colón Santana*, Univ. of Nebraska-Lincoln, *L. Rosa*, Univ. of Nebraska-Lincoln, Univ. of Puerto Rico, *L. Routaboul*, *P. Braunstein*, Maître de conférences de l'Université de Strasbourg, France, *B. Doudin*, Institut de Physique et Chimie des Matériaux de Strasbourg, France, *C.-M. Lee*, *J. Choi*, Kyung Hee Univ., Korea, *P.A. Dowben*, Univ. of Nebraska-Lincoln

Both gold and graphene are excellent conductors, and one might expect that both conductors would fully screen the photoemission and inverse photoemission final states of a molecular adsorbate, but in fact this is not the case. The comparison of the electronic structure of p-quinonoid zwitterionic type molecules with a large intrinsic dipole of 10 Debyes adsorbed on both gold and graphene on copper substrates, shows that the interaction between the adsorbate molecules and graphene is very weak, confirming that graphene is chemically inert. We find that the photoemission and inverse photoemission final states are well screened for p-quinonoid zwitterionic dipolar molecules on gold. This is not observed in the case of this quinonoid zwitterion adsorbed on graphene on copper. This weaker screening is evident in a larger highest occupied molecular orbital to lowest unoccupied molecular orbital gap for the molecules on graphene. The larger highest occupied molecular orbital to lowest unoccupied molecular orbital gap for the molecules on graphene indicates that a much weaker screening on the photoemission and inverse photoemission final states for these dipolar molecules on graphene than that on gold. This work is reviewed in the context of other studies of molecular adsorption on graphene.

4:20pm **GR+EM+ET+NS+TF-MoA8 Growth of and Interactions in Epitaxial Graphene Layers**, *A. Bostwick*, Lawrence Berkeley National Laboratory, *A. Walter*, *Th. Seyller*, Lawrence Livermore National Laboratory, *K. Horn*, *E. Rotenberg*, Lawrence Berkeley National Laboratory **INVITED**

The electronic properties of graphene has been investigated using angle-resolved photoemission spectroscopy at the MAESTRO* facility of the ALS** synchrotron in Berkeley, California. This laboratory is unique in its ability to grow sophisticated samples for *in situ* study using angle-resolved photoemission spectroscopy, and to subtly alter their properties by engineering their surfaces by chemical doping or thickness control. In this talk I will discuss the electronic properties of graphene, focusing on the role of dopants to control the charge density and as defects to disrupt the metallic conduction. By measuring the spectrum of "plasmasonic" quasiparticle excitations, we can demonstrate the scale-free nature of the Coulomb interaction in Dirac systems. Such effects are readily observed on quasi-free standing graphene samples doped with long-range scatterers. Doping with short-range scatterers, on the other hand, results in a loss of conduction which we interpret as a manifestation of strong (Anderson) localization.

*Microscopic and Electronic Structure Observatory

**Advanced Light Source

5:00pm **GR+EM+ET+NS+TF-MoA10 Squeezing of the Graphene Dirac Cone Observed by Scanning Tunneling Spectroscopy**, *J. Chae*, *S. Jung*, *Y. Zhao*, *N.B. Zhitenev*, *J.A. Stroscio*, Center for Nanoscale Science and Technology / NIST, *A. Young*, *C. Dean*, *L. Wang*, *Y. Gao*, *J.C. Hone*, *K.L. Shepard*, *P. Kim*, Columbia University

The single-particle spectrum of graphene is described by massless Dirac quasiparticles with a linear energy-momentum dispersion relation. In this talk I examine the effect of electron interactions on the graphene energy dispersion as a function of both excitation energy *E* away from the Fermi energy and density *n*. To analyze the dispersion, we measure the Landau levels (LLs) in graphene on a hexagonal boron nitride (hBN) insulator in low magnetic fields by scanning tunneling spectroscopy. The experiments were performed in a custom designed cryogenic scanning tunneling microscope system operating at 4 K with applied magnetic fields from 0 T to 8 T. The graphene devices were fabricated by the method detailed in Dean *et al.* [1]. The disorder in graphene on hBN is reduced in comparison with the previous measurements in graphene on SiO₂ [2] allowing us to observe the LLs in fields as low as 0.5 T. By fitting the LL energies obtained at constant density, we find that the energy dispersion remains linear, characterized by a momentum-independent renormalized velocity.

However, the renormalized velocity is density dependent, showing a strong increase as the charge neutrality point is approached. The overall spectrum renormalization can be described as a *squeezing* of the Dirac cone angle due to electron-electron interactions at low densities. Interestingly, we also find that the renormalization of the dispersion velocity is affected by the local disorder potential and magnetic field, which is not described by current theory.

[1]. C. Dean, A. Young, I. Meric, C. Lee, L. Wang, S. Sorgenfrei, K. Watanabe, T. Taniguchi, P. Kim, K. L. Shepard, and J. Hone, *Nature Nanotech.* 5, 722–726 (2010).

[2]. S. Jung, G. M. Rutter, N. N. Klimov, D. B. Newell, I. Calizo, A. R. Hight-Walker, N. B. Zhitenev, and J. A. Stroscio, *Nature Phys.* 7, 245–251 (2011).

5:20pm **GR+EM+ET+NS+TF-MoA11 Interfacial Interaction of Graphene and Metal Surfaces Investigated by Resonant Inelastic X-ray Scattering**, **L. Zhang**, University of Science and Technology of China, Advanced Light Source, *J.H. Guo*, Advance Light Source, *J.F. Zhu*, University of Science and Technology of China

The synthesis of graphene on metal surfaces by chemical vapor deposition (CVD) is the most promising method to prepare single-layer and large-area graphene, which is a prerequisite for the fabrication of graphene-based electronic devices. Therefore, the graphene/metal interfaces have attracted much attention due to their importance in graphene synthesis by CVD processes. In this presentation, we report our recent studies on the electronic structure and band dispersion of graphene on different metal surfaces (Cu, Ir and Ni) by the means of X-ray absorption spectroscopy (XAS), X-ray emission spectroscopy (XES) and resonant inelastic X-ray scattering (RIXS). The XAS spectra for graphene on metal surfaces show strong π^* and σ^* resonant features, indicating that the single-layer graphene films preserve the intrinsic symmetry of graphite. The resonant XES spectra of graphene on different metal surfaces change dramatically, especially for the features of π^* resonances, which can be directly related to the different strength of hybridization between graphene and metal substrates. These significant spectra changes have been proved to be an effective measure for the bonding strength of graphene on different substrates: strong band dispersion can be observed when the interaction between graphene and metal substrate is weak (such as Cu), while the band dispersion is seriously disturbed when a strong hybridization between graphene and metal substrate (such as Ni) exists. These results provide basic understanding of graphene/metal interfacial interaction, which helps to develop graphene-based electronic devices with high performances.

Oxide Heterostructures-Interface Form & Function

Focus Topic

Room: 7 - Session OX+SS+TF+MI-MoA

Chemistry of Oxide Surfaces and Interfaces

Moderator: M. Engelhard, EMSL, Environmental

Molecular Sciences Laboratory

2:00pm **OX+SS+TF+MI-MoA1 Investigation of Al₂O₃ Nanostructure Surfaces Using Charge Optimized Many Body Potentials**, **D.E. Yilmaz**, *T. Liang*, *S.B. Sinnott*, *S.R. Phillpot*, University of Florida

Aluminum oxide nanostructures have drawn attention due to their interesting physical and optical properties. In particular, photoluminescence peaks for these systems are attributed to oxygen vacancies and surface effects. Here, we apply third-generation Charge Optimized Many Body (COMB) potentials for the Al-A1₂O₃ system to investigate the properties of Al₂O₃ nanoparticle surfaces. In particular, the elastic properties and local atomistic strain distribution of nanoparticles with a range of sizes are determined, and the corresponding vibrational spectra are determined. The effect of oxygen vacancies and adsorbed surface atoms on the local strain and vibrational spectra are also determined. This work is supported by the National Science Foundation (DMR-1005779).

2:20pm **OX+SS+TF+MI-MoA2 Manipulating Ferroelectric Surfaces for Direct NO_x Decomposition**, **M.W. Herdiech**, **A. Kakekhani**, **S. Ismail-Beigi**, **E.I. Altman**, Yale University

Current technology for removing nitrogen oxides from engine exhausts relies on nearly stoichiometric air to fuel ratios. Under these conditions, the concentrations of CO and unburned hydrocarbons in the exhaust stream are high enough to efficiently remove adsorbed oxygen from the platinum based catalysts in catalytic converters, ensuring that the catalysts do not become saturated with adsorbed oxygen. Direct catalytic decomposition of NO_x to N₂ and O₂ in the presence of excess O₂ would eliminate the need for

reducing species in automobile engine exhaust streams, allowing these engines to be run more efficiently. We have been investigating the potential of ferroelectric supports to modify the behavior of supported layers to enable direct NO_x decomposition. Our approach involves first principles density functional theory and surface science techniques. Using both approaches we have investigated the interactions of N, O, and NO with bare ferroelectric lead titanate surfaces and surfaces modified to expose catalytic layers, in particular Ru oxides. Theory indicates that the behavior of the PbTiO₃ surface towards these species is sensitive to the polarization direction and termination of the ferroelectric and that stable RuO₂-terminated surfaces can be created by manipulating the termination of the substrate. Experiments take advantage of plasma sources that allow the behavior of O and N atoms to be studied individually and epitaxial growth to manipulate the termination of the ferroelectric support. Favored reaction pathways are assessed using theory and temperature programmed desorption and related mass spectrometry methods.

2:40pm **OX+SS+TF+MI-MoA3 Catalyst Synthesis by Atomic Layer Deposition**, **P.C. Stair**, Northwestern University & Argonne National Laboratory

INVITED

Atomic Layer Deposition (ALD) has enormous potential for the synthesis of advanced heterogeneous catalysts with control of composition and structure at the atomic scale. The ability of ALD to produce conformal oxide coatings on porous, high-surface area materials can provide completely new types of catalyst supports. At the same time ALD can achieve highly uniform catalytically active metal and oxide phases with (sub-) nanometer dimensions.

Vanadium oxide species supported on high surface area oxides are among the most important catalytic materials for the selective, oxidative conversion of hydrocarbons to useful chemicals. In our laboratory ALD has been used to synthesize both the catalytic vanadium oxide and the supporting oxide on both high surface powders and anodic aluminum oxide (AAO) nanoliths. These materials have been characterized by SEM, XRF, ICP, UV-Vis absorption spectroscopy, Raman spectroscopy and evaluated for the oxidative dehydrogenation (ODH) of cyclohexane.

More recently we have studied the synthesis of supported metal particles and developed what we call “ABC-type” ALD in which metal nanoparticles and support materials are grown sequentially in each ALD cycle. This method makes possible the synthesis exceptionally small particles, ca. 0.5 nm. Using additional ALD support layers at the conclusion of the growth, the metal particles can be stabilized against sintering while still remaining active at high temperatures and reaction conditions. Moreover, the catalysts resist coke formation which is a leading cause of catalyst deactivation. These properties are imparted as a result of anchoring step and edge atom sites while leaving facet sites open for catalysis.

3:40pm **OX+SS+TF+MI-MoA6 Energy Alignment at Organic/Oxide Interfaces: The Influence of Adsorption Geometry and Chemical Bond on Interface Dipole**, **S. Rangan**, **C. Ruggieri**, **S. Coh**, **R.A. Bartynski**, **K. Chitre**, **E. Galoppini**, Rutgers University

The lack of control of the energy alignment at the interface between an organic layer and an oxide substrate remains a limitation to the performance of promising technologies such as dye sensitized solar cells, organic light emitting diodes or organic thin film transistors. The energy alignment depends not only on the choice of the starting materials, but also on more subtle parameters such as oxide surface termination or defects, and molecular layer preparation mode.

In an effort to disentangle the different aspect of the interface of an organic/oxide system, we have studied simultaneously the adsorption geometry and the energy alignment of the Zn(II) tetraphenylporphyrin (ZnTPP) molecule on the TiO₂(110) and ZnO(11-20) surfaces. Two approaches have been pursued: 1) in-situ evaporation of the ZnTPP on a clean oxide surface prepared in ultra-high vacuum resulting in weakly bound multilayers or monolayers 2) ex-situ sensitization in a solution of ZnTPP derivative, modified with COOH anchoring group for chemisorption at the oxide surface.

Scanning tunnel microscopy has been used to characterize the clean oxides and the ZnTPP adsorption modes. X-ray photoemission, ultra-violet photoemission and inverse photoemission spectroscopies have allowed the exploration of both occupied and unoccupied states of the electronic structure, resulting in the full characterization of the energy alignment at the surface as a function of the molecular overlayer thickness. The electronic transport gap, obtained from the latter experimental techniques has also been compared to the optical gap obtained from reflection electron energy loss spectroscopy, thus allowing the characterization of bound excitonic states.

The effect of the ZnTPP/oxide interface preparation, as well as the effect of the oxide substrate on the energy alignment will be presented. The

discussion will be extended to metallic substrates such as Ag(100) and Au(111) surfaces

4:00pm **OX+SS+TF+MI-MoA7 Energy-Level Alignment at Organic/Oxide Interfaces**, *M.T. Greiner, Z.-H. Lu*, University of Toronto, Canada **INVITED**

Oxide/organic interfaces play an important role in many organic electronic device designs. Oxides are frequently used as buffer layers to tune the energy-level alignment between electrodes and organic semiconducting layers, and thus allow for efficient hole/electron injection. As per the 'integer charge-transfer' (ICT) model, energy-level alignment at electrode/organic interfaces is governed by the electrode's Fermi level and the organic molecule's oxidation/reduction potential. While the ICT model was originally proposed for organic/organic interfaces, it also applies to a broad range of transition metal oxides. In this presentation we will discuss the energy-level alignment (ELA) of several organic semiconductors with transition-metal oxides. We will show that ELA is primarily governed by an oxide's work function, and that ELA is relatively insensitive to oxide electronic structure. As transition metal oxides can exhibit a wide range of work functions (~ 2 - 7 eV), and can possess a wide range of electronic properties (p-type to n-type) they are very versatile materials for use in organic electronics. We will their properties—such as work function and electronic structure—can best be utilized for use as buffer layers in organic light-emitting diodes and organic photovoltaics.

4:40pm **OX+SS+TF+MI-MoA9 Variable Kinetic Energy XPS of the Buried P3HT/ITO Interface**, *M.T. Brumbach*, Sandia National Laboratories, *J.C. Woicik*, National Institute of Standards and Technology

The characterization of buried interfaces is difficult and often has to be performed by post-processing methods where the interface is revealed, disturbed, and possibly altered by environmental exposure. Variable kinetic energy X-ray photoelectron spectroscopy (VKE-XPS) offers the ability to tune the depth of analysis while the use of hard X-rays allows for a deeper analysis. The combination of variable energy hard X-rays for XPS (HAXPES) allows for systematic evaluation through a buried interfacial region. An important inorganic/organic interface for use in organic photovoltaic devices is the poly(3-hexylthiophene) (P3HT) interface with indium tin oxide (ITO). In this work P3HT/ITO buried interfaces were examined using X-ray energies from 2.2-3.9 keV. The ITO surface was additionally prepared using different pretreatment conditions. The P3HT film protected the ITO surface from adventitious adsorbents and allowed for sensitivity to the buried ITO surface. Robust peak fitting parameters were obtained to model the O 1s and In 3d lineshapes. The deconvolution of these lineshapes allowed for the clear identification of a surface layer on the ITO which is oxidized to a greater extent than the underlying bulk ITO. The surface oxide layer, composed of indium oxide and indium hydroxide, is deficient of oxygen vacancies and would therefore be expected to act as an insulating barrier on the ITO surface. Peak fitting conditions allowed for an estimation of the thickness of this insulating layer. Sandia National Laboratories is a multi-program laboratory managed and operated by Sandia Corporation, a wholly owned subsidiary of Lockheed Martin Corporation, for the U.S. Department of Energy's National Nuclear Security Administration under contract DE-AC04-94AL85000.

5:00pm **OX+SS+TF+MI-MoA10 Organic Molecules Adsorbed on the ZnO(10-10) Surface: An Infrared Reflection Absorption Spectroscopy Study**, *M. Buchholz*, Karlsruhe Institute of Technology, Germany, *H. Noei, Y. Wang*, Ruhr University Bochum, Germany, *A. Nefedov, Ch. Wöll*, Karlsruhe Institute of Technology, Germany

Except for gold, every metal forms an oxide on its surface when exposed to the ambient atmosphere. The understanding of chemical processes taking place on metal oxide surfaces are thus of crucial importance. One of the most important oxides is ZnO. As a result of its semiconducting and optical properties, this material is used in many applications such as gas sensors, thin film solar cells, as well as in photocatalysis and photooxidation[1]. The important surfaces of ZnO are the polar Zn- or O-terminated ZnO(0001) and ZnO(000-1) as well as the mixed-terminated ZnO(10-10) surface. The latter is the dominating surface for ZnO powder particles and energetically most favorable.

Here we report on the adsorption of formic acid and maleic anhydride (MA) molecules on the mixed-terminated ZnO(10-10) surface. Formic acid is a good model molecule for understanding the anchoring of carboxylic dye molecules in dye-sensitized solar cells. The choice of MA is motivated by the importance of the industrial process where MA is hydrogenated using Cu/ZnO catalysts. The identification of the reaction mechanism requires the identification of intermediates using IR-spectroscopy[2].

In last decades numerous IR investigations of oxide powders have been reported. An unambiguous assignment of the features present in the complex powder IR spectra, however, is only possible on the basis of

reference data recorded for well-defined systems, e.g. surfaces of single crystals with defined orientation. Unfortunately, Infrared Reflection Absorption Spectroscopy (IRRAS) studies of molecular adsorbates on oxide single crystals, and, in particular on ZnO, are extremely scarce due to the fact that the sensitivity of IRRAS to adsorbate vibrations is two orders of magnitude lower for oxides than for metals. Whereas in case of TiO₂ recently with improved experimental setups adsorbate vibrations have been observed for a number of cases[3], to our knowledge molecular vibrations on clean ZnO single crystal surfaces have not yet been reported. With our novel UHV-IRRAS setup[4] high-quality IR spectra of different molecular adsorbates on ZnO(10-10) could be recorded in a routine fashion. In this presentation the obtained results will be presented and discussed.

M. Buchholz gratefully acknowledges the financial support from the Helmholtz Research School "Energy-Related Catalysis".

[1] C. Wöll, *Prog. in Surf. Sci.* **2007**, *82*, 55-120.

[2] S. G. Girol, T. Strunskus, M. Muhler, C. Wöll, *J. Phys. Chem. B* **2004**, *108*, 13736-13745.

[3] M. C. Xu, H. Noei, M. Buchholz, M. Muhler, C. Wöll, Y. M. Wang, *Catal. Today* **2012**, *182*, 12-15.

[4] Y. Wang, A. Glenz, M. Muhler, C. Wöll, *Rev. Sci. Instrum.* **2009**, *80*, 113108-113106.

5:20pm **OX+SS+TF+MI-MoA11 In Situ Interface Analysis of Self-Assembled Monolayers on Metal Surfaces at High Water Activities by Means of a PM-IRRAS/QCM-Setup**, *I. Giner, M. Maxisch, G. Grundmeier*, University of Paderborn, Germany

Aluminum and its alloys are widely used as engineering material and in a wide range of applications ranging from the aviation industry to the automotive and construction industries. As almost all engineering metals, aluminum under ambient conditions is covered by a native oxide film which alters significantly its surface physical and chemical properties. For corrosion protection and adhesion promotion, oxide covered aluminum surfaces are coated with organic films. Ultra-thin films or even monomolecular layers of organic acids like self-assembled monolayers (SAMs) of organophosphonic and organocarboxylic acids have been investigated as new advanced interfacial layers for aluminum alloys.¹ However, the stability of the self-assembled monolayers under environmental conditions is an aspect for technical applications. Different studies concerning to the stability and structure of the self-assembly monolayers under high humidity's conditions have been performed.² These studies revealed that the organic film decreased the amount of interfacial water layer but cannot prevent the water diffusion through the monolayer.³ The aim of the present work is to establish an in-situ setup combining quartz crystal microbalance (QCM) and PM-IRRAS to study the chemistry of passive films and adsorbed organic monolayers at high humidity. The metal coated quartz was used as the reflecting substrate for the PM-IRRAS measurement. Thereby, the structure of the monolayer, the amount of adsorbed water and the chemical state of the surface layer in the presence of an adsorbed water layer could be analysed in-situ. The surface hydroxyl density prior to organic molecule adsorption was adjusted by means of low temperature Ar- and H₂O- plasma treatments. Adsorption studies of H₂O on nonadecanoic carboxylic acid (NDA) monolayer modified surfaces in comparison to bare oxide covered aluminum surfaces showed, that the NDA monolayer leads to a reduced amount of adsorbed water based on the inability of water to form hydrogen bonds to the low energy aliphatic surface chemistry. Moreover the kinetics of chemisorption of water indicated by the oxyhydroxide peak growth at SAM/metal interfaces could be significantly inhibited. Furthermore, it is noticeable that interfacial carboxylate group coordinatively bound the oxide as well as the orientation of the NDA monolayer is not affected by the adsorption of several monolayers water. *Bibliography* 1. Thissen, P et al. *Langmuir* **2010**, *26*, (1), 156-164 2. Thissen, P et al. *Surface & Coatings Technology* **2010**, *204* (21-22), 3578-3584. 3. Maxisch, M et al. *Langmuir* **2011**, *27* (10), 6042-6048

Thin Film

Room: 11 - Session TF+EN-MoA

ALD for Energy

Moderator: R.K. Grubbs, Sandia National Laboratories

2:00pm **TF+EN-MoA1 Atomic Layer Deposition for the Synthesis of Nanostructured Catalysts**, *J.W. Elam, C. Marshall*, Argonne National Lab, *E. Stach, F. Ribeiro*, Purdue Univ., *J. Greeley*, Argonne National Lab, *J. Notestein, K. Poepelmeier*, Northwestern Univ., *L. Curtiss*, Argonne National Lab, *M. Kung, P.C. Stair*, Northwestern Univ., *L. Winans*, Argonne National Lab, *S. Nguyen*, Northwestern Univ. **INVITED**

The successful transition to an energy economy based on biomass will require radical advances in catalyst science. This challenge demands a new paradigm in catalyst synthesis whereby inorganic components can be assembled at the atomic scale to yield complex, multifunctional catalysts rivaling Nature's enzymes in their specificity. To this end, we have developed a novel approach combining templated synthesis for shape-selectivity with the atomically-precise positioning of discrete functionalities. In this approach we begin with a supporting scaffold for catalyst growth upon which we chemically attach molecular templates. Next, atomic layer deposition is used to build a structure around each template in an atomically precise, layer-by-layer fashion where the thickness and composition can be tuned at each layer. Finally, the template is removed yielding a "nanobowl" defining a structured catalytic environment. The molecular template can be synthesized to contain bulky organic ligands surrounding a catalytic atom or cluster which remains anchored to the bottom of the bowl after ligand removal. Furthermore, one or more layers in the bowl wall can be selected to serve as a co-catalyst (e.g. Lewis acid group) positioned at a well-defined distance from the catalyst at the bottom of the bowl. This presentation will review our recent progress synthesizing, characterizing, modeling, and testing these unique catalytic materials.

2:40pm **TF+EN-MoA3 Using Metalcone Films Grown by Molecular Layer Deposition to Form Conducting Metal Oxide-Carbon Composite Films**, *A. Abdulagatov, K. Terauds, J. Travis, A. Cavanagh, R. Raj*, CU Boulder, *S.M. George*, University of Colorado, Boulder

Metalcone films grown using molecular layer deposition (MLD) techniques with metal and organic precursors are metal alkoxide polymers. These hybrid organic-inorganic films can serve as precursors to conducting metal oxide-carbon composite films. In this study, titanicone MLD films were deposited by sequential, self-limiting exposures of TiCl_4 and glycerol at 150°C . These films were then annealed in argon at temperatures ranging from 500 to 1200°C . Under argon, the hydrogen is removed from the hybrid organic-inorganic titanicone films and the carbon remains. Raman spectroscopy measurements showed the progressive growth and sharpening of the D and G signature peaks for graphitic carbon after annealing from 600 to 900°C . The sheet resistance of the annealed films was also found to progressively decrease with increasing annealing temperature. X-ray photoelectron spectroscopy depth profiling confirmed the presence of carbon throughout the annealed film. X-ray diffraction measurements also observed the formation of rutile TiO_2 diffraction peaks. The annealing of metalcone MLD films in argon is a general method to deposit metal oxide-carbon composite films. Conducting metal oxide-carbon composite films are desirable because many electrochemically important metal oxides have low electrical conductivities. The metal oxide-carbon composite films with graphitic carbon have much higher electrical conductivities that will enable their electrochemical application for Li ion batteries and pseudocapacitance supercapacitors.

3:00pm **TF+EN-MoA4 In Situ Growth Study and Material Characterization of Plasma-Assisted Atomic Layer Deposition of Palladium**, *M.J. Weber, A.J.M. Mackus, M.A. Verheijen, N. Leick-Marius, A. Bol, W.M.M. Kessels*, Eindhoven University of Technology, Netherlands
Palladium thin films are object of great interest in catalysis, as well as in hydrogen sensing, storage and generation. Noble metals such as Palladium are the most effective if deposited as ultrathin films on a large surface area. Atomic layer deposition (ALD) is considered to be the method of choice to grow ultrathin films on various substrates with demanding surface topologies. This contribution will present *in situ* and *ex situ* studies of Palladium films grown by plasma-assisted ALD. The Pd films were deposited on alumina at 100°C using $\text{Pd}(\text{hfac})_2$ (hfac= hexafluoroacetylacetonate) as the precursor, and H_2 gas and H_2 plasma as reducing agents. *In situ* spectroscopic ellipsometry (SE) has been used to monitor the film growth and obtain detailed information about the optical properties of Palladium. The nucleation and subsequent island growth have been characterized by Transmission Electron Microscopy (TEM). X-Ray

diffraction, X-ray photoelectron spectroscopy and Rutherford backscattering spectrometry have been carried out in order to characterize the grown films. The thermal ALD process only allowed for growth of Pd on a Pd or Pt seed layer, while the plasma-assisted ALD process also led to growth on an alumina surface. In both cases the steady-state growth rate was $\sim 0.17 \text{ \AA/cycle}$ as determined by *in situ* SE. The observed selective growth on catalytic Pd or Pt seed layer of the thermal process holds promises for nanopatterning applications, whereas the plasma-assisted process can be used to deposit Pd nanoparticles and films at low-temperature on oxide substrates, which has considerable potential for catalysis and hydrogen sensor applications.

3:40pm **TF+EN-MoA6 ALD-enabled Nanostructures for High Rate Li-ion Storage**, *X. Chen, H. Zhu, L. Hu, G.W. Rubloff*, University of Maryland
A major challenge for Li-ion batteries is to achieve high rates (power) by overcoming the long charge/discharge time caused by low Li diffusivity in active storage materials. Nanostructured electrodes provide a potential solution by reducing the thickness of active storage layers, since the diffusion time is proportional to the square of diffusion length. Our strategy to improve the rate performance of Li-ion battery is to use atomic layer deposition (ALD) to grow thin active battery materials on highly conductive current collecting scaffolds with high surface area. The unprecedented conformality of ALD allows maximum utilization of high surface area, while the highly conductive scaffold facilitates easy electron transport and Li^+ migration in electrolyte as also needed for high power. We report two embodiments of this heterogeneous nanostructure configuration, both with ALD V_2O_5 storage layers.

First, we used highly porous multiwall carbon nanotube (MWCNT) sponge as the scaffold. The V_2O_5 -MWCNT coaxial sponge achieves a stable high areal capacity as $816 \mu\text{Ah/cm}^2$ over voltage range 4.0 - 2.1 V at current density of 1.1 mA/cm^2 (i.e., 1C rate). This capacity is 450X that of a corresponding planar V_2O_5 thin film cathode. For the same voltage range but 50X higher current, the areal capacity of the V_2O_5 -MWCNT sponge is $155 \mu\text{Ah/cm}^2$, giving a high power density of 21.7 mW/cm^2 . The areal capacity increases further to $1284 \mu\text{Ah/cm}^2$, when cycled over a larger voltage window (4.0 - 1.5 V), but this incurs deteriorated cycling performance as expected from the intrinsic properties of V_2O_5 .

Second, we employed well-ordered anodic aluminum oxide (AAO) templates to with ALD current collecting layers as a scaffold for the storage material. ALD TiN was first deposited into the AAO nanopores to form current collecting nanostructures, after which ALD V_2O_5 was deposited on TiN as the active Li storage medium, with both layer thicknesses precisely controlled and highly conformal. The resulting structures, with electrolyte filling the remaining pore volume, provide test structures to understand regimes where either Li^+ transport or electron transport can be rate-limiting.

4:00pm **TF+EN-MoA7 Enhancement of the Heat Recovery Mechanism in Infrared Photovoltaic Devices Promoted by Thin Planar ALD Oxide Films**, *A.J. Vincent-Johnson, H.S. Mann, Y. Schwab*, James Madison University, *A.E. Masters*, Custom Thermoelectrics Inc., *X. Hu, G. Scarel*, James Madison University

Infrared photovoltaic devices absorb infrared radiation and transform it into electricity through the heat recovery mechanism [1,2]. In thin planar oxide films, the mechanism is mediated by the excitation of radiative polaritons, as shown by investigations carried out immediately after beginning the exposition to infrared radiation [1,2]. Here we present the results of our investigation on the evolution of the heat recovery mechanism; and the electricity production over time through illumination by infrared radiation. We compare the results on systems including atomic layer deposited (ALD) Al_2O_3 , Al foil, and the bare thermoelectric power generator used for the detection of the heat recovery mechanism. We show that ALD oxide films promote the largest amount of electricity production under long term exposition to both polarized and non-polarized infrared radiation.

[1] A.J. Vincent-Johnson, K.A. Vasquez, J.E. Bridstrup, A.E. Masters, X. Hu, and G. Scarel, Appl. Phys. Lett. **99**, 131901 (2011).

[2] A.J. Vincent-Johnson, A.E. Masters, X. Hu, and G. Scarel. Submitted.

4:20pm **TF+EN-MoA8 Ultra-thin TiO_2 Blocking Layer by Atomic Layer Deposition for Dye-Sensitized Solar Cells**, *D.H. Kim, M. Woodroof, K.M. Lee, B. Kalanyan, G.N. Parsons*, North Carolina State University

In dye-sensitized solar cells (DSSCs), one of major recombination routes occurs at the interface of fluorine-doped tin oxide (FTO) glass and electrolyte solution. Typically, a thin and compact blocking layer (B/L) on the FTO-glass has been introduced to reduce electron loss before mesoporous TiO_2 layer integration. A variety of deposition methods have been tried and studied to make efficient B/L on the FTO-glass. Optimal thickness that suppresses the recombination on the interface of FTO glass

and electrolyte, is typically 25 to 450 nm, depending on deposition methods and conditions. Compared to other methods, atomic layer deposition (ALD) with TiO_2 is not well established and investigated for blocking layers even though it is a valuable process in making pin-hole, crack-free, and dense TiO_2 films.

In this study, ALD TiO_2 was performed on FTO-glass with titanium isopropoxide and H_2O as precursors, producing B/L thickness from 5 to 100 nm. Cells without mesoporous titania but with ALD TiO_2 B/L were also made. We find the optimal thickness of the ALD TiO_2 blocking layer is 10 nm. This blocking layer thickness significantly reduces recombination, resulting in an average overall efficiency of 8.5%, compared to 7.1% for similar cells without the blocking layer present. We also find that a blocking layer of 4.3 nm effectively prevents electrons of FTO surface from recombining with I_3^- in the electrolyte. On the other hand, a thick ALD TiO_2 blocking layer in excess of 10 nm tended to reduce the overall efficiency because the thick ALD TiO_2 film increases the charge transfer resistance and hinders the electron transport to FTO-glass. This work contributes to understand effective blocking layer from TiO_2 ALD process for DSSCs and other high-performance electrical devices

Tuesday Morning, October 30, 2012

Energy Frontiers Focus Topic

Room: 15 - Session EN+TF-TuM

Chalcogenide Solar Cells II

Moderator: H.W. Hillhouse, University of Washington

8:00am EN+TF-TuM1 Thin Film Solar Cells: Present Status and Future Prospects, C.S. Ferekides, University of South Florida INVITED

Thin film photovoltaics (TF PV) have long been viewed as a low cost option for solar electricity. Two very promising TF technologies are based on Cu(In,Ga)(S,Se)₂ (CIGS) and CdTe. The former has achieved the highest thin film laboratory efficiency (over 20%) and the latter is the lowest cost PV product on the market today (@ \$0.74/Watt). Recently, another thin film technology based on the kesterites Cu₂ZnSn(S,Se)₄ (CZTS) has received significant attention due to the abundance of the constituent elements, and small area cells have reached the 10% efficiency level. Despite all the successes achieved at the laboratory and manufacturing environments, TF technologies continue to face challenges some of which are unique to the specific material system. The presentation will provide an overview of thin film photovoltaics by comparing and contrasting the devices and technologies described above. Material, device and fabrication issues will be discussed with emphasis placed on some of the unique aspects of each technology: the need for sodium for CIGS and the importance of the co-evaporation process, the use of a chloride based treatment for CdTe and the challenge in forming back contacts to this device, and the loss of tin for CZTS.

8:40am EN+TF-TuM3 Materials and Process Options for Cu(InGa)Se₂ Thin Film Solar Cells, W.N. Shafarman, University of Delaware INVITED

Two approaches to depositing thin films of Cu(InGa)Se₂ and related alloys have been developed in the laboratory and are being implemented in large scale photovoltaics manufacturing. Precursor reaction processes use precursor films containing Cu, Ga, and In deposited by methods such as sputtering, printing, or electrodeposition chosen to provide potential manufacturing benefits. These are reacted in hydrogen selenide gas or elemental Se vapor to form the semiconductor absorber layer. Elemental co-evaporation is a single step process in which fluxes of all species are delivered to a hot substrate. Advantages and critical issues for these processing approaches will be compared. One of the materials options for Cu(InGa)Se₂-based absorber layers is the opportunity to alloy the film to increase its bandgap. This is desirable because the increased solar cell voltage can be advantageous for large scale module performance. Wider bandgap can be achieved by increasing the relative Ga content or by alloying with S, Al or Ag, but in all cases the cell efficiency decreases as the absorber layer bandgap increases beyond 1.2-1.3 eV. Alloying and composition control is generally straightforward using co-evaporation since these alloys form continuous solutions. With precursor reaction, however, chemical pathways to film formation are partly controlled by preferential reaction of Se with In instead of Ga, leading to aggregation of the Ga at the back of the film and, effectively, low bandgap. Multi-step reaction profiles can be used to control through-film composition in this case. For wide bandgap cells, recent results with the combination of Ag alloying and higher Ga content show promise. This includes improved optical properties, evidence of reduced structural disorder and improved performance with high open circuit voltage solar cells. The incorporation of Ag in both the precursor reaction and co-evaporation processes will be described.

9:20am EN+TF-TuM5 Why Are We Making CIGS Solar Cells from Cu-poor Material?, S. Siebentritt, University of Luxembourg INVITED

CIGS can be prepared single phase in a large range of Cu-poor compositions. When prepared under Cu-excess a secondary phase of Cu selenide is formed which can be etched. Record solar cells as well as commercial modules are prepared from Cu-poor absorbers. However, the transport and recombination properties of material prepared under Cu-excess are superior. It has been known that the interface in cells with absorbers prepared under Cu-excess leads to increased recombination and thus limits the efficiency. The properties of the surface of CIGS absorbers prepared under Cu-excess is not well understood so far. We are preparing solar cells with absorbers grown under Cu-excess, where we make the surface Cu-poor to get the best from both worlds.

10:40am EN+TF-TuM9 Zn_xCd_{1-x}S Thin Films for Chalcopyrite Solar Cells Deposited through Batch and Continuous-Flow Chemical Bath Deposition, B.S. Tosun, C. Pettit, S.A. Campbell, E.S. Aydil, University of Minnesota

Copper indium gallium diselenide (CIGS) thin film solar cells already exceed 20 % overall power conversion efficiencies. These high efficiencies are achieved using an n-type cadmium sulfide (CdS) buffer layer deposited on the p-type CIGS absorber using chemical bath deposition. CdS buffer layers are also used in the emerging copper zinc tin sulfide/selenide (CZTSSe) based solar cells. In some cases, it is desired to grade and widen the band gap of the buffer layer away from the CdS-absorber interface by alloying CdS with Zn to form Zn_xCd_{1-x}S films. In this work, we demonstrate the ability to manipulate Zn fraction, x, as a function of distance from the absorber-buffer layer interface and investigate the fundamental factors that govern the evolution of the film composition as a function of depth. Specifically, Zn_xCd_{1-x}S films were grown from solutions containing cadmium sulfate ammonium hydroxide, ethylenediaminetetraacetic acid disodium, zinc sulfate and thiourea in two different types of chemical baths, a traditional batch-type chemical bath and a continuous-flow chemical bath. By changing the initial concentrations of Zn and Cd sulfate in the batch-type chemical bath deposition, the entire range of overall compositions ranging from primarily cubic ZnS to primarily hexagonal CdS could be deposited. Using Auger depth profiling, we show that a CdS rich layer forms at the film/substrate interface due to the faster reaction of Cd than Zn. The formation of Cd-rich Zn_xCd_{1-x}S layer at film/substrate interface followed by Zn-rich Zn_xCd_{1-x}S is favorable for solar cells. Thicker films with increasing band gap towards the surface can be deposited to increase the shunt resistance without sacrificing light transmission. In addition, we have developed a continuous chemical bath deposition system that allows deposition of Zn_xCd_{1-x}S films on 4-inch diameter substrates at temperatures as high as 80 °C without significant liquid temperature rise and without homogeneous nucleation and growth. Structure and composition of the films from the batch and continuous flow systems will be discussed and compared.

11:00am EN+TF-TuM10 Selenization of Cu-Ga-In Precursors for Synthesis of CIGS Absorbers: Equilibrium and Kinetic Studies, C. Muzzillo, R. Krishnan, University of Florida, W.K. Kim, Yeungnam University, Republic of Korea, E.A. Payzant, Oak Ridge National Laboratory, Y.H. Sohn, B. Yao, University of Central Florida, J. Shen, General Research Institute for Non-ferrous Metals of Beijing, China, C. Campbell, National Institute of Standards and Technology, T.J. Anderson, University of Florida

The emerging CuIn_xGa_{1-x}Se₂ (CIGS) PV industry is primarily differentiated on the basis of the process used to synthesize the CIGS absorber. The most common approach is a 2-step metal deposition/selenization with differentiation occurring on the method of metal deposition and Se source for selenization. Typical champion cell efficiencies, however, are slightly lower for 2-step processes as compared to co-evaporation. This has been attributed to difficulty in creating a 'U-shaped' Ga profile, void formation near the back contact, and differences in diffusion/reaction rates of Ga and In during synthesis. Furthermore, cost pressures are driving reduction of the selenization time (up to 8 hr) and thinning of the absorber layer. A better understanding of the thermodynamic and kinetic elements of the precursor Cu-Ga-In metal system offers the potential to exploit faster pathways, assist in scale-up, and ensure robust processing of CIGS. This study includes a critical assessment of thermochemical and phase equilibria data of the Cu-Ga-In ternary metal system. The calculated phase diagram includes 11 binary intermetallic phases and no ternary compounds. Of particular interest are the 4 phases which exhibit ternary solubility: α-Cu (fcc), γ-Cu₉(Ga_xIn_{1-x})₄ (sc), and η-Cu₁₆(In_xGa_{1-x})₉ (hcp) are all modeled with a sublattice formalism, and an ionic two-sublattice liquid model is employed. Time-resolved *in situ* high temperature X-ray diffraction data for selenization of metallic precursors have also been collected. Reaction pathways and kinetics of temperature ramp and isothermal anneal experiments have both been examined, and kinetic rate parameters for the Avrami and parabolic growth models have been estimated from the data. As examples, MBE deposited bilayer metal precursor structures (e.g. CuIn/CuGa) and elemental stacked layers (e.g. (Cu/Ga/In)_n) were selenized and the Ga distribution measured. The formation of Cu₁₁In₉, textured indium, and the solid solution γ-Cu₉(Ga_xIn_{1-x})₄ were also evident as well as formation of CuGaSe₂ and CIGS simultaneously for selected structures. Rietveld refinement of temperature ramped selenized samples was performed to estimate the Ga distribution. TEM-EDS results confirm that the Ga distribution after selenization depended on the order of deposition of the precursor structure. The samples were further characterized by SEM (microstructure) and ICP (final composition). The activation energy for formation of CIGS was

estimated from isothermal studies, and gave values of 76(±14) for the glass/Mo/CuIn/CuGa and 93(±4) and 101(±9) kJ/mole for the glass/Mo/CuGa/CuIn precursor.

11:20am **EN+TF-TuM11 Fabrication of $\text{CuIn}_{1-x}\text{Ga}_x\text{S}_2$ Thin-Film Solar Cells on Single Layer Molybdenum**, A. Kaul, E. Schneller, N. Shiradkar, S. Pethe, N. Dhere, Florida Solar Energy Center, University of Central Florida

Considering the various advantages of a single pass operation, efforts have been made to develop a recipe for device quality single layer molybdenum back contact film that has good adhesion to the soda-lime glass substrate and at the same time lower resistivity values. $\text{CuIn}_{1-x}\text{Ga}_x\text{S}_2$ (CIGS2) thin film solar cells with reasonable efficiencies were successfully fabricated on the single layer molybdenum film without any signs of peeling or back contact degradation during processing. The molybdenum films were also subjected to various processing conditions of temperature and gas ambient and the subsequent results from these tests are also being presented.

11:40am **EN+TF-TuM12 Investigation of Elemental Composition for $\text{Cu}(\text{InGa})\text{Se}_2$ Thin Films by Various Analytical Techniques**, J.H. Lee, S.H. Kim, J.-H. Yoon, S.-O. Won, Y.H. Lee, Korea Institute of Science and Technology, Republic of Korea

$\text{Cu}(\text{InGa})\text{Se}_2$ (CIGS) solar cells are very promising films for use in photovoltaic devices, as they feature a high absorption coefficient and a high conversion efficiency at a relatively low manufacturing cost. In order to develop an efficient CIGS solar cell, the relative ratio of the major elements should be determined quantitatively. In this study, a quantitative analysis of $\text{Cu}(\text{InGa})\text{Se}_2$ (CIGS) was performed using an electron probe micro analysis (EPMA), x-ray fluorescence (XRF), inductively coupled plasma-optical emission spectrometry (ICP-OES), Auger electron spectroscopy (AES), time-of-flight secondary ion mass spectrometry (TOF-SIMS), and dynamic secondary ion mass spectrometry (dynamic SIMS). Surface roughness was observed by using atomic force microscopy (AFM) to identify the effect of the surface roughness on the reproducibility of the measurements. The relative sensitivity factors (RSF) of AES and SIMS were obtained by using ungraded CIGS thin film of known composition as the standard sample. Quantitative analysis of several CIGS samples were performed using the relative sensitivity factor (RSF) value calculated from the depth profile results of the standard film. The Cu/(In+Ga) ratio and the Ga/(In+Ga) ratio of SIMS results are relatively reproducible and close to those of the AES results. Overall, results from Composition of CIGS thin films by a variety of analytical methods were compared and their discrepancies were interpreted.

Thin Film

Room: 11 - Session TF-TuM

ALD Reactions and Film Properties

Moderator: H. Kim, Yonsei University, Korea

8:40am **TF-TuM3 Growth Simulations for Atomic Layer Deposition: Adsorption, Elimination and Densification Reactions**, S. Elliott, M. Shirazi, Tyndall National Institute, Ireland

INVITED

The central idea in chemical vapour deposition (including atomic layer deposition, ALD) is that the thermodynamic tendency of atoms to aggregate and bond into a solid film can be delayed by surrounding the atoms with ligands and transporting the molecular complex as a vapour. Deposition thus involves adsorption of the molecule, removal of ligands and a concomitant increase in atomic coordination number as the solid is formed. The focus is often on adsorption and ligand removal, while the change in coordination during growth, which has been termed 'densification' [1], has often been neglected.

We apply first principles density functional theory (DFT) to the $\text{Hf}(\text{NR}_2)_4 + \text{H}_2\text{O}$ system for the ALD of HfO_2 , which reveals how important densification can be in explaining the characteristics of oxide ALD. We consider $\text{R}=\text{Me}$ but expect that similar reactions occur for larger R. Transfer of H from the surface to the ligand is strongly affected by rotation of the ligand around the Hf-N bond, which in turn depends on the crowding associated with proximity of Hf to the surface. Dissociation of HfNR_2 is facilitated if multiple ligands on an adsorbed Hf centre are protonated, contrary to the usual assumption of dissociation one by one. Once sufficient protonated ligands have desorbed, Hf is freed up to bond to more surface O (densification), with substantial release of energy. Thus this example illustrates the importance of densification reactions in transforming molecular precursors into solid films.

Next, we use the DFT activation energies for this reaction mechanism as inputs to a Kinetic Monte Carlo (KMC) model to explicitly model film growth over multiple ALD cycles. KMC allows a large set of inter-dependent events (such as growth reactions) to be combined into a sequence over a variety of timescales. It is therefore suitable for the coarse-graining in time that is necessary in order to simulate ALD cycles [2]. We have modified the KMC modules of the SPPARKS code [3] for oxide growth by ALD. We include 162 possible reactions (each with DFT-derived activation energies) at 8000 reaction sites under typical values of temperature and pressure. The results show which reactions predominate, how layer-by-layer growth takes place and how roughness evolves in time.

We gratefully acknowledge funding from Science Foundation Ireland under the Strategic Research Cluster 'FORME' (www.tyndall.ie/forme) and coding support and computing time at the SFI/HEA funded 'Irish Centre for High End Computing'.

[1] S. Olivier et al., Chem. Mater., 2008, 20, 1555–1560.

[2] A. Esteve et al., J.Chem. Theory Comput., 2008, 4, 1915–1927.

[3] A. Slepoy et al., J. Chem. Phys., 2008, 128, 205101.

9:20am **TF-TuM5 Optimization of Properties of Al-doped ZnO Films Deposited by Atomic Layer Deposition**, Y. Wu, P.M. Hermkens, B.W.H. van de Loo, H.C.M. Knoops, F. Roozeboom, W.M.M. Kessels, Eindhoven University of Technology, the Netherlands

ZnO is widely used in solar cell windows, and as active layers in gas sensors. Often Al-doping is applied to decrease its resistivity. However, the chemical environment and electrical properties of Al-doped ZnO are not fully understood and the doping efficiency of Al is not optimized yet. In this work, 40 nm Al-doped ZnO layers were deposited on 450 nm SiO_2/Si -substrate at 250 °C by ALD using ZnEt_2 , AlMe_3 and water vapor as precursors. The Zn-O/Al-O cycle ratios were varied corresponding to an Al-content ranging from 0 at.% to 17.4 at.%. The resistivity improved from 8.2 $\text{m}\Omega\text{-cm}$ for intrinsic ZnO to an optimum of 2.2 $\text{m}\Omega\text{-cm}$ at 6.8 at.% Al-content. The stoichiometry, distribution and chemical environment of Zn, Al and O elements were studied by angular-resolving and depth-profiling X-ray photoelectron spectroscopy (XPS). With XPS sputter depth profiling we could distinguish the individual ZnO and Al-O lamellae in the films grown with high cycle ratios, whereas films grown with low cycle ratios showed a more homogeneous composition. The binding energies of Al 2p3 and Zn 2p3 increase by 0.23eV and 0.44eV for intrinsic ZnO to highest doped AZO, respectively. This shift is ascribed to an increase of the Fermi level, and secondly, to the delocalization of bonded electrons from Zn_{Zn}^0 to Al_{Zn}^+ .

Ex-situ SE and Fourier transform infrared spectroscopy were applied to measure the optical properties, from which the carrier concentration and intra-grain mobility were extracted by modeling. The relative permittivities ϵ_1 and ϵ_2 were obtained from the modeling as well and the optical band gap was determined by Tauc-plot fitting. The optical band gap increases from 3.29 eV for intrinsic ZnO to 3.77eV for the highest doped AZO (17.4 at.% Al), corresponding to the Burstein-Moss effect and an increase of the Fermi level. Meanwhile, the total mobility was determined by Hall measurement. Combined with the intra-grain mobility, the mobility at grain boundaries (GB) can be calculated. The result shows that with increasing Al%, the barrier at GB decreases at first due to an increased Fermi level and increases next due to alumina clustering at the GB. The Al-doping efficiency, as calculated from the carrier concentration, shows that the doping of Al in ZnO phase is saturated at 6.8 at.% Al. Above this value, the Al incorporated mainly forms alumina at GB, which decreases the mobility while hardly leading to higher carrier concentrations.

In summary, the chemical and electrical properties of Al-doped ZnO were measured and explained properly, and the doping efficiency was optimized at 6.8 at.% Al, which is useful for further study and applications.

9:40am **TF-TuM6 Growth Inhibition of Al_2O_3 on InGaAs by Atomic Layer Deposition**, B. Granados, A.J. Muscat, University of Arizona

The chemical composition of the $\text{In}_{0.53}\text{Ga}_{0.47}\text{As}(100)$ interface during the growth of an aluminium oxide (AlO_x) layer deposited by ALD was studied after each half-cycle using *in-situ* X-ray photoelectron spectroscopy (XPS) to understand film nucleation and interface formation. Native oxide was removed from InGaAs using liquid HF (49%, followed by water rinse) and gas phase HF and compared to deposition directly on native oxide. *In situ* gas phase $\text{HF}/\text{H}_2\text{O}$ etching was run at 29°C and 100 Torr with an HF to water partial pressure ratio of 1.23. The ALD process consisted of pulses of trimethylaluminum (TMA) and H_2O at 170°C. The AlO_x film thickness was estimated from the Al 2p peak area and the attenuation of the As 3d bulk signal due to an assumed homogenous Al_2O_3 overlayer. An AlO_x film with a thickness of 11.2 ± 2.5 Å was deposited during the first pulse of TMA on both liquid and gas phase HF treated samples and a film with a thickness of 12.8 ± 2.5 Å was deposited on InGaAs covered by native oxide. These

thicknesses correspond to approximately 3 ML of Al₂O₃, which could indicate the formation of islands. Remarkably the thickness was equivalent starting from an As-rich interface in the case of liquid HF, a Ga-rich interface in the case of gaseous HF that contained both oxides and fluorides, and an nearly stoichiometric surface in the case of native oxide. After three complete ALD cycles the thickness of the AlO_x film was 12.9 ± 2.5 Å on liquid HF treated, 9.2 ± 2.5 Å on gas phase HF treated, and 14.1 ± 2.5 Å on the native oxide of InGaAs, indicating that the first pulse reacts with most of the sites on the surface. The density of methyl groups after the first pulse was estimated to be 12 methyl groups/nm² on the liquid HF treated surface based on XPS. Approximately half of the methyl groups were hydrolyzed by the first water pulse, depositing an estimated 6 hydroxyl groups/nm². The second TMA pulse returned the methyl density to approximately the same value after the first TMA pulse. After the first ALD cycle the samples entered into a growth inhibition period. The growth rate per cycle (GPC) during cycles two and three dropped from 2.5 ML/cycle to 0.4 ML/cycle on the liquid HF treated surface and to 0.0 ML/cycle on the gas phase HF treated surface, and from 3.4 ML/cycle to 0.2 ML/cycle on the native oxide of InGaAs. This growth inhibition after the first pulse of TMA must be caused by the formation of Al-CH₃ moieties on the surface that are less reactive than both the initial surface and Al₂O₃. Understanding the surface reactions involved in the nucleation phase and early cycles of ALD is important in achieving control of the III-V-dielectric interface.

10:40am **TF-TuM9 Nanoindentation and Flexure Related Effects Due to Reactive Subsurface Growth of Atomic Layer Deposition Aluminum Oxide on Polyamide-6**, *Y. Sun*, North Carolina State University, *M.P. Goertz, J.A. Palmer*, Sandia National Laboratories, *R.P. Padbury, J.S. Jur*, North Carolina State University

In this study, we investigate the nanoindentation characteristics and crack formation with flexure of nanoscale atomic layer deposition (ALD) alumina on polyamide-6 (PA-6) films. Initial ALD processing PA-6 is shown to form a subsurface hybrid layer by reaction between ALD precursors and the polymer backbone, followed by standard Al₂O₃ surface formation in subsequent cycling. Over an exposure temperature from 60 to 120 °C, the degree of hybrid layer formation varies significantly. Transmission electron microscopy shows that the thickness of the underlying hybrid layer is increased at lower temperatures, up to 120 nm for 100 ALD cycles of trimethylaluminum and water on PA-6. At 120 °C processing, no hybrid layer is observed. The elastic modulus and hardness evaluated by nanoindentation show a corresponding decrease in value with the thickness of the hybrid layer. Flexure testing shows that both crack density and critical tensile strain is decreased for films processed at lower temperatures that have an increased thickness of the underlying hybrid layer. This analysis shows that the nucleation behavior of the ALD thin films on polymers plays an important role in understanding the mechanical performance of the thin films. This work has important consequences in the how ALD materials need to be applied and evaluated on polymers for application as diffusion barrier layers.

11:00am **TF-TuM10 The Importance of Oxygen-Induced Ripening in the Nucleation of Platinum Atomic Layer Deposition**, *A.J.M. Mackus, M.A. Verheijen, N. Leick, W.M.M. Kessels*, Eindhoven University of Technology, Netherlands

Platinum thin films and particles on oxide surfaces are interesting for various applications in microelectronics and catalysis. Atomic layer deposition (ALD) of Pt from MeCpPtMe₃ precursor and O₂ gas has recently emerged as a promising technique to fabricate these structures on demanding topologies such as high-aspect ratio surfaces or porous catalyst supports. The surface reactions of Pt ALD are governed by dissociative chemisorption of O₂ at the Pt surface, and catalytic combustion and dehydrogenation of the MeCpPtMe₃ precursor ligands,¹ which is limited during nucleation on oxides due to the absence of a catalytic surface. In this work, it is established that a parameter that has not been investigated so far, the O₂ exposure (i.e. pressure × time) during the reactant half-reaction of the ALD cycle, plays a crucial role during the nucleation of Pt ALD. Under influence of the oxygen, deposited Pt atoms diffuse over the surface and form small islands, and these islands subsequently catalyze the surface reactions of Pt ALD. As a result, the nucleation delay for Pt growth decreases with increasing O₂ exposure. It is shown that the particle ripening is absolutely essential for the Pt ALD growth to occur. For low O₂ exposures, there is no growth at all on Al₂O₃ substrates. The O₂ exposure can be used as a parameter to tune the nucleation behavior, and this has some important consequences for the applications. For example, the O₂ exposure dependence can be exploited to minimize the nucleation delay for the deposition of ultrathin closed Pt films, to fabricate particles with a narrow size distribution for catalysis applications, or to obtain selective growth on seed layer patterns for nanopatterning applications.²

[1] A.J.M. Mackus, N. Leick, L. Baker, W.M.M. Kessels, *Chem. Mater.*, (accepted for publication).

[2] A.J.M. Mackus, J.J.L. Mulders, M.C.M. van de Sanden, W.M.M. Kessels, *J. Electrochem. Soc.* **157**, G241-G249 (2010)

11:20am **TF-TuM11 Plasma Assisted Atomic Layer Deposition of Pt and PtO_x in High Aspect Ratio 3D Structures**, *I.J.M. Erkens, M.A. Verheijen, F. Roozeboom, W.M.M. Kessels*, Eindhoven University of Technology, Netherlands

High aspect ratio (AR) nanostructured films of noble metals and noble metal oxides with large specific surface areas can have a wide variety of applications in many fields such as catalysis, sensing and energy storage. Atomic layer deposition (ALD) has become the method of choice for depositing thin films conformally in high AR structures. (1) To achieve high conformality, saturation of the surface reactions has to be achieved throughout the three-dimensional (3D) structure. For plasma assisted ALD, reaching conformal deposition in high AR structures is less straightforward than for thermal ALD due to surface recombination loss of plasma radicals. (2) In our contribution we demonstrate that plasma assisted ALD can be used to deposit Pt in high AR 3D structures with high conformality. We also describe the sample preparation technique that allowed the conformality to be analyzed using transmission electron microscopy (TEM). Depositions were performed on high AR trenches, pre-etched in silicon (AR = 1.3 - 34), and in anodized aluminum oxide (AAO) (pore diameter = 70 nm, depth = 20 μm). The results for coating the Si trenches demonstrate that for the plasma assisted ALD process, pulses of 3 s (MeCp)PtMe₃ and 3 s O₂ plasma are sufficient to deposit Pt coatings with 95-100% conformality up to AR = 20. For AR = 20 the conformality was quantified using TEM. For this purpose, a cross-sectional TEM sample of a trench was prepared by first cleaving the Si substrate exactly through the trench heartline. A lift-out TEM sample was subsequently prepared using Focused Ion Beam (FIB) milling orthogonal to the cleavage plane (i.e. to the side wall of the trench). This provided a TEM sample in which the entire sidewall of the 20 μm deep trench was electron transparent, which allowed the layer thickness as a function of depth to be determined with high precision. The TEM images of individual Pt nanotubes deposited in the AAO pores were used to determine wall thickness as a function of depth, and showed the grain structure of the deposited Pt in great detail. In our contribution we will also report on the high AR conformality of other noble metal and noble metal oxide plasma assisted ALD processes (e.g., PtOx and Ir).

(1) P. Banerjee, I. Perez, L. Henn-Lecordier, S. B. Lee, and G. W. Rubloff, *Nature Nanotechnology* **4**, 292 (2009).

(2) H. C. M. Knoops, E. Langereis, M. C. M. van de Sanden, and W. M. M. Kessels, *J. Electrochem. Soc.* **157**, G241-G249 (2010).

Tuesday Afternoon, October 30, 2012

Energy Frontiers Focus Topic

Room: 15 - Session EN+TF-TuA

Thin Film, Heterostructured, and Organic Solar Cells

Moderator: M. Filler, Georgia Institute of Technology

2:00pm EN+TF-TuA1 **Photonic Materials for Solar Energy Conversion at the Thermodynamic Limit**, H.A. Atwater, California Institute of Technology **INVITED**

Ever since serious scientific thinking went into improving the efficiency of photovoltaic energy conversion more than 50 years ago, thermodynamics has been used to assess the limits to performance, guiding advances in materials science and photovoltaic technology. Photovoltaics have advanced considerably, resulting in single-junction solar cells with a record efficiency of 28.8% and multi-junction cells with an efficiency of 43.5%. As impressive as these advances are, these record efficiencies and also today's manufactured cell efficiencies in the 10–18% range fall far short of the thermodynamic limits. Why such a large gap? There is no fundamental reason, and in this talk, I will discuss methods for systematically addressing the thermodynamic efficiency losses in current photovoltaics that can enable a next phase of photovoltaic science and engineering – ultrahigh efficiency photovoltaics. This development takes advantage of recent advances in the control of light at the nanometer and micron length scales, coupled with emerging materials fabrication approaches, and will allow the development of solar cells with efficiencies in the 50–70% range.

Web resources:

<http://www.lmi.caltech.edu/>

<http://daedalus.caltech.edu/>

2:40pm EN+TF-TuA3 **Semiconducting Carbon Nanotubes as Polymer-Like Near-Infrared Bandgap Photoabsorbers**, M.S. Arnold, D.J. Bindl, M.-Y. Wu, M.J. Shea, University of Wisconsin Madison **INVITED**

We are pioneering the exploration of semiconducting carbon nanotubes as the light-absorbing components of polymer-inspired solar cells and photodetectors.[1-2] Carbon nanotubes are conjugated polymer-like materials with built-in long-range crystallinity that gives rise to exceptional charge and energy transport characteristics, strong light absorption tunable throughout the visible and near-infrared spectra, and outstanding stability in air. We have discovered how to efficiently harvest photogenerated charges and excitons from optically excited nanotubes by pairing them in donor / acceptor heterojunctions with more electronegative electron accepting semiconductors. In particular, semiconducting nanotubes form a type-II heterojunction with C60 fullerenes and C60 derivatives with energy offsets sufficient to drive electron transfer from the optically excited nanotubes to C60, with an internal quantum efficiency (QE) for exciton dissociation and charge transfer > 75%, for nanotubes of diameter < 1 nm and gaps > 1 eV. Thus, we have identified the nanotube / C60 materials pair as a promising basis for future nanotube-based light harvesting devices.

In order to further guide the implementation of nanotubes in devices, we have also characterized exciton transport in nanotube films and shown that excitons can migrate in films by two mechanisms: (i) over short distances of ~ 5 nm via slow inter-nanotube diffusion and (ii) potentially over much longer distances via rapid intra-nanotube diffusion. As a proof-of-principal, we have fabricated both bilayer and blended nanotube / C60 heterojunction devices, which are analogous to polymer solar cells with nanotubes taking on the role of the semiconducting “polymer”. Thus far, we have realized a peak external QE > 20% across 1000 – 1365 nm and a monochromatic power conversion efficiency of 7% at 1050 nm. Our results show that AM1.5G photovoltaic power conversion efficiency > 10% should be possible with future optimization of: (a) the nanotube bandgap (and diameter) distribution and (b) improved control over morphology.

[1] D. J. Bindl, M.-Y. Wu, M. S. Arnold, *Nano Letters* (2011).

[2] D. J. Bindl, A. S. Brewer, M. S. Arnold, *Nano Research* (2011).

4:00pm EN+TF-TuA7 **Understanding Vertical Stratification in Polymer:Fullerene Bulk Heterojunction Solar Cells**, M.D. Clark, Air Force Research Laboratory, M.L. Jespersen, University of Dayton Research Institute, B.J. Leever, Air Force Research Laboratory

In the bulk heterojunction architecture of polymer-based solar cells (PSCs), the separate acceptor-donor phases form a bi-continuous inter-penetrating network by simultaneous casting from solution with morphological control stemming from external parameters such as thermal annealing, co-solvent inclusion, and drying conditions. While such treatments enhance device performance, a fundamental understanding of vertical concentration gradients within the fabricated active layer has been limited. In an effort to understand such morphological changes, several reports have explored 3D bulk heterojunction nanostructure using electron tomography,¹ ellipsometry,² neutron scattering,³ and spectroscopic techniques.⁴ This work, however, has yielded somewhat contradictory conclusions about fundamental network development and the origin of emerging concentration gradients. For example, some studies reported nearly equal blends at the PEDOT:PSS surface of annealed samples,^{2,4c} while others found P3HT^{1,4a,4c} or PCBM^{3,4b,4d,4f} preferentially decorating the buried interface. Several groups^{2b,3,4c,4f} further reported annealing causes PCBM diffusion towards the exposed surface, suppressing as cast vertical composition gradients. However, Xu et al.^{4b} detected PCBM migration towards the PEDOT:PSS interface upon annealing, while Xue et al.^{4a} suggested PCBM diffusion away from both interfaces. Here we report a combined experimental and theoretical analysis of phase segregation. The vertical stratification within a P3HT:PCBM bulk heterojunction solar cell is examined by depth profiling using both x-ray photoelectron spectroscopy (XPS) and time of flight secondary ion mass spectrometry (ToF-SIMS), with the effects of thermal annealing and P3HT:PCBM ratio being explored. In addition, the vertical phase stratification is predicted on thermodynamic grounds based on measured interfacial energies of the PSC constituents. Using these results, a fundamental understanding of the thermodynamic driving force for bulk heterojunction phase segregation and vertical stratification is then presented.

References

1 van Bavel, S.S. et al. *Nano Lett.* **9**, 507 (2009).

2 (a) Germack, D.S. et al. *Macromolecules* **43**, 3828 (2010); (b) Campoy-Quiles, M. et al. *Nat. Mater.* **7**, 158 (2008).

3 Parnell, A.J. et al. *Adv. Mater.* **22**, 2444 (2010).

4 (a) Xue, B. et al. *J. Phys. Chem. C* **114**, 15797 (2010); (b) Xu, Z. et al. *Adv. Funct. Mater.* **19**, 1227 (2009); (c) Yu, B.-Y. et al. *ACS Nano* **4**, 833 (2010); (d) Vaynzof, Y. et al. *ACS Nano* **5**, 329 (2011); (e) Wang, H. et al. *Chem. Mater.* **23**, 2020 (2011); (f) Germack, D.S. et al. *Appl. Phys. Lett.* **94**, 233303 (2009).

4:20pm EN+TF-TuA8 **Novel, Single-Crystalline-like Silicon on Low-Cost, Flexible Substrates for High Efficiency Thin Film Photovoltaics**, V. Selvamani, P. Dutta, R. Wang, Y. Gao, M. Yang, G. Majkic, E. Galtysyan, University of Houston

Thin film photovoltaics (PV) is being pursued by several institutions as a lower cost alternative to crystalline wafer technologies. The use of much less materials and roll-to-roll continuous processing in thin film technologies have been touted as the pathway to low-cost PV. However, the efficiencies of production thin film Si solar cells are about one half that achieved with crystalline silicon. Hence, achievement of single-crystalline-like silicon photovoltaics on flexible, low-cost substrates can be game changing by combining high efficiency with low cost. We are developing such a technology by creation of an architecture that yields single-crystalline-like thin films even on polycrystalline or amorphous substrates. This technology has been very successfully demonstrated and being commercialized in the superconductor field and inserted in the U.S. electric power grid [1].

The enabler that we have employed in this work is a single-crystalline-like thin film template of MgO made by Ion Beam-Assisted Deposition (IBAD). Such IBAD films have been successfully employed as templates for epitaxial growth of cube-textured superconducting films on polycrystalline substrates with critical current densities as high as those achieved on single crystal substrates [1].

MgO templates made by IBAD on flexible metal substrate have been used for epitaxial growth of germanium films using intermediate oxide layers. All layers were deposited by reel-to-reel magnetron sputtering and strongly (400) textured Ge films with an in-plane texture spread of just 1° FWHM

were achieved [2]. Optical properties of the germanium films are found to be comparable to that single crystal Ge and Hall mobility values over 700 cm²/Vs have been achieved. Epitaxial (400) textured silicon films have been grown by reel-to-reel magnetron sputtering on the Ge films. A continuous grading of germanium to silicon has been done to accommodate for the lattice mismatch. While excellent epitaxial growth has been achieved in Si and Ge on flexible metal substrates, the defect density of the films showed a high value of 10⁸ per cm². Cross sectional TEM of the multilayer architecture showed concentration of threading dislocations near the semiconductor-oxide interface. Defect reduction strategies are being employed and recent progress in use of single-crystalline-like templates on low-cost, flexible substrates for high-efficiency silicon photovoltaics will be discussed in this presentation.

1. V. Selvamanickam et al. *IEEE Trans. Appl. Supercond.* **19** (2009) 3225.
2. V. Selvamanickam et al. *J. Crystal Growth* **311**, (2009) 4553.

4:40pm **EN+TF-TuA9 High-Efficiency Multijunction Solar Cells Employing Dilute Nitrides**, V.A. Sabnis, H.B. Yuen, M. Wiemer, Solar Junction **INVITED**

Concentrating photovoltaic (CPV) systems have the opportunity to provide the lowest cost of electricity in hot, sunny climates. The advantages of CPV are based, in part, from the high performance offered by multijunction solar cells made from group III-V compound semiconductors. Unlike traditional PV, high concentration systems utilize mm-scale solar cells that comprise only 10-15% of the overall system cost. This low cost share means that increasing cell efficiency has significant leverage in driving down upfront capital costs and the leveled cost of electricity of a CPV project.

Production cell efficiencies for triple junction solar cells have reached 40% under concentration (25°C, AM 1.5D spectrum). We will review a number of exciting approaches for increasing cell efficiency that are being investigated world wide. Solar Junction has developed a set of dilute-nitride compound semiconductors that offer broad bandgap tunability over the infrared while retaining lattice matching to GaAs and Ge substrates. While significant efforts have been undertaken to develop dilute nitrides for multijunction solar cells over the last 15 years, these approaches have resulted in films that exhibited poor minority carrier properties resulting in low current drives and output voltages. Solar Junction has developed a molecular beam epitaxy process utilizing antimony as a surfactant that significantly enhances the minority carrier properties. Triple junction cells utilizing GaInNAsSb bottom junctions have achieved a world record efficiency of 43.5% under concentration. When used in conjunction with well known InAlGaP and AlGaAs compounds, GaInNAsSb films complete a lattice-matched epitaxial platform for enabling 4-, 5-, and 6-junction cells for achieving > 50% efficiencies in the coming years.

5:20pm **EN+TF-TuA11 Non-Radiative Carrier Recombination in InGaAs/GaAsP Strain-Balanced Superlattice Solar Cell**, T. Aihara, University of Miyazaki, Japan

An inserting of the quantum wells (QWs) to GaAs p-i-n solar cells could be a promising candidate to solve the current matching issue in the multi-junction solar cells[1]. We have successfully obtained the non-radiative recombination process for excitonic and subband absorptions in the GaAs/AlAs multiple QWs (MQWs) by using PPT methods [2]. In this study, we investigate escape, radiative and non-radiative recombination mechanisms of photo-generated carriers in the strain-balanced InGaAs/GaAsP MQWs or superlattice (SL) inserted into GaAs p-i-n solar cell structure to improve the photovoltaic performance. We then evaluated above three processes by using the surface photovoltage (SPV), photoluminescence (PL), and piezoelectric photothermal (PPT) spectroscopies, respectively. A InGaAs/GaAsP MQWs absorbing layer that inserted into GaAs p-i-n junction was composed of 10 stacks of 7.4-nm-thick InGaAs well and 10.8-nm-thick GaAsP barrier. For SL absorbing layer, ultra-thin GaAsP barriers of 3.7 nm thickness with 0.56-nm-thick GaAs buffer were prepared. All the layers were grown by metal-organic vapor phase epitaxy on the GaAs substrate. The PPT detects a heat generated by the non-radiative recombination by the PZT directly attached to rear surface of the sample. Figures 1 and 2 show the temperature change of PPT spectra of MQWs and SL with GaAs thin buffer samples, respectively. For MQWs sample, three peaks were observed and A-peak was concluded to be due to the excitonic transition associated with the electron transition between first electron (e1) and heavy-hole subbands (hh1) in QW. On the other hand, B-peak was concluded to be the electron transition between 1st minibands in conduction and valence bands in SL. As the temperature decreased, peak intensities of A and B increased, whereas corresponding SPV peaks decreased. The temperature dependence of PL, PPT, and SPV signal intensities can be fitted with the Arrhenius equation. Figure 3 shows the fitting results of PPT A (MQWs) and B (SL) and SPV A peaks. As shown in Fig. 3, activation energy of SL was smaller than that of

MQWs. This result implied that carrier escape from the QWs was enhanced for the case of SL. References [1] K. W. J. Barnham and G. Duggan, *J. Appl. Phys.* **67** (1990) 3409. [2] P. Wang et al.: *Jpn. J. Appl. Phys.* **46** (2007) 6857.

5:40pm **EN+TF-TuA12 Piezoelectric Photothermal Spectra and Carrier Nonradiative Recombination in InGaAs/GaAsP Super Lattice Structured Solar Cells**, T. Ikari, T. Aihara, Y. Nakano, University of Miyazaki, Japan, Y. Wang, M. Sugiyama, Y. Nakano, University of Tokyo, Japan, A. Fukuyama, University of Miyazaki, Japan

Fabrication of multi quantum well (MQW) or superlattice (SL) structures embedded in an absorption layer of solar cell is a promising idea for developing higher efficient devices. This is because the quantum well can extend the absorption to longer wavelength region and enhance the short-circuit current. However, recombination centers for carriers are simultaneously generated at the boundaries, leading to the degradation of conversion efficiency. Although optical absorption and spectral response spectroscopy are usually used for investigating absorption and recombination mechanism in the solar cell, no direct technique for characterizing nonradiative recombination is presented. We have developed the piezoelectric photothermal (PPT) spectroscopy for detecting such nonradiative recombination in the QW [1]. Heat generated by a nonradiative recombination of photoexcited carriers were detected as PPT signal by using a piezoelectric transducer. In this paper, we report on the PPT spectra of InGaAs/GaAsP SL layer and show that this technique is sensitive and powerful to investigate the absorption spectra of SL. It is, then, becomes possible to discuss a recombination mechanism of the photo-excited carriers in the solar cell structure from the non-radiative transition point of view.

A strain-balanced InGaAs/GaAsP SL layer embedded into the intrinsic region of the GaAs p-i-n solar cell were prepared. The SL absorbing layer was prepared in the structure of InGaAs(3.7nm)/GaAsP(5.4nm) with 0.56-nm-thick GaAs buffer layer by MOVPE technique on the GaAs substrate [2]. PPT spectrum at 100K shows two dominant peaks. The conventional absorbance of SL and the PPT spectrum of the MQW (InGaAs(7.4nm)/GaAsP (10.8nm)) samples were also discussed for comparison. A signal from SL is more clearly observed in the PPT than the absorbance spectra. Although the step like signals accompanied with the exciton transition are well resolved for MQW samples, no step but broad peaks around 1.395 and 1.45 eV were observed for SL sample. The energies of these peaks were as expected from the calculation of the single QW without any interaction of the neighboring QW, i.e. tunneling. Since the wave function of quantized level spread into the next well for the SL structure, broad peaks were, then, observed. Although the step like density of states should appear even in the SL, drastic decrease of the PPT signal beyond the peak was observed. One possible reason is that the number of carriers that recombine nonradiatively inside the quantum well decreases by tunneling.

- [1] T. Ikari, et al., *Phys. Rev. B* **77** (2008) 125311.
- [2] M. Sugiyama et al.: *J. Cryst. Growth* **315** (2011) 1.

Thin Film

Room: 10 - Session TF+AS-TuA

Modeling and Analysis of Thin Films

Moderator: D. Irving, North Carolina State University

2:00pm **TF+AS-TuA1 Nanoconfined Fluids: Fundamentals and Application to Ionic-Liquid-Based Supercapacitors**, G. Feng, S. Li, P.T. Cummings, Vanderbilt University **INVITED**

Phase transitions in nanoconfined fluids have been contentious for two decades. In the 1980s and early 1990s a large number of surface force apparatus (SFA) experiments on a variety of ultrathin nonpolar liquid films (e.g., such as dodecane, cyclohexane and octamethylcyclotetrasiloxane (OMCTS)), reached a common conclusion: When their confinement between molecularly smooth mica sheets reached the order of several molecular diameters (approximately 3 or less, depending on the fluid being studied) they exhibited behavior typical of the stick-slip response of a crystalline solid structure.

In contrast to the solid-like behavior under extreme nanoconfinement, when the mica surface separation is sufficiently large, the confined fluid exhibits bulk-like liquid behavior. Thus, a phase transition as a function of separation must exist. In this talk, we review the two-decade-old debate on the nature of this phase transition (first order vs continuous), and its effective resolution using very high fidelity molecular dynamics simulations. In particular, the origin of the phase transition from fluid to solid-like behavior is, unexpectedly, driven by electrostatic interactions

between ions in mica and partial charges on the atoms in the nonpolar organic molecules.

More recently, our interest in nanoconfined fluids has focused on novel energy storage devices: electrical double layer (EDL) capacitors, also called supercapacitors. Supercapacitors have attracted considerable attention, owing to their desirable properties, such as high power density, high capacitance, and excellent durability. As emerging electrolytes for these supercapacitors, room-temperature ionic liquids (RTILs) have attracted considerable attention due to their wide electrochemical windows, excellent thermal stability, non-volatility, relatively inert nature, and high ionic conductivity. With high specific surface area and electrical conductivity, nanoporous carbon-based materials are the most widely used electrodes for supercapacitors, including activated carbons, templated and carbide-derived carbons (CDC). Using molecular simulations, model porous carbon electrodes (e.g., CDC), supercapacitors composed of slit-shaped micropores ranging in size from 0.67 nm to 1.8 nm in an IL were studied to investigate the dependence of capacitance on pore size. The capacitance was found to show an oscillatory behavior with pore size. In good agreement with experiment, we find that, as the pore shrinks from 1.0 nm to 0.7 nm, the capacitance of the micropore increases anomalously. The persistence of oscillations in capacitance beyond 1.0 nm is a new theoretical prediction currently being probed experimentally.

2:40pm TF+AS-TuA3 XPS Analysis of Monomolecular Films Prepared by Self-Assembly and Langmuir-Blodgett Techniques, G.G. Jernigan, F.K. Perkins, M.G. Ancona, A.W. Snow, Naval Research Laboratory

Characterization of self-assembled monolayers (SAMs) using x-ray photoelectron spectroscopy (XPS) measurements of the gold (4f) attenuation from increasing molecular length alkane thiols were pioneered by Bain and Whitesides[1]. Since then, the gold attenuation has been used by many others as a method for determining the length/thickness of molecular films formed as SAMs on gold. We have done similarly with carboxylic acid (COOH) terminated alkane thiols SAMs deposited on gold with the aid of additives[2], and we obtained similar results. We discovered, however, that the attenuation of the sulfur (2p) signal did not correspond with the gold attenuation. Additionally, neither the gold or sulfur attenuation could correctly account for the observed carbon (1s) signal in the XPS measurements. This fact was originally noted, but not addressed, by Bain and Whitesides.

In conjunction with experiments, we will present our successful solution to the modeling of XPS measurements of molecular films prepared by self-assembly and by the Langmuir-Blodgett (LB) technique. In a classic alkanethiol SAM, one third of the surface gold atoms, typically, are bound to a thiol-terminated molecule, due to the steric effect of a radial shell created by the molecule. Thus, the gold signal is only partially attenuated by the molecule. Use of the attenuation of the sulfur signal associated with the S-Au bond (obtained by fitting the XPS signal), we find that we are able to correctly determine the electron escape depth (λ) for sulfur and carbon through the molecular film. Using a poly(thiomethyl methacrylate) thin film as a carbon and sulfur XPS standard combined with the correct λ , we developed a model for the packing density and molecular orientation of COOH terminated alkane thiols that is consistent with gold, sulfur, and carbon XPS measurements as a function of molecule length. We have expanded our model to include SAMs formed of sterically crowded tertiary thiols, where fewer molecules per gold atom can attach to the surface, and to LB films formed from carboxylic acid terminated alkanes on gold surfaces, where no sulfur linkage is made. The consistent interpretation provided by our model will be presented at the talk.

[1] C.D. Bain and G.M. Whitesides, *J. Phys. Chem.* **93**, 1670 (1989).

[2] A.W. Snow, G.G. Jernigan, and M.G. Ancona, *Analyst* **136**, 4935 (2011).

3:00pm TF+AS-TuA4 The Dynamics of Atomic-Scale Transport on the Anisotropic Compound Surface TiN(001), D.G. Sangiovanni, V. Chirita, L. Hultman, Linköping University, Sweden, I. Petrov, J.E. Greene, University of Illinois at Urbana Champaign

We use classical molecular dynamics (MD) and the modified embedded atom method (MEAM) formalism to investigate the dynamics of atomic-scale transport on a low index anisotropic model compound, TiN(001). Our simulations, totaling 0.25 ms for each case study, follow the pathways and migration kinetics of Ti and N adatoms, as well as TiN_x complexes with x = 1, 2 and 3, all of which are known to contribute to the growth of TiN thin films by reactive deposition from Ti, N₂, and N precursors. The simulations

are carried out at 1000 K, a reasonable temperature for TiN(001) epitaxial growth. We find Ti adatoms to be the highest mobility species on TiN(001), with the primary migration path involving jumps of one nearest-neighbor distance d_{NN} between four-fold hollow sites along in-plane $\langle 100 \rangle$ channels. Long jumps, $2d_{NN}$, are also observed, but at much lower frequency. N adatoms exhibit much lower migration rates than Ti, diffuse only along in-plane $\langle 110 \rangle$ directions, and are unstable to associative formation of N₂ molecules which desorb at kinetic rates. As expected, TiN and TiN₃ complexes migrate at even lower rates with complex diffusion pathways involving rotations, translations, and roto-translations. TiN₂ trimers, however, are shown to have surprisingly high diffusion rates, comparable to that of Ti adatoms, due to, as revealed in our density functional theory (DFT) investigations, the significantly more symmetric charge transfer between trimer and terrace atoms, as compared with the charge distributions observed for dimers and tetramers.

4:00pm TF+AS-TuA7 Multi-Method Calculations of the Thermodynamics of Film Deposition on Fuel Rods in Light Water Reactors, D.W. Brenner, A.D. Dongare, C.J. O'Brien, North Carolina State University

INVITED

Corrosion products in light water reactors are driven to deposit on the fuel rods, which reduces their efficiency and lifetime. The thermodynamics and kinetics that lead to this deposition are notoriously difficult to characterize *in situ* experimentally due to the extreme conditions of temperature and radiation within the reactor, and the relationship of deposits studied *ex situ* to processes under reactor conditions is unclear. It is thought that deposition is related to bubbles that form at the surface of the fuel rods due to sub-cooled boiling, but further details are lacking. We have been using first principles methods combined with molecular modeling to understand the thermodynamic driving force for this deposition, including how pH, pressure, temperature, and aqueous versus semi-aqueous "bubble" environments affects this driving force. The results of these calculations, which include studies of solvated ions, clusters and solid surfaces containing Ni, Fe, O, B, C and H will be presented along with ideas for suppressing deposition based on these results. The broader implications of our calculations for understanding and controlling film deposition in various types of aqueous environments will also be discussed.

This research is supported by the Department of Energy

4:40pm TF+AS-TuA9 Toughness Enhancement in Transition Metal Nitride Thin Films by Alloying and Valence Electron Concentration Tuning, D.G. Sangiovanni, V. Chirita, L. Hultman, Linköping University, Sweden

Enhanced toughness in hard and superhard thin films is a primary requirement for present day ceramic hard coatings, known to be prone to brittle failure during *in-use* conditions, in modern applications. Based on the successful approach and results obtained for TiN- and VN-based ternary thin films [1,2], we expand our Density Functional Theory (DFT) investigations to TiAlN-based quaternary thin films. (TiAl)_{1-x}M_xN thin films in the B1 structure, with $0.06 \leq x \leq 0.75$, are obtained by alloying with M = V, Nb, Ta, Mo and W, and results show significant ductility enhancements, hence increased toughness, in these compounds [3]. Importantly, these thin films are also predicted to be hard/superhard, with hardness values comparable to TiAlN. For (TiAl)_{1-x}W_xN these results have been experimentally confirmed [4]. The general, electronic mechanism responsible for the ductility increase is rooted in the enhanced occupancy of d-t_{2g} metallic states, induced by the valence electrons of substitutional elements (V, Nb, Ta, Mo, W). This effect is more pronounced with increasing valence electron concentration (VEC), and, upon shearing, leads to the formation of a layered electronic structure, consisting of alternating layers of high and low charge density in the metallic sublattice. This unique electronic structure allows a selective response to tetragonal and trigonal deformation: if compressive/tensile stresses are applied, the structure responds in a "hard" manner by resisting deformation, while upon the application of shear stresses, the layered electronic arrangement is formed, bonding is changed accordingly, and the structure responds in a "ductile/tough" manner, as dislocation glide along the {110}<1-10> slip system becomes energetically favored [2]. The findings presented herein open new avenues for the synthesis of hard, yet tough, ceramic coatings, by tuning the VEC of alloying elements to optimize the hardness/toughness ratio in relevant applications.

[1] D. G. Sangiovanni et. al. *Phys. Rev. B* **81** (2010) 104107.

[2] D. G. Sangiovanni et. al. *Acta Mater.* **59** (2011) 2121.

[3] D.G Sangiovanni et. al. *Thin Solid Films* **520** (2012) 4080.

[4] T. Reeswinkel et. al. *Surf. Coat. Technol.* **205** (2011) 4821.

5:00pm **TF+AS-TuA10 Non-Destructive Element Specific Density Depth Profiling by Resonant Soft X-ray Reflectometry**, *S. Macke*, Max Planck - UBC Centre for Quantum Materials, Canada, *A. Radi*, University of British Columbia, Canada, *R. Sutarlo*, Canadian Light Source, Canada, *G. Christiani*, *G. Logvenov*, Max-Planck-Institute for Solid State Research, Germany, *G. Sawatzky*, University of British Columbia, Canada, *B. Keimer*, Max-Planck-Institute for Solid State Research, Germany, *V. Hinkov*, Max Planck - UBC Centre for Quantum Materials, Canada

X-ray resonant reflectometry (XRR) is the ideal tool to study the depth resolved and element-specific electronic structure of multilayer films. Besides the structural parameters of thin films like thicknesses and roughnesses one is sensitive to the dielectric tensor of the film which allows to retrieve depth profiles of the magnetic, orbital[1] and valence configuration.

Due to the complex physics of reflectometry this measurement method needs sophisticated tools to analyze the results quantitatively [2]. The issues arising with this method are addressed and discussed.

By changing angle, energy and polarization of the incoming beam complete reflectivity maps can be measured leading in principle to an accurate picture of the depth resolved electronic states of thin films. The standard model used in reflectometry is based on compound layers with a defined thickness, roughness and dielectric tensor. But such a simple model is usually not capable to reproduce a full measured reflectivity map. The main reasons are especially contaminations, additional oxide layers and interdiffusion between layers.

However, introducing a layer system based on the element specific atomic density and scattering factors instead of dielectrics tensors allows more degrees of freedom for the system and allows to reproduce the reflectivity maps. Thereby the advanced model is capable to retrieve the element specific density profiles of thin films.

The method is introduced by analyzing a simple film of PrNiO₃ grown on an LSAT substrate. The reflectivity map is measured from 500eV to 1100eV.

[1] E. Benckiser et al., Nature Materials 10, 189 (2011)

[2] ReMagX, www.simulationcorner.net/ReMagX/

5:20pm **TF+AS-TuA11 Monte Carlo Radiation Model for Heat Transfer of Lamp for Advanced Thermal Annealing Process**, *K. Bera*, *J. Ranish*, *U. Kelkar*, Applied Materials, Inc.

Advanced thermal annealing process of semiconductor wafer uses lamp heating, specially for rapid thermal oxidation, silicidation, ion-implant anneal and spike anneal. As the technology node shrinks and the wafer size increases, wafer temperature uniformity becomes significant. The thermal modeling challenge includes complexity of the lamp filament and chamber configuration, and complex optical properties of semitransparent media. In order to analyze lamp heating, two-dimensional Monte-Carlo based radiation, and thermal conduction model for a single lamp is built using CFD-ACE+. The Tungsten lamp filament is immersed in Nitrogen. The single lamp is enclosed by a reflector, and protected at the top by a quartz plate. For the single lamp thermal model, effective surface area and volume of the coil are considered. The irradiance profile of the lamp at a distance of a few cm from the quartz plate compared well with the experimental data. The single lamp model is simplified using a cylindrical filament structure that matches the irradiance profile. The cylindrical filament structure is used in 3D chamber model that considers thermal convection in addition to radiation and conduction. In both single lamp and chamber models, for semi-transparent non-gray media, wavelength dependent real and imaginary parts of refractive indices are used in optical database to calculate thermal absorption. For gray material, surface emissivity of the material is defined. For reflective material, the degree of specularity on the surface is defined as well. For gas conduction, temperature dependent thermal properties are used. The single lamp power is varied by several hundreds of Watts. The irradiance profile shows a peak at the center that decays substantially as we move radially outwards. The effect of quartz plate thickness on irradiance profile is evaluated. The chamber model is used to determine wafer temperature distribution and transient thermal response for a range of lamp assembly power.

5:40pm **TF+AS-TuA12 First Principles Studies of Oxygen Transfer at Buried Metal/Metal Oxide Interfaces**, *C. Goldstein*, *E. Mily*, *J.-P. Maria*, *D.W. Brenner*, *D. Irving*, North Carolina State University

Heterogeneous material interfaces between metals and metal-oxides provide a unique opportunity to create active functional materials. The functionality of these heterostructures can hinge either on limiting or enabling oxygen transfer across the interface. For example, there has been recent research on how to use thin film metal/metal-oxide super-structures to control the power output generated by the exothermic exchange of oxygen across the as-deposited interface. In all of these heterogeneous systems, it is imperative to

fundamentally understand the mechanisms that facilitate oxygen exchange, as the dynamics are not currently well understood. In the work presented here, chemically accurate Density Functional Theory calculations have been used to predictively determine likely reaction pathways for oxygen transport in energetic nanocomposite materials and to characterize the stability of novel heterogeneous material interfaces. Our ultimate goal is to tune power output through an understanding of the mechanisms of oxygen transport across heterogeneous interfaces and within the super-structure. Several systems have been investigated, including more traditional thermite materials such as Al and Ti paired with Cu₂O. In these systems, the energy release is large, but there is also a high degree of strain when ideal systems are modeled. Other model systems were chosen based on structural similarity, minimal lattice mismatch, and the degree of exothermicity associated with oxygen transfer. Results on these systems will also be presented. Preliminary calculations simulate systems at various early stages to isolate factors that could influence the reaction, such as strain or initial barrier height. The results presented here show qualitative agreement between calculations and experimental observations. This project has been supported by the Army Research Office through grant # W911NF-10-1-0069 and the NSF Graduate Research Fellowship Grant # DGE0750733.

Thin Film

Room: 11 - Session TF2-TuA

ALD for Hybrid Films and Bioapplications

Moderator: S.M. Rossnagel, IBM T.J. Watson Research Center

2:00pm **TF2-TuA1 Characteristics of Nanomaterials Embedded in Atomic Layer Deposition Thin Films**, *J.S. Jur*, *P.J. Krommenhoek*, *J.C. Halbur*, North Carolina State University, *H.O. Everitt*, Duke University, *J.B. Tracy*, *G.N. Parsons*, North Carolina State University

Atomic layer deposition (ALD) is demonstrated as a method to fabricate NP embedded thin films, and provides new opportunities to alter the characteristic properties of nanomaterials. This work examines conducting and semiconducting ALD materials growth on nanoparticles and nanowires for opportunities to alter the optical behavior and conductive behaviors of nano-enabled materials. For example, gold nanoparticles (15 nm diameter) are embedded into dense inorganic zinc oxide nanofilms deposited by atomic layer deposition onto a fibrous textile template. By changing the dielectric field surrounding the nanoparticle with the ALD ZnO, the surface plasmon resonance is dampened, resulting in significant changes to the optical absorption behavior of the textile. The alteration of the surface plasmon resonance is examined with increasing nanoparticles concentration on the fiber surface and with increasing ALD coating thickness. For example, the absorption at 900 nm is enhanced by up to 4.8x for a 45 nm ZnO ALD coating. Minimal increase in absorption is observed with additional ZnO growth. Cathodoluminescence evaluation of ZnO ALD on Au nanoparticles -loaded nylon-6 produces a ~65% decrease in the defect luminescence and a corresponding ~80% increase in the band edge luminescence. In addition, an analysis of the electrical properties of nanoparticle and nanowire embedded ALD thin films are provided. Using externally fabricated nanomaterials and embedding them in ALD thin films offers the ability to study and understand near surface interactions that can alter the characteristics of the nanomaterials.

2:20pm **TF2-TuA2 ALD-Based Fabrication and Chromatographic Separations on Binder-Free, Carbon Nanotube-Templated Thin Layer Chromatography Plates**, *M.R. Linford*, *R.C. Davis*, *D.S. Jensen*, *S. Kanyal*, Brigham Young University, *M.A. Vail*, *A.E. Dadson*, Diamond Analytics

We recently reported the use of patterned carbon nanotube (CNT) forests as scaffolds for the microfabrication of silica-based thin-layer chromatography plates (TLC) (*Advanced Functional Materials* 2011, 21(6), 1132 – 1139). In this fabrication, CNTs were infiltrated by low pressure chemical vapor deposition of silicon using SiH₄, which was then oxidized and hydrated. Thorough characterization by RBS, XPS, TEM, SEM, and ToF-SIMS has been performed on these materials, which has given us a considerable understanding of them, e.g., the structure of the Si/SiO₂/Al₂O₃(30 nm)/Fe(6 nm) stack deposited prior to CNT growth has been confirmed, multiwall CNTs are grown in our process, CNT growth is base (bottom up) and not tip (top down), the thickness of the Fe catalyst layer plays a key role in the fabrication of our plates – when the catalyst layer is too thick CNT structures are unstable, etc. Fast and efficient separations were demonstrated on these plates.

Nevertheless, the oxidation of silicon in these materials leads to a volume expansion of the support, which appears to affect the A-term of the van

Deemter equation in our separations. That is, distortions in the material appear to adversely affect separations performed on them. Accordingly, we have now shown that TLC plates can be fabricated by (i) priming patterned nanotube forests with a few nanometers of amorphous carbon, followed by a layer of Al₂O₃ deposited by atomic layer deposition (ALD), (ii) deposition of SiO₂ in a fast (pseudo) ALD of this material, and (iii) oxidizing at a lower temperature (ca. 600 K) than was used previously to remove the CNTs. An amino bonded phase was created. The resulting TLC plates show 125,000 – 225,000 N/m in a baseline separation of four fluorescent dyes. An even more recent and newly developed microfabrication method in our laboratory of CNT-templated TLC plates also shows fast separations with 400,000 – 500,000 N/m in preliminary results. These separations rival (or exceed) those of HPLC/UPLC in both speed and efficiency. Separations of biological interest will be shown.

4:00pm **TF2-TuA7 Conductivity and Mechanical Stretching of Conductive ALD Coatings on Nonwoven Fiber Mats**, *W.J. Sweet, C.J. Oldham, G.N. Parsons*, North Carolina State University

Advanced sensing, responsive and protective electronic systems integrated with fibers and flexible textile media may lead to new solutions for functional device deployment and integration. A challenging aspect of conductive coatings on fibers is the observation that most good conductors, including doped metal oxides or metallic films, are not readily flexible when coated in thin film form onto polymer fibers. For this work, we use atomic layer deposition (ALD) to produce conformal coatings of conductive ZnO, Al:ZnO and others on complex nonwoven polypropylene and nylon fibers. We measured conductivity of the as-formed coated fibers as a function of deposition temperature and other process parameters. We also measured the mechanical response of the coated and uncoated fiber mats, including measuring the change in conductivity upon fiber mat stretching. We find that in all materials measured to date, the conductivity of the fiber mat decreases with increasing applied tensile stress. For example, for Al-doped ZnO on nylon deposited at 115°C, we obtained fiber mats with conductivity of 33 S/cm, and after a 10% strain, the conductivity drops to ~3.3 S/cm. Generally, the largest conductivity decrease occurs for the materials that are most conductive to start. However, results indicate a correlation between some process parameters, such as deposition temperature, and conductivity resiliency, showing possible directions to attain highly flexible and reliable conductive material integration. In this presentation we will summarize our results regarding mechanical resiliency and conductivity and identify key parameters needed to achieve stretchable fibers that are also highly conductive.

4:20pm **TF2-TuA8 Molecular Layer Deposition of Alucones and Zincones Using Hydroquinone**, *Y. Lee, S.M. George*, University of Colorado, Boulder

Alucones and zincones are metal alkoxide polymer films that can be grown using molecular layer deposition (MLD) techniques. In this study, alucones and zincones were grown using trimethylaluminum (TMA) and diethylzinc (DEZ) as the metal precursors and hydroquinone (HQ) as the organic reactant. HQ is an aromatic diol that has a rigid structure with a central benzene ring. The benzene ring may lead to interesting electrical conductivity and the rigid structure may help to avoid “double reactions”. Quartz crystal microbalance measurements and X-ray reflectivity (XRR) studies were employed to examine film growth. Individual mass gains after the TMA and HQ exposures were consistent with a TMA:HQ stoichiometry of 4:3 in the MLD film. This TMA:HQ stoichiometry suggests the presence of Al₂O₃ dimeric core species. In comparison, individual mass gains after the DEZ and HQ exposures were consistent with a DEZ:HQ stoichiometry of 1:1 in the MLD film. XRR studies measured growth rates at 150°C of 2.6 Å/cycle for TMA/HQ and 2.7 Å/cycle for DEZ/HQ. The alucone and zincone MLD films were also annealed in air at temperatures up to 350°C. There is evidence that the benzene rings polymerize after heating to 200°C. The films turn brown and a strong absorbance observed at ~320 nm is consistent with an expanded π -conjugated system. The polymerization of the benzene rings should change the mechanical properties of these annealed MLD films. Alucone and zincone films were also grown using tetrafluorohydroquinone to observe the effect of fluorination of the benzene ring.

4:40pm **TF2-TuA9 Organic-Inorganic Hybrid Thin Films Prepared by Ozone Assisted Molecular Layer Deposition (MLD)**, *J. Huang, M. Lee, A.T. Lucero, J. Kim*, The University of Texas at Dallas

Recently, organic thin films have been attracting attentions due to their flexibility and transparency which are suitable for large-scale display and flexible electronics applications. Alternatively, inorganic thin films have several benefits over organic thin films such as high functionality (e.g. high conductance, high dielectric constant or high polarization, etc). Potentially, organic-inorganic hybridization can widen the range of their applications, for both worlds, with new functionalities. A novel technique has been

reported using a modified atomic layer deposition (ALD) method, named molecular layer deposition (MLD), which can be applied to build an organic and inorganic hybrid stack. Hybrid thin films by MLD minimized the formation of defects during the growth of the organic and inorganic layers because they are deposited by sequential, self-limiting surface reactions similar to ALD process.

In this study, we investigated the growth characteristics of organic-inorganic laminates. We focused on 7-octenyltrichlorosilane (7-OTS) and metal-oxide hybrid thin film, using ozone based MLD. 7-OTS is deposited by an exchanging reaction between functional group and water. The terminal vinyl group (C=C) of 7-OTS is converted into a carboxylic group (-COOH) through in-situ ozone (O₃) modification. Metal oxide is then deposited as a linker layer in-between of each OTS layers using conventional ALD precursors, such as diethyl zinc (DEZ) and water. We found out that MLD process is kinetically control, which mean for a very limited of time, if we need organic molecules to form chemical bonding on top of certain surface, some special process would be required. In our experiment, we used repeating pulse to get a good coverage of organic molecules. Besides, effect of depositing temperature, dosing time, even in-situ UV activation with variety of time, location and power will also be discussed.

Characterization of organic-inorganic hybrid thin films have been extensively investigated using transmission electron microscopy (TEM), scanning electron microscopy (SEM), atomic force microscopy (AFM), X-ray diffraction (XRD), X-ray photoelectron spectroscopy (XPS) and Fourier transform infrared spectroscopy (FTIR). Electrical characteristics of the hybrid films will also be reported.

This research is partially funded through Korea-US collaboration R/D program by MKE-COSAR-KETI.

5:00pm **TF2-TuA10 Organic-Inorganic Hybrid Structure Formation via Sequential Vapor Infiltration**, *H. Akyildiz, M. Yokus, R.P. Padbury, J.S. Jur*, North Carolina State University

Hybrid film formation onto polymer surfaces during atomic layer deposition (ALD) has inspired a number of processing schemes that promote precursor infiltration to increase the extent of hybrid reaction. These hybrid materials have shown opportunity in mechanical, electronic, biomedical and catalytic applications. In this work we utilize a sequential vapor infiltration (SVI) process, defined by subsets of consecutive precursor exposures, to understand the minimum precursor exposure required to saturate the formation of the hybrid material. As a test system, we examine consecutive exposures of trimethylaluminum followed by a H₂O exposure onto polyamide 6 (PA6). We investigate the effect of temperature, pressure, and exposure time on the mass change of high surface area PA6 fabrics (3 m²/g). A saturation in the mass increases is reached after ~10 TMA (0.2 sec dose, 30 sec hold) exposure cycles, resulting in a ~14 wt% increase at 30 °C and 1.5 wt% increase at 150 °C. Cross-sectional transmission electron microscopy shows a conformal surface modification of ~75 nm at 60 °C. The influence of water resident in the PA6 is examined by conducting a 120 °C *in situ* anneal prior to SVI processing, which results in a decreased of ~4 wt % at lower exposure temperatures. Still, the total mass increase is inversely proportional to temperature. A reaction-diffusion mechanism for the precursor penetration is proposed that considers a decrease in diffusion with an increased extent of reaction near the outer surface of the fiber. Application of these hybrid modifications to the mechanical and dielectric properties of the fabric is explored.

Tuesday Afternoon Poster Sessions

Spectroscopic Ellipsometry Focus Topic

Room: Central Hall - Session EL+TF+AS+EM+SS-TuP

Spectroscopic Ellipsometry Poster Session

EL+TF+AS+EM+SS-TuP1 Ellipsometric Characterization of Iron Pyrite (FeS₂) and Samarium Sesquisulfide (Sm₂S₃) Thin Films. A. Sarkar, N.J. Ianno, University of Nebraska-Lincoln, J.R. Brewer, Rare Earth Solar

Iron pyrite (FeS₂) and samarium sesquisulfide (Sm₂S₃) are transition metal chalcogenides characterized as absorbing semiconductors with bandgaps of 0.95 eV and 1.8 eV respectively. Synthesis of both *n*-type and *p*-type samples have been reported in the form of single crystals and thin films for both materials. As a result of these properties they have received considerable interest as photovoltaic absorber materials. We present the characterization of FeS₂ and Sm₂S₃ thin films using spectroscopic ellipsometry. FeS₂ thin films were synthesized by sulfurizing DC magnetron sputtered iron films and reactive ion sputtered iron (III) oxide films in H₂S / Ar atmosphere. Sm₂S₃ thin films were synthesized by reactive ion sputtering of Sm in an H₂S / Ar atmosphere. This analysis gives the optical properties of chalcogenide films from near-UV (300 nm) to the mid-IR (20 μm). This can then be correlated to the structural and electronic properties as well. The analysis is corroborated with results obtained from Raman spectroscopy, scanning electron microscopy, profilometry, X-ray diffraction (XRD), and Van der Pauw measurements. The ellipsometric results can be used to access different processing methods for synthesizing FeS₂ and Sm₂S₃, to determine the presence of different phases and intermediate products. This work will lay the foundation for employing *in situ* ellipsometry as a process monitor and quality control tool during manufacture of earth abundant chalcogenide thin films.

EL+TF+AS+EM+SS-TuP2 Temperature Dependence of the Dielectric Function of Germanium by Spectroscopic Ellipsometry. A.A. Medina, L.S. Abdallah, S. Zollner, New Mexico State University

Germanium has important applications in photovoltaics as a substrate for III/V triple-junction solar cells, especially in space vehicles and for terrestrial concentrator-based applications. Unfortunately, the optical properties of germanium (complex refractive index and absorption coefficient) and their temperature dependence (important to consider the effects of the space environment or the radiation-induced heating in concentrators) are not as well known as for silicon, which limits the accuracy of modeling for solar cells and Ge-based optical interconnects. In this work, we report precision measurements of the complex refractive index of germanium from 0.5 to 6.6 eV at room temperature using variable-angle spectroscopic ellipsometry. To improve accuracy, especially at photon energies below 2 eV, we used a Berek waveplate compensator. By cleaning a commercial Ge wafer in isopropanol followed by deionized water, we were able to reduce the native oxide thickness to 1.3 nm. Heating the wafer in UHV at 700 K did not reduce the oxide thickness further. (The oxide thickness can be determined with precision measurements of Δ below the band gap on a single-side polished wafer.) From the ellipsometric angles of the Ge wafer measured at three angles of incidence (65, 70, and 75°), we calculated the dielectric function from 0.5 to 6.6 eV, by correcting for the effects of a native oxide.

Mounting our wafer in a compact UHV cryostat allowed temperature-dependent measurements from 80 to 700 K at 70° angle of incidence. Using similar methods as described above, we determined the dielectric function at different temperatures. We also determined the critical-point parameters (amplitude, energy, phase angle, and broadening) of the E_0 , E_1 , $E_1+\Delta_1$, E_0' , and E_2 critical points as a function of temperature. To separate the non-resonant contributions from the critical-point line shapes, we calculated the second derivative of the dielectric function with respect to photon energy and fitted the result to analytical line shapes with two-dimensional critical points. In general, our results are in good agreement with those of Viña *et al.* However, our results cover a wider spectral range and are more accurate because of the use of a compensator. Work is in progress to form thermal oxides on Ge wafers by annealing in oxygen, which will allow a multi-wafer analysis for Ge similar to work on Si by Herzinger *et al.*

This work was supported by NSF (HRD-0803171 and DMR-11104934) and the New Mexico Louis Stokes Alliance for Minority Participation.

Reference: L. Viña, S. Logothetidis, M. Cardona Phys. Rev. B **30**, 1979 (1984).

Wednesday Morning, October 31, 2012

Electronic Materials and Processing

Room: 9 - Session EM+TF-WeM

Hybrid Electronic Materials and Interfaces

Moderator: M.R. Linford, Brigham Young University, A.J. Muscat, University of Arizona

8:00am **EM+TF-WeM1 Versatile Electron Beam Chemical Lithography on the Basis of Monomolecular Films, M. Zharnikov, University of Heidelberg, Germany** **INVITED**

The talk reviews recent progress in Electron Beam Chemical Lithography (EBCL) on the basis of monomolecular templates provided by self-assembled monolayers (SAMs). Due to the monolayer thickness of SAMs and molecular size of their structural building blocks, patterning down to few nanometers is in principle possible. Depending on the architecture of the SAM constituents, different EBCL strategies can be used [1]. In the case of aromatic backbone, selective modification of specific tail groups at the SAM-ambient interface can be exploited [1]. In the case of aliphatic backbone, irradiation-promoted exchange reaction between the molecules in the primary SAM and potential molecular substituents can be used [2]. A further promising technique within the EBCL framework is Electron Beam Activation Lithography which involves activation of the amino tail groups of the primary SAM template disabled by specific quencher moieties [3]. This method is especially useful for the fabrication of morphological patterns. EBCL can also be adapted for biological applications, based on protein-repelling templates [4]. One can either perform a direct writing in such a template, which can be both SAM-based and polymer-like, or apply irradiation-promoted exchange reaction with well-controlled parameters. Using the above techniques, chemical patterning and surface engineering on the length scale ranging from cm to nm can be performed. Not only simple dot or stripe structures, but complex gradient-like and biology-inspired patterns can be fabricated as will be demonstrated by representative examples.

[1] M. Zharnikov and M. Grunze, *J. Vac. Sci. Technol. B* **20**, 1793-1807 (2002).

[2] N. Ballav, S. Schilp, and M. Zharnikov, *Angew. Chem. Int. Ed.* **47**, 1421-1424 (2008).

[3] S. Schilp, N. Ballav, and M. Zharnikov, *Angew. Chem. Int. Ed.* **47**, 6786-6789 (2008).

[4] N. Ballav, H. Thomas, T. Winkler, A. Terfort, and M. Zharnikov, *Angew. Chem. Int. Ed.* **48**, 5833-5836 (2009); *Nature*, **460**, 308 (2009).

8:40am **EM+TF-WeM3 Covalently Linked Organic Monolayers on Silicon Surfaces: Making Them Better, Stronger, Faster!, H. Zuilhof, Wageningen University, Netherlands**

Covalently linked organic monolayers on silicon surfaces provide a prime example of hybrid electronic materials. Such systems are required on the one hand to passivate the Si surface, and on the other hand provide an optimal electrical link between the bulk of the Si semiconductor and the liquid with which it interacts.

To obtain an optimal passivation a highly dense monolayer is required, and we present novel agents and methods that yield a denser formation of the monolayers. At the same time monolayer formation can be made faster, which reduces the chance for competing silicon oxide formation. Finally, this combination of properties is desired for really thin monolayers, which drives research to allow attachment of small molecules. The paper will present a combination of such newly developed methods, properties of the resulting monolayers and an approach for further systematic improvements.

9:00am **EM+TF-WeM4 Probing the Intrinsic Organic/Semiconductor Interface, W. Peng, O. Seitz, R. Chapman, University of Texas at Dallas, E.M. Vogel, Georgia Institute of Technology, Y.J. Chabal, University of Texas at Dallas**

The electronic properties of organic/semiconductor interfaces are crucial for a variety of applications, such as organic dielectrics and organic/inorganic hybrid solar cells. However, the accurate characterization of these interfaces is prevented by the large tunneling current through the molecular layer. Moreover, standard fabrication methods, such as the formation of top metal contact via evaporation, cause damages during the processing even if applied directly with extreme caution. We present here a novel method to protect the interface with a layer of high- κ dielectric (Al_2O_3) gently deposited on top of the organic layer using atomic layer deposition. The metal precursor reacts with the carboxylic head group of the self-assembled

monolayer (SAM) layer without affecting the underlying SAM/Si interface. Due to the increase of the dielectric layer thickness ($\text{SAM}+\text{Al}_2\text{O}_3$), a large reduction in tunneling leakage current occurs, and conductance voltage measurements can be implemented with a mercury probe setup. Moreover, the gate stack shows enough robustness to survive the entire MOS capacitor fabrication. Capacitance voltage measurements show small frequency dispersion and a low D_{it} , on the order of $10^{11} \text{ cm}^{-2}\text{eV}^{-1}$, for the intrinsic SAM/Si interface demonstrating inherent high quality when it is protected by the Al_2O_3 layer.

9:20am **EM+TF-WeM5 Towards Organic Electronics: Methods for the Selective Deposition of Semiconductors and Metals, J. Yang, Z. Shi, K. Borner, A.V. Walker, University of Texas at Dallas**

We describe recent progress in our laboratories to build robust complex two- and three-dimensional molecular constructs. This work has important applications in photovoltaics, molecular and organic electronics, sensing, photonics and other technologies. Several recent developments are discussed including the chemical bath deposition of PbS, the UV photoassisted chemical vapor deposition of Al, and the formation of Ni and Cu nanowires on micron-scale patterned surfaces. Optimization and further development of these techniques requires a detailed understanding of the reaction pathways involved in the interaction of organic thin films with metals, organometallic compounds, ions, and other compounds.

9:40am **EM+TF-WeM6 Electroless Deposition of Co on SiO_2 Surfaces Modified by an Aminosilane Self-Assembled Monolayer, R. Jain, A. Ng, E. White, A.J. Muscat, University of Arizona**

As device interconnects continue to shrink in size, the formation of diffusion barriers between dielectric and metal surfaces becomes more difficult. Self-assembled monolayers (SAMs) can be used to chemically activate a variety of surfaces, and their potential for uniform and defect-free monolayer formation makes them attractive alternatives for barrier layers. SAMs can also serve as adhesion layers to promote the electroless deposition (ELD) of metals on some dielectric surfaces. A 3-aminopropyltrimethoxysilane (APTMS) SAM was formed on a well-hydroxylated SiO_2 surface and studied as a function of solvent (methanol, IPA, and toluene), APTMS concentration (5.72 mM and 57.2 mM), and post-deposition rinsing in methanol, IPA or chloroform depending on the solvent used. An aminopropylsilane monolayer with a thickness of $7.8 \pm 0.2 \text{ \AA}$ and roughness of $3 \pm 1 \text{ \AA}$ was formed at an APTMS concentration of 5.72 mM in methanol and IPA, but multilayers were formed in toluene, which were deposited at a rate of $0.4 \pm 0.06 \text{ \AA/min}$ and roughness of $31 \pm 18 \text{ \AA}$. The N 1s XPS peak at a binding energy (BE) of 398.8 eV verified that a primary amine group ($-\text{NH}_2$) was present together with an equal coverage of protonated amine ($-\text{NH}_3^+$). Based on N 1s XPS peak areas, the molecular density of the aminopropylsilane monolayer was $4.2 \pm 0.6 \text{ molecules/nm}^2$, which is about equal to the accepted value of the OH group density on the Si surface. ELD processes are known to be sensitive to surface termination and require a metal catalyst, such as palladium, to activate the surface. A layer of Pd atoms was deposited by immersing the APTMS SAM surfaces in an 80 mM $\text{PdCl}_2\text{-HCl}$ solution for 2 min, yielding one Pd atom bonded to two amine groups based on XPS peak areas. These results suggest that Pd atoms are bonded to primary amines rather than protonated amines resulting in a coverage of half of the N sites. Cobalt was plated by immersing the Pd-coated surface in a solution of 0.05 M CoSO_4 , 0.2 M dimethylaminoborane (DMAB), and 0.01 M diethylenetriamine (DETA). Cobalt replaced the Pd atoms on the surface depositing a seed layer that auto-catalytically yielded a thick cobalt film on the surface. The thickness of the Co increased with the deposition time as verified by both the Co 2p peak at a BE of 777.2 eV and attenuation of the Si 2p peak with time. These results demonstrate that an aminopropyl silane adhesion layer binds metals such as Co. The next step is to test the effectiveness as a diffusion barrier.

10:40am **EM+TF-WeM9 Polymer-Colloidal Nanocrystal Hybrid Materials for Photovoltaic Applications, J. Xue, R. Zhou, P.H. Holloway, University of Florida** **INVITED**

Hybrid photovoltaic (PV) cells based on conjugated polymers and colloidal inorganic semiconductor nanoparticles have attracted significant attention as an alternative for all-organic solar cells. However, so far the highest efficiencies for hybrid PV cells have been limited to 2-3%, significantly lower than that of all-organic PV cells. One main reason for the lower performance is attributed to the complex interfaces and surfaces involving the inorganic nanocrystals.

Here we report our recent work that significantly improves the efficiency of hybrid PV cells to the 5% level. First, a 30-70% increase in the device efficiency was achieved by incorporating a solution-processed ZnO nanoparticle layer between the active layer and the cathode. This was

attributed to a combination of electronic, optical, chemical, and morphological effects, including blocking leakage of photogenerated holes to the cathode, optimizing the optical intensity profile in the hybrid active layer, minimizing recombination or quenching of photogenerated excitons and charge carriers. Maximum power conversion efficiencies of 2.5% and 3.5% were achieved with a high-gap polymer P3HT and a low-gap polymer PCPDTBT, respectively. The incorporation of the ZnO nanoparticle layer also drastically improves the stability of the hybrid PV cells.

We further demonstrated another 30-50% improvement in the efficiencies of hybrid PV cells by treating the hybrid active layer in an acetonitrile solution with 1% ethanedithiol (EDT). This leads to a maximum efficiency of ~5.0% for the EDT-treated hybrid PV cell with a PCPDTBT:CdSe nanorod active layer. Detailed characterizations of the hybrid active layers before and after the EDT treatment revealed no appreciable differences in their morphology and absorption spectra; however the phosphonic acid organic ligands on CdSe nanocrystals are more completely removed, and an improved electron mobility was obtained upon EDT treatment. We attribute the enhanced efficiency to more complete removal of exciton/charge recombination centers and the subsequent atomic layer passivation of the CdSe nanorod surface.

11:20am **EM+TF-WeM11** **Obtention of Deterministic Patterns through Wrinkling Formation**, *J.L. Yague, J. Yin, D. Eggenstiele, M.C. Boyce, K.K. Gleason*, Massachusetts Institute of Technology

Formation of wrinkles through buckling of a stiff coating on a compliant substrate can be found very commonly in nature. For instance, the epidermal ridges, which form our fingerprints, show a very unique pattern due to out-of-plane bending of the epidermis. The use of wrinkling to obtain patterned surfaces has become increasingly significant for a wide range of applications, such as: microfluidic, tunable wettability, stretchable electronics, photonics or anti-fouling surfaces. In this work, we demonstrate the ability to obtain labyrinth and herringbone patterns using a 2D stretching-releasing approach.

On top of a compliant substrate, an acrylate-based polymer is deposited by initiated chemical vapor deposition (iCVD). iCVD is a solvent-free method that yields a conformal thin coating on virtually any substrate, giving a controllable thickness and tunable structural, mechanical, thermal, wetting, and swelling properties. Monomer together with an initiator is introduced into a reactor chamber under vacuum, where the initiator is decomposed over resistively heated filaments to obtain radicals. Radicals and monomer are then adsorbed on a surface, which is kept at a controlled temperature to promote adsorption, to yield the polymer by the classical free-radical mechanism. Here, deterministic herringbone patterns are achieved through wrinkling of the polymer thin film. Furthermore, a simplified theoretical model is developed to predict the geometry of the ordered herringbone pattern. Depending on the experimental conditions is possible to control the features of such pattern. We report, for first time, the obtention of herringbone patterns with a jog angle lower than 90°. Finally, this method also provides a tool to determine the Young's modulus of the films based only on the characteristic wavelengths of the pattern.

11:40am **EM+TF-WeM12** **Surface Dynamics of Hybrid Silicon Interfaces Explored via Helium Atom Scattering**, *Z.M. Hund, R.D. Brown*, University of Chicago, *L.E. O'Leary*, California Institute of Technology, *D. Campi, M. Bernasconi, G. Benedek*, Università di Milano-Bicocca, Italy, *N.S. Lewis*, California Institute of Technology, *S.J. Sibener*, University of Chicago

Surface dynamical properties of methyl-terminated silicon(111) were investigated with energy and momentum resolved inelastic helium atom scattering measurements. The narrow energy distribution and nondestructive nature of neutral helium atom beams allow us to probe the vibrational dynamics of this hybrid organic-semiconductor interface. Time-of-flight experiments identify single phonon inelastic scattering events including, but not limited to, those attributed to Rayleigh wave excitations. We have mapped out the entire surface Brillouin zone along the nearest neighbor and next nearest neighbor azimuths, $\langle 011 \rangle$ and $\langle 121 \rangle$, respectively. Our experimental results are in excellent agreement with density functional perturbation theory calculations, which provide a detailed description of the dispersion curves. The combination of experimental measurements with theoretical calculations allows us to determine the interfacial Si-Si force constants, including coupling between the molecular adlayer and the substrate, displacement fields, and mode polarizations. Helium atom scattering complemented with DFPT calculations allow us to quantify these effects. Additionally, isotopic effects were probed by mapping the dispersion curves for the perdeutero-methylated silicon surface. Our results will be discussed with respect to hydrogen-terminated Si(111).

Scanning Probe Microscopy Focus Topic

Room: 16 - Session

SP+AS+BI+ET+MI+NM+NS+SS+TF-WeM

Probe-Sample Interactions, Nano-Manipulation and Fabrication

Moderator: S. Allen, The University of Nottingham, UK, A.-P. Li, Oak Ridge National Laboratory

8:20am **SP+AS+BI+ET+MI+NM+NS+SS+TF-WeM2** **Controlled Coupling of Silicon Atomic Quantum Dots at Room Temperature: A Basis for Atomic Electronics?**, *R.A. Wolkow*, University of Alberta and The National Institute for Nanotechnology, Canada, *J. Pitters*, The National Institute for Nanotechnology, Canada, *G. DiLabio, M. Taucer, P. Piva, L. Livadaru*, University of Alberta and The National Institute for Nanotechnology, Canada **INVITED**

Quantum dots are small entities, typically consisting of just a few thousands atoms, that in some ways act like a single atom. The constituent atoms in a dot coalesce their electronic properties to exhibit fairly simple and potentially very useful properties. It turns out that collectives of dots exhibit joint electronic properties of yet more interest. Unfortunately, though extremely small, the finite size of typical quantum dots puts a limit on how close multiple dots can be placed, and that in turn limits how strong the coupling between dots can be. Because inter-dot coupling is weak, properties of interest are only manifest at very low temperatures (milliKelvin). In this work the ultimate small quantum dot is described – we replace an “artificial atom” with a true atom - with great benefit.

It is demonstrated that the zero-dimensional character of the silicon atom dangling bond (DB) state allows controlled formation and occupation of a new form of quantum dot assemblies - at room temperature. Coulomb repulsion causes DBs separated by less than ~2 nm to experience reduced localized charge. The unoccupied states so created allow a previously unobserved electron tunnel-coupling of DBs, evidenced by a pronounced change in the time-averaged view recorded by scanning tunneling microscopy. It is shown that fabrication geometry determines net electron occupation and tunnel-coupling strength within multi-DB ensembles and moreover that electrostatic separation of degenerate states allows controlled electron occupation within an ensemble.

Some speculation on the viability of a new “atomic electronics” based upon these results will be offered.

9:00am **SP+AS+BI+ET+MI+NM+NS+SS+TF-WeM4** **Atomic Forces and Energy Dissipation of a Bi-Stable Molecular Junction**, *C. Lotze*, Freie Universität Berlin, Germany, *M. Corso, K.J. Franke, F.V. Oppen, J.I. Pascual*, Freie Universität Berlin, Germany

Tuning Fork based dynamic STM/AFM is a well established method combining the advantages of scanning tunneling and dynamic force microscopy. Using tuning forks with high stiffness, stable measurements with small amplitudes, below 1 Å can be performed. In this way, conductance and frequency shift measurements of molecular junction can be obtained simultaneously [1] with intramolecular resolution [2].

One of the most intriguing aspects of molecular junctions relates to the effect of structural bi-stabilities to the properties of the junction. These lead, for example, to conductance fluctuations, telegraph noise and the possibility to switch the electrical transport through the junction.

In this presentation, we characterize a model bi-stable molecular system using dynamic force spectroscopy. The effect of current-induced stochastic fluctuations of conductance are correlated with fluctuations in force. In our experiment we identified the last from both, frequency shifts and energy dissipation measurements, picturing a regime in which electrical transport and mechanical motion are coupled.

[1] N. Fournier *et. al*, PhysRevB 84, 035435 (2011),

[2] L. Gross *et. al*, Science 324, 1428 (2009)

9:20am **SP+AS+BI+ET+MI+NM+NS+SS+TF-WeM5** **Acetylene on Cu(111): Imaging a Molecular Pattern with a Constantly Rearranging Tip**, *Y. Zhu, J. Wyrick, K.D. Cohen, K. Magnone, C. Holzke, D. Salib, Q. Ma, D.Z. Sun, L. Bartels*, University of California Riverside

Abstract: Using variable temperature STM and DFT simulation, we identify the phases of acetylene adsorbed on the Cu(111) surface. Depending on the coverage, a diffraction-derived surface pattern of acetylene on Cu(111) is validated by STM. The modification of the STM image transfer function

through the adsorption of an acetylene molecule onto the tip apex is taken into account. In this case, the images of acetylene patterns on Cu(111) also include direct evidence of the **rotational orientation and dynamics of the acetylene species attached to the tip apex**. DFT modeling of acetylene/Cu(111) reveals that the molecular orientation and separation is governed by a balance of repulsive interactions associated with stress induced in the top surface layer and attractive interactions mediated by the electronic structure of the substrate. Computationally modeling of the substrate with 3 layers obtains the periodicity of the intermolecular interaction that provides a theoretical underpinning for the experimentally observed molecular arrangement.

9:40am **SP+AS+BI+ET+MI+NM+NS+SS+TF-WeM6 Atomic Scale Imaging and Electronic Structure of Trimethylaluminum Deposition on III-V Semiconductor (110) Surfaces, T.J. Kent*, M. Edmonds, E. Chagarov, A.C. Kummel**, University of California San Diego

Silicon based metal oxide semiconductor field effect transistors (Si-MOSFETs) are quickly approaching their theoretical performance limits, as a result many semiconductors are being explored as an alternative channel material for use in MOSFETs. III-V semiconductors are an appealing alternative to Si because of their higher electron mobilities. The limiting factor in III-V based MOSFET performance is defect states which prevent effective modulation of the Fermi level. The InGaAs (001) As-rich (2x4) surface contains two types of unit cells: ideal unit cells with double As-dimers and defect unit cells with single As-Dimers. The missing As-dimer unit cells, which comprise ~50% of the surface, are believed to cause electronic defect states at the semiconductor-oxide interface, specifically at the conduction band edge of the semiconductor. *In-situ* scanning tunneling microscopy and spectroscopy (STM/STS) and density function theory (DFT) modeling show that TMA readily passivates the As-As dimers in the ideal unit cell but the missing InGaAs(001)-2x4 may not be fully passivated by TMA. To improve the electronic structure of the interface, the sidewalls of the finFETs on InGaAs(001) can be fabricated along the (110) direction. The (110) surface contains only buckled III-V heterodimers in which the lower group III atom is sp² hybridized with an empty dangling bond and the upper group V atom is sp³ hybridized with a full dangling bond. This results in an electrically unpinned surface.

To investigate the benefits of using a (110) surface as a channel material, the atomic and electronic structure of the ALD precursor trimethylaluminum (TMA) monolayer deposited on III-V (110) surfaces has been studied using *in-situ* STM and STS. Both GaAs and InGaAs samples were studied. GaAs wafers were obtained from Wafertech with a Si doping concentration of 4x10¹⁸/cm³. The (001) samples were cleaved *in-situ* to expose the (110) surface. Samples were transferred to the STM chamber (base pressure 1x10⁻¹¹ torr) where the atomic bonding structure of the precursor monolayer unit cell was determined. STS, which probes the local density of states (LDOS), was used to determine Fermi level pinning. A model of TMA chemisorption was developed in which TMA chemisorbs between adjacent As atoms on the surface, giving a highly ordered monolayer with a high nucleation density which could allow for aggressive effective oxide thickness (EOT) scaling.

10:40am **SP+AS+BI+ET+MI+NM+NS+SS+TF-WeM9 A New Experimental Method to Determine the Torsional Spring Constants of Microcantilevers, G. Haehner, J.D. Parkin**, University of St Andrews, UK
Cantilever based technologies have seen an ever increasing level of interest since the atomic force microscope (AFM) was introduced more than two decades ago. Recent developments employ microcantilevers as stand-alone sensors by exploiting the dependence of their oscillating properties on external parameters such as adsorbed mass [1], or the density and the viscosity of a liquid environment [2,3]. They are also a key part in many microelectromechanical systems (MEMS) [4]. In order to quantify measurements performed with microcantilevers their stiffness or spring constants have to be known. Following calibration of the spring constants a change in oscillation behavior can be quantitatively related to physical parameters that are probed. The torsional modes of oscillation have attracted significant attention due to their high sensitivity towards lateral and friction forces, and recent developments in torsional-tapping AFM technology [5]. However, the methods available to determine the torsional spring constants experimentally are in general not simple, not very reliable, or risk damage to the cantilever [6].

We demonstrate a new method to determine the spring constants of the torsional modes of microcantilevers experimentally with high accuracy and precision. The method is fast, non-destructive and non-invasive. It is based on measuring the change in the resonance frequencies of the torsional

modes as a function of the fluid flow escaping from a microchannel. Results for rectangular cantilevers will be presented and compared to results obtained with other methods [7].

- [1] J. D. Parkin and G. Hähner, Rev. Sci. Instrum. **82** (3), 035108 (2011).
- [2] N. McLoughlin, S. L. Lee, and G. Hähner, Appl. Phys. Lett. **89** (18), 184106 (2006).
- [3] N. McLoughlin, S. L. Lee, and G. Hähner, Lab Chip, 1057 (2007).
- [4] S. Beeby, G. Ensell, N. Kraft, and N. White, *MEMS Mechanical Sensors*. (Artech House London, 2004).
- [5] O. Sahin and N. Erina, Nanotechnology **19** (44), 445717 (2008).
- [6] M. Munz, Journal of Physics D-Applied Physics **43** (6), 063001 (2010).
- [7] C. P. Green, H. Lioe, J. P. Cleveland, R. Proksch, P. Mulvaney, and J. E. Sader, Rev. Sci. Instrum. **75** (6), 1988 (2004).

11:00am **SP+AS+BI+ET+MI+NM+NS+SS+TF-WeM10 A Torsional Device for Easy, Accurate and Traceable Force Calibration of AFM Cantilevers, J.F. Portoles, P.J. Cumpson**, Newcastle University, UK

Accurate measurement of biologically-relevant forces in the range of pN to µN is an important problem in nanoscience.

A number of force probe techniques have been applied in recent years. The most popular is the Atomic Force Microscope (AFM). Accuracy of force measurement relies on calibration of the probe stiffness which has led to the development of many calibration methods[1], particularly for AFM microcantilevers. However these methods typically exhibit uncertainties of at best 15% to 20% and are often very time consuming. Dependency on material properties and cantilever geometry further complicate their application and take extra operator time. In contrast, one rapid and straightforward method involves the use of reference cantilevers (the "cantilever-on-cantilever" method) or MEMS reference devices. This approach requires that a calibrated reference device is available, but it has been shown to be effective in providing measurement traceability[2].

The main remaining difficulty of this approach for typical users is the positional uncertainty of the tip on the reference device, which can introduce calibration uncertainties of up to around 6%. Here we present a new reference device based on a torsional spring of relatively large dimensions compared to the typical AFM cantilever and demonstrate how it is calibrated. This method has the potential to calibrate the reference device traceably[3] to the SI with a 1% accuracy by applying techniques typically used for the characterisation of micromechanical devices. The large dimensions of the device reduce the positional uncertainty below 1% and simultaneously allow the use of the device as an effective reference array with different reference stiffnesses at different positions ranging from 0.090 N/m to 4.5 N/m

- [1] P J Cumpson, C A Clifford, J F Portolés, J E Johnstone, M Munz Cantilever Spring-Constant Calibration in Atomic Force Microscopy, pp289-314 in Volume VIII of Applied Scanning Probe Methods, Ed. B Bhushan and H Fuchs (Springer, New York, 2009)
- [2] P J Cumpson PJ, J Hedley, Nanotechnology 14 (2003) pp. 1279-1288
- [3] J F Portolés, P J Cumpson, J Hedley, S Allen, P M Williams & S J B Tendler, Journal of Experimental Nanoscience 1 (2006) pp51-62.

11:20am **SP+AS+BI+ET+MI+NM+NS+SS+TF-WeM11 Nanoscale Surface Assembly by Single-Molecule Cut-and-Paste, H.E. Gaub**, Ludwig-Maximilians Universität, Germany

INVITED
Bottom up assembly of functional molecular ensembles with novel properties emerging from composition and arrangement of its constituents is a prime goal of nanotechnology. With the development of Single-Molecule Cut-and-Paste (SMC&P) we provided a platform technology for the assembly of biomolecules at surfaces. It combines the Å-positioning precision of the AFM with the selectivity of DNA hybridization to pick individual molecules from a depot chip and allows to arrange them on a construction site one by one. An overview on different applications of this technology will be given in this talk. One recent example demonstrates the functional of receptors for small molecules. By SMC&P we assembled binding sites for malachite green in a molecule-by-molecule assembly process from the two halves of a split aptamer. We show that only a perfectly joined binding site immobilizes the fluorophore and enhances the fluorescence quantum yield by several orders of magnitude. To corroborate the robustness of this approach we produced a micron-sized structure consisting of more than 500 reconstituted binding sites. To the best of our knowledge this is the first demonstration of a one by one bottom up functional bio-molecular assembly. Figure included in supplemental document. S. Kufer, Puchner E. M., Gump H., Liedel T. & H. E. Gaub *Science* (2008), Vol 319, p 594-S. Kufer, Strackham, M., Stahl S.W., Gump H., Puchner E. M. & H. E. Gaub *Nature Nanotechnology* (2009), Vol 4, p 45-M. Erdmann, R. David. A.N. Fornof, and H. E. Gaub, *Nature*

* ASSD Student Award Finalist

Thin Film

Room: 11 - Session TF+SE+NS-WeM

Glancing Angle Deposition (GLAD)

Moderator: T. Karabacak, University of Arkansas at Little Rock

8:00am **TF+SE+NS-WeM1 Tunable-Refractive-Index Materials – A New Class of Optical Thin-Film Materials with Applications in Solid-State Lighting and Solar Photovoltaics**, *E.F. Schubert*, Rensselaer Polytechnic Institute **INVITED**

Among the properties of optical materials, the refractive index is a most fundamental one. It determines many optical characteristics such as Fresnel reflection, Bragg reflection, Snell refraction, diffraction, and the phase and group velocity of light. The refractive index was introduced centuries ago by Isaac Newton who correlated the refractive index with the relative strength of refraction at the liquid-to-air interface. He realized that the degree of refraction is proportional to the mass density of the liquid, and therefore called the new optical quantity the “optical density.” Nowadays, this key quantity is known as the “refractive index.”

Among transparent dense materials, MgF₂ has the lowest refractive index: $n = 1.39$. Air and other gases have a refractive index very close to 1.0 but these materials are not viable for thin-film optoelectronic applications. Therefore, there are no dense materials with a refractive index in the range $1.0 < n < 1.39$. That is, this range has remained unavailable and unexplored.

Over the last few years, a new class of materials, tunable-refractive-index materials, has been developed. Optical thin-film materials, with a refractive index as low as 1.05, have been demonstrated. The tunable-index materials are based on nano-porous materials, such as, for example, nano-porous SiO₂, nano-porous indium-tin oxide (ITO), and nano-porous TiO₂. The porosity can be precisely controlled by using oblique-angle deposition, a technique in which the substrate is at non-normal angle with respect to the deposition source. Whereas dense films form for normal-incidence deposition, porous films with a self-organizing nano-structure form for oblique-angle deposition.

In this presentation, we will present examples of novel structures and devices that exploit the newly gained controllability of the refractive index. Devices to be discussed include distributed Bragg reflectors, light-emitting diodes, and solar cells, along with the performance enhancements enabled by the control of the refractive-index.

8:40am **TF+SE+NS-WeM3 Nanostructured Homogenous CdSe/TiO₂ Composite Visible Light Photoanodes Fabricated by Oblique Angle Codeposition**, *G.K. Larsen*, University of Georgia, *B.C. Fitzmorris*, University of California Santa Cruz, *C. Longo*, University of Campinas, Brazil, *J.Z. Zhang*, University of California Santa Cruz, *Y.-P. Zhao*, University of Georgia

A unique fabrication method, oblique angle codeposition, is used to deposit well-aligned nanorod arrays and thick films of homogeneously mixed CdSe/TiO₂ composites. The structural, optical, and photoelectrochemical properties of the films are investigated using a variety of experimental techniques. Ultrafast exciton dynamics are studied using femtosecond transient absorption (TA) spectroscopy. The CdSe/TiO₂ composites are compared with pure CdSe and TiO₂ films in order to determine their utility for photoelectrochemical (PEC) applications and to understand the mechanisms underlying the observed behaviors. The morphology of the deposited nanorods changes with film composition due to atomic collisions occurring in the vapor column, which can be modeled using a simplified Keller-Simmons expression. Furthermore, the two phase evaporation process of CdSe creates three different cluster types within the TiO₂ film structures: isolated Se, Se-deficient CdSe, and Se-rich CdSe. The prevalence of each cluster type is dependent on predicted film composition, and each is affected differently by open-air annealing. Isolated Se can be incorporated into the TiO₂ lattice, resulting in low energy rutile phase. Se-deficient CdSe clusters crystallize preferentially into cubic CdSe and are easily oxidized into CdO, while Se-rich CdSe clusters crystallize into hexagonal CdSe and are more stable. Furthermore, each of these cluster types interacts differently with the surrounding TiO₂ matrix, resulting in diverse optical and PEC behaviors. Interestingly, the stoichiometry of the CdSe domains is more important than overall CdSe content within the film in determining the structural, optical, and PEC properties of the films. The composite nanorod structure is a more efficient photoanode under visible light illumination than both the pure CdSe and TiO₂ nanorod array films.

The higher efficiency of the composite films is attributed to efficient charge transfer and separation in the homogeneously mixed composite. This is confirmed by the extremely high electron injection rate from CdSe into TiO₂ observed in the ultrafast TA studies.

9:00am **TF+SE+NS-WeM4 Control the Biaxial Texture of Vertically Aligned Nanostructures using Oblique Angle Sputtering Deposition with Substrate Flipping Rotation**, *G.-C. Wang*, *L. Chen*, *T.-M. Lu*, Rensselaer Polytechnic Institute

It is known that oblique angle deposition can be used to grow 3D nanostructures with a variety of morphology such as nanorods and nanospirals. For a selective set of materials, the technique can also produce a preferred crystal orientation, particularly a biaxial texture where the texture selection occurs in both the out-of-plane and in-plane directions. Most frequently biaxial texture created using the oblique angle deposition is in the form of slanted nanorods. It is desirable to produce a biaxial structure in the form of vertically aligned nanostructures which may be useful as a buffer layer to grow functional films on top of it. In this talk we will discuss several strategies to grow vertically aligned nanostructures including nanorods with a biaxial texture by dynamically varying the incident flux angle with respect to the surface normal during deposition. A particularly robust technique to achieve this goal is a flipping rotation scheme where the substrate is rotated continuously at a fixed speed around an axis lying within and parallel to the substrate [1]. This is very different from the conventional substrate rotation mode where the rotational axis is perpendicular to the substrate surface. In the flipping rotational mode the incident flux is perpendicular to the rotational axis, and the incident flux angle changes continuously. For vertical nanorod films, grown on amorphous substrates under three orders of magnitude different rotation speeds, different flipping directions, and different ending deposition angles, were characterized using scanning electron microscopy. For texture characterization of these Mo nanostructures we used our newly developed reflection high energy electron diffraction surface pole figure technique [2]. Despite very different morphologies, such as 'C'-shaped, 'S'-shaped, and vertically aligned nanorods grown by the flipping rotation, the same (110)[1-10] biaxial texture with an average out-of-plane dispersion of ~15° was observed. In contrast, we showed that only a fiber-textured Mo film was obtained by using the conventional rotation mode with a fixed incident flux angle. These biaxial Mo vertical nanorod films have potential applications as buffer layers to grow near-single crystal semiconductor films through nanoheteroepitaxy. These films may find important applications in energy conversion and light emitting devices.

Work was supported by the NSF DMR-1104786.

[1] L. Chen, T.-M. Lu, and G.-C. Wang, *Nanotechnology* 22, 505701 (2011).

[2] F. Tang, T. Parker, G.-C. Wang, and T.-M. Lu, *J. of Physics D: Applied Physics* 40, R427 (2007).

9:20am **TF+SE+NS-WeM5 Flux Engineering to Control In-Plane Crystal and Morphological Orientation**, *J.M. LaForge*, *G. Ingram*, *M.T. Taschuk*, *M.J. Brett*, University of Alberta, Canada

Texture evolution during oblique angle deposition (OAD) and glancing angle deposition (GLAD) is of fundamental interest and important applications. As the distribution of size, shape and orientation of crystal grains impacts film electrical, optical, magnetic and mechanical properties control over texture evolution is important to optimizing performance. Morphology and crystal texture of OAD or GLAD nanostructured films is influenced by the orientation of the substrate relative to the collimated vapor flux, namely angle of incidence and the azimuthal angle, during deposition. Previous work has demonstrated control over the out-of-plane orientation through changes in the angle of incidence or azimuthal motion of substrate (e.g. stationary or continuous rotation).^{[1][2]} However, work on the development of in-plane orientation has focused on material kinetic effects, such as deposition temperature, residual gas concentration, and deposition rate rather than substrate motion.^{[3][4]}

We have deposited iron nanocolumns that have a tetrahedral apex and an out-of-plane texture (fiber texture) at a deposition angle of 88° under continuous substrate rotation. It is possible to induce in-plane crystal texture and morphological orientation by engineering the azimuthal distribution of the flux to match the symmetry of the nanocolumns (i.e. 3-fold rotational symmetry). Thus, biaxially textured nanocolumns with an in-plane alignment that is predominantly controlled by substrate motions (or flux configuration) can be created using this technique. In principle, this method could be generalized to nanocolumns with 4-fold and 6-fold azimuthal symmetry and therefore provides a mechanism to form biaxially textured, nanostructured films from a variety of materials deposited on amorphous or crystalline substrates.

[1] P. Morrow, F. Tang, T. Karabacak, P.-I. Wang, D.-X. Ye, G.-C. Wang, T.-M.T.-M. Lu, *Journal of Vacuum Science & Technology A: Vacuum, Surfaces, and Films* **2006**, *24*, 235.

[2] R. Krishnan, T. Parker, S. Lee, T.-M. Lu, *Nanotechnology* **2009**, *20*, 465609.

[3] K. Okamoto, T. Hashimoto, K. Hara, M. Kamiya, H. Fujiwara, *Thin Solid Films* **1985**, *129*, 299-307.

[4] K. Okamoto, T. Hashimoto, K. Hara, M. Kamiya, H. Fujiwara, *Thin Solid Films* **1987**, *147*, 299-311.

9:40am **TF+SE+NS-WeM6 Bi-axial Texture Development in AlN Layers during Off-axis Sputter Deposition**, R. Deng, D. Gall, Rensselaer Polytechnic Institute

Polycrystalline AlN layers were deposited by pulsed-DC reactive magnetron sputtering from a variable deposition angle $\alpha = 0-84^\circ$ in 5 mTorr pure N₂ at room temperature. X-ray diffraction pole figure analyses show that layers deposited from a normal angle ($\alpha = 0^\circ$) exhibit fiber texture, with a random in-plane grain orientation and the c-axis tilted by $42 \pm 2^\circ$ off the substrate normal, yielding wurtzite AlN grains with the {10-12} plane approximately parallel ($\pm 2^\circ$) to the substrate surface. However, as α is increased to 45° , two preferred in-plane grain orientations emerge, with populations I and II having the c-axis tilted towards and away from the deposition flux, by $53 \pm 2^\circ$ and $47 \pm 1^\circ$ off the substrate normal, respectively. Increasing α further to 65 and 84° , results in the development of a single population II with a $43 \pm 1^\circ$ tilt. This developing bi-axial texture is attributed to a competitive growth mode under conditions where the adatom mobility is sufficient to cause inter-grain mass transport but insufficient for the thermodynamically favored low energy {0001} planes to align parallel to the layer surface. Consequently, AlN nuclei are initially randomly oriented and form a kinetically determined crystal habit exposing {0001} and {11-20} facets. The expected direction of its highest growth rate is $49 \pm 5^\circ$ tilted relative to the c-axis, in good agreement with the $42-53^\circ$ measured tilt. The in-plane preferred orientation for $\alpha > 0^\circ$ is well explained by the orientation dependence in the cross-section of the asymmetric pyramidal nuclei to capture off-normal directional diffusion flux. The observed tilt is ideal for shear mode electromechanical coupling, which is maximized at 48° .

10:40am **TF+SE+NS-WeM9 Engineered Indium Tin Oxide Nanowhiskers via Vapour Liquid Solid Glancing Angle Deposition**, A.L. Beaudry, R.T. Tucker, J.M. LaForge, M.T. Taschuk, University of Alberta, Canada, M.J. Brett, University of Alberta, Canada and The National Institute for Nanotechnology

The vapour liquid solid (VLS) nanowire growth technique has been recently modified with spatially modulated vapour flux through glancing angle deposition (GLAD).^{1,2} Using this new technique, named VLS-GLAD, our group has demonstrated improved morphological control over indium tin oxide (ITO) nanowhiskers.¹ Single crystal ITO nanowhiskers are grown via a self-catalyzed VLS growth mechanism, resulting in branched structures.³ VLS-GLAD exhibits improved control over the diameter, spacing, branching density and branching orientation of ITO nanowhiskers. As the angle of deposition is increased to glancing angles, there is a transition from a dense interconnected network to a porous film of individual ITO nanowhisker structures. In addition, branching was found to increase significantly with increasing deposition angle. This result is attributed to an increase in the proportion of vapour flux incident on the sides of the structures, resulting in an increase in self-catalytic VLS growth of branches. This effect has been used to engineer branch morphology and orientation. Vapour flux rate modulation at glancing angles results in further in-situ control over ITO nanowhisker features. HRTEM imaging revealed a continuation of crystal planes from the trunk into the branch. XRD results indicated single crystal cubic bixbyite structures with a $\langle 400 \rangle$ growth direction. Haacke's figure of merit was used to assess the suitability of ITO nanowhisker films as transparent electrodes.⁴

¹ Beaudry, A.L. et al. *Nanotechnology* **23**, 105608 (2012).

² Alagoz, A.S. and Karabacak, T. *MRS Proceedings* **1350**, (2011).

³ Castañeda, S.I. et al. *Journal of Applied Physics* **83**, 1995 (1998).

⁴ Haacke, G. *Journal of Applied Physics* **47**, 4086 (1976).

11:00am **TF+SE+NS-WeM10 CoPt Nanopillars for Advanced Media by Glancing Angle Deposition**, H. Su, A. Natarajathinam, S. Gupta, The University of Alabama

We report for the first time the fabrication of CoPt+AlN "granular nanorods" utilizing glancing angle deposition (GLAD) on a multi-gun, planetary sputtering system. Initially, AlN was deposited by reactive sputtering from an Al target while CoPt multilayers were simultaneously sputtered using cobalt and platinum targets. Various ratios of Co and Pt, ranging from Co80Pt20 to Co50 Pt50, were used to deposit CoPt-AlN

nanorods with different AlN volume percentages. X-ray diffraction (XRD), electron dispersive X-rays (EDX), scanning electron microscopy (SEM), and alternating gradient magnetometry (AGM) were employed to characterize the structural and magnetic properties, respectively. SEM micrographs indicated that the nanorods were approximately 16 nm in diameter, the angle between the substrate plane and the growth direction was about 78 degrees, while the lengths of the nanorods ranged from 30 to 50 nm, depending on deposition time. The angles between the substrate plane and incident flux ranged from 47 degrees to 82 degrees as the substrate presented itself at different angles to the target during the planetary deposition. The composition of CoPt-AlN has been studied by EDX for different ratios of AlN. M-H loops showed that the planetary GLAD sample had twice the coercivity of the flat sample.

We have also compared stationary vs. planetary GLAD, and sequential deposition of AlN/CoPt multilayers with true co-deposition, using an annular CoPt target with an Al insert. Simulations of the deposition have been carried out to gain a better understanding of where the AlN segregates with respect to the CoPt grains. These preliminary results indicate a novel and promising approach to nanopatterned graded media that is the subject of intense research in the data storage industry.

11:20am **TF+SE+NS-WeM11 Through-post Electrical Characterization of GLAD Thin Films**, A. Lalany, R.T. Tucker, M.T. Taschuk, University of Alberta, Canada, M.D. Fleischauer, University of Alberta and The National Institute for Nanotechnology, Canada, M.J. Brett, University of Alberta, Canada

Glancing Angle Deposition (GLAD) [1] thin films are increasingly used in optoelectronic applications that benefit from their unique optical properties or ultra-high surface area. GLAD produces porous nanostructured thin films which have found applications as high surface area electrodes. Potential performance benefits of these nanostructured thin-films for optoelectronic devices include, but are not limited to, increased charge extraction [2]. Suitable electrical conductivity along the length of GLAD structures (normal to substrate plane) is necessary to exploit a GLAD film's high surface area for electronic devices. However, optimization of GLAD films for these devices has proven difficult without direct measurements of post resistivity.

In-plane resistivity measurements of metals and conductive oxide GLAD films have been performed [3-5], showing increasing in-plane resistivity with increasing oblique deposition angle (due to decreased film density resulting in fewer conductive pathways). Electrical anisotropy has also been observed, with differing in-plane resistivity for different nanocolumn orientations [3-5]. Through post conductivity measurements present additional challenges - it has been shown that as crystallite grain size approaches the range of bulk electron mean free path, column-boundary scattering effects begin to dominate standard bulk-scattering mechanisms [6]. As such, the extensive boundaries present in GLAD structures can result in complex electrical behavior. While several attempts have been made to access through-post electrical properties, results have been limited to relative measures or are extremely low yield processes [7, 8].

We require a measurement technique that is both time and cost effective, statistically robust, and has high yield. This has been achieved with a Kelvin Cross-Bridge Resistor architecture specifically designed to measure through-post resistivity. Our devices can measure resistivities between $100 \mu\Omega \text{ cm} < \rho < 11 \text{ G}\Omega \text{ cm}$, and we have successfully measured through-post conductivities for Indium-tin-oxide (ITO) and Cr GLAD films. Here, we will present device fabrication, validation and current experimental results.

[1] M.M. Hawkeye et al., *J. Vac. Sci. Technol. A* **25** (2007) 1317.

[2] D.A. Rider et al., *Nanotech.* **22** (2007) 0857060.

[3] J. Lintymer et al., *Surf. & Coat. Tech.* **174-175** (2003) 316.

[4] K.D. Harris et al., *Adv. Funct. Mater.* **18** (2008) 2147.

[5] D. Vick et al., *J. Vac. Sci. Technol. A* **24** (2006) 156.

[6] A. Besnard et al., *J. Phys. D: Appl. Phys.* **44** (2001) 215301.

[7] M.F. Cansizoglu et al., *ACS Nano.* **4** (2010) 733.

[8] S.P. Chiu et al., *Nanotech.* **20** (2009) 105203.

11:40am **TF+SE+NS-WeM12 Direct Label-Free Detection of microRNA Using a Multi-well SERS Chip Fabricated By Oblique Angle Deposition**, J.L. Abell, University of Georgia, J.M. Garren, Georgia Health Science University, J.D. Driskell, Illinois State University, R.A. Tripp, Y.-P. Zhao, University of Georgia

Direct label-free nucleic acid detection is a desirable yet challenging task. The current mainstay detection and screening technologies, namely polymerase chain reaction (PCR) and DNA microarrays (i.e. DNA chips), rely heavily upon the use of extrinsic reporter molecules to detect the

hybridization of a probe sequence to a target sequence. Removing the need for external labels reduces the cost and complexity of DNA detection assays. This, however, requires a sensing platform capable of highly sensitive, specific, direct chemical analysis. Surface-enhanced Raman spectroscopy (SERS) is an analytical technique capable of detecting highly resolved chemical signatures with superior sensitivity, and can be used to determine the relative quantities of a compound adsorbed on a nanostructured metal surface. The challenge for SERS detection is to produce a large area, uniform and highly sensitive substrate. Here, we report the use of Ag nanorod (AgNR) SERS substrates fabricated by oblique angle deposition (OAD) for microRNA (miRNA) detection. With such a large area (wafer size) and uniform response (signal intensity variation $\leq 10\%$) of the AgNR substrates, we have developed a simple molding technique to pattern the substrates into multi-well arrays. We demonstrate a 40-well 1" x 3" glass slide allowing for parallel screening of multiple specimens with uniform response. This multiwell substrate has been used in conjunction with a linear least squares (LS) analysis method by assuming that the SERS spectrum of miRNA is a convolution of the individual signals of each of the four A, C, G, and T components, where the contribution of each source signal to the total DNA signal is weighted by the relative quantities of A, C, G, and T present within the sequence. Experimentally we have demonstrated this method for detection and differentiation of four different DNA sequences. In addition, we show for the first time the subtle spectral changes observed after label-free hybridization can be quantified with LS to confirm the capture of the target sequence. This study reveals that the use of OAD SERS substrate could be a potential technique to replace to current microarray technique for DNA/RNA detection.

Thin Film

Room: 10 - Session TF-WeM

Thin Films for Encapsulation, Packaging, and Biomedical Devices

Moderator: L.W. Rieth, University of Utah

8:00am TF-WeM1 **Optimizing a Spatial Atomic Layer Deposition Cell for High Throughput, Low Temperature, Roll-to-Roll Applications.** *M.J. Dalberth, L. Lecordier, M.J. Sershen, M. Ruffo, R. Coutu, G. Sundaram, J.S. Becker*, Cambridge Nanotech, Inc.

Atomic layer deposition (ALD) has established itself as a technique capable of producing uniform, dense, pin-hole free films with extremely fine thickness control. The surface reactions involved in many ALD processes are thermally active at temperatures less than 200°C which makes it attractive for emerging applications coating substrates with a limited thermal budget- for example, a barrier layer for organic photovoltaics on a flexible substrate. Many of these applications demand high throughput, however, and traditional ALD is too slow due to its temporally spaced pulses of reactant A and reactant B, and its need for a vacuum system requiring time consuming evacuation. Spatial ALD replaces the temporal separation of reactants with their spatial separation by confining them to separate gas channels in a deposition cell. Plus, it's a process that takes place at atmospheric pressure and can eliminate system evacuation times. In spatial ALD, the substrate and cell move relative to one another, and the number of A/B channels determines the thickness of material deposited. At speeds of 10m/min or more, equivalent throughput of 2000-4000 wafers can potentially be achieved with equivalent cycle time $\ll 0.1s/\text{\AA}$. As of today, Cambridge Nanotech has implemented two 150 mm x 150 mm cells based on two and six-cycle designs. 150mm Si wafer and PEN/PET substrates were processed using TMA and water at atmospheric pressure, 100-120°C, 10m/min speed and 0.1-0.5 mm gap size between cell and substrate. The impact of key process metrics on process performance such as GPC or uniformity was evaluated, including reactant dosage, temperature or stage velocity. Not surprisingly, the ability to maintain the spatial confinement of TMA and water in order to limit parasitic CVD-like reactions (which induces higher GPC and particle formation) is shown to be critically dependent on gap size and flow rate for the inert gas barriers. Data showing the impact of different cell designs (e.g., orifice distribution and size) on wafer- and process-scale metrics will also be discussed. While development on new cells is continuing, the data taken so far support the outlook that spatial ALD could be a key technology for rapid deposition of functional layers in high throughput applications.

8:20am TF-WeM2 **Encapsulation of Implantable Devices by Atomic Layer Deposited Al_2O_3 and Parylene C Bi-layer.** *X. Xie, L.W. Rieth, F. Solzbacher*, University of Utah

Encapsulation of 3-D electronic biomedical implants with complex geometries and tight gaps between components is one of the greatest

challenges to achieve long-term functionality and stability. We have investigated a new encapsulation scheme that combines atomic layer deposited (ALD) Al_2O_3 and Parylene C for biomedical implantable system and will present results to quantify the performance of this system. Our approach combines the highly effective moisture barrier properties of ALD alumina, and Parylene as a barrier to many ions and for preventing contact of alumina with liquid water. 52 nm of Al_2O_3 was deposited by plasma-assisted (PA) ALD on interdigitated electrodes (IDEs). AFM micrographs show that as-deposited Al_2O_3 films on fused silica substrate have RMS surface roughness of 0.48 nm. XPS spectra determined that PA-ALD films had nearly stoichiometric O/Al ratio of 1.4. A 6- μm thick Parylene-C layer was deposited by CVD using Gorman process on top of Al_2O_3 and used A-174 (Momentive Performance Materials), an organosilane, as adhesion promoter. The IDEs coated with Al_2O_3 -Parylene C were soaked in phosphate buffered saline (PBS) solution for a period of about 9 months at both body temperature (37 °C) and elevated temperatures (57 to 80 °C) for accelerated lifetime testing. Electrochemical impedance spectroscopy (EIS) and chronoamperometry were used to evaluate the integrity and insulation performance of the soft encapsulation. The leakage current was ~ 20 pA by applying 5 V DC bias and impedance was ~ 3.5 M Ω at 1 kHz with phase of close to -87° by using EIS for samples under 67°C about 9 months (approximately equivalent to 72 months at 37°C), indicating no significant degradation. The encapsulation performances of combining alumina and Parylene C, Parylene C only and alumina only coatings were compared and the bi-layer coating shows its superiority of at least 5 times longer lifetime than the rest two coating approaches. The continuous 5 V bias voltage has no obvious effect on alumina and Parylene coated samples while it shortened the lifetime of Parylene coating by at least a factor of 4. Complex topography can shorten the lifetime of coating dramatically comparing with planar structures, especially with the existence of micromotion inside the body. The lifetime of alumina and Parylene coated devices with hand-wound coils and SMD capacitors was only about 50% or less of that of planar test structures. The long-term (more than 6 years of equivalent lifetime) insulation performance of the novel double-layer encapsulation shows its potential usefulness for chronic implantable electronic microsystems.

8:40am TF-WeM3 **Ultra-barrier Technology for Moisture-Sensitive Electronics.** *P.F. Carcia*, DuPont Central Research and Development
INVITED

Organic materials are driving future electronic technologies in the direction of lighter weight, more robust, flexible, and lower cost manufacturing. Organic solar cells have reached 10% efficiency in the lab and are becoming an attractive low-cost option for generating electricity in isolated regions in the undeveloped world. Organic light emitting diodes (OLEDs) are poised to succeed LCDs as the next generation of more vibrant color displays for TVs, computer tablets, and mobile phones. However, one obstacle to the broad utilization of organic electronic materials, and also some inorganic materials, is their sensitivity to atmospheric gases, especially moisture. In the case of OLED displays, hermetic packaging with glass or metal may be an interim solution for early product introduction, but this precludes advantages of lighter weight and flexibility, which could have cost penalties. But for organic photovoltaics (OPV), and for some thin-film inorganic PV technologies, e.g. CIGS, to be cost competitive, they will need to be fabricated with flexible polymer materials, which are permeable. These polymer materials will require low permeation coatings to exclude atmospheric gases that can readily degrade moisture sensitive electronic materials. For OLEDs, the barrier coating must uniformly reduce permeation through the polymer by $\sim 10^6$ times for the display to be defect-free. Solar cells will need a similar (10^4 - 10^5 times) reduction in permeation, if they are to have a reasonable outdoor lifetime. In our laboratory, we have discovered that single-layer, inorganic, barrier coatings grown by atomic layer deposition (ALD) can meet the demanding requirements of an ultra-barrier to protect sensitive electronic devices on a flexible polymer substrate. In this talk we will discuss many of the materials and processing insights we have learned about ALD barriers, their performance protecting sensitive electronic devices, and the outlook for practical, high-speed ALD manufacturing.

9:20am TF-WeM5 **Multilayer Barrier Coatings for Organic Photovoltaics.** *A.M. Coclite, F. De Luca, K.K. Gleason*, Massachusetts Institute of Technology

Encapsulant barrier coatings, which prevent the permeation of water through flexible plastic substrates, are an enabling technology for the commercialization of OPV devices. Such protective coatings are made of multilayer stacks where multiple dense, inorganic layers are alternated with soft, organic ones. The inorganic layer contains inevitably some pinholes and defects. The roles of the organic layer are creating a tortuous and longer path among the defects of two successive inorganic layers, filling the pores of the inorganic underlayer limiting the propagation of defects from one

inorganic layer to the other and smoothening the substrate surface roughness.

We obtained good barrier properties ($WVTR = 10^{-2}$ g/cm²/day at 25°C, RH=85%) with a bilayer obtained by coupling initiated-PECVD (iPECVD) and plasma enhanced CVD (PECVD) at very low thickness of inorganic layer (25 nm).

SiO_x layers were deposited through PECVD in MW plasma at high power and high oxygen dilution. The silanol and organic groups were not detectable by IR spectroscopy, resulting in dense film with high flexibility and high critical tensile strain. High critical tensile strain implies that the coating can be bent and stretched to a relatively big extent before cracking. Inorganic films obtained by other technologies (i.e. Al₂O₃ ALD coatings) showed smaller critical strain values.

Organic coatings were deposited through a new process named iPECVD with enhanced monomer structure retention compared to a conventional plasma deposition and faster deposition rate if compared to conventional iCVD processes from organosilicon monomer. The deposition conditions were tuned to obtain good planarizing properties. The deposition of planarizing organic layers was demonstrated by depositing the coating on the top of some microspheres (1 μm in diameter) which served as model defects on the surface. Increasing the thickness of the coating, the degree of planarization (DP), both local (DLP) and global (DGP), increases. The DLP increases much faster than the DGP: when the coating is 1 μm-thick the DLP is already 99%, for the global planarization instead a 1.8 μm-thick-coating is needed to reach DGP= 99%.

The great advantage of a similar approach is that we deposit the multilayer in a large-area reactor, maintaining the same organosilicon precursor and the same reactor configuration for both deposition of silica-like and organosilicon layers. A detailed investigation of the barrier and mechanical properties changing the number of layers in the stack and the measurements conditions will be presented in order to demonstrate the robustness of the following approach to create flexible ultra-high barrier layer.

9:40am TF-WeM6 Preparation of Hydrophobic Coatings on Si/SiO₂ by Incorporation of Nano- and Microdiamond in a Layer-By-Layer Deposition, A. Diwan, J. Wilcock, M.R. Linford, Brigham Young University

Hydrophobic coatings are required in a wide variety of applications. We are preparing robust hydrophobic coatings on silicon from nano-/microdiamond and polyallylamine (PAAm) deposited in a layer-by-layer fashion. After deposition of PAAm/diamond multilayers, two different approaches were considered for preparing hydrophobic surfaces. The first involved the reaction of the amine groups of PAAm with the epoxy groups of 2-(1H,1H-perfluoroundecyl)oxirane to yield hydrophobic surfaces. However, due to the formation of hydroxyl groups in this ring opening reaction, the roll off of water drops, i.e., their receding contact angles, was poor although the surface showed high static and advancing water contact angles. The other approach, which appears to produce more robust coatings, used only nano-diamond and PAAm for the growth of electrostatically bound layers. The amine of the PAAm was reacted with (3-glycidyloxypropyl)trimethoxysilane (GPTMS) in a closed pressure vessel at 100°C, which should provide crosslinking to the film and also active sites for subsequent reaction. The final step involved the chemical vapor deposition of a fluorinated silane (F-13 silane) to give a hydrophobic surface. The static water contact angle of a flat PAAm/GPTMS/F-13 silane surface was 107°, which showed good roll off properties. The prepared coatings are evaluated and analyzed at every step using atomic force microscopy (AFM), x-ray photoelectron spectroscopy (XPS), time-of-flight secondary ion mass spectroscopy, ellipsometry for thickness measurements and water contact angles measurements.

Wednesday Afternoon, October 31, 2012

Applied Surface Science

Room: 20 - Session AS+NS+SS+TF-WeA

3D Imaging & Nanochemical Analysis - Part 2 (2:00-3:20 pm)/ Advanced Data

Analysis and Instrument Control (4:00-6:00 pm)

Moderator: V.S. Smentkowski, General Electric Global Research Center, M.R. Linford, Brigham Young University, S.J. Pachuta, 3M Company

2:00pm AS+NS+SS+TF-WeA1 From Atomic Scale to Materials Behavior: Using Atom-Probe Tomography to Understand the Behavior of Alloys and Ceramics, E.A. Marquis, University of Michigan INVITED

The ability to improve the performance of functional materials is driven by how well microstructure can be understood and controlled. The three-dimensional distribution of solutes, dopants or impurities in particular, in relation to structural features determines such properties as fracture toughness, strength, ductility, as well as electrical and magnetic response. After a brief introduction to atom-probe tomography, I will illustrate how high resolution characterization approaches can be used systematically to understand the atomic scale processes controlling materials microstructures and their evolution, focusing on alloys and ceramic systems. Several topics will be presented: precipitation and coarsening behavior of Al-based alloys, grain boundary chemistry and role of impurities during irradiation in ferritic steels which may play an important role in fracture and corrosion resistance, the development of oxide-dispersion strengthened steels for structural applications in future nuclear reactors and the role of minor elements in controlling the oxidation behavior of Ni-base alloys for high temperature power generation applications.

2:40pm AS+NS+SS+TF-WeA3 Three Dimensional Atomic Scale Characterization of Binary and Complex Oxides using Atom Probe Tomography, A. Devaraj, R. Colby, D.E. Perea, S. Thevuthasan, EMSL, Pacific Northwest National Laboratory

The development of three dimensional, high spatial and mass resolution characterization techniques is important for several materials used in applications ranging from catalysis, sensors to optoelectronics. Laser assisted atom probe tomography (APT) technique offers such an opportunity to perform atomic scale three dimensional analysis of materials including metals, semiconductors and dielectrics, with subnanometer spatial resolution and sub-ppm level mass resolution. The Cameca LEAP 4000XHR Atom Probe equipped with 355nm UV pulsed laser is used to analyze technologically important binary bulk oxides like MgO, Al₂O₃, TiO₂ and CeO₂. A strong correlation between applied UV laser energy and measured stoichiometry was observed for all these binary oxides. Using those results the importance of laser energy optimization on obtaining accurate stoichiometric composition analysis for oxides will be highlighted. Extension of such laser parametric investigation to complex oxides including SrTiO₃, LaCrO₃ and LaSrMnO₃ will also be presented. In addition the impact of laser pulsing on atomic scale structure of the oxide APT sample surface was studied by a direct cross correlation with aberration corrected TEM. The information on the atomic scale structure of the field evaporated oxide APT samples will be utilized to postulate the laser-oxide material interaction occurring during APT analysis of such oxides leading to the dependency of applied laser energy on measured stoichiometry.

3:00pm AS+NS+SS+TF-WeA4 Atom Probe Tomography of Complex Heterogeneous Low Dimensional Materials, S. Thevuthasan, A. Devaraj, R. Colby, D.E. Perea, V. Subramanian, V. Shutthanandan, Pacific Northwest National Laboratory

EMSL, a national scientific user facility of the DOE, is developing a comprehensive chemical imaging capability combining atom probe tomography with high resolution (scanning) transmission electron microscopy(HR(S)TEM) and high resolution Rutherford back scattering spectrometry (HRRBS) to provide solutions to problems pertaining to energy and environmental applications. We will emphasize on a chemical imaging effort aimed at atomically-resolved composition and structural analysis of low dimensional materials such as nanowires and embedded metal nanoparticles highlighting the benefits and challenges for APT. A unique benefit of APT is the ability to characterize the ppm level concentration and distribution of dopants across semiconducting nanowire heterojunctions. The preferential incorporation of dopants at specific atomic facets at the heterojunction interface in Si-Ge nanowires can only be characterized by using APT. Another important class of low dimensional

materials includes embedded metal nanoparticles in oxides with applications in catalysis, sensors and optoelectronic applications. In order to extent APT analysis capability to such materials a cross correlative approach of combining APT with aberration corrected HRSTEM is employed. The results from the model system of ion beam synthesized Au and Ag nanoparticles embedded in MgO will be presented.

4:00pm AS+NS+SS+TF-WeA7 Upgrading a 25 Year Old ims-4f Magnetic Sector SIMS Instrument: Teaching an Old Dog New Tricks and Keeping Research in its Future, A.J. Fahey, B.E. Naes, G. Hager, Pacific Northwest National Laboratory

The CAMECA ims-4f at PNNL is nearly 25 years old. Although much of the vacuum system, electrostatic optics and associated apertures and slits have been maintained and remain operational the electronics that control the critical components of this machine has gone beyond the typical "mean-time-between failure" of nearly all components, which is typically 10 years.

The original electronics designs, many of which are no longer employed on the newer CAMECA models, incorporated multiple series of relays to control lens voltages that allowed isolation of low control and high voltage output. These relays, among other components, are failing.

Some components of the electrostatic optics and vacuum system are targeted to be replaced to upgrade the capabilities of the instrument and to use physical components from our "surplus" ims-4f system than would enhance the operation of the PNNL ims-4f giving in near-equivalence to the operation of an ims-7f.

The upgraded electronics and control systems are being designed in a modular way using as many commercial components as possible, such as modular high voltage power supplies and commercially available high-voltage operational amplifiers. The new system will allow for complete control of all subsystems on the instrument and will improve repeatability of settings and measurements. We will be able to perform measurements sets and sequences that are currently not possible on any existing SIMS instrument. In addition, the new computer controlled system should make operation of the SIMS instrument more accessible to other investigators as it should reduce the level of training needed to operate the instrument. Currently, the operator must adjust "knobs" to tune the instrument and reproduce prior operating conditions. With the upgraded system conditions will be recalled from saved files.

All modular components are being housed in ANSI-standard DIN modules and sub-racks. Control, monitoring and data acquisition will largely be performed via PXI subsystems. The Vacuum will be controlled and monitored via a commercial process control system. Also, several other individual instruments will be used in critical positions around the instrument.

Details of the upgrade will be discussed as well as improvements to the flexibility of measurements and the performance of the system. An outline of the types of measurements that should be available with all modern systems will be presented and discussed as well as the results of improvements implemented to the PNNL ims-4f SIMS instrument.

4:20pm AS+NS+SS+TF-WeA8 Automated Processing of X-ray Photo-Electron Spectra, K. Macak, E. Macak, S.J. Coultas, S.J. Hutton, A.J. Roberts, R. Raso, S.J. Page, C.J. Blomfield, Kratos Analytical Ltd, UK

Modern XPS instruments are capable of generating a large amount of data in a hands-off automated fashion. Many new material challenges are increasingly reliant upon XPS for sample screening and other high throughput, low operator intervention applications.

The interpretation of XPS data and reliable quantification from the acquired results presents an opportunity to improve the whole experimental automation still further. We present an algorithm for fully automated processing of X-ray photo-electron spectra. The analysis is split into three stages: background subtraction, peak identification and quantification of element composition.

Each step can be carried out separately and the user can provide prior knowledge of the sample by manually selecting regions, assigning their labels and/or explicitly include/exclude specific elements. This additional information then helps to improve the accuracy of the results.

The algorithm was tested on more than 1000 spectra, selected from a wide range of different materials; including steels, polymers, semiconductors and ceramics. These spectra were processed using the automated procedure and the outcomes were compared to those determined by expert users. The average element detection success rate was 87 %.

The influence of various experimental conditions (such as signal-to-noise ratio and operating conditions) on the identification procedure is also discussed.

4:40pm AS+NS+SS+TF-WeA9 Correlating Structure and Chemistry – A Multitechnique Study using Light Microscopy (LM), SEM and XPS, M.L. Pacholski, P.Y. Eastman, The Dow Chemical Company

Understanding the distribution of carbon-rich chemistries on organic substrates can be very difficult, particularly when the substrates are not uniform, such as cellulose fibers. Recently we have been challenged to measure the distribution of an olefin polymer on a fibrous cellulose sheet. In order to verify that measured chemical distributions were definitively from polymer, as well as to understand the morphology of the deposited polymer, it was highly desired to study identical areas using SEM and other imaging techniques. Although several chemical imaging methods were investigated, it became apparent that XPS imaging was the only chemical technique capable of obtaining distributions over the desired fields of view (1 mm-3 mm). Registry of the SEM images with XPS images proved to be difficult since many of the traditional registry methods, such as marking with ink or gluing markers to the surface are ill-suited to absorbent cellulose. The first step was to align relatively low magnification light microscope images from a stereoscope with optical images captured directly in the XPS instrument. These images were then used as a “bridge” to align the higher magnification SEM and XPS images. With this method, deposited polymer and chemical information were correlated with high spatial accuracy. Composite images showing the chemical information as colored overlays on the SEM images were generated to clearly display the correlation.

**Energy Frontiers Focus Topic
Room: 15 - Session EN+TF-WeA**

Thin Films for Energy Applications

Moderator: M. Filler, Georgia Institute of Technology

2:00pm EN+TF-WeA1 Batteries and Battery Materials by Vapor Deposition, N. Dudney, Oak Ridge National Laboratory INVITED

Although most commercial rechargeable batteries are prepared by bulk and powder processing methods, vapor deposition of materials has led to important advances for fundamental research, for modification of battery materials and interfaces, and also for commercialization of thin film batteries. Each of these areas will be illustrated with our studies of thin film materials for the electrolyte, anode, and cathode components of rechargeable lithium and lithium-ion batteries with both planar and 3-dimensional architectures.

4:00pm EN+TF-WeA7 Efficient Radiative and Non-Radiative Energy Transfer from Quantum Dots to Silicon Nanomembrane. Evidence of Waveguiding Phenomena, O. Seitz, H.M. Nguyen, W. Peng, Yu.N. Gartstein, Y.J. Chabal, A.V. Malko, University of Texas at Dallas

Nanostructured materials attract a considerable attention as potential candidates for practical photovoltaic (PV) devices. The majority of current hybrid PV architectures are based on charge transfer schemes, which frequently suffer from bad interface quality and poor carrier transport, consequently lowering the light conversion efficiency. An alternative is offered by non-contact *energy transfer*-based hybrid nanostructures, which combine strongly absorbing components, such as inorganic nanocrystal quantum dots (NQDs), and high-mobility semiconductor (SC) layers. It is envisioned that in such hybrid systems, the excitonic energy would be transferred via non-radiative energy transfer (NRET) and radiative (RET) waveguide coupling across the interface with the subsequent separation and transport of charge carriers entirely within the SC-based component. In this talk, we demonstrate the efficient excitonic sensitization of crystalline Si nanomembranes via combined effects of radiative (RET) and non-radiative (NRET) energy transfer from a proximal monolayer of colloidal semiconductor nanocrystals. Ultrathin, 25–300 nm Si films are prepared on top of insulating SiO₂ substrates and grafted with a monolayer of CdSe/ZnS nanocrystals via carboxy-alkyl chain linkers. The wet chemical preparation ensures that Si surfaces are fully passivated with a negligible number of non-radiative surface state defects and that the separation between nanocrystals and Si is tightly controlled. Combining atomic force microscopy (AFM), ellipsometry, time-resolved photoluminescence measurements and theoretical modeling, we could identify and quantify the individual contributions from RET and NRET, which all combined exceed 85% efficiency of energy transferred into the Si substrate when the nanocrystals are at about 4 nm from the interface. This demonstration supports the feasibility of an advanced thin-film hybrid solar cell concept

that relies on energy transfer between strong light absorbers and adjacent high-mobility Si layers.

4:40pm EN+TF-WeA9 Synthesis of a Thin-Film Ytria-Stabilized-Zirconia (Y₂O₃-ZrO₂) Thin Films by Radical Enhanced Atomic Layer Deposition for μ -Solid Oxide Fuel Cell Applications, J. Cho, D. Membreno, B. Dunn, J.P. Chang, University of California, Los Angeles

Solid Oxide Fuel Cells (SOFCs) is one outstanding alternative energy devices, owing to its significantly higher fuel conversion efficiency than that of fossil fuel based ones while being more environmentally benign. Despite its tremendous advantages and potentials, however, the commercial applications of this technology have been restrained due to its intrinsic problems such as the use of expensive interconnectors and long start-up time, which are inevitably tied to its high operation temperatures (650-1000°C) to maintain high ionic conductivity of electrolytes. To fully utilize the revolutionary potentials of SOFCs in commercial applications, it is imperative to lower its operation temperatures to intermediate temperatures, below 700°C without sacrificing the efficiency of the cell.

Ytria-Stabilized-Zirconia (YSZ, (Y₂O₃)_x-(ZrO₂)_(1-x)) has been implemented as the electrolyte material of choice in SOFCs because of their high structural, chemical stability with along with high ionic conductivity at the operation temperatures of the cell. While the temperature of the cell could not be lowered as it compromises its conductivity, recent pioneering studies of YSZ in nanoscales have reported significantly enhanced ionic conductivities which could not only lower the working temperature of the cell much below 700°C, but will also allow an expansion in their potential applications even to power portable electronics, resulting in strong scientific and technological interests in investigating the feasibility of developing YSZ in nanoscale for electrolyte applications in next-generation SOFCs, including μ -SOFCs for portable electronics. A thin-film YSZ has been synthesized by Radical Enhanced Atomic Layer Deposition (REALD), with thickness and composition controllability. The metal precursors, Tris(2,2,6,6-tetramethyl-3,5-heptanedionato)yttrium(III) [Y(tmhd)₃] and Bis(cyclopentadienyl)dimethylzirconium [Cp₂Zr(CH₃)₂] with Oxygen radicals as oxidant, were used to deposit Y₂O₃ and ZrO₂ with the deposition rates of 0.47 Å/cycle and 0.62 Å/cycle, respectively at ~250°C. The composition of each metal cations in YSZ thin films synthesized as a solid solution of Y₂O₃-ZrO₂ was found to correlate closely to the number of ALD cycles of each constituent oxide. The crystalline structures as well as the local environment of the deposited YSZ thin films were studied by X-ray diffraction (XRD) and Extended X-ray absorption fine structure (EXAFS). The conductivities of REALD YSZ films were found to be both a function of the thickness of YSZ film and the yttrium content in the film. The presence of conductivity enhancement effect on YSZ-SrTiO₃ nanoparticles are investigated as well.

5:00pm EN+TF-WeA10 ALD-enabled Tunneling and Transparent Conductive Oxide Layers for Novel Silicon Nanowire Solar Cells, M. Toivola, Picosun, Finland, C.L. Dezelah, Picosun USA, LLC

In order to enable more efficient harvesting of solar energy in the future, the recently ended (Dec 2011) EU 7th FP project ROD-SOL has successfully developed a novel, high efficiency solar cell based on Si nanostructures. The photoactive layer of this solar cell is a dense “forest” of adjacent Si nanowires (SiNW) deposited on metal or glass substrates. The 3D nanostructure of the NW forests offers various benefits over planar cell geometry, namely, more efficient light absorption due to light scattering in the NW forest, i.e. the NWs work as a light-trapping, antireflective layer.

The best solar cells in the project have already reached a promising value of near 10% efficiency and good long term stability. They were prepared with semiconductor-insulator-semiconductor concept, in which a 1-2 nm layer of ALD-deposited Al₂O₃ functions as a tunneling layer for the minority charge carriers between the SiNWs and the current collecting transparent conductive oxide (TCO) layer on the front side of the cell. Due to the high aspect ratio of the SiNWs ALD is the only method with which ultra-thin but highly uniform, conformal and pinhole-free tunneling layers can be coated on them. Also ALD-deposited, few hundreds of nm thick Al-doped ZnO (AZO) layer works as the TCO in SiNW solar cells, and we have investigated and optimized the electrical and optical properties of these layers.

AZO layers were prepared from trimethyl aluminum (TMA), diethyl zinc (DEZ) and deionized water (DIW). The varied parameters in AZO layers were deposition temperature (100 - 250 °C) and the percentage of Al in the ZnO matrix (0 - 11 %). The effects of post-ALD annealing and different TMA/DEZ/DIW pulsing orders were also tested.

The best conductivity (1-2 * 10⁻³ Ωm specific resistance) was achieved at 200 °C with a pulsing ratio of 5 % TMA and 95 % DEZ, equaling ~2 % elemental Al in ZnO. Reverse pulse order, i.e. starting the process with oxidant pulse instead of metal precursor, didn't result in significant performance improvement, neither did the annealing.

Optically, the ALD AZO films had high transparency over the visible wavelengths (no significant dependence on deposition temperature and/or Al doping-%) and refractive index $1.8 - 2$, so the films work efficiently as conformal antireflective coatings on Si.

In short, ALD-deposited TCO layers offer a potential alternative to indium-doped tin oxide (ITO) and other scarce element containing TCO materials in solar cells. In the novel nanostructured photovoltaic devices ALD is typically the only method with which thin enough coatings of high quality material (i.e. dense, uniform, conformal, crack- and pinhole-free) can be deposited.

5:20pm EN+TF-WeA11 Effect of Top Electrodes on the Photovoltaic Properties of Ferroelectric PLZT Thin Film Capacitors, V. Nampoori, S. Kotru, The University of Alabama

Ferroelectrics are emerging as potential candidate materials for energy harvesting and storage. A recent report suggesting the possibility of above band gap voltages from ferroelectric materials has attracted the interest of research community to study these materials for the applications towards non-conventional solar cells devices. Although these ferroelectric solar cells materials do not exhibit very high conversion efficiency compared to the conventional solar devices, but the control of the PV characteristics with controlled polarization in these materials, gives it an edge over the semi-conducting counterparts. It is now, widely agreed that the PV effect in a ferroelectric material is induced by internal polarization of the material which in turn separates the photo generated electron-hole pairs. However apart from controlling the polarization of the material, there are various other factors which could contribute to the PV output, choice of electrodes, is one among them.

In this work, PV response of ferroelectric PLZT thin film capacitors was investigated. The films were prepared using chemical solution deposition process. Capacitor type solar cells were fabricated from these films using various top electrodes. The IV curves were measured for each device. The ferroelectric/metal barrier as well as the bulk depolarizing field was shown to influence IV characteristics. Use of a metal top electrode with lower work function was found to increase the open circuit voltage (V_{oc}) from 0.17 V to 0.37 V. It was seen that use of a transparent conducting electrode could increase the V_{oc} further to $\sim 1.3V$. This in turn resulted in enhancement of PV efficiency of the devices. Such increase is attributed from the contribution of ferroelectric/metal barrier rather than from the bulk ferroelectric. These results indicate that choosing an appropriate top electrode can result in significant increase in the efficiency of the ferroelectric photovoltaic devices.

5:40pm EN+TF-WeA12 Synthesis of Nano-structured Zn_3P_2 as a Solar Cell Absorber, P.S. Vasekar, S.P. Adusumilli, D. Vanhart, T. Dhakal, Binghamton University

With rise in the prices and non-abundance of the materials like indium and gallium current research trends in thin film solar cells have been moving toward development of earth-abundant solar cell materials which can be synthesized using low-cost processes. Also zinc based hetero-junction partners are getting preference over toxic cadmium based compounds such as cadmium sulfide. Zn_3P_2 is also an important semiconductor from the II-V group and is used for optoelectronic applications. Zinc phosphide exhibits favorable optoelectronic properties such as direct bandgap of 1.5 eV which corresponds to the optimum solar energy conversion range. Also zinc phosphide has a large optical absorption coefficient of $>10^4 \text{ cm}^{-1}$, hence it can be positively used as a p-type absorber. Also due to its long minority diffusion length of $\sim 10 \mu\text{m}$, high current collection efficiency can be yielded. Zinc and phosphorous are quite abundant in earth's crust. It makes their cost-effective development quite feasible when it comes to large scale production. We have developed a very simple process using chemical reflux technique with Tri-octyl-phosphine (TOP) as a source of phosphorous. Zn_3P_2 has been synthesized in both nanowire and bulk form on zinc foil as well as glass substrates and initial results are quite encouraging. It has been observed that depending on the exposure method with TOP, either nanowire or bulk phase forms. Zinc metal when in contact with liquid TOP, develops nanowires in the range of 50-100 nm and the formation of nanowires exhibits a solution-liquid-solid (SLS) mechanism at the reaction temperature around 350 °C. To the best of our knowledge, zinc phosphide nanowire formation at this low temperature has been observed for the first time. Analysis has been carried out using SEM, XRD, TEM, XPS and PL.

Scanning Probe Microscopy Focus Topic

Room: 16 - Session SP+AS+BI+ET+MI+TF-WeA

Emerging Instrument Formats

Moderator: A. Belu, Medtronic, Inc.

2:00pm SP+AS+BI+ET+MI+TF-WeA1 Electrochemical Strain Microscopy: Nanoscale Imaging of Solid State Ionics, S. Jesse, Oak Ridge National Laboratory **INVITED**

Electrochemical reactions in solids underpin multiple applications ranging from electroresistive non-volatile memory and neuromorphic logic devices memories, to chemical sensors and electrochemical gas pumps, to energy storage and conversion systems including metal-air batteries and fuel cells. Understanding the functionality in these systems requires probing reversible (oxygen reduction/evolution reaction) and irreversible (cathode degradation and activation, formation of conductive filaments) electrochemical processes. Traditionally, these effects are studied only on the macroscopically averaged level. In this talk, I summarize recent advances in probing and controlling these transformations locally on nanometer level using scanning probe microscopy. The localized tip concentrates an electric field in a nanometer scale volume of material, inducing local ion transport. Measured simultaneously, the electromechanical response (piezo response) or current (conductive AFM) provides the information on bias-induced changes in a material. Here, I illustrate how these methods can be extended to study local electrochemical transformations, including vacancy dynamics in oxides such as titanates, $\text{La}_x\text{Sr}_{1-x}\text{CoO}_3$, BiFeO_3 , and $\text{Y}_x\text{Zr}_{1-x}\text{O}_2$. The formation of electromechanical hysteresis loops indistinguishable from those in ferroelectric materials illustrate the role ionic dynamics can play in piezoresponse force microscopy and similar measurements. In materials such as lanthanum-strontium cobaltite, mapping both reversible vacancy motion and vacancy ordering and static deformation is possible, and can be corroborated by post mortem STEM/EELS studies. The possible strategies for elucidation ionic motion at the electroactive interfaces in oxides using high-resolution electron microscopy and combined ex-situ and in-situ STEM-SPM studies are discussed. Finally, the future possibilities for probing electrochemical phenomena on in-situ grown surfaces with atomic resolution are discussed. This research was conducted at the Center for Nanophase Materials Sciences, which is sponsored at Oak Ridge National Laboratory by the Scientific User Facilities Division, Office of Basic Energy Sciences, U.S. Department of Energy.

2:40pm SP+AS+BI+ET+MI+TF-WeA3 Probing Electrochemical Phenomena in Reactive Environments at High Temperature: In Situ Characterization of Interfaces in Fuel Cells, S.S. Nonnenmann, R. Kungas, J.M. Vohs, D.A. Bonnell, University of Pennsylvania

Many strategies for advances in energy related processes involve high temperatures and reactive environments. Fuel cell operation, chemical catalysis, and certain approaches to energy harvesting are examples. Scanning probe microscopy provides a large toolbox of local and often atomic resolution measurements of phenomena at a scale that enables understanding of complex processes involved in many systems. Inherent challenges exist, however, in applying these techniques to the realistic conditions under which these processes operate. To overcome some of these challenges, we have designed a system that allows SPM at temperatures to 850° C in reactive gas environments. This is demonstrated with the characterization of an operating fuel cell. Solid oxide fuel cells (SOFCs) offer the highest conversion efficiencies with operating temperatures ranging from 400° C - 1000° C; and operate under variable gaseous fuel environments – H_2 -based environments (anode side) and O_2 -based environments (cathode side). Topography and the temperature dependence of surface potential are compared to impedance. While not (yet) at atomic levels of spatial resolution, these probes are at the scale to examine local interface properties.

3:00pm SP+AS+BI+ET+MI+TF-WeA4 High-Resolution Scanning Local Capacitance Measurements, M. Brukman, University of Pennsylvania, S. Nanayakkara, National Renewable Energy Laboratory, D.A. Bonnell, University of Pennsylvania

Spatial variation of dielectric properties often dictates the behavior of devices ranging from field effect transistors to memory devices to organic electronics, yet dielectric properties are rarely characterized locally. We present methods of analyzing 2nd harmonic-based local capacitance measurements achieved through non-contact atomic force microscopy. Unlike contact-based methods, this technique preserves tip shape and allows the same probe to realize high-resolution topographic imaging and scanning surface potential imaging. We present an improved analysis of the electrical fields between tip and sample, yielding high sensitivity to the capacitance-induced frequency shift.

The techniques are applied to thin-film ceramics (SrTiO₂ and HfO₂), metals (Pt and Ti), and mixed-phase self-

assembled monolayers to illustrate application over all orders of dielectric constant. Conversion from frequency shift signal to dielectric constant κ is demonstrated, with sub-5 nm spatial resolution and dielectric constant resolution between 0.25 and 1.

4:00pm **SP+AS+BI+ET+MI+TF-WeA7 Experimental Calibration of the Higher Flexural Modes of Microcantilever Sensors**, J.D. Parkin, G. Hähner, University of St Andrews, UK

Microcantilevers are widely employed as probes not only in atomic force microscopy [1], but also as sensors for mass [2], surface stress [3], chemical identification [3], or in measuring viscoelastic properties of cells [4].

Use of the higher flexural modes of microcantilever sensors is an area of current interest due to their higher Q-factors and greater sensitivity to some of the properties probed [2]. A pre-requirement for their exploitation, however, is knowledge of their spring constants [5]. None of the existing cantilever calibration techniques can calibrate the higher flexural modes easily.

We present a method that allows for the determination of the spring constants of all flexural modes. A flow of gas from a microchannel interacts with the microcantilever causing a measurable shift in the resonance frequencies of all flexural modes [6]. The method is non-invasive and does not risk damage to the microcantilever. From the magnitude of the frequency shifts the spring constants can be determined with high accuracy and precision. Experimental data for the response of the first four flexural modes of microcantilever beams used in AFM with spring constants in the range of ~0.03-90 N/m will be presented.

The spring constants of the first mode determined using our method are compared to those obtained with the Sader method [7]. Finite element analysis computational fluid dynamics (CFD) simulations of the experimental setup are used to provide an insight into the interaction of the flow with the microcantilever.

References

- [1] F.J. Giessibl, Rev. Mod. Phys. **75**, 949 (2003).
- [2] J.D. Parkin and G. Hähner, Rev. Sci. Instrum. **82**, 035108 (2011).
- [3] A. Boisen *et al.* Rep. Prog. Phys. **74**, 036101 (2011).
- [4] M. Radmacher *et al.* Biophys. J. **70**, 556 (1996).
- [5] G. Hähner, Ultramicroscopy **110**, 801 (2010).
- [6] G.V. Lubarsky and G. Hähner, Rev. Sci. Instrum. **78**, 095102 (2007).
- [7] J.E. Sader, J.W.M. Chon, and P. Mulvaney, Rev. Sci. Instrum. **70**, 3967 (1999).

4:20pm **SP+AS+BI+ET+MI+TF-WeA8 Atomic Imaging with Peak Force Tapping**, B. Pittenger, Y. Hu, C. Su, S.C. Minne, Bruker AFM, I. Armstrong, Bruker Nano Surfaces Division

As its name implies, Atomic Force Microscopy (AFM) has long been used to acquire images at the atomic scale. However these images usually only show the lattice of atoms in the crystal and do not show individual atomic defects. In order to achieve atomic resolution, researchers have typically had to design their systems for the ultimate in noise performance, sacrificing ease of use, flexibility, and scan size. Recently we have demonstrated that, by using Peak Force Tapping, our large sample platforms (Dimension Icon, Dimension FastScan) are capable of obtaining atomic resolution imaging along with maps of the tip-sample interaction. Unlike standard TappingMode, or FM-AFM, Peak Force Tapping uses instantaneous force control, allowing the system to be insensitive to long range forces while maintaining piconewton level control of the force at the point in the tapping cycle that provides the highest resolution – the peak force. Since the modulation frequency is far from resonance, the technique is less sensitive to the cantilever thermal noise (Brownian motion). In addition to topography, this technique can provide maps of the interaction between the tip and the sample. This is possible since Peak Force Tapping has access to the instantaneous force between tip and sample at any point in the modulation cycle. To study the details of a tip-sample interaction, Atomic Peak Force Capture can acquire the entire force distance curve used to create the interaction maps. These curves can be exported for easy analysis with models of tip-sample interaction. In this talk we will discuss the latest atomic resolution results using Peak Force Tapping and the implications of this with regard to studies of dissolution, crystallization, ordered liquids, and corrosion.

4:40pm **SP+AS+BI+ET+MI+TF-WeA9 Nanoscale Chemical Composition Mapping with AFM-based Infrared Spectroscopy**, C.B. Prater, M. Lo, Q. Hu, Anasys Instruments, C. Marcott, Light Light Solutions, B. Chase, University of Delaware, R. Shetty, K. Kjoller, E. Dillon, Anasys Instruments **INVITED**

The ability to identify material under an AFM tip has been identified as one of the "Holy Grails" of probe microscopy. While AFM can measure mechanical, electrical, magnetic and thermal properties of materials, until recently it has lacked the robust ability to chemically characterize unknown materials. Infrared spectroscopy can characterize and identify materials via vibrational resonances of chemical bonds and is a very widely used analytical technique. We have successfully integrated AFM with IR spectroscopy (AFM-IR) to obtain high quality infrared absorption spectra at arbitrary points in an AFM image, thus providing nanoscale chemical characterization on the sub-100 nm length scale. Employing the AFM-IR technique, we have mapped nanoscale chemical, structural and mechanical variations in multilayer thin films, nanocomposites, polymer blends, organic photovoltaics, and biological materials including hair, skin, and bacterial and mammalian cells. Light from a pulsed infrared laser is directed at a sample, causing rapid thermal expansion of the sample surface at absorbing wavelengths. The rapid thermal expansion creates an impulse force at the tip, resulting in resonant oscillations of the AFM cantilever. The amplitude of the cantilever oscillation is directly related to the infrared absorption properties of the samples, enabling measurements of IR absorption spectra far below the conventional diffraction limit. AFM-IR can be used both to obtain point spectra at arbitrary points and to spatially map IR absorption at selected wavelengths. Simultaneous measurement of the cantilever's contact resonance frequency as excited by the IR absorption provides a complimentary measurement of relative mechanical properties. We have used these techniques to chemically identify individual chemical components in polymer nanocomposites and multilayer films and performed subcellular spectroscopy and chemical imaging on biological cells. Using self-heating probes we have been able to locally modify the state of a semicrystalline polymer and observe the resulting change in absorption spectra on the nanoscale. Using polarization sensitive AFM-IR, we have mapped spatial variations in molecular orientation in electrospun fibers.

5:20pm **SP+AS+BI+ET+MI+TF-WeA11 Quantifying Nanomechanical Properties with Simultaneous AM-FM and $\tan\delta$ Imaging**, T. Mehr, A. Moshar, R. Proksch, I. Revenko, N. Geisse, S. Hohlbauch, D. Walters, J. Cleveland, J. Bemis, C. Callahan, D. Beck, Asylum Research

Frequency-Modulated (FM) is a powerful, quantitative technique for mapping interaction forces between an oscillating tip and sample. Since FM-AFM typically requires the use of three feedback loops, one ongoing challenge has been stable and cross-talk free operation. Amplitude-modulated Atomic Force Microscopy (AM-AFM), also known as tapping mode, is a proven, reliable and gentle imaging method with wide spread applications. Recently, the phase signal of the first resonant mode has been recast in terms of the tip-sample loss tangent.[1] This allows quantitative imaging of a response term that includes both the dissipated and stored energy of the tip sample interaction. Combining AM and FM imaging allows reaping the benefits of both techniques.[2] Because the feedback loops are decoupled, operation is more robust and simple than conventional FM imaging. In this mode, the topographic feedback is based on the AM signal of the first cantilever resonance while the second resonance drive is frequency modulated. The FM image returns a quantitative value of the frequency shift that in turn depends on the sample stiffness and can be applied to a variety of physical models. We will present results on a wide variety of materials as well as discussing quantitative separation of the elastic and dissipative components of the tip-sample interactions.[3]

References

- [1] R. Proksch and D. Yablon, Appl. Phys. Lett. **100**, 073106 (2012) and R. Proksch, D. Yablon, and A. Tsou, ACS Rubber Division 180th Technical Meeting, 2011-24 (2011).
- [2] G. Chawla and S. Solares, Appl. Phys. Lett., **99**, 074103 (2011) and R. Proksch and R. C. Callahan, US Patents 8,024,963 and 7,603,891.
- [3] R. Proksch and S. V. Kalinin, *Nanotechnology* **21**, 455705/1 (2010).

5:40pm **SP+AS+BI+ET+MI+TF-WeA12 Simultaneous Scanning Tunneling and Atomic Force Microscopy with Subatomic Spatial Resolution**, F.J. Giessibl, University of Regensburg, Germany

Frequency-modulation AFM can be combined with scanning tunneling microscopy, yielding a simultaneous data set for current and average force gradient. Ternes *et al.* [1] have shown that for some metallic contacts, force and current are proportional. The interaction of a tungsten tip with a CO molecule adsorbed on Cu(111), however, yields a much different symmetry and distance dependence of tunneling current and force [2]. The tunneling current yields a gaussian dip over the CO molecule, while the forces show a

strong angular dependence with force fields that vary strongly by distance and angle within the extent of the single front atom, displaying subatomic variations. While the simultaneous acquisition of current and force can reveal new information about the atomic and electronic structure of matter, the tunneling current can modify the atomic forces. This “phantom force” [3,4], a modification of the electrostatic attraction between tip and sample, originates in an alteration of the effective potential difference between tip and sample caused by strongly localized voltage drop induced by the tunneling current. The talk discusses the potential of combined STM/AFM as well as the challenges, in particular with respect to tip preparation and characterization.

- [1] M. Ternes et al., *Phys. Rev. Lett.* **106**, 016802 (2011).
- [2] J. Welker, F. J. Giessibl, *Science* **326**, 444 (2012).
- [3] A.J. Weymouth et al. *Phys. Rev. Lett.* **106**, 226801 (2011).
- [4] T. Wutscher et al. *Phys. Rev. B* **85**, 195426 (2012).

Thin Film

Room: 11 - Session TF+AS-WeA

Thin Films: Growth and Characterization-I

Moderator: M.R. Davidson, University of Florida

2:00pm **TF+AS-WeA1 Studying the Microstructure of Cu₂ZnSn(S,Se)₄ Thin Film Solar Cells**, *L. Zhang, Y. Cao, D.H. Rosenfeld, M. Lu, J. Caspar, C. Chan*, DuPont Central Research and Development

To advance the next generation photovoltaic technology, the new ink-based Cu₂ZnSn(S,Se)₄ (CZTSSe) solar cells have attracted rapid growth attention in the thin film photovoltaic areas. As a potential alternative to CIGS, the CZTSSe technology offers a non-vacuum based and likely low manufacturing cost process with active area efficiency above 9%. In particular, the fact that CZTSSe utilizes only earth abundant elements enables the sustainability & renewability for future green energy demand.

The overall CZTSSe solar cell developed by DuPont scientists consists of multi-layer inorganic structures of ITO/ ZnO/ CdS / CZT(S,Se) / Mo on sodalime glass substrate. A novel synthetic method has been developed to produce the active CZTSSe layer. During the process, binary and ternary chalcogenide nanoparticles are first synthesized as starting materials, formulated into a precursor ink, applied onto a substrate, and then converted into CZTSSe upon a thermal annealing process. To aid product development for optimum efficiency, chemical and structural characterization of the active CZTSSe layer and interfaces between different layers are performed using multiple analytical techniques. For example, sputter depth profiling with XPS and Auger, and cross-section SEM/EDX helped us to visualize the structural chemistry at specific locations in the films which enabled the team to adjust ink formation as well as processing conditions for better and more efficient cell production. This presentation will cover the characterization of CZTSSe solar cells, including the study of film composition and morphology, inter-layer diffusion, and their correlation with device performance.

2:20pm **TF+AS-WeA2 Seed-Mediated Growth of 1D Pyrite (FeS₂) Structures**, *Y.J. Kwon, N. Berry, M. Law, J.C. Hemminger*, University of California Irvine

Iron pyrite is a promising semiconductor for use in solar cells due to its earth-abundance, suitable bandgap, and high absorption coefficient. Pyrite device efficiency is only about 3% due to a low open-circuit photovoltage and high dark current, possibly as a result of sulfur deficiency at the surface resulting in thermionic field emission. Although fabrication of pyrite thin films has been studied by various methods, specific details of the pyrite growth process in the presence of homogeneous nucleation sites has not been studied. In this project, the role of pyrite nucleation sites is investigated in the growth of pyrite thin films by atmospheric-pressure chemical vapor deposition (AP-CVD). The pyrite nanoparticle nucleation sites are fabricated by sulfurization of pre-deposited Fe₂O₃ grains on the step edges of highly oriented pyrolytic graphite (HOPG) using H₂S, elemental sulfur or a combination of the two annealing treatments and characterized by transmission electron microscopy (TEM), X-ray photoelectron spectroscopy (XPS), X-ray diffraction (XRD) and Raman spectroscopy. H₂S-sulfurized Fe₂O₃ nuclei coalesce to form FeS₂ nanowires containing both pyrite and marcasite phases. A subsequent elemental sulfur treatment on either H₂S-sulfurized samples or pre-deposited Fe₂O₃ samples yield pure pyrite; however, the nanowires convert to a less desirable morphology of randomly sized spherical grains as a result of this annealing treatment. Atmospheric Pressure-CVD of FeS₂ from iron-(III) acetylacetonate and *tert*-butyl disulfide was performed to grow pyrite on

these seeded substrates. Initial deposition on the H₂S-annealed samples leads to only seed-mediated growth and the formation of linear arrays of polycrystalline FeS₂ nanowires. However, due to marcasite phase presence on pre-covered FeS₂ nanoparticle seeds, both marcasite and pyrite phases could be observed. Initial deposition on elemental sulfur treated samples with pure pyrite phase showed deposition occurring throughout the substrate. No preferential growth on seeded pyrite nucleation sites was observed. It is proposed that during elemental sulfur treatment, new nucleation sites form, leading to deposition covering the substrate. Further work is in process to clearly determine or identify the growth mechanism of pyrite. In this work, we will gain a greater understanding of early stages of pyrite growth process in the presence of homogeneous nucleation sites.

2:40pm **TF+AS-WeA3 Investigation of Recrystallization in Low-Temperature Grown CdTe Solar Cells in Substrate and Superstrate Configuration**, *L. Kranz, C. Gretener, J. Perrenoud, S. Buecheler, A.N. Tiwari*, EMPA, Switzerland

INVITED
CdTe solar cells and modules on glass substrates have already shown high performance and low cost. Production costs and energy payback time can be further reduced by minimizing the thermal budget of the production process, increasing the throughput and by the use of low-cost substrates. We developed a process for the conventional superstrate configuration which involves substrate temperatures below 450°C. The low temperatures enable the growth on flexible polyimide foil. Efficiencies up to 15.6% and 13.8% on glass and polyimide were achieved, respectively.

In the conventional superstrate configuration sputtered ZnO:Al/ZnO was used as transparent front electrical contact. CdS and CdTe were evaporated at low temperatures of 160 and 350°C followed by an annealing treatment in the presence of CdCl₂ at 420°C and the cells were finished with a metallic electrical back contact. The annealing treatment is essential for highly efficient CdTe solar cells as it leads to grain growth of CdTe, improves electronic properties of CdTe and leads to an intermixing between CdTe and CdS.

For the growth on opaque substrates like flexible metal foils, we developed a growth process of CdTe solar cells in substrate configuration, where light does not need to pass the substrate. It enabled efficiencies of 11.3% and 8.7% on glass and flexible steel foil, respectively.

A combination of Mo, MoO₃ and Te was deposited as back contact and in some cases Cu was added. Evaporated MoO₃ grew with low crystallinity and recrystallized during subsequent processing. CdTe was deposited by vacuum evaporation while CdS was grown by chemical bath deposition. In substrate configuration, the CdTe and CdS layers were annealed separately as a combined annealing step would lead to excessive CdS-CdTe intermixing. The annealing treatment of the CdTe layer leads to similar grain growth as in superstrate configuration. The CdCl₂ treatment after deposition of CdS was optimized, resulting in increased grain size and wurtzite structure. CdS-CdTe intermixing, which is commonly observed in superstrate configuration was less pronounced in substrate configuration. The effects of the recrystallization treatments in substrate configuration are compared to the conventional superstrate configuration.

4:00pm **TF+AS-WeA7 High Quality ZnMgO Thin Films Grown on Sapphire and ZnO Substrates by Molecular Beam Epitaxy**, *M. Wei, R.C. Boutwell, W.V. Schoenfeld*, University of Central Florida

Zinc oxide (ZnO) based material is attractive for high efficiency ultraviolet (UV) optoelectronics devices. We will report growth of high quality ZnMgO on both sapphire and ZnO substrate by plasma-assisted molecular beam epitaxy (MBE). With relatively low growth rate and optimized growth condition, we were able to achieve step flow growth of ZnO thin films. ZnO thin films grown on sapphire showed high crystalline quality, low carrier concentration, high mobility and sub-nanometer surface roughness with terrace steps, indicating suitability for UV application. Homoepitaxial ZnO films were grown on both c-plane and miscut ZnO substrates with atomically flat surface, no threading dislocation and same crystallinity as the substrate. Ga doping was demonstrated for ZnMgO films on sapphire and ZnO substrates. This work may lead to the realization of high efficient UV emitters such as Laser diodes.

4:20pm **TF+AS-WeA8 Epitaxial Growth of Zirconium Diboride Thin Film on Ge(111) Wafer**, *C. Hubault, A. Baba, A. Fleurence, Y. Yamada-Takamura*, Japan Advanced Institute of Science and Technology

GaN-based semiconductors are widely used in optoelectronic devices. To grow these films, substrates such as sapphire, SiC and Si are used. However, recently, Lieten *et al.* [1] have proposed to grow GaN on Ge(111) substrate to have a more closely matching thermal expansion coefficient and to decrease the lattice mismatch. Despite the good quality of the film, misoriented domain and voids can be found in it. While the domains can be suppressed, the voids cannot, as they come from a diffusion of Ge atoms in

the film. This is a problem for the growth of p-type or semi-insulating GaN layers.

Using ZrB₂ as a buffer layer on Ge substrate could help by providing a diffusion barrier. Moreover, ZrB₂ substrate has already been used as a conductive growth template for GaN and has proven to be interesting thanks to the low lattice mismatch and close in-plane thermal expansion coefficient [2]. Therefore, ZrB₂ has been used as a buffer layer for the growth of GaN films on Si wafer [3] and those films were shown to be promising.

It was also demonstrated that on top of ZrB₂(0001) thin film on Si(111) substrate, silicene, which has a similar structure to graphene was present [4]. In the periodic table, C, Si and Ge are in the same column. Therefore, we can envisage the possibility of the formation of germanene in the same manner as silicene on top of the ZrB₂ layer grown on germanium substrate.

Here, we report on the epitaxial growth of ZrB₂ thin films on Ge(111) by thermal decomposition of Zr(BH₄)₄ in a dedicated UHV-chemical vapour deposition system. The growth was monitored *in situ* by RHEED, and the samples were further analysed by XRD and TEM. The film grows with epitaxial relationship of ZrB₂(0001)//Ge(111). Under slow growth conditions (substrate temperature, T_s=750°C), two types of in-plane orientations, which are rotated by 30° can be observed, while under faster growth condition (T_s=650°C), the layer is monocrystalline. The single-crystalline film has in-plane orientation of ZrB₂[11-20]//Ge[-110], similar to the case of single-crystalline ZrB₂ film on Si(111) [4], but with a different surface reconstruction of ($\sqrt{3}\times\sqrt{3}$) when cooled down under 450°C. There is a good epitaxy between the layer and the substrate with the presence of a second phase at the interface, which tends to disappear when the growth was carried out at 550°C.

[1] R.R. Lieten *et al.*, J. Cryst. Growth, 314, 71 (2011).

[2] H. Kinoshita *et al.*, Jpn. J. Appl. Phys., 42, 2260 (2003).

[3] Y. Yamada-Takamura *et al.*, Phys. Rev. Lett., 95, 266105 (2005).

[4] A. Fleurence *et al.*, Phys. Rev. Lett., accepted for publication.

4:40pm TF+AS-WeA9 Effect of Growth Conditions on Cubic ZnMgO films, C. Boutwell, M. Wei, W.V. Schoenfeld, University of Central Florida
ZnMgO films were grown on MgO substrates by Plasma-Enhanced Molecular Beam Epitaxy. Epilayer morphology, stoichiometry, and crystalline orientation were investigated. Films were produced by varying cation source temperature/flux, substrate temperature, and oxygen plasma power and flow rate. Crystalline immiscibility was determined in the phase mixed cubic/wurtzite range. Growth rate varied from 30nm/hr to 175nm/hr while roughness varied from 4nm to 110nm in cubic to mixed-phase samples. Wurtzite ZnO peaks at (002) and (101) were apparent from θ -2 θ X-Ray Diffraction on phase separated films, indicating multiplanar ZnO crystallite growth on the (001) MgO substrate. Growth condition information will be useful for optimization of optoelectronic devices functional in the deep ultraviolet/solar-blind range.

5:00pm TF+AS-WeA10 Properties of Ytterium Doped Zinc Oxide Thin Films Deposited by r.f. Magnetron Sputtering, K. VanSant, T. Barnes, J. Burst, J. Duenow, T.A. Gessert, National Renewable Energy Laboratory

Transparent conducting oxides (TCOs) based on zinc oxide (ZnO) and aluminum (Al) doped ZnO (AZO) are important for many large-scale commercial applications because they exhibit good optical and electrical properties. Further, their constituent elements are non-toxic and abundant, and high-quality thin-films can be deposited at room temperature using a variety of deposition processes. These characteristics make AZO appealing for use as part of the top contact in copper indium gallium diselenide (CIGS) PV modules. Although the present generation of ZnO-based TCOs meet many of the technical requirements of present-generation technologies, it is known that the material could be much more widely applied if some of its properties were more consistent with another important TCO, In₂O₃:Sn (i.e., ITO). In this comparison, the main properties requiring improvement include increasing the mobility from ~20 to ~50 cm² V⁻¹s⁻¹ while maintaining carrier concentrations > 5x10²⁰ cm⁻³ and improving the moisture-tolerance of the films. Earlier work has already shown that AZO with mobility approaching 50 cm²V⁻¹s⁻¹ can be achieved by careful control of the sputtering ambient and the dopant concentration. This study investigates the use of the Group IIIA material yttrium (Y) as a dopant, as well as the impact it has on the optical properties of ZnO. The Y-doped ZnO films are deposited on glass by r.f. magnetron sputtering using pressed powder targets, and the Y concentration is varied by simultaneous co-sputtering from a ZnO:Y target. The films will be analyzed using a combination of Hall measurements, UV-Vis-NIR spectrophotometry, spectroscopic ellipsometry, and Auger/X-ray photoelectron spectroscopy (XPS) and Secondary Ion Mass Spectrometry (SIMS). Based on prior research related to the addition of zirconium (Zr) to ITO, it is suspected that the addition of Y in ZnO may lead to similar changes in the optical

properties of this material. Understanding the functionality of these changes could have significant implications for device applications requiring greater control of the dielectric properties of ZnO.

5:20pm TF+AS-WeA11 Effect of Process Parameters on Molybdenum Thin Films and Development of Single Layer Molybdenum Film for CIGS Thin Film Solar Cells, S. Pethe, A. Kaul, N. Dhere, Florida Solar Energy Center, University of Central Florida

Molybdenum back contact in CuIn_{1-x}Ga_xSe_{2-y}S_y (CIGSeS) solar cells is usually deposited using DC magnetron sputtering. Properties of thin films are dependent on process parameters. Films deposited at high power and low pressure, tend to be more conductive. However, such films exhibit poor adhesion strength since the films are under compressive stress. Films deposited at low power and high pressure tend to be under tensile stress and exhibit higher roughness and resistivity, while the films adhere very well to the sodalime glass substrate. Therefore, it has been a practice to deposit multi-layered Mo back contact to achieve properties of good adhesion and higher conductivity. Deposition of multi-layered back contact results in either increase in deposition time if a single target is used or increase in footprint if multiple targets are used resulting in increase in the total cost of production. Experiments were carried out to understand effects of working pressure, sputtering power and working distance on molybdenum film properties with the final aim to develop a process recipe for deposition of a single molybdenum film with acceptable properties of both good adhesion and higher conductivity. Experiments were carried out at a fixed working distance by varying the working pressure and keeping the sputtering power constant and then varying the sputtering power keeping the working pressure constant. The same set of experiments were repeated with varying working distance. Moreover, the effect of the relative position of the substrate with respect to the sputtering target for a moving target was studied. Adhesive tape test was performed on each film to determine the adhesion strength of the films. Moreover, the sheet resistance and the average roughness for each film were measured using a four probe measurement setup and the Dektak Profilometer, respectively. All experiments were also carried out on narrow and long glass strips in order to estimate the residual stress in the film by using the bend test method. Based on the results obtained from the experiments carried out a process recipe was developed for depositing on a moving substrate, a single layer molybdenum film with acceptable properties of good adhesion and higher conductivity.

5:40pm TF+AS-WeA12 Oxygen Reservoir Effect and its Impact on HfO₂, C. Vallee, C. Mannequin, P. Gonon, L. Latu-Romain, LTM (CNRS / UJF-Grenoble1 / CEA), France, A. Salain, H. Grampeix, V. Jousseau, CEA, LETI, MINATEC Campus, France

ReRAM device is a non-volatile memory based on resistive switching phenomena in a dielectric in a MIM (Metal Insulator Metal) structure. Depending on the nature of the oxide and the metallic electrode, the switching is based on a unipolar thermochemical mechanism (TCM), a bipolar valence change mechanism (VCM), as well as a bipolar electrochemical metallization mechanism (ECM). For all these devices, the choice of the oxide (nature, crystallization, density, doping, vacancies), the metal (inert electrode, its free energy formation of the oxide) as well as the interfacial layer (role of the electrode, role of the process) are impacting the operation sets and reliability of the device. For example, it has been shown that electrode reaction is one of the major factors determining the functionality of ECM cells [1].

This work is focused on HfO₂ based ReRAMs which are good candidates for embedded non-volatile memories [2-4]. For this material, forming/set and reset processes are correlated with the respective generation of oxygen vacancies and recombination of Vo²⁺ positive charges with oxygen ions (O²⁻). It has been recently proposed that during the negative reset the passivation occurs by the back-diffusion of oxygen ions stored in the oxide portion near the conductive filaments and at the electrode, which serve as oxygen reservoir [5].

With this work we propose to discuss on the reservoir effect by studying HfO₂ memories obtained with top electrodes of different chemical compositions and morphologies. The HfO₂ dielectric (10 nm) is deposited by Atomic Layer Deposition on Pt and TiN. X-ray Photoelectron Spectroscopy and Transmission Electron Microscopy characterization have been used to investigate the chemical composition, morphology and crystalline structure of the oxide and metallic layers. It is hence demonstrated that devices with gold deposited by a PVD process give better results than those obtained with gold deposited by evaporation. This can be related to a modification of oxygen diffusion through the top electrode via a difference in the electrode morphology (roughness, thickness...) induced by the process. Moreover, it is shown that alloying the gold target of the PVD process with a suitable metal considerably helps to improve the reliability of the memory. This is discussed in terms of catalytic effect and modification of the electrode morphology and reservoir effect.

- [1] I. Valov *et al*, *Nanotech.* **22** (2011) 254003
 [2] P. Gonon *et al*, *J. Appl. Phys.* **107** (2010) 074507
 [3] J.J. Yang *et al*, *Appl. Phys.* **A102** (2011) 785
 [4] Ch. Walczyk *et al*, *J. Vac. Sci. Technol.* **B29** (2011) 01AD02-1
 [5] S. Yu *et al*, *IEDM* (2011) 17.3.1

Thin Film

Room: 10 - Session TF+MI-WeA

Thin Films for Memory and Data Storage

Moderator: S. Gupta, The University of Alabama

2:00pm **TF+MI-WeA1 Spin Transport Properties and Applications in Magnetic Multilayers**, *R.H. Victora, S.H. Hernandez, T. Qu*, University of Minnesota **INVITED**

Since the discovery of giant magnetoresistance (GMR) in 1988, spin transport has rapidly evolved as a research area examining effects such as Current Perpendicular to Plane (CPP) GMR and spin torque transfer (STT). Giant Magnetoresistance is caused by spin-dependent scattering. High electrical resistance (R_{AP}) is measured for antiparallel magnetizations of adjacent layers, while low resistance (R_P) is measured for parallel magnetizations. CPP GMR shows an advantage in MR ratio ($(R_{AP}-R_P)/R_P$), because all electrons must pass through all layers. This geometry is widely used as the reader in high areal magnetic recording, where it is likely that the current non-magnetic insulator will ultimately be replaced by a metallic layer in order to limit resistance. The reciprocal effect, STT, occurs when an electric current passes through a pinned ferromagnetic layer and the angular momentum (magnetic moment) is transferred to a neighboring free magnetic layer. The magnetization in the free layer may stably oscillate or may achieve a collinear state to the pinned layer. Magnetization switching with the help of a current has been proposed as potential magnetoresistive random access memory (MRAM). However, the mechanism of spin transport is not fully understood for these effects.

We consider multiple reflections between the interfaces of the adjacent magnetic layers. If the ferromagnetic material is not 100% polarized, electrons with different polarizations are not perfectly transmitted or reflected. We show that reflections, although typically neglected, strongly affect the spin transport properties. They explain the experimentally observed nonlinearity of GMR dependence on $\beta = \cos^2(\theta/2)$ (θ is the angle between the magnetizations of the fixed and free layers). Also the spin torque is decreased² by the reflection. The more orders of reflection we include in the spin torque, the more critical current is needed to switch the magnetization state. The spin torque oscillator (STO) is an attractive replacement for current microwave devices owing to its very small (nanoscale) size. However, a single STO does not provide sufficient power for many applications. An array of oscillators in series or parallel has been proposed to generate more power. The problem is to phase lock the non-uniform oscillators. We calculate the power spectrum of serial oscillators. We show that the oscillators could be closely synchronized by a feedback ac current, even at room temperature.

1. T. Qu and R.H. Victora, *J. Appl. Phys.* **111**, 07C516 (2012)
 2. S. Hernandez and R.H. Victora, *Appl. Phys. Lett.* **97**, 062506 (2010)

2:40pm **TF+MI-WeA3 Ta Seeded Ultrathin Free Layer for Fully Perpendicular Magnetic Tunnel Junctions**, *A. Singh, A. Natarajathinam, B.D. Clark, S. Gupta*, The University of Alabama

Studies of the effect of seed and capping layers on CoFeB free layers of magnetic tunnel junctions (MTJ's) originated from reports (1) of the crystallization of the CoFeB through diffusion of the B into the cap, as well as inducing an interfacial perpendicular magnetic anisotropy in the free layer (2, 3). We have also seen that CoFeB can be made perpendicular [3, 4] with seed layers of certain materials, such as Ta and Ru. We deposited Ta and Ru seed layers with the following stack structure: (Ta/Ru/Hf/Zr) 2/[tCoFeBx]/MgO 0.9/TaN5 nm. The thickness of CoFeB, tCoFeB, was varied between 0.8 to 1.4 nm. Samples with the Ta seed layer showed higher perpendicular anisotropy than that of Ru, Hf and Zr because of the B diffusion into Ta after annealing. At tCoFeB = 1nm, high perpendicular anisotropy was seen, with anisotropy energy density $K_{ut} = 0.24$ erg/cm². The optimized Ta-seeded CoFeB was used as the free layer in a fully perpendicular MTJ stack with a Co/Pd multilayer synthetic antiferromagnet pinned layer [5]. These MTJ stacks were then patterned into devices with photolithography and planarized at each step of fabrication with a novel sputtered aluminum oxide passivation layer. After fabrication, these devices were subjected to a variety of annealing conditions: a) furnace annealed with a field of 0.5T applied in the plane of the sample at 1500C for 2 hours,

b) rapid thermally annealed (RTA) at 3500C, 4000C and 5000C for various time periods. Magnetometry of the minor loops indicated that, as the RTA time was increased at each temperature, the free layer became fully perpendicular at 8 minutes and then went in-plane with longer annealing times of 12 minutes. These results matched closely with the transport measurements. Increase of annealing time improved the tunneling magnetoresistance (TMR) to a maximum of 50% at room temperature (nearly 60% at 4.2K). Further increase in annealing time degraded the TMR at all temperatures tested. Thus for the first time, we have found that magnetometry on the free layer of fully perpendicular magnetic tunnel junctions (pMTJ) can be used to optimize the annealing conditions.

References

1. E. Chen *et al*, *IEEE Trans. Magn.* **46**, 1 (2010).
 2. S. M. Watts *et al*, *Digest FV-11*, 11th Joint MMM-Intermag Conference, Washington, DC(2010)
 3. D. Worledge *et al*, *Digest HB-10*, 11th Joint MMM-Intermag Conference, Washington, DC(2010)
 4. D. C. Worledge, G. Hu, David W. Abraham, J. Z. Sun, P. L. Trouilloud, J. Nowak, S. Brown, M. C. Gaidis, E. J. O'Sullivan, and R. P. Robertazzi. *Appl. Phys. Lett.* **98**, 022501 (2011).
 5. A. Natarajathinam, R. Zhu, P.B. Visscher and S. Gupta, *J. Appl. Phys.* **111**, 07C918 (2012).

3:00pm **TF+MI-WeA4 Epitaxial Fe_{38.5}Pd_{61.5} Films Grown by Pulsed Laser Deposition: Structure and Properties**, *M.A. Steiner, R.B. Comes, J.A. Floro, W.A. Soffa, J.M. Fitz-Gerald*, University of Virginia

Thin films of 3d-4d/5d metallic alloys such as Fe-Pt, Co-Pt, and Fe-Pd are of technological interest due to their ordered L1₀ tetragonal phase which exhibits high magnetocrystalline anisotropy comparable to that of 3d-4f rare earth magnets. A combination of hard magnetic properties with ductility and corrosion resistance makes this family of alloys ideal for applications including micro-electro-mechanical systems and ultra-high-density magnetic storage. These alloys are known to develop unique microstructures, including a novel strain-induced chessboard eutectoid microstructure featuring exchange coupling effects that has been found between the hard L1₀ and soft L1₂ magnetic phases of the Co-Pt system. Within this class of materials, Fe-Pd alloys possess a somewhat lower magnetocrystalline anisotropy compared to Co-Pt and Fe-Pt, but the Fe-Pd phase diagram showing considerably lower order-disorder transition temperatures renders them well-suited for nanostructured magnetic applications and study.

Epitaxial films of Fe_{38.5}Pd_{61.5} at the L1₂-L1₀ eutectoid composition have been grown on MgO 001 oriented substrates by pulsed laser deposition. These films exhibit atomic ordering with increasing temperature, transitioning from the disordered A1 (FCC) phase to the ordered L1₂ phase. Fe_{38.5}Pd_{61.5} films grown at 550°C have been found to possess a two-phase microstructure of prismatic 50-100 nm disordered A1 secondary phases with 110 oriented facets embedded within an ordered L1₂ matrix. These secondary phases exhibit single domain magnetic axis rotation, while the easy magnetic axis of the ordered L1₂ matrix lies in plane due to strain induced by epitaxy. The growth these two-phase films has been studied as a function of deposition time. The films grown in this study were characterized by x-ray diffraction, vibrating sample magnetometry, atomic and magnetic force microscopy, and high resolution scanning electron microscopy.

Thursday Morning, November 1, 2012

Transparent Conductors and Printable Electronics

Focus Topic

Room: 7 - Session TC+EM+AS+TF+EN-ThM

Transparent Conductors and Devices

Moderator: L.M. Porter, Carnegie Mellon University

8:20am **TC+EM+AS+TF+EN-ThM2 High Conductivity in Thin ZnO:Al Deposited by Means of the Expanding Thermal Plasma Chemical Vapor Deposition**, K. Sharma, H.C.M. Knoops, M.V. Ponomarev, Eindhoven University of Technology, The Netherlands, R. Joy, M. Velden, D. Borsa, R. Bosch, Roth and Rau BV, Germany, W.M.M. Kessels, M. Creator, Eindhoven University of Technology, The Netherlands

Session: Transparent Conductors and Devices

The ever-increasing demand for transparent conducting oxides (TCO) for application in flat panel displays, light emitting diodes (LEDs), and thin film photovoltaics drives the present research in the field of TCOs. Aluminum-doped zinc oxide (ZnO:Al) is often referred to as a potential alternative to e.g. indium tin oxide. The ZnO:Al is considered appealing due to the relatively low cost, high abundance, non-toxicity, resistance to H₂ etching and, under specific conditions, surface texturing for light management/trapping. Thin ZnO:Al films (~ 100 nm) with low resistivity ($2.5 \cdot 10^{-4}$ ohm*cm) along with high transmission (> 85 %) are desirable in many devices. Furthermore, large area processing/ high throughput are essential pre-requisites for industrial applications.

ZnO:Al thin films (< 150 nm) have been deposited by using an in-line industrial expanding thermal plasma chemical vapor deposition (ETP-CVD) technique,^{1,2,3} by means of O₂/diethylzinc/trimethylaluminium mixtures. High diethyl zinc flow rate conditions² were applied, which enable the development of a conductive ($5 \cdot 10^{-4}$ Ω·cm), 300 nm-thick ZnO:Al layer by promoting the development of a densely packed structure at early stages of growth, as very recently reported.²

In the present contribution, the effect of the dopant, i.e. trimethylaluminium, is investigated to further improve the electrical quality of even thinner ZnO:Al layers. ZnO:Al films were analyzed with spectroscopic ellipsometry, four point probe, hall measurements, X-ray photon spectroscopy (XPS), Rutherford backscattering (RBS), elastic recoil backscattering (ERD), and X-ray diffraction (XRD).

A remarkable low resistivity of $5 \cdot 10^{-4}$ Ω·cm was measured for a ZnO:Al film with thickness of only 120 nm, characterized by a carrier concentration of $1 \cdot 10^{21}$ cm⁻³, with an electron mobility in the range of 10-25 cm²/V · s.^{2,3} The obtained mobility values are higher than previously reported value of 13 cm²/V · s for 300 nm thick ZnO:Al.² The improvement in terms of conductivity is attributed to the large hydrogen content ($2-4 \cdot 10^{21}$ at/cm³) promoting the chemical passivation of the grain boundaries.

A broad characterization of highly conductive thin ZnO:Al films along with insights on charge transport process will be presented.

Reference List

1. B. Hoex *et al.*, Progress in Photovoltaics **13**, 705 (2005).
2. M. V. Ponomarev *et al.* Journal of Applied Physics **112**, 043708 (2012).
3. M. V. Ponomarev, *et al.*, Journal of Applied Physics **111**, 063715 (2012).

8:40am **TC+EM+AS+TF+EN-ThM3 Recent Progress in Oxide Semiconductors and Oxide TFTs**, H. Hosono, Tokyo Institute of Technology, Japan **INVITED**

Transparent conductive oxides (TCOs) and transparent oxide semiconductors (TOSS) have a long history since 1950s. The material design concept for TCOs looks almost established, i.e., ionic oxides of block metals with an electronic configuration of (n-1)d¹⁰ns⁰ and a spatial spread of ns orbitals which is enough to have large overlap with neighboring metal ns orbitals irrespective of intervening oxygen ion¹⁾. Concretely, most of the TCOs have been realized in the material systems of In₂O₃-SnO₂-CdO-Ga₂O₃-ZnO. Materials based on light metal oxides such as Al₂O₃ and SiO₂ have not been regarded as the candidates of TCOs. In 2002, we²⁾ reported high electronic conductivity in 12CaO·7Al₂O₃(C12A7) which had been a typical insulator and this discovery was followed by transparent conductivity in cubic SrGeO₃ in 2011.³⁾ These two materials are TCOs realized by a new material design concept.

As for TOS, the striking advances are seen in transparent amorphous oxide semiconductors (TAOS) in science and technology due to strong demand for

active layer materials in thin film transistors (TFTs). Amorphous In-Ga-Zn-O (IGZO) TFTs, which was first reported in late 2004,⁴⁾ has adopted to drive high resolution displays of new iPad.⁵⁾ This is a first mass production of TOS family. The major reasons for this adoption are high electron mobility (an order of larger than that of a-Si:H) and easy fabrication process. A major advance in TOS-TFTs is realization of p-channel TFTs and subsequent fabrication of C-MOS using ambipolar SnO.⁶⁾

In this talk, I review these progresses viewed from electronic state of these materials.

- 1) H. Kawazoe, H. Yanagi, K. Ueda, and H. Hosono. *MRS Bull.*, **25**, 28 (2000)
- 2) K. Hayashi, S. Mitsuishi, T. Kamiya, M. Hirano, H. Hosono, *Nature* **419**, 462 (2002).
- 3) H. Mizoguchi, T. Kamiya, S. Mitsuishi, H. Hosono: *Nat. Commun.*, **2**, 470 (2011).
- 4) K. Nomura, H. Ohta, A. Takagi, T. Kamiya, M. Hirano, H. Hosono, *Nature* **432**, 488 (2004).
- 5) Sharp Press Release April 6, 2012
- 6) K. Nomura, T. Kamiya, and H. Hosono: *Adv. Mater.*, **23**, 3431 (2011)

9:20am **TC+EM+AS+TF+EN-ThM5 Surface Functionalization of Amorphous Zinc Tin Oxide Thin Film Transistors**, G.S. Herman, M.S. Rajachidambaram, Oregon State University, A. Pandey, S. Vilayrganapathy, P. Nachimuthu, S. Thevuthasan, Pacific Northwest National Laboratory

Amorphous zinc tin oxide semiconductor materials have been studied primarily as the active semiconducting material for thin film transistors (TFT) for applications including transparent and flexible electronics. Due to the amorphous nature of these materials excellent uniformity can be obtained over large areas while still having reasonably high electron mobilities (>10 cm²/Vs). Considerable control over the electrical properties of ZTO can be maintained, where insulating, semiconducting, and conductive films can be obtained by varying the processing and post-annealing conditions. We have recently characterized sputter-deposited zinc tin oxide (ZTO) as the active material for TFTs and found that the switching properties of ZTO are closely related to deposition, post-annealing, and electrical test conditions. In this presentation we will discuss bias stress induced instabilities for ZTO TFTs. We have found that devices with a backchannel exposed to the atmosphere have a positive subthreshold shift under positive bias, which can be well explained by a stretched exponential model. Using this model the shifts may be related to either electron trapping at the dielectric semiconductor interface or due to metastabilities of the active material. We have found that the adsorption of a self-assembled monolayer (SAM) on the backchannel of the TFT effectively passivates the device and significantly reduces the bias stress induced instabilities. In this study we will present contact angle measurements and x-ray photoelectron spectroscopy to better understand the interaction of the SAM with the ZTO surface, and the improved stability of the ZTO TFTs will be discussed in regards to the interfacial chemistry of the backchannel.

9:40am **TC+EM+AS+TF+EN-ThM6 Work Function and Valence Band Structure of Oxide Semiconductors and Transparent Conducting Oxides Grown by Atomic Layer Deposition**, A. Yanguas-Gil, Argonne National Laboratory, R.T. Haasch, University of Illinois at Urbana Champaign, J.A. Libera, J.W. Elam, Argonne National Laboratory

Atomic Layer Deposition offers a low-temperature, scalable route to the synthesis of a wide range of oxide semiconductors and transparent conducting oxides both in flat and high aspect ratio surfaces. We have carried out studies on the influence of concentration and spatial distribution on the electrical properties within the ZnO-SnO₂-In₂O₃ compositional map, including standard TCO materials such as Al:ZnO and ITO. We will present results on the work function and valence band structure of transparent conducting oxides grown by ALD using ex-situ UPS measurements, including the influence of the surface termination on the interfacial properties of the materials. Finally, the ability of ALD to tailor the surface and interfacial properties of TCOs based on its layer-by-layer nature will be discussed.

10:40am **TC+EM+AS+TF+EN-ThM9 Low Temperature, High Performance Solution-Processed Metal Oxide Thin Film Transistors formed by a 'Sol-Gel on Chip' Process**, H. Sirringhaus, University of Cambridge, UK **INVITED**

N-type amorphous mixed metal oxide semiconductors, such as ternary oxides, where M¹ and M² are metals such as In, Ga, Sn, Zn, have recently gained momentum because of high carrier mobility and stability and good optical transparency, but they are mostly deposited by sputtering. To date

only limited routes are available for forming high-performance mixed oxide materials from solution at low process temperature $< 250^{\circ}\text{C}$. Ionic mixed metal oxides should in principle be ideal candidates for solution processible materials because the conduction band states derived from metal s-orbitals are relatively insensitive to the presence of structural disorder and high charge carrier mobilities are achievable in amorphous structures. Here we report the formation of amorphous metal oxide semiconducting thin films via a 'sol-gel on chip' hydrolysis approach from soluble metal alkoxide precursors, which affords unprecedented high field-effect mobilities of $10\text{ cm}^2/\text{Vs}$, reproducible and stable turn-on voltages $V_{\text{on}} \gg 0\text{V}$ and high operational stability at maximum process temperature as low as 230°C . We discuss the effect of film composition on device performance and stability.

11:20am **TC+EM+AS+TF+EN-ThM11 *In Situ* Measurements of Interface States and Junction Electrical Properties of Electrically Biased Metal / $\beta\text{-Ga}_2\text{O}_3$ Structures**, *H. Pham, X. Zheng, B. Krueger, M.A. Olmstead, F.S. Ohuchi*, University of Washington

A significant issue in application of wide-band-gap transparent conducting oxides is formation of reliable ohmic and rectifying metal contacts. The metal-oxide interface properties are dominated by chemical reactions during growth and the resultant interface state distribution once the interface is formed. We have investigated interface formation between the wide band gap TCO $\beta\text{-Ga}_2\text{O}_3$ ($E_g = 4.8\text{ eV}$) and the metals Pd, Ni, Ti and Al with in-situ xray photoemission spectroscopy (XPS) both during growth and during sputter profiling. The two techniques give very similar results, demonstrating that in this case sputter profiling does not significantly alter the interface chemistry. Consistent with the relative compound heats of formation, Ni and Pd show very little interface reaction with either Ga or O, while Ti interacts strongly with both Ga and O and Al interacts primarily with oxygen. Electrically, Ni and Pd have similar Schottky barriers on the intrinsically n-type oxide (about 0.9 eV), Ti forms a symmetric, nearly ohmic contact, while Al exhibits a smaller barrier (about 0.6 eV). To probe the nanoscopic origins of the Schottky contact behavior through the interface state energy distribution, we combined *in-situ* deposition of thin metal layers and application of forward/reverse biases to the metal-oxide junction with XPS measurements of the relative positions of the Ga_2O_3 bands (via the Ga 3d or O 1s core level) and the metal Fermi level. The density of interface states determines the rate at which the Fermi level can be moved through the oxide band gap, so variation of the oxide core-level shift with respect to the bias voltage yields the interface state density. We find the metal and oxide bands maintain their relative alignment under forward bias (back-plane negative with respect to metal), while they separate at a rate about half that of the applied bias under reverse bias (positive bias with respect to metal).

11:40am **TC+EM+AS+TF+EN-ThM12 Atmospheric Pressure Dielectric Barrier Discharge (DBD) Post Annealing of Aluminium Doped Zinc Oxide (AZO) Films**, *Y.L. Wu, E. Ritz, J. Hong, T.S. Cho, D.N. Ruzic*, University of Illinois at Urbana Champaign

Aluminum-doped Zinc Oxide (AZO) is a material that has high electrical conductivity while being highly transparent at the same time. It could find many useful applications in our daily lives such as displays, mobile devices, solar cells, etc. Currently AZO films are considered as attractive alternatives to materials such as Indium Tin Oxide (ITO) due to its much cheaper cost and comparable high electrical conductivity. A process of depositing AZO film by dual DC magnetron system has been developed. Film thicknesses were measured to be about 300nm by stylus contact profilometer and transparency of greater than 90% in the visible range were measured with spectrophotometry methods. Film conductivities were in the order of 10^3 Ohm-cm with the four-point probe method. By using a Dielectric Barrier Discharge operating at atmospheric pressure, conductivity of film can be further lowered. A $500\text{mm} \times 30\text{mm}$ line source operating at a Nitrogen flow of $250\text{L}/\text{min}$ was used and $\sim 0.4\text{L}/\text{min}$ Hydrogen gas was also introduced into the discharge system to create Hydrogen radicals. A 10% - 15% decrease in electrical resistance was observed with no changes in the optical properties of the AZO films. The elemental composition of the film was measured by X-ray photoelectron spectroscopy (XPS) and the change of crystal structure after DBD post annealing was measured by X-ray diffraction (XRD).

Thin Film

Room: 10 - Session TF+EM+SE+NS-ThM

Nanostructuring Thin Films

Moderator: R.C. Davis, Brigham Young University

8:00am **TF+EM+SE+NS-ThM1 Plasma Effects in Nanostructuring Thin Films**, *K. Ostrikov*, CSIRO Materials Science and Engineering, Australia **INVITED**

In this presentation, several examples of uniquely plasma-enabled nanostructuring of thin film materials for applications in energy conversion and storage, environmental monitoring, and bio-sensing. Strong emphasis is made on atom-, energy-efficiency, and environment-friendliness of plasma-based nanotechnologies.

1. Introduction: Atom- and energy-efficient nanotechnology is the ultimate Grand Challenge for basic energy sciences as has recently been road-mapped by the US Department of Energy. This ability will lead to the energy- and matter-efficient production of functional nanomaterials and devices for a vast range of applications in energy, environmental and health sectors that are critical for a sustainable future. Here we present examples related to atom- and energy-efficient nanoscale synthesis of advanced nanomaterials for energy conversion and storage, environmental sensing, and also discuss effective cancer cell treatment using low-temperature plasmas.

2. Atom- and energy-efficient nanostructure production for energy storage: Here we show an example of a recent achievement of a very low amount of energy per atom ($\sim 100\text{ eV}/\text{atom}$) in the synthesis of MoO_3 nanostructures for energy storage (e.g., Li-ion battery) applications. This was achieved by using time-programmed nanosecond repetitive spark in open air between Mo electrodes. Highly-controlled dosing of Mo and O atoms was achieved through the controlled evaporation and dissociation reactions and maintaining reactive chemistry in air. These nanomaterials show excellent electrochemical and energy storage performance.

3. Environment-friendly, single-step solar cell production: Highly-efficient (conversion efficiency 11.9% , fill factor 70%) solar cells based on the vertically-aligned single-crystalline nanostructures have been produced without any pre-fabricated p-n junctions in a very simple, single-step process of Si nanorod formation by etching p-type Si wafers in low-temperature environment-friendly plasmas of argon and hydrogen mixtures. The details of this process and the role of the plasma are discussed.

4. Metal-nanotube/graphene environmental and bio-sensors: Plasma processing was successfully applied for the fabrication of hybrid nanomaterials based on metal-decorated carbon nanotubes and vertically aligned graphenes. The applications of these structures in environmental (gas) and bio-sensing (SERC/plasmonic) platforms are presented. The vertically-aligned graphene structures have been grown without catalyst and any external substrate heating, owing to the unique plasma properties.

8:40am **TF+EM+SE+NS-ThM3 Directed, Liquid Phase Assembly of Patterned Metallic Films by Pulsed Laser Dewetting**, *Y. Wu*, University of Tennessee, *J.D. Fowlkes, M. Fuentes-Cabrera*, Oak Ridge National Laboratory, *N.A. Roberts, P.D. Rack*, University of Tennessee

Self-assembly of materials offer the potential to synthesize complex systems by defining the *initial and bounding* conditions if the fundamental scientific principles guiding the assembly are known. Much work has been performed studying the assembly of continuous thin polymer and metal films which reveal interesting dewetting phenomenon. Less work has been devoted to the directed assembly and pattern formation of confined or patterned metallic thin films. Meanwhile, the synthesis of functional metallic nanomaterials via self-assembly has been an effective and low-cost approach to realize many critical applications of nanoscience and nanotechnology. In this study, the dewetting and nanopattern formation of nanolithographically pre-patterned thin films of various shapes via pulsed nanosecond laser melting were investigated to understand how initial boundary conditions facilitate precise assembly. Specifically we will show experimental and computational results (continuum and molecular dynamics) illustrating how so-called synthetic perturbations can vary the dispersion of the resultant nanoparticle size and shape distribution of pseudo-one-dimensional liquid metal wires. Furthermore, we will show how controlling the shape and size of bi-metallic nanostructures, the assembly of multifunctional nanoparticles can be assembled.

9:00am **TF+EM+SE+NS-ThM4 Nanosphere Lithography for Bit Patterned Media**, *A.G. Owen, H. Su, A.M. Montgomery, S.M. Kornegay, S. Gupta*, University of Alabama

Nanosphere lithography¹⁻⁴ has been used to pattern perpendicular magnetic anisotropy Co/Pd multilayers into nanopillars for the first time for bit-

patterned media applications. A multilayer stack of Pd₁₀/[Co_{0.3}Pd₁]₉/Pt₅ nm nanolayers was deposited onto a bare silicon wafer. The nanospheres were spin-coated into a uniform monolayer and then reduced in size by plasma ashing in oxygen. The Co/Pd multilayer films were subsequently ion milled into nanopillars using the reduced nanospheres as masks. We tested two ranges of nanosphere sizes, one at about 100 nm, and the other at about 1000 nm. In order to optimize the ashing of the nanospheres, response surface methodology (RSM) was performed to optimize the ashing power and time. It was seen that ashing at low powers of less than 100 W for longer times was more effective than higher powers for short times in shrinking the nanosphere masks without damage. The subsequent ion milling of the Co/Pd films was performed at a near-perpendicular angle to minimize shadowing by the nanospheres. We will discuss some of the complex shapes the nanospheres were patterned into after ashing, and how they translated into variously sized and shaped nanopillars of Co/Pd multilayers after ion milling. Magnetometry was used to characterize the films before and after patterning, showing an improvement in the coercivity and squareness of the media after patterning with nanospheres that were shrunk, but not damaged, by ashing. Micromagnetic simulations using Object Oriented Micromagnetic Framework (OOMF) have been carried out to produce a simulated hysteresis loop which is then compared with the experimental results.

Acknowledgements

The NSF ECCS 0901858 grant, entitled "GOALI: Nanopatterned graded media" is acknowledged for support. Alton Highsmith is acknowledged for support in the UA Microfabrication Facility.

References

1. Xiao Li, T. R. Tadisina, S. Gupta, J. Vac. Sci. Technol. A **27**, Jul/Aug 2009, 1062
2. Kosmas Ellinis, A. Smyrnakis, A. Malainou, A. Tserepi, E. Gogolides, Microelectronic Engineering, **88**, 2011, 2547-2551
3. C. L. Haynes, R. P. Van Duyne, J. Phys. Chem. B **105**, 5599, 2001
4. S. M. Weekes, F. Y. Ogrin, W. A. Murray, Langmuir **20**, 11208, 2004

9:20am TF+EM+SE+NS-ThM5 Effects of Nanometer Scale Periodicity on the Self-Propagating Reaction Behaviors of Sputter-Deposited Multilayers, D. Adams, R. Reeves, Sandia National Laboratories

Nanometer-scale, vapor-deposited multilayers are an ideal class of materials for systematic, detailed investigations of reactive properties. Created in a pristine vacuum environment by sputter deposition, these high-purity materials have well-defined reactant layer thicknesses between 1 and 1000 nm, minimal void density and intimate contact between layers. If designed appropriately, these energetic materials can be ignited at a single point and exhibit a subsequent, high-temperature, self-propagating formation reaction. The nanometer-scale periodicity set through design tailors the effective diffusion length of the subsequent self-propagating reaction.

With this presentation, we describe effects of the nanometer-scale, multilayer periodicity on i) the reactivity of multilayers in different surrounding gaseous environments and ii) the reaction front morphology as viewed in the plane of the multilayer. We show that nickel/titanium and titanium/boron multilayers are affected by the surrounding gaseous environment, and describe how the magnitude of average propagation speed depends on multilayer periodicity. Fine multilayer designs are characterized by fast reaction waves, and there is no difference in average propagation speed when reacted in air (atm. pressure) versus vacuum (1 mTorr). Coarse multilayer designs are generally slower and are affected by secondary oxidation reactions when conducted in air. These thick multilayer designs are affected by the pressure of the surrounding gaseous environment with enhanced propagation speeds owing to the highly exothermic reaction of Ti with O. Regarding the effects of nanometer-scale multilayer periodicity on reaction front morphology, we show that reactive multilayers often have a smooth reaction front when layer periodicity is small. However, multilayers having larger periodicity (and hence larger effective diffusion lengths) exhibit reaction front instabilities and complex reaction front morphologies.

In this talk, we also stress how the propensity to oxidize and the propensity to form reaction front instabilities (as affected through nanometer-scale design) impact final properties of the multilayers for applications such as localized joining.

Sandia is a multiprogram laboratory managed and operated by Sandia Corporation, a wholly owned subsidiary of Lockheed Martin Company, for the United States Department of Energy's National Nuclear Security Administration under Contract DE-AC04-94AL85000.

9:40am TF+EM+SE+NS-ThM6 Ag Nanoparticles Supported by (111) Facets on Biaxial CaF₂ Nanoblades, M. Auer, D. Ye, Virginia Commonwealth University

Silver nanoparticles of different diameters were grown in an effort to study methods of preferentially orienting the geometry of metal nanoparticles. Arrays of calcium fluoride nanorods were grown on silicon substrates using oblique angle deposition at 75° incident angle. A method was then developed to grow silver nanoparticles exclusively on the (111) facet of the calcium fluoride tips. Cross sectional scanning electron microscopy and transmission electron microscopy imaging was used to verify that the nanoparticles adhered exclusively to the desired facet of the tip. Using selected area diffraction and dark field in the TEM, it was shown that the nanoparticles did grow at a [111] orientation at the interface between them and the calcium fluoride rods. Different thicknesses and diameters of nanoparticles were then grown to determine what an ideal size was to achieve the most [111] orientation of the nanoparticles.

Thin Film

Room: 11 - Session TF+NS+EM-ThM

Thin Films: Growth and Characterization-II

Moderator: C. Vallee, LTM - MINATEC - CEA/LETI, France

8:00am TF+NS+EM-ThM1 Plasma-enhanced Atomic Layer Epitaxy of AlN Films on GaN, N. Nepal, J.K. Hite, N. Mahadik, M.A. Mastro, C.R. Eddy, Jr., U.S. Naval Research Laboratory

AlN and its alloys with GaN and InN are of great interest for number of applications. In a device structure that employs an ultrathin layer of these materials, thickness control at the atomic scale is essential. Atomic layer epitaxy (ALE) is one of the most promising growth methods for control of epilayer thickness at the atomic scale. There are reports on atomic layer deposition of AlN on GaN and Si substrates [1]. In those reports, the AlN layers were either amorphous or composed of nm-sized crystallites. Since ALE is a low temperature growth process, there is significantly reduced thermal energy for adatoms to bond at preferred lattice sites and promote growth of crystalline material, therefore, surface preparation plays a very important role to ensure a crystalline layer.

In this work, we present recent efforts to improve the crystalline quality of ALE AlN layers on MOCVD grown GaN/sapphire templates, including the influence of *ex situ* and *in situ* surface pretreatments to promote uniform two-dimensional (2D) nucleation of AlN layers and ALE growth of crystalline AlN films thereupon. AlN layers were grown at 500 °C by ALE simultaneously on Si(111) and GaN/sapphire templates and characterized using spectroscopic ellipsometry (SE), x-ray diffraction (XRD), and atomic force microscopy measurements. The SE measurements indicate that the AlN growth on Si(111) is self-limited for trimethylaluminum (TMA) pulse of length 0.04 to 0.06 sec. However, the AlN nucleation has a bimodal island size distribution for TMA pulses < 0.06 sec. The AlN nucleation becomes uniform and 2D for a pulse length of 0.06 sec, therefore, this pulse length was used to study the GaN surface pretreatment on the nucleation of AlN layer. GaN surfaces were pre-treated *ex situ* with HF and HCl wet chemical etches. Alternating pulses of trimethylgallium and hydrogen plasma followed by an hour of annealing at 500 °C (emulating a Ga-flash-off process) were employed *in situ* before growing an AlN layer. For 3 cycles of Ga-flash-off the AlN nucleation is uniform and replicates the GaN surface morphology on both HF and HCl pretreated GaN. XRD measurements on 36 nm thick AlN films reveal that the ALE AlN on GaN/sapphire is crystalline with only a wurtzite structure and a (0002) peak rocking curve FWHM of 630 arc-sec, which is close to the typical value for AlN grown by MBE and MOCVD [2,3]. Electrical characterization of 2D electron gas at the AlN/GaN interface will also be presented.

References:

1. M. Alevli et al., Phys. Status SolidiA **209**, 266 (2012), and references therein.
2. T. Koyama et al., Phys. Stat. Sol. (a) **203**, 1603 (2006).
3. K. Balakrishnan et al., Phys. Stat. Sol. (c) **3**, 1392 (2006).

8:20am TF+NS+EM-ThM2 *In Situ* Infrared Spectroscopy Study of Cobalt Silicide Thin Film Growth by Atomic Layer Deposition, K. Bernal Ramos, University of Texas at Dallas, M.J. Saly, SAFC Hitech, J. Kwon, University of Texas at Dallas, M.D. Halls, Materials Design Inc., R.K. Kanjolia, SAFC Hitech, Y.J. Chabal, University of Texas at Dallas
Cobalt silicide has potential applications in microelectronics. For instance, the drive to scale down integrated circuitry (IC) has led to the consideration

of cobalt silicide (CoSi₂) as an alternative contact material for titanium silicide (TiSi₂) in future self-aligned silicide technology due to its wider silicidation window and superior thermal and chemical stability. Studies of the growth mechanisms during film deposition are critical to better understand and control thin film formation.

This work focuses on the atomic layer deposition (ALD) of cobalt silicide (CoSi₂), using (tertiarybutylallyl)cobalttricarboxyl ((tBuAllyl)Co(CO)₃) and trisilane on H-terminated silicon to uncover the film growth mechanisms. The first pulse of (tBuAllyl)Co(CO)₃ reacts completely with the H-terminated Si surface forming one monolayer of metallic silicide through the reduction of the allyl ligand by transfer of the surface hydrogen and the formation of Co-Si bonds¹. In situ infrared absorption spectra show the complete loss of H-Si bonds, and the appearance of surface-bound carbonyl and CH_x ligands after the first (tBuAllyl)Co(CO)₃ pulse on H/Si(111). Further deposition of CoSi₂ is possible only after the linear carbonyl groups (initially observed, on the surface after the first (tBuAllyl)Co(CO)₃) are removed by subsequent ALD cycles. Further ALD cycles give rise to cobalt silicide growth through ligand exchange after a nucleation period of 2–4 cycles. The resultant CoSi₂ films are characterized by a low concentration of carbon impurities in the bulk according to X-ray photoemission spectroscopy (XPS).

1 Kwon et al. Chem. Mater. 2012, 24, 1025–1030

8:40am **TF+NS+EM-ThM3 Thin Film Growth: From Gas Phase to Solid Phase – Links and Control**, *P. Raynaud*, CNRS and University Paul Sabatier – Toulouse – France **INVITED**

PECVD, PVD, ALD, sputtering processes, are widely used for thin film growth. Nevertheless, the growth mechanisms need to be controlled and understood to be able to propose stable, adaptable and reproducible processes. Gas, plasma or "volume" phase is one parameter; interaction with surfaces to be treated is the second one, the last one being the final property (ies) to be reached. The Gas phase is controlled by external parameters (pressure, power, polarization, temperature, gas mixture, type of power supply in plasma processes, type of target, duty cycle,). Moreover, these external parameters are linked to internal parameters such as: density and energy of species, type of species (neutrals, ions, electrons, radicals, photons ...), temperature, bombardment energy... Thus, interaction with surfaces and growth process (growth mode, growth rate...) are obviously controlled by these internal parameters and the couple "Gas phase/surface (nature of substrate)". The purpose of this talk is to explain through examples (In situ Infrared spectroscopy of gas phase, OES, MS, Growth modes characterization by in situ ellipsometry, RBS, ARXPS...) how to characterize (in or ex situ) the gas phase et solid phase to find links between these two phases and give some explanation of the processes "from power supply to final properties of the layer".

9:20am **TF+NS+EM-ThM5 Investigation of Precursor Infiltration and ALD Growth on Polymers and Effect on Fiber Mechanical Properties**, *R.P. Padbury*, *J.S. Jur*, North Carolina State University

Atomic layer deposition (ALD) provides the opportunity to unite the properties of organic fiber forming polymers and nanoscale inorganic films creating a hybrid material interface. Prior research has shown that ALD materials nucleation on polymers varies in composition and structure based on how the precursor interacts with the polymer chemistry and the process conditions. The purpose of this work is to explore the effect of this processing on the mechanical behavior of fibrous materials. To study this in more detail, *in-situ* quartz crystal microgravimetry (QCM) is employed to understand the material growth mechanisms of ALD TiO₂, ZnO, and Al₂O₃ on poly (acrylic acid), polyamide-6, and polyethylene terephthalate. Particular emphasis is placed on controlling the ALD precursor diffusion into the sub-surface region of these polymers. *In-situ* QCM data was complemented by *ex-situ* characterization methods such as FT-IR and TEM to examine the interaction between the precursor and polymer and the compositions of the inorganic films. Finally, these results are correlated to the mechanical performance of the ALD treated fabrics. This work has important implications on sustainable textiles processes as well as the introduction of hybrid material properties to textile systems.

9:40am **TF+NS+EM-ThM6 Atomic Layer Deposition Enabled Synthesis of Nanostructured Composite BiFeO₃/CoFe₂O₄ Thin Films for Multiferroic Applications**, *C.D. Pham*, *J.P. Chang*, University of California at Los Angeles

Multiferroic materials, that can either exist as single-phase materials or multi-phase composites, exhibit two or more forms of ferroic order such as (anti)ferroelectricity, (anti)ferromagnetism, or ferroelasticity and have been proposed for use in future non-volatile memory technology. Atomic layer deposition (ALD) is proposed as a scalable approach to synthesize multiferroic thin films and to enable the synthesis of multiferroic

composites which utilize conformal deposition onto 3-D nanostructures. Challenges that must be overcome in the ALD of multiferroic materials is the amorphous nature of as-deposited films and the difficulty in attaining the desired crystallinity and structure that would enable multiferroic properties to emerge from these materials.

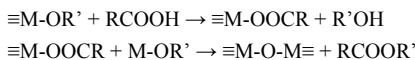
In this work, multiferroic BiFeO₃ was deposited by ALD as a single-phase multiferroic thin film as well as the ferroelectric component in a composite multiferroic using a ferrimagnetic CoFe₂O₄ mesoporous template that was synthesized using an evaporation induced di-block copolymer self-assembly technique. The ALD process used the metallorganic precursors Bi(tmhd)₃ (tmhd = 2,2,6,6-tetramethylheptane-3,5 dione) and Fe(tmhd)₃ alongside oxygen atoms produced from a coaxial waveguide microwave powered atomic beam source. A variety of ALD process conditions were studied, such as the effects of process temperature, precursor pulsing time, and precursor pulsing ratio on film composition, growth rate, and crystallization. The ALD films were able to be grown with a composition ratio Bi:Fe close to unity and with a controlled nanostructure and growth rate of ~0.7 Å/cycle. In order to achieve the desired crystalline material after rapid thermal processing, the composition and nanostructure of the as-deposited films must first be controlled via the ALD process to fit within narrow windows.

To compare the performance of the multiferroic ALD films to more well established synthesis methods, measurements of magnetic and ferro/piezoelectric properties were accomplished using SQUID magnetometry and piezoresponse force microscopy, respectively. Magnetic measurements showed that the out-of-plane remnant magnetization of a composite film at room temperature was approximately 66.4 emu/cm³ while the coercive field was approximately 1950 Oe which was comparable to epitaxial films grown by other methods such as PLD. The magnetoelectric coupling effects in the composite films were studied to assess the effectiveness of the nanostructured material approach.

10:40am **TF+NS+EM-ThM9 In Situ Infrared Spectroscopic Study of Atomic Layer Deposited TiO₂ Thin Film Formation Using Non-Aqueous Routes**, *K. Bernal Ramos*, University of Texas at Dallas, *G. Clavel*, Université Montpellier 2, France, *C. Marichy*, Universidade de Aveiro / CICECO, Portugal, *W. Cabrera*, The University of Texas at Dallas, *N. Pinna*, Universidade de Aveiro / CICECO, Portugal, *Y.J. Chabal*, University of Texas at Dallas

Atomic layer deposition (ALD) is a unique technique for the deposition of conformal and homogenous thin films, by the use of successive self-limited surface reactions. Non-aqueous sol-gel routes are elegant approaches for the synthesis of metal oxide nanomaterials.¹ High quality inorganic nanocrystals,¹ ordered hybrid materials² or ALD thin films³ can be obtained.

Our ALD approach makes use of metal alkoxides and carboxylic acids as metal and oxygen source, respectively.⁴ It is expected that the reaction of carboxylic acids with the surface alkoxide species leads to surface carboxylate species (eq. 1), in a second step an aprotic condensation reaction between surface carboxylate species and metal alkoxides leads to metal-oxide bond formation (eq. 2).



Characterization of interface properties by in situ investigation of surface reaction mechanisms during deposition of high-*k* materials provides critical information for the development of semiconductor devices, where sharp interfaces and impurity free films are sought after.

In this work, in-situ IR spectroscopy is used to investigate the mechanisms for TiO₂ growth using either acetic acid or O₃ as oxygen source and titanium isopropoxide as metal source. It is believed to avoid intermediate OH group and to lead to sharp Si-high-*k* interfaces.

The IR results of the acetic acid process show clearly a ligand exchange leading to formation of acetates at the surface (vibrational bands at 1527 and 1440 cm⁻¹) during the acetic acid pulse and then to their removal during the metal alkoxide pulse. These findings confirm the expected mechanism and demonstrate the absence of OH intermediate. However, the ligand exchange does not seem to be complete leading to accumulation of C impurities.

The in-situ study of O₃ based ALD demonstrates similarities with the above process. Indeed, formation of formate, carboxylate or carbonate species are observed function of the O₃ flow.⁵ The formation of surface carboxylic species upon reaction with O₃ leads then to similar surface states as in the case of the reaction with carboxylic acids.⁴ The mechanism of both approaches and their similarities and differences will be discussed.

1. N. Pinna and M. Niederberger, *Angew. Chem.-Int. Edit.*, 2008, **47**, 5292-5304

2. N. Pinna, *J. Mater. Chem.*, 2007, **17**, 2769-2774

3. G. Clavel, E. Rauwel, M. G. Willinger and N. Pinna, *J. Mater. Chem.*, 2009, **19**, 454-462
4. E. Rauwel, G. Clavel, M. G. Willinger, P. Rauwel and N. Pinna, *Angew. Chem.-Int. Edit.*, 2008, **47**, 3592-3595
5. J. Kwon, M. Dai, M. D. Halls, E. Langereis, Y. J. Chabal and R. G. Gordon, *J. Phys. Chem. C*, 2009, **113**, 654-660

11:00am **TF+NS+EM-ThM10 Nanomechanical Shaft-Loading Blister Testing of Thin Films**, *M. Berdova, A. Baby, J. Lyytinen*, Aalto University, Finland, *K. Grigoros, L. Kilpi, H. Ronkainen*, VTT Technical Research Center, Finland, *J. Koskinen, S. Franssila*, Aalto University, Finland

Atomic Layer Deposition (ALD) is important in micro- and nanoelectromechanical systems, since it provides smooth, uniform, pin-hole free, and conformal layers. In particular, ALD aluminum oxide has excellent properties such as high mechanical strength and hardness, and chemical inertness.

We propose a new technique to measure the mechanical properties of ALD thin films. In the present work, a MEMS version shaft-loading blister test used to evaluate the adhesion between ALD alumina and Cu, Cr/Cu, SiN_x, SiC_x, and Pt thin films. The test structure consists of microcylinders with diameters 1000 μm and 2000 μm, surrounded by etched annular rings making 50 μm, 100 μm and 200 μm gaps (Figure 1). The test structures are examined by applying the load along the microcylinder with a help of CSM Microindenter, inducing displacement which then causes the delamination between thin films and therefore, contributing to obtain the work of adhesion (Figure 2).

The fabrication of the test structure begins from the cleaning of double-side polished silicon wafer in hydrogen-peroxide-based (RCA) wet cleans. The following step is Atomic Layer Deposition of alumina on both sides of the wafer using trimethyl aluminum and water as precursors at 220 °C. 20 nm of Al₂O₃ is grown on one side as the etch mask, and 200 nm of Al₂O₃ is grown on another side to act both as an etch-stop mask and a testing layer. Next, the top layer is patterned to create alumina etch mask; and the rings are etched through silicon wafer by dry anisotropic Bosch process, forming this way a microcylinders supported only by 200 nm of Al₂O₃ layer. Then, thin films (300 nm thick) are deposited by sputtering, or by PECVD techniques. The silicon nitride and silicon carbide were deposited at 300 °C. Magnetron sputtering was used for deposition of Pt, Cu, and Cr/Cu thin films at room temperature. Finally, those films are released by wet etching supporting alumina layer around the microcylinder.

As a result, we have not observed the delamination for nitride and carbide films: after certain reached displacement point (7 μm for nitride, 12 μm for carbide) the films start to break. For soft films as Pt and Cu, at similar displacement values we observed the starting of delamination. Comparing copper and copper with chromium layer underneath, the delamination of the film with adhesive layer starts at higher displacement and load values, proving the adhesive action of chromium. In the case of metal films large displacement and delamination can be achieved without breaking of the film (Table 1). The proposed MEMS shaft-loading blister test might become a valuable tool for all thin film adhesion testing.

11:20am **TF+NS+EM-ThM11 Phase Formation and Thermal Stability of Arc-Evaporated ZrAlN Thin Films**, *L. Rogström*, Linköping University, Sweden, *M.P. Johansson*, SECO Tools AB, Sweden, *M. Ahlgren*, Sandvik Tooling AB, Sweden, *N. Ghafoor*, Linköping University, Sweden, *J. Almer*, Advanced Photon Source, Argonne National Lab, *L. Hultman, M. Odén*, Linköping University, Sweden

Transition metal nitrides are widely used as wear protective coatings due to their high hardness also at elevated temperatures. Hence, TiAlN is one of the most common materials for coating of cutting tools. Its attractive mechanical properties are connected with the phase separation of the cubic TiAlN phase when the coating is exposed to high temperatures. The related ZrAlN system is less studied while its large miscibility gap with possibility for phase separation at elevated temperatures makes this material interesting for high temperature applications. Here, we present a comprehensive study of the phase formation in arc-evaporated ZrAlN thin films and their mechanical properties and thermal stability. Zr_{1-x}Al_xN thin films with a wide range of compositions (0.12 < x < 0.73) were grown by cathodic arc-evaporation. The structure of as-deposited and annealed films was characterized by x-ray diffraction and transmission electron microscopy and the mechanical properties were determined by nanoindentation.

The structure of the as-deposited ZrAlN thin films was found to depend on the Al-content. A low Al-content (x < 0.38) results in cubic (c) structure films while for high Al-content (x > 0.70) a hexagonal (h) ZrAlN phase is obtained [1]. In the compositional range between x = 0.38 and x = 0.70, the films exhibit a nanocomposite structure with a mixture of cubic, hexagonal, and amorphous phases [1, 2]. In all films, separation of ZrN and AlN takes place during annealing. In films with a nanocomposite structure, the phase

transformation is initiated by nucleation and growth of c-ZrN in the ZrN-rich domains while the AlN-rich domains remain largely amorphous at 1100 °C [3]. Nucleation and growth of h-AlN is hindered by a high nitrogen content in the film and takes place at annealing above 1300 °C, simultaneously to loss of the excess nitrogen. The depletion of amorphous phase during annealing results in an improved hardness of the film. In the h-ZrAlN films, ZrN- and AlN-rich domains form within the hexagonal lattice during annealing above 900 °C. The formation of domains with different composition results in an increased hardness, from 24 GPa of the as-deposited film to 31 GPa of the annealed film. The c-ZrAlN phase is found to be stable to annealing temperatures of 1000 °C, while at higher temperatures, h-AlN nucleates and grows. This is different from the c-TiAlN system where spinodal decomposition occurs resulting in age hardening of the films.

[1] L. Rogström et al., *J. Vac. Sci. Technol. A* 30 (2012) 031504.

[2] L. Rogström et al., *Scr. Mater.* 62 (2010) 739.

[3] L. Rogström et al., *J. Mater. Res.*, In press (2012)

11:40am **TF+NS+EM-ThM12 Ion-assisted Epitaxial Sputter-Deposition and Properties of Metastable Zr_{1-x}Al_xN(001) (0.05 x 0.25) Alloys**, *AR.B. Mei, B.M. Howe*, University of Illinois at Urbana Champaign, *N. Ghafoor, E. Broitman*, Linköping University, Sweden, *M. Sardela*, University of Illinois at Urbana Champaign, *L. Hultman*, Linköping University, Sweden, *A. Rockett, J.E. Greene, I. Petrov*, University of Illinois at Urbana Champaign, *M. Oden, H. Fager*, Linköping University, Sweden

Single-phase epitaxial metastable Zr_{1-x}Al_xN/MgO(001) (0.05 x 0.25) thin films were deposited by ultra-high vacuum magnetically-unbalanced reactive magnetron sputtering from a single Zr_{0.75}Al_{0.25}target at a substrate temperature of 650°C. We control the AlN content, x, in the films by varying the ion energy (5 < E_i < 55 eV) incident at the film growth surface with a constant ion to metal flux ratio of 8. The net atomic flux was decreased from 3.16 to 2.45x10¹⁵ atoms cm⁻²s⁻¹, due to efficient resputtering of deposited Al atoms (27 amu) by Ar⁺ ions (40 amu) neutralized and backscattered from heavy Zr atoms (91.2 amu). Consequentially, films varied in thickness from 400 nm to 290 nm during 20 min depositions. HfN buffer layers were deposited on the MgO(001) substrates to reduce the lattice mismatch from ~8 to ~0.5%. High resolution x-ray diffraction ω-2θ scans and reciprocal lattice mapping revealed single-phase NaCl structure with a cube-on-cube orientation relative to the substrate, (001)_{Zr1-x Alx N}|| (001)_{MgO}, and relaxed lattice parameters varying from 4.546 with x = 0.25 to 4.598 Å with x = 0.05. Film nanoindentation measurements showed that hardness decreases from 28.6 to 23.3 Gpa and Young's modulus increases from 263 Gpa to 296.8 GP as x is varied from 0.25 to 0.05. For the same range in x, electronic transport measurements established the films to have electron mobilities increasing from 2.67 to 462 cm²V⁻¹s⁻¹, resistivities decreasing from 162.4 to 25.4 μΩ-cm, and positive temperature coefficients of resistivity spanning from 0.3164 to 1.307 Ω-cm K⁻¹. Films deposited with incident ion energy above 35 eV (x < 0.08) exhibited superconductivity with T_c of 8.26 K.

Thursday Afternoon, November 1, 2012

Electronic Materials and Processing
Room: 14 - Session EM+TF+AS-ThA

Growth and Characterization of Group III-Nitride Materials

Moderator: N. Dietz, Georgia State University

2:00pm EM+TF+AS-ThA1 AlN-based Technology for Deep UV and High-power Applications, Z. Sitar, HexaTech, Inc. & North Carolina State University, *B. Moody, S. Craft, R. Schlessler, R. Dalmau, J. Xie, S. Mita,* HexaTech, Inc., *T. Rice, J. Tweedy, J. LeBeau, L. Hussey, R. Collazo, B. Gaddy, D. Irving,* North Carolina State University **INVITED**

For the first time in history of III-nitrides, the availability of low defect density ($<10^3 \text{ cm}^{-2}$) native AlN substrates offers an opportunity for growth of AlGaIn alloys and device layers that exhibit million-fold lower defect densities than the incumbent technologies and enable one to assess and control optical end electrical properties in absence of extended defects. Epitaxial AlN wafers are fabricated from AlN boules grown by physical vapor transport at temperatures between 2200 and 2300°C. Gradual crystal expansion is achieved through a scalable, iterative re-growth process in which the high crystal quality is maintained over many generations of boules. Despite the excellent crystal quality, below bandgap optical absorption bands in the blue/UV range affect the UV transparency of wafers. We use density functional theory (DFT) to develop a model to understand the interplay of point defects responsible for this absorption. We show a direct dependence of the mid-gap absorption band with the carbon concentration within the AlN. Low defect density AlN and AlGaIn epitaxial films are grown upon these wafers that exhibit superior optical properties in terms of emission efficiency and line width and can be doped with an efficiency that is several orders of magnitude higher than possible in technologies using non-native substrates. UV LED structures and Schottky diodes were fabricated on these materials that exhibit low turn-on voltages and breakdown fields greater than 10 MV/cm. This presentation will review state-of-the-art of AlN-based technology and give examples of potential applications in future devices and contrast these with other wide bandgap technologies.

2:40pm EM+TF+AS-ThA3 Atomic Layer Deposition of AlN Thin Films as Gate Dielectrics for Wide Bandgap Semiconductors, Y.-C. Perng, J.P. Chang, D. Chien, University of California at Los Angeles

Aluminum nitride (AlN) is a potential dielectric layer for wide bandgap semiconductor based power electronic devices, such as those demanded in radio frequency, high-speed and high-temperature communication, because of its wide bandgap and high dielectric constant. In particular, for 4H-SiC, AlN is also a promising interfacial layer due to their similar atomic arrangement, small lattice mismatch (1.3%) and comparable thermal expansion coefficients. Although various deposition techniques have been investigated to synthesize AlN thin films with atomic controllability over a large substrate remains a challenge. Atomic layer deposition (ALD) was thus used in this work to grow AlN thin films.

AlN deposition was performed in an ultra-high vacuum chamber with base pressure of 10^{-7} Torr using trimethylaluminum (TMA) and ammonia (NH₃) as precursors. It was discovered that ALD of AlN is possible only when the minute amount of moisture in NH₃, which competed with and inhibited the nitride growth, was completely eliminated. The ALD window was found to be 500-570°C with a growth rate of 1.5 Å/cycle. The deposited film composition was evaluated via *in-situ* x-ray photoelectron spectroscopy (XPS) with Al/N determined to be 1.2. *In-situ* reflective high-energy electron diffraction (RHEED) measurements showed as-deposited AlN films were crystalline, which was confirmed by x-ray diffraction (XRD). AlN/4H-SiC MIS capacitors were fabricated to examine the electrical properties with the dielectric constant of AlN determined to be 8.3 and a leakage current density of 10^{-3} A/cm^2 at 4.3 MV/cm. The 150 Å ALD AlN passivated AlGaIn/GaN hetero-structure demonstrated 11% increase in the carrier density and 3% decrease in mobility compared to those of non-passivated hetero-structure as $8.3 \times 10^{12} \text{ cm}^{-2}$ and $1100 \text{ cm}^2/\text{V}\cdot\text{s}$. While with amorphous 150 Å Al₂O₃ surface passivation, the mobility decrease by 22% with carrier density increase by 12%, showing that the crystalline AlN providing a superior property on passivating the hetero-structure.

3:00pm EM+TF+AS-ThA4 Low-Temperature Behavior of the Surface Photovoltage in p-type GaN, J.D. McNamara, M. Foussekis, A.A. Baski, M.A. Reshchikov, Virginia Commonwealth University

The effect of low temperature on the surface photovoltage (SPV) in semiconductors is rarely studied and not well understood. We studied the

SPV behavior for Mg-doped, p-type GaN using a Kelvin probe at temperatures from 80 to 300 K. Under band-to-band UV illumination at room temperature, the measured SPV signal in p-type GaN becomes negative as electrons are swept to the surface. However, we observed that at low temperatures, the SPV signal becomes positive under UV illumination, contrary to the SPV behavior of p-type GaN at room temperature. This positive SPV resembles the behavior of an n-type semiconductor. We assume that under UV illumination and at low temperatures, the conductivity of Mg-doped GaN does indeed convert from p- to n-type. This conversion was predicted from photoluminescence studies on Zn-doped GaN.^[1] At low temperatures, photo-generated electrons may accumulate in the conduction band which causes an upward shift in the bulk Fermi level towards the conduction band. This results in a positive SPV signal, since the Kelvin probe uses the bulk Fermi level as a reference for the measured SPV signal. Interestingly, the characteristic temperature at which we observe this transition from p- to n-type behavior depends on illumination intensity. As the excitation intensity increases from 10^{15} to $10^{17} \text{ cm}^{-2} \text{ s}^{-1}$, the characteristic temperature increases from 130 to 170 K. This result also agrees with previously reported photoluminescence data and further authenticates the above assumption.^[1]

[1] M. A. Reshchikov, A. Kvasov, T. McMullen, M. F. Bishop, A. Usikov, V. Soukhoveev, and V. A. Dmitriev, *Phys. Rev. B* **84**, 075212 (2011).

3:40pm EM+TF+AS-ThA6 Controlling GaN Polarity on GaN Substrates, J.K. Hite, M.E. Twigg, J.A. Freitas, Jr., M.A. Mastro, J.R. Meyer, I. Vurgaftman, S. O'Connor, N.J. Condon, F.J. Kub, S.R. Bowman, C.R. Eddy, Jr., U.S. Naval Research Laboratory

Gallium nitride is a high quality semiconductor widely used in both optical and electronic devices. The polarity of GaN (+/- c-direction) influences many properties of the resultant material, including chemical reactivity and electric field in these 'piezoelectric' materials. Control over the polarity of GaN grown on sapphire and SiC substrates has been previously demonstrated by controlling the growth conditions, doping levels, and buffer or nucleation layer properties. Further, in the case of heavily doped p-type layers, spontaneous polarity inversion has been demonstrated in GaN homoepitaxial layers, switching the doped layer from Ga-polar to N-polar. However, this approach leads to uncontrolled inversion domain boundaries and often results in dopant clustering within the film, impacting film quality and resultant device performance.

In this work we investigate the fabrication of Mg-free inversion layers (ILs) to control the polarity of MOCVD-grown GaN on GaN substrates. By changing the IL material, we demonstrate conversion of GaN polarity in both directions (N-polar to Ga-polar and Ga-polar to N-polar). By employing a patented selective growth method to deposit the IL, the lateral polarity of the GaN can also be alternated, allowing control of the polarity in both vertical and lateral directions. A one-dimensional grating of periodically oriented (PO) GaN stripes was achieved over square-centimeter (or large) areas. The boundaries between polarities are found to be both sharp and vertical, and the growth conditions have been adjusted to result in equal growth rates of both polarities. Chemical etching of the material verifies the polarity of the material. Transmission electron microscopy (TEM) rules out the presence of alternating polar inclusions in the inverted material while showing a strong inversion domain boundary at the vertical interfaces. Dislocation density and grain size are determined through the use of electron channeling contrast imaging. The MOCVD-grown PO GaN structures have been extended in thickness by further HVPE growth. TEM and photoluminescence imaging confirms that the PO GaN structure is maintained throughout the extended growth (up to 80 μm in thickness). This method of GaN polarity inversion offers the promise of engineering both lateral and vertical polarity heterostructures and the potential of novel engineered polarity-based devices.

4:00pm EM+TF+AS-ThA7 Direct Green and Yellow Light Emitting Diodes – Polarization Control and Epitaxy, C. Wetzel, T. Detchprohm, Rensselaer Polytechnic Institute **INVITED**

Solid state lighting by means of GaInN/GaN light emitting diodes (LEDs) is rapidly progressing to a major factor in energy savings technology. By convergence of lighting and lighting control, however, smart lighting is an opportunity to elevate lighting to a holistic experience of human wellbeing beyond the obvious economic benefits. Full epitaxial control of the GaInN/GaN active region is prime to fulfill the promise of an optical bandgap tunable across the entire visible spectrum. As such it will serve both, as tunable absorption layer for multijunction solar cells and emitter for direct emitting LEDs. The later aspect is of particular promise to outperform the traditional phosphor conversion approach known from historic fluorescence lamps and current white light LEDs.

Rigorous defect reduction approaches have enabled us to continuously improve the emission efficiency in ever longer wavelength emission reaching beyond green, deep green to yellow and orange (590 nm). In contrast to conventional phosphor or AlGaInP-based LED, such emitters show a superior temperature stability of their light output performance. A further leap in defect reduction has been demonstrated by the implementation of heteroepitaxy on nanotextured templates. Unlike widely explored lateral epitaxial overgrowth, growth zones primarily coalesce without the generation of threading dislocations. Implemented at the sapphire substrate level in green LEDs, the texturing substantially boosts both, internal quantum efficiency and light extraction. Furthermore, by control of the crystallographic orientation of growth we achieve a modulation of the piezoelectric polarization within the active region. This for once results in the emission of highly linear polarized light but on the other hand holds the promise to move the actual sweet spot of LED performance from the blue into the green and yellow spectral region. We discuss our approaches in light of our latest achievements.

This work was supported by a DOE/NETL Solid-State Lighting Contract of Directed Research under DE-EE0000627. This work was supported in part by the Engineering Research Centers Program of the National Science Foundation under NSF Cooperative Agreement No. EEC-0812056.

4:40pm EM+TF+AS-ThA9 The Influence of Substrate and Gas Phase Temperatures on the Properties of InN Epilayers, M.K.I. Senevirathna, S.D. Gamage, R. Atalay, R.L. Samaraweera, A.G.U. Perera, Georgia State University, **B. Kucukgok, A.G. Melton, I. Ferguson,** University of North Carolina at Charlotte, **N. Dietz,** Georgia State University

The influence of the substrate growth temperature on the structural and optoelectronic properties of group III-nitride layers grown by various growth techniques has been extensively studied and reported on, due to the close relationship of substrate temperature with crystalline quality and the point defect chemistry of the alloy. Most thin film growth systems only control the substrate temperature and have limited control to adjust the gas phase decomposition dynamic independent to influence to growth surface chemistry.

In this contribution, we present results on the growth of InN epilayers grown the high-pressure chemical vapor deposition (HPCVD), studying in influence of and independent from the substrate temperature controlled gas phase temperature above the substrate reactor zone. The HPCVD reactor system has two heater elements: one that controls the substrate temperature and a second radiative heat source above, which allows the control of the gas phase temperature. While the substrate temperature dominantly controls the growth process and the crystalline layer properties, the heater above the substrate surface influences strongly the precursor decomposition processes and the diffusion and concentrations of the precursor fragments in the boundary layer and at the growth surface. InN epilayers grown with different gas phase heating settings where grown and analyzed with the respect to their short- and long-range crystalline ordering and their optoelectronic properties as function of the gas phase temperature. The long-range and the short-range crystalline order of the layers have been analyzed by x-ray diffraction $2\theta-\omega$ scans FWHM and the Raman E_2 (high) FWHM, respectively. The optoelectronic properties have been studied by reflectance spectroscopy and are related to the structural properties and the additional gas phase heating.

The figure depicts the FWHM values of Raman- E_2 (high) peak of the InN epilayers as a function of reactor pressure for higher (red line) and lower (blue line) gas phase temperature. The results indicate that there is an improvement of the short-range crystalline order of the layers with lower gas phase temperature. However, the FWHM values of XRD $2\theta-\omega$ scans, which are not shown here, are indicating that there is an improvement of long-range crystalline order of the layers with increasing gas phase heating.

5:00pm EM+TF+AS-ThA10 Absence of Electron Accumulation at InN(11-20) Cleavage Surfaces, H. Eisele, Technische Universität Berlin, Germany, **S. Schaafhausen,** Forschungszentrum Jülich, Germany, **A. Lenz,** Technische Universität Berlin, Germany, **A. Sabitova,** Forschungszentrum Jülich, Germany, **L. Ivanova, M. Dähne,** Technische Universität Berlin, Germany, **Y.-L. Hong, S. Gwo,** National Tsing-Hua University, Taiwan, **P. Ebert,** Forschungszentrum Jülich, Germany

InN in principle opens up the possibility of using only one ternary III-V semiconductor alloy (InGaN) in optoelectronic devices to cover the whole visible spectral range. Despite this, key material properties of InN are still under debate. The intrinsic energetic position of the Fermi level is unclear, i.e., whether the Fermi level is located within the fundamental band gap or shifted slightly into the conduction band. The latter case induces electron accumulation at the surfaces of the crystal. Such an electron accumulation is typically observed at InN surfaces upon air contact, raising the question whether it is an intrinsic material property or not?

In order to probe intrinsic bulk properties by STM and not only contamination or surface effects, a clean and stoichiometric surface is necessary. This can be achieved by cleaving InN along non-polar planes. To analyze the origin of the different electronic states in detail, we investigated the clean non-polar (11-20) cleavage surface using cross-sectional scanning tunneling microscopy (XSTM) and spectroscopy (XSTS).

Using combined XSTM and XSTS we were able to locate an InN layer grown on an AlN buffer layer on top of a Si(111) substrate [1]. XSTS spectroscopy on the InN(11-20) cleavage surface yield normalized conductivity spectra, where three contributions to the tunneling current can be observed: (i) the contribution from the conduction band density of states for biases above the conduction band minimum at +0.3 V, (ii) a defect induced current, dominating the spectra between biases of 0 and -0.4 V, and (iii) a valence band related tunneling current rising at a bias of about -0.4 V and dominating the spectrum for biases below. The defect induced current arises from semi-filled defect states being present at the surface steps, and probably also from other (point) defects at the surface. Within the bulk band gap of $E_G = 0.7$ eV no intrinsic surface states could be observed. Furthermore, the Fermi level pinning at about 0.3 eV below the conduction band minimum indicates the absence of an electron accumulation layer.

The results illustrate that electron accumulation at InN surfaces is not a universal property on InN. For clean stoichiometric cleavage surfaces no electron accumulation is observed. Thus, electron accumulation results primarily from the details of the surface structure and is hence not an intrinsic property of the bulk InN material.

[1] Ph. Ebert, S. Schaffhausen, A. Lenz, A. Sabitova, L. Ivanova, M. Dähne, Y.-L. Hong, S. Gwo, and H. Eisele, *Appl. Phys. Lett.* **98**, in press (2011).

5:20pm EM+TF+AS-ThA11 Dependence of Gallium Incorporation and Structural Properties of Indium-rich In_xGa_{1-x}N Epilayers on Ammonia - MO Precursor Pulse Separation, S.D. Gamage, R. Atalay, M.K.I. Senevirathna, R.L. Samaraweera, Georgia State University, **A.G. Melton, I. Ferguson,** University of North Carolina at Charlotte, **N. Dietz,** Georgia State University

The large band gap tunability of ternary In_xGa_{1-x}N alloys has opened new avenues in the field of advanced optoelectronics devices fabrication. However, the growth process of the epilayers of these materials is yet to be well explored. In this contribution, the growth of In_xGa_{1-x}N epilayers under super atmospheric pressure is studied. In order to mitigate the gas phase reactions and the gap of dissociation temperatures between the binary alloys GaN and InN, and to improve the phase stability, high growth chamber pressure has been used together with a pulsed precursor injection system. This pulsed precursor injection scheme introduces two important process parameters; the precursor separation times between the metal organic (MO) sources (TMI and TMG) and ammonia (S₁), and ammonia and MO (S₂).

With the aim to find the optimum S₂ separation for high quality indium-rich InGaN epilayers, a set of In_xGa_{1-x}N samples with nominal x=0.9 has been grown with different S₂ timings. It will be shown that the S₂ separation is critical for the incorporation of gallium into the epilayers. In order to maintain single-phase epilayers, the S₂ separation has to be increased from S₂=400 ms for InN to over 1200 ms for In_xGa_{1-x}N. Raman spectroscopy and X-ray diffraction (XRD) spectroscopy are used to study the structural properties while the Fourier Transform Infra-red (FTIR) and transmission spectroscopy are utilized to investigate the electrical and optical properties of the epilayers.

5:40pm EM+TF+AS-ThA12 MBE-Growth of Coherent-Structure InN/GaN Short-Period Superlattices as Ordered InGaN Ternary Alloys for III-N Solar Cell Application, A. Yoshikawa, K. Kusakabe, N. Hashimoto, T. Okuda, T. Itoi, Chiba University, Japan

We have recently proposed "SMART" III-N tandem solar cells in which all sub-cells could be coherent-structure high-quality pn junctions with low leakage current, resulting in high performance solar cells. SMART means "Superstructure Magic Alloys fabricated at Raised Temperature". The most important feature in the proposed SMART solar cell is a novel idea for realizing ordered and/or quasi InGaN-ternary alloys with InN/GaN Short-Period Superlattices (SPS) enabling coherent-structure band engineering for the (InN)_n/(GaN)_m SPSs with simple integer pairs of (n, m) ≤ 4. In this symposium, detailed epitaxy processes, structural and physical properties of SPSs, and also the idea and features of proposed "SMART" III-N tandem solar cells are reported.

We have ever reported successful growth of fine and coherent-structure 1-ML InN/GaN matrix QWs, and they can be fabricated so under self-limiting and self-ordering growth processes at remarkably higher and/or "raised" temperatures (~650 °C) than the critical one (~500 °C) for growing thick InN layer under +c growth regime in MBE. We are now underway to extend this understanding and the corresponding epitaxy technology to realize the proposed (InN)_n/(GaN)_m SPSs, and we have started to achieve

(InN)₁/(GaN)_m (m=1-20) SPSs. When fabricating high structural quality those SPSs, very careful surface stoichiometry control such as (In+Ga)/N and In/Ga composition in adlayers, and also periodical complete surface dry-up of In and Ga for each one-cycle growth of SPSs are necessary and quite important.

In brief, 50-100 periods of (InN)₁/(GaN)_m SPSs were grown on MOCVD-grown +c-GaN template at 650 °C by a conventional plasma-assisted MBE. Surface stoichiometry and surface dry up were quite carefully monitored and controlled by in-situ Spectroscopic-Ellipsometry. First, structural properties of 50 periods of (InN)₁/(GaN)_m SPSs were characterized with XRD diffraction patterns taking the *m* as a parameter. It was found that coherent structure SPSs could be fairly easily fabricated even when the *m* was decreased down to 4. Generally, much more careful surface stoichiometry control was necessary with decreasing the *m*, though it was confirmed coherent structure (InN)₁/(GaN)₄ SPSs could be grown finally after quite careful control, such as selective re-evaporation between In and Ga consuming a long time. This leads to complete In re-evaporation leaving only some Ga metals on the surface. Of course those Ga metals must be completely dried up with irradiating plasma-excited nitrogen just before the following deposition of 1ML InN on it. It is still difficult at present, however, to grow fine structure InN/GaN SPSs with the *m* below 3.

Graphene and Related Materials Focus Topic Room: 13 - Session GR+EM+NS+SS+TF-ThA

Beyond Graphene: BN and Other 2D Electronic Materials; 2D Heterostructures

Moderator: I.I. Oleynik, University of South Florida

2:00pm **GR+EM+NS+SS+TF-ThA1 X-ray Photoelectron Spectroscopy Investigation of the Valence and Conduction Band Offset at Hexagonal a-BN:H/Si Interfaces**, S. King, M. French, J. Bielefeld, Intel Corporation, M. Jaehnig, Intel Corporation, M. Kuhn, B. French, Intel Corporation

Due to a wide band gap (~ 6 eV) and close lattice matching, hexagonal boron nitride (h-BN) is of interest as a potential gate dielectric in graphene channel transistor devices. A key property for the success of h-BN as a gate dielectric in such devices is the valence and conduction band offsets at the h-BN/graphene and h-BN/gate electrode interfaces. In many graphene channel devices, amorphous or poly-Si is a desirable gate electrode material for compatibility in standard CMOS processing. In this regard, we have utilized x-ray photoelectron spectroscopy (XPS) to determine the valence band offset present at the interface between plasma enhanced chemically vapor deposited hexagonal a-BN:H and a (100) Si substrate. Combined with Reflection Electron Energy Loss Spectroscopy measurements of the a-BN:H band gap, we have also been able to determine the conduction band offset at this interface. The combined measurements indicate a type I alignment with valence and conduction band offsets of 1.95±0.1 and 2.15±0.17 eV respectively.

2:20pm **GR+EM+NS+SS+TF-ThA2 Monolayer Graphene-Boron Nitride 2D Heterostructures**, R. Cortes, J. Lahiri, E. Sutter, P.W. Sutter, Brookhaven National Laboratory

Unusual electronic properties have been predicted for monolayer graphene-boron nitride heterostructures, but access to these properties depends on methods for controlling the formation of graphene-boron nitride interfaces [1]. Here we report on the growth and interface formation of monolayer graphene (MLG)-hexagonal boron nitride (h-BN) 2D heterostructures on Ru(0001), investigated by a combination of real-time low-energy electron microscopy (LEEM) and scanning tunneling microscopy (STM).

LEEM observations of sequential chemical vapor deposition growth show that h-BN attaches preferentially to the edges of existing MLG domains, while nucleation of h-BN on the Ru surface away from MLG is not observed at the conditions considered here. With increasing coverage, h-BN expands anisotropically and, ultimately, the substrate is covered by a continuous 2D membrane of MLG domains embedded in h-BN. The study of the 1D interface between MLG and h-BN in these membranes by STM demonstrates that, following sequential growth at high temperatures, the interface is not abrupt, but contains an intermixed zone consisting of h-BN with embedded carbon atoms. Using quantitative LEEM, we have identified processes that eliminate this intermixing and pave the way to atomically sharp graphene-boron nitride boundaries, as confirmed by STM. The application of a similar growth procedure to terminate the edges of atomically controlled graphene nanoribbons with h-BN, embedding them in a h-BN membrane, will be considered.

[1] P. Sutter, R. Cortes, J. Lahiri, and E. Sutter. *Submitted* (2012).

2:40pm **GR+EM+NS+SS+TF-ThA3 Large Area Vapor Phase Growth and Characterization of MoS₂ Atomic Layers**, J. Lou, S. Najmaei, Z. Liu, Y. Zhan, P. Ajayan, Rice University **INVITED**

Monolayer Molybdenum disulfide (MoS₂), a two-dimensional crystal with a direct bandgap, is a promising candidate for 2D nanoelectronic devices complementing graphene. Unlike conductive graphene and insulating h-BN, atomic layered MoS₂ is a semiconductor material with a direct bandgap, offering possibilities of fabricating high performance devices with low power consumption in a more straight-forward manner.

In this talk, we will discuss our recent efforts on the large area growth of MoS₂ atomic layers by a scalable chemical vapor deposition (CVD) method. The as-prepared samples can either be readily utilized for further device fabrication or be easily released from the growth substrate and transferred to arbitrary substrates. High resolution transmission electron microscopy and Raman spectroscopy on the as grown films of MoS₂ indicate that the number of layers range from single layer to a few layers. Our results on the direct growth of MoS₂ layers on dielectric leading to facile device fabrication possibilities show the expanding set of useful 2D atomic layers, on the heels of graphene, which can be controllably synthesized and manipulated for many applications.

3:40pm **GR+EM+NS+SS+TF-ThA6 Formation of Silicene and 2D Si Sheets on Ag(111): Growth Mode, Structural and Electronic Properties**, P. Vogt, Technical University of Berlin, Germany, T. Bruhn, A. Resta, B. Ealet, CNRS CiNaM, Marseille, France, P. De Padova, CNR-ISM, Rome, Italy, G. Le Lay, CNRS CiNaM, Marseille, France

Since the discovery of graphene enormous efforts have been invested to discover other similar 2-dimensional materials, like e.g. silicene. These 2D materials share similar structural, electronic and optical properties as graphene but are expected to differ in terms of their respective chemical reactivity and thus their applicability for electronic devices. In particular silicene could more easily be integrated into current Si-based electronics than graphene. Silicene has been predicted theoretically [1,2] but does not seem to exist in nature.

Recently, we could synthesize silicone layers grown epitaxially by depositing Si on Ag(111) surfaces. The electronic properties of these silicene layers were shown to behave as theoretically predicted [3] and the structural and electronic properties are very similar to graphene. In STM images the hexagonal 2D silicone sheet gives rise to triangular structures situated in a honeycomb arrangement with (4×4) symmetry with respect to the Ag(111) surface. A structural model derived from the STM measurements showed a very good agreement with DFT results and exhibited a downward conical electronic dispersion resembling that of relativistic Dirac fermions at the Si K-points [3]. Depending on the growth conditions the formation of different 2D silicon arrangements can be observed: 1) Si-clusters at low deposition temperatures, 2) the formation of less ordered 2D hexagonal Si-based structures at temperatures up to 180°C, 3) the formation of the (4×4) silicene sheet around 220°C and 4) a 2D Si structure with a (√13×√13)-like periodicity at higher growth temperatures exhibiting a very regular, wide range ordered Moiré-like surface pattern in STM.

Here, we will discuss the formation and epitaxial growth mode of these different 2D Si structures and the dependence on the growth parameters. We will also investigate whether these different 2D Si layers all refer to similar silicene sheets which give rise to different appearances in STM due to a varying rotation with respect to each other.

Keywords: silicene, 2D materials, graphene, Dirac fermions

References:

- [1] S. Cahangirov et al., Phys. Rev. Lett. **102**, 236804 (2009)
- [2] G. G. Guzman-Verri and L. C. Lew Yan Voon, Phys. Rev. B **76**, 75131 (2007)
- [3] P. Vogt et al., Phys. Rev. Lett. **108**, 155501 (2012)

4:00pm **GR+EM+NS+SS+TF-ThA7 Yttria-monolayer on Pt(111) Supported Graphene: A Novel Two Dimensional Heterostructure and its Affect on Charge Doping of Graphene**, R. Addou, A. Dahal, M. Batzill, University of South Florida

Yttrium oxide (Y₂O₃) is a high-k dielectric material, with promising wetting behavior of graphene [1]. In our study we grew yttria by reactive MBE on Pt(111) supported graphene to investigate the structural and electronic properties of the graphene/yttria interface. Photoemission measurements

indicate that the graphene layer is covered by yttria. Scanning tunneling microscopy (STM) and low energy electron diffraction reveal that at annealing temperatures higher than 600 °C yttria forms an ordered monolayer on top of graphene. In STM, a moiré pattern is observed that is a consequence of super-positioning of a hexagonal yttria monolayer lattice with that of graphene. X-ray photoemission indicates a shift of the C1s peak by 1 eV to higher binding energy upon depositing of the yttria film. This peak shift is explained by charge doping of graphene by the underlying Pt substrate due to the change in the work function of the yttria coated graphene.

[1] Z. Wang et al. *Nano Lett.* **2010**, *10*, 2024–2030; L. Ding et al. *Nano Lett.* **2009**, *9*, 4209–4214.

4:20pm **GR+EM+NS+SS+TF-ThA8 Probing the BCN-triangle by Computations—Outside the Carbon Corner, Jakobson, Rice University INVITED**

We will discuss recent work on modeling 2D-materials “beyond graphene” [1-2]: two dimensional hexagonal h-BN, pure B polymorphs, MoS₂, etc. Lessons from graphene studies remain invaluable as they offer general approach and views on the edges [3] and interface structures and energies, and especially organization of the grain boundaries [4,5]. New dislocation cores in BN (both 5/7 and 4/8 types) lead to accordingly new physical properties of emerging polar GB [6]. Similarly, we identify the dislocation cores and the grain boundary structure for more complex polar layer-material, MoS₂ (X. Zou, unpublished). Our analysis of edge and cleavage energies helps to explain fracture patterns emerging in the course of synthesis. In principle, computations suggest possibility of metastable 2D-layers of GaN or ZnO or even their hybrids. Finally, it is important to mention clear opportunities of designing 2D-circuits by combining 2D-materials in specific functional patterns like proposed nanoroads and quantum dots [7-8] which now become a subject of experimental laboratory work.

[1] Y. Liu et al. *Nano Lett.* **11**, 3113 (2011). [2] E. Penev, et al, *Nano Lett.* **12**, 2441 (2012). [3] Y. Liu et al. *Phys. Rev. Lett.* **105**, 235502 (2010). [4] BIY and F. Ding, *ACS Nano* **5**, 1569 (2011). [5] Ajayan and BIY, *Nature Mater.* **10**, 415 (2011). [6] Y. Liu et al. *ACS Nano* (2012). [7] A. Singh and BIY, *Nano Lett.*, **9**, 1540 (2009). [8] A. Singh, E. Penev, and BIY, *ACS Nano*, **4**, 3510 (2010).

5:00pm **GR+EM+NS+SS+TF-ThA10 Single-layer MoS₂ Devices and Circuits, A. Kis, EPFL, Switzerland INVITED**

Single layer MoS₂ is a recent addition to the family of 2D materials and is reminiscent of graphene except that it is an intrinsic direct band gap semiconductor with a 1.8 eV gap. We have exfoliated single layers 6.5 Angstrom thick from bulk crystals of semiconducting MoS₂, using the micromechanical cleavage technique commonly used for the production of graphene. Our nanolayers are mechanically and chemically stable under ambient conditions. We have fabricated transistors based on single-layer MoS₂ which demonstrate that this material has several advantages over silicon for potential applications in electronics. Our transistors have room-temperature current on/off ratios higher than 10⁸, mobility higher than 780 cm²/Vs and leakage currents in the fA range. Integrated circuits based on MoS₂ have the capability to amplify signals and perform logic operations. Finally, I will show our work on suspended MoS₂ membranes that show ripples similar to those observed in graphene. MoS₂ also has superior mechanical properties: higher stiffness than steel and 30 times its breaking strength which makes it suitable for integration in flexible electronics.

References

1. B. Radisavljevic, A. Radenovic, J. Brivio, V. Giacometti, and A. Kis. Single-layer MoS₂ transistors. *Nature Nanotechnology* **6**, 147, 2011. doi: 10.1038/nnano.2010.279
2. M.M. Benameur, B. Radisavljevic, J.S. Heron, S. Sahoo, H. Berger, and A. Kis. Visibility of dichalcogenide nanolayers. *Nanotechnology* **22**, 125706, 2011. doi: 10.1088/0957-4484/22/12/125706
3. B. Radisavljevic, M.B. Whitwick, and A. Kis. Integrated circuits and logic operations based on single-layer MoS₂. *ACS Nano* **5**, 9934, 2011. doi: 10.1021/nn203715c
4. J. Brivio, D.T.L. Alexander, and A. Kis. Ripples and Layers in Ultrathin MoS₂ Membranes. *Nano Letters* **11**, 5148, 2011. doi: 10.1021/nl2022288
5. S. Bertolazzi, J. Brivio, and A. Kis. Stretching and Breaking of Ultrathin MoS₂. *ACS Nano* **5**, 9703, 2011. doi: 10.1021/nn203879f

Thin Film

Room: 11 - Session TF+AS+SS-ThA

Thin Films: Growth and Characterization-III

Moderator: M.R. Davidson, University of Florida

2:00pm **TF+AS+SS-ThA1 Atomic Force Microscopy (AFM)-Based Nanografting for the Study of Self-Assembled Monolayer Formation of Organophosphonic Acids on Al₂O₃ Single Crystal Surfaces, B. Torun, B. Oezkaya, G. Grundmeier, University of Paderborn, Germany**

The surface chemistry of aluminum oxides plays a crucial role in the field of catalysis, corrosion and adhesion. Alumina (Al₂O₃) covered aluminum alloys are employed in the construction of lightweight automotive and aerospace parts. In order to protect these materials from environmental factors organic coatings are commonly used. In this context the adhesion between polymer and oxide surfaces is of utmost importance to improve the longevity of industrial parts. Using self-assembled adhesion promoting monolayers the complexity of surface pretreatment processes could be reduced tremendously. Long aliphatic phosphonic acids, such as octadecylphosphonic acid (ODPA), were found to be suitable for forming dense self-assembled monolayers on native oxide covered aluminum substrates. However in contrast to amorphous oxide films, single crystal surfaces provide a much more well-defined experimental and theoretical platform for studies on the adsorption mechanisms and the stability of organophosphonic acids.

In the presented study^[1], adsorption, stability, and organization kinetics of organophosphonic acids on single-crystalline alumina surfaces were investigated by means of atomic force microscopy (AFM)-based imaging, nanoshaving, and nanografting. The latter, nano-shaving and -grafting, are rather new techniques to study self-assembly processes. Since they were first reported^[2] in 1997, atomic force microscopy based nanografting has been used as a tool to investigate the adsorption of organic monolayers mostly on noble metals, such as gold.^[3] Moreover recent studies focused on influences of the confinement between AFM-tip and background monolayer on the adsorption of molecules during the grafting process. [about:blank#_ENREF_1]

AFM friction and phase imaging have shown that chemical etching and subsequent annealing led to heterogeneities on single-crystalline surfaces with (0001) orientation indicating differences in the local surface termination. These findings were supported by angle resolved X-Ray photoelectron spectroscopy (AR-XPS) measurements suggesting a partially hydroxide terminated surface. Self-assembly and stability of ODPA were shown to be strictly dependent upon the observed heterogeneities of the surface termination, where it was locally shown that ODPA can loosely or strongly bind on different terminations of the crystal surface. Furthermore, organization kinetics of ODPA was monitored with nanografting on (0001) surfaces. Supported by measurements of surface wettability and diffuse reflectance infrared Fourier transform spectroscopy (DRIFTS), it was demonstrated that the lack of organization within the protective adsorbed hexylphosphonic acid (HPA) monolayer on alumina surfaces facilitated the reduced confinement effect during nanografting, such that kinetics information on the organization process of ODPA could be obtained.

[1] Torun, B. et al., *Langmuir* **2012**, *28*, (17), 6919-6927.

[2] Xu, S. et al., *Langmuir* **1997**, *13*, (2), 127-129.

[3] Yu, J. et al., *Langmuir* **2008**, *24*, (20), 11661-11668.

[4] Xu, S. et al., *J. Amer. Chem. Society* **1998**, *120*, (36), 9356-9361.

2:20pm **TF+AS+SS-ThA2 SIMS as a Method for Probing Stability of the Molecule-Substrate Interface in SAMs, J. Ossowski, J. Rysz, Jagiellonian University, Poland, A. Terfort, Goethe University, Germany, P. Cyganik, Jagiellonian University, Poland**

Despite the numerous structural studies of Self-Assembled Monolayers (SAMs) available nowadays, the structure and stability of the SAM-substrate interface is still poorly understood and controversial even for the most simple SAM system. As a consequence, the experimental and theoretical analysis of the bonding geometry and the stability of the molecule-substrate interface for technologically relevant, and therefore more complicated SAMs, is extremely difficult.

In this presentation we report extensive static secondary ion mass spectrometry (SIMS) studies¹ on homologous series of thiols (BPnS, CH₃-C₆H₄-C₆H₄-(CH₂)_n-S-Au(111), n = 2-6) and selenols (BPnSe, CH₃-C₆H₄-C₆H₄-(CH₂)_n-Se-Au(111), n = 2-6) where structure and stability of molecule-substrate interface was systematically modified as verified by our previous experiments²⁻⁵. Correlating SIMS data with previous microscopic², spectroscopic³ and very recent neutral mass spectrometry studies^{4,5} we show that SIMS can be successfully applied to monitor fine

changes in the molecule-substrate interface stability of these model SAMs. Further, to demonstrate general applicability of SIMS for such analysis, we report use of this method for monitoring influence of S versus Se substitution in purely aliphatic (heksadecanethiol/selenol) and aromatic (anthracenethiol/selenol) SAMs on Au(111). In summary our experiments show that a new approach for probing the stability of molecule-substrate interface in SAMs can be proposed by using SIMS. Importantly, this technique is relatively fast and can be applied for virtually all complicated and technologically relevant SAMs.

References

- (1) J. Ossowski, P. J. Rysz, A. Terfort and P. Cyganik *in preparation*.
- (2) P. Cyganik, K. Szelagowska-Kunstman, et al. *J. Phys. Chem. C* **2008**, *112*, 15466.
- (3) K. Szelagowska-Kunstman, P. Cyganik, et al. *Phys. Chem. Chem. Phys.* **2010**, *12*, 4400.
- (4) S. Wyczawska, P. Cyganik, A. Terfort, P. Lievens, ChemPhysChem (communication) **2011**, *12*, 2554.
- (5) F. Vervaecke, S. Wyczawska, P. Cyganik, et al. ChemPhysChem (communication) **2011**, *12*, 140.

2:40pm TF+AS+SS-ThA3 Wet Chemical Surface Modification of Silicon Oxide and Oxide Free Silicon by Aluminum Oxide, P. Thissen, A. Vega, T. Peixoto, Y.J. Chabal, University of Texas at Dallas

Wet chemical surface modification is a powerful method to change the chemical properties of surfaces. Although it has been used extensively, there are still many issues that limit the applicability of these reactions. Substrate dip coating in aqueous solutions is particularly useful to facilitate both organic and inorganic layer functionalization. For instance, the bonding of phosphonic acid to silicon oxide is weak in water because the Si-O-P bond is easily hydrolyzed. We demonstrate here that this problem is alleviated by the addition of an ultra-thin aluminum oxide layer to the silicon oxide surface via dip-coating a silicon substrate in an aqueous solution of aluminum chloride. The growth kinetics of the aluminum oxide layer are characterized by several surface sensitive techniques and found to follow a Stranski-Krastanov mechanism. Once the aluminum oxide layer is in place, a self assembled monolayer (SAM) of octadecylphosphonic acid (ODPA) is attached by the "tethering by aggregation and growth" (T-BAG) method performed in a controlled environment. We demonstrate that this ODPA layer grafted on the aluminum oxide interlayer remains stable in water. We also show that, following the same wet chemical approach, we are able to attach aluminum hydroxyl directly on oxide-free silicon surfaces previously functionalized with 1/3 monolayer OH. [1] Finally, we show that our approach can easily be transferred to other metal oxides and discuss the most influencing parameters.

[1] Michalak, D. J.; Amy, S. R.; Aureau, D.; Dai, M.; Esteve, A.; Chabal, Y. J. *Nat. Mater.* **2010**, *9*, 266-271.

3:00pm TF+AS+SS-ThA4 Static and Dynamic Depth Profiling of Thin Films with Low Energy Ion Scattering (LEIS), H.R.J. ter Veen, M. Fartmann, Tascon GmbH, Germany, T. Grehl, ION-TOF GmbH, Germany, B. Hagenhoff, Tascon GmbH, Germany

With the ever increasing demand of thinner and better defined thin layer structures, good depth resolution becomes more and more critical in depth profiling techniques. Low Energy Ion Scattering (LEIS) is known as the most surface sensitive chemical analysis technique (see [1] for a review of LEIS technique). It is considerably less known that LEIS can also be applied for so called "static depth profiling" by interpreting the backgrounds on the low energy side of the LEIS peaks. The energy that the particles lose while travelling through the sample is a measure for the depth of the scattering atom, in a way similar to Rutherford Back Scattering (RBS) but for a much smaller depth range. New models have been developed to understand the process that gives rise to these backgrounds and that contains the information from layers below the surface up to depths of 10 nm. These models will be presented.

The models for this static depth profiling can be verified by dynamic (sputter) depth profiling. After each sputter step a full LEIS spectrum is recorded, which contains the surface information as well as the static depth profile at that point in the dynamic depth profile. In this way, the static depth profile can forecast the dynamic depth profile. This technique will be demonstrated for an Si/SiO₂/W/Al₂O₃ system.

LEIS is particularly suited for dynamic depth profiling. Since LEIS is so surface specific, the depth resolution is excellent, as long as the sputter conditions are chosen with care. Furthermore, LEIS can be quantified easily, in many cases - such as in depth profiles - without the use of references. However, any dynamic depth profile suffers from artifacts, such as preferential sputtering and ion beam mixing. By combining the dynamic depth profiling with static depth profiling there is an independent check on

these artifacts. Furthermore, it will be shown how static depth profiling can give relevant information also at shallow depths where in a dynamic depth profile sputter equilibrium will not have been reached yet.

[1] H.H. Brongersma et al, Surf. Sci. Rep. 62 (2007)63

3:40pm TF+AS+SS-ThA6 Paul Holloway Award Talk: Surface Chemistry and Structure of Alloy Thin Films under Reaction Conditions and their Correlations to Catalytic Performances of CO₂ Conversion and Methane Partial Oxidation, F. Tao*, University of Notre Dame

Formation of alloys is one of the important approaches to design of new catalysts with high activity and selectivity as a second metal could tune electronic structure of the first metal or/and create thermodynamically favorable sites for an ideal reaction channel. Co-Ru alloys are active catalysts for conversion of CO₂ into fuel molecules CH₄. Pd-based alloys are important catalysts for methanol partial oxidation to produce hydrogen. Thin films of model catalysts of alloys Co-Ru and Pd-Co were prepared through e-beam evaporation in UHV. In-house ambient pressure X-ray photoelectron spectroscopy using monochromatic Al K α were used to examine the evolution of surface compositions of alloy catalysts and the oxidation states of the constituting elements under reaction conditions and during catalysis in contrast to those before or after a reaction; Surface chemistry (composition and oxidation state) of active phases of Co-Ru and Pd-Co was revealed. High pressure STM provided visible information of surface structure at nano and atomic scale under reaction conditions. These studies clearly suggest a modification of the coordination state through coordinating Ru atoms and thus tuning the adsorption energy of intermediates on Co in CO₂ conversion, which enhances the selectivity to production of CH₄. The formed Co_{0.85}Ru_{0.15} alloy exhibits 100% selectivity to the production of CH₄ and a conversion of 40% which is higher than both pure Co and pure Ru. The promotion effect of the alloy film for CO₂ conversion was rationalized by electronic effects of Ru to Co in the alloy thin films under reaction conditions. In terms of Pd-Co alloy catalysts, segregation of Co to surface under reaction conditions was observed. Through the measurement of surface composition using AP-XPS and the coordination of Pd on surface visualized with STM, a correlation between surface chemistry and structure of Pd-Co alloy surface under reaction conditions and the corresponding catalytic performances were built. The modification of Co to the catalytic behaviors of Pd was identified.

4:20pm TF+AS+SS-ThA8 Time-resolved and Surface Plasmon Resonance Studies in Metal-Insulator Phase Transition in VO₂ Thin Films, L. Wang, C. Clavero, K. Yang, E. Radue, M.T. Simons, I. Novikova, R.A. Lukaszew, College of William and Mary

Vanadium dioxide (VO₂) is a prominent example for a material exhibiting a metal-insulator transition (MIT) as a function of temperature with a phase transformation around 340 K from a low-temperature insulator state to a high-temperature conducting state. During the MIT the lattice structure of VO₂ transforms from a monoclinic (insulator) to a tetragonal structure (conductor). Whether these structural changes are solely responsible for the nature of the transition or whether correlation effects also play a role, has been a subject of much debate. Two mechanisms have been generally considered to explain the origin of the MIT in VO₂. The Mott-Hubbard mechanism suggests that electron-electron correlation drives the first-order MIT whereas the Peierls mechanism proposes that a strong electron-lattice interaction leads to the MIT. In order to have a better understanding of the phase transition mechanism and the optical properties of this material across the MIT, we present our research studies on epitaxial VO₂ thin films. We have investigated the optical transmission of a VO₂ thin film during the thermally induced MIT in two different optical spectral regions, with cw THz light and low power (1 mW) IR light (1520 nm HeNe), to identify different mechanisms at play. We have found that the transmission of the THz light starts to decrease at higher temperature than that of the IR light thus probing different stages during the thermally induced MIT. We also investigated surface plasmon polariton excitation in VO₂ thin films in the IR region, and observed a clear trend from non-absorption in the insulator phase to a high absorption in the metallic phase while changing the VO₂ temperature. Our studies are aimed at helping to understand the evolution of the metallic phase in VO₂ thin films after the MIT and relaxation back to the insulator phase upon the MIT which is of paramount importance for ultra-fast switch applications. Finally, we note that Cavalleri *et al.* [1] reported that the light-induced phase transition happens in less than half a pico-second thus hinting at electronic processes, although they also found that it strongly depended on pump-laser power which is suggestive of lattice interactions. We will compare our time-resolved measurements also using pump-probe techniques but with the sample held at low-temperature vs.

* Paul Holloway Award Winner

room-temperature to illustrate the role of the pump-power on the photo-induced MIT.

[i] A. Cavalleri, Cs. Tóth, C.W. Siders, J. A. Squier, F. Ráksi, P. Forget and J. C. Kieffer, Phys. Rev. Lett. **87** (23), 237401 (2001).

4:40pm TF+AS+SS-ThA9 Growth, Microstructure and Optical Properties of Sputter-Deposited Gallium Oxide Thin Films, S.K. Samala, C.V. Ramana, The University of Texas at El Paso

Gallium oxide (β -Ga₂O₃), which is a stable oxide of gallium, is a wide band gap material. The high melting point coupled with stable structure makes of β -Ga₂O₃ the best candidate for high temperature sensing. β -Ga₂O₃ thin films can be used for developing oxygen sensors operating at higher temperatures (≥ 900 °C). This feature opens the possibility of developing the integrated of β -Ga₂O₃ based oxygen sensors for power generation systems. The present work was performed on the analysis of growth behavior, microstructure, and optical properties of β -Ga₂O₃ films grown by sputter deposition. Ga₂O₃ thin film were deposited on Si(100) and quartz substrate by varying the growth temperature from room temperature to 800 °C. The characteristic analysis of the samples was performed employing grazing incidence X-ray diffraction (GIXRD), scanning electron microscopy (SEM), and spectrophotometry measurements. GIXRD analyses indicate that the samples grown at lower temperatures were amorphous while those grown at ≥ 400 °C. SEM results indicate that the morphology evolution is dependent on the temperature. The characteristic shape of the grains changed from triangular to square and finally to spherical morphology with increasing temperature. Optical characterization indicates that the band gap varies from 4.1 to 5.1 eV as a function of increasing temperature. The correlation between growth conditions, microstructure and band gap is established.

5:00pm TF+AS+SS-ThA10 Optical and Structural Properties of Hafnium Oxide Thin Films Prepared Using Different Deposition Techniques, L. Sun, N.R. Murphy, J.T. Grant, J.G. Jones, R. Jakubiak, Air Force Research Laboratory

The high dielectric constant and optical transparency of hafnium oxide makes it a useful component in leading-edge integrated circuitry and optical coatings. The optical and structural properties of stoichiometric HfO₂ films vary significantly depending on the deposition mechanism. We prepared 200 nm thick films of HfO₂ on silicon (100) substrates derived from DC magnetron sputtering (DCMS), high power impulse magnetron sputtering (HiPIMS) and pulsed laser deposition (PLD). Analysis of x-ray diffraction data revealed that films deposited via PLD are amorphous, while those deposited using the magnetron sputtering methods had peaks at 2θ of 28.3°, 31.3°, 34.3° and 50.0° indicative of polycrystalline monoclinic HfO₂. This is further supported by the FT-IR data collected in the far-IR regime where absorption bands at 258, 341, 410 and 514 cm⁻¹ were present. AFM and SEM images indicate that the sputtered samples had rougher surface morphology and larger grain sizes than the PLD films where the surface was uniform and smooth (RMS surface roughness less than 0.1nm). The degree of surface roughness and grain size is inversely proportional to the refractive index. At 632 nm PLD films had an index of refraction of 2.10 while the index of the sputter coated films was 1.98, presumably due to presence of voids. The high refractive index and homogeneity of the PLD films indicate that they were highly packed without voids during growth. Additionally, the influence of the O₂/Ar ratio, working pressure, HiPIMS pulse profile and duty cycle on optical properties, surface roughness, particle size and structural properties of the HfO₂ thin films were characterized and evaluated.

5:20pm TF+AS+SS-ThA11 Nitrogen Induced Changes in the Structure and Electronic Properties of WO₃ Thin Films, C.V. Ramana, R.S. Vemuri, The University of Texas at El Paso, M. Engelhard, S. Thevuthasan, Pacific Northwest National Laboratory

Tungsten oxide (WO₃) is a wide band gap semiconductor (~ 3.2 eV), which exhibits excellent physical, chemical and electronic properties. WO₃ thin films have been widely used in electrochromics and chemical sensors. Recently, the band gap modification with anionic and cationic doping of WO₃ was gained importance to utilize these materials in photo-catalysis for energy production and utilization. The present work was performed on nitrogen incorporated WO₃ (N-WO₃) films to explore the options to engineer the microstructure and electronic properties. Specifically, the effect of nitrogen incorporation and processing parameters on the microstructure evolution and band gap of WO₃ thin films is investigated. The samples were grown using reactive RF magnetron sputtering where the nitrogen concentration in the films is varied by varying partial pressure of nitrogen during deposition while keeping all other process parameters constant.

Quantitative measurements employing X-ray photoemission spectroscopy indicate the nitrogen content increases with increasing nitrogen partial pressure. Structural analysis employing grazing incidence X-ray diffraction demonstrated that the nitrogen atoms embedded in WO₃ crystal matrix changes the crystal-texturing and thus induce changes in the physical properties. Optical spectrophotometry analysis on the N-WO₃ films revealed a shift in the fundamental absorption edge which is in linear relation with the corresponding nitrogen concentration. The correlation between microstructure, dopant profile, dielectric constant and band gap in WO₃ films will be presented and discussed.

Thin Film

Room: 10 - Session TF+EM+SS-ThA

Applications of Self-Assembled Monolayers and Layer-by-Layer Assemblies

Moderator: M.R. Linford, Brigham Young University

2:00pm TF+EM+SS-ThA1 Light-Directed Nanosynthesis: Near-Field Optical Approaches to Integration of the Top-Down and Bottom-Up Fabrication Paradigms, G.J. Leggett, University of Sheffield, UK
INVITED

The integration of top-down (lithographic) and bottom-up (synthetic chemical) methodologies remains a major goal in nanoscience. At larger length scales, light-directed chemical synthesis, first reported two decades ago, provides a model for this integration, by combining the spatial selectivity of photolithography with the synthetic utility of photochemistry. Work in our laboratory has sought to realise a similar integration at the nanoscale, by employing near-field optical probes to initiate selective chemical transformations in regions a few tens of nm in size. A combination of near-field exposure and an ultra-thin resist yields exceptional performance: in self-assembled monolayers, an ultimate resolution of 9 nm (ca. $1/30$) has been achieved. A wide range of methodologies, based on monolayers of thiols, silanes and phosphonic acids, and thin films of nanoparticles and polymers, have been developed for use on metal and oxide surfaces, enabling the fabrication of metal nanowires, nanostructured polymers and nanopatterned oligonucleotides and proteins. Strategies based upon the use of nitrophenyl-based photocleavable protecting groups have enabled the introduction of synthetic chemical methodology into nanofabrication. Nanoscale control of chemistry over macroscopic areas remains an important challenge. Recently parallel near-field lithography approaches have demonstrated the capacity to pattern macroscopic areas at high resolution, yielding feature sizes of ca. 100 nm over an area four orders of magnitude larger; they have also demonstrated the ability to function under fluid, yielding feature sizes of ca. 70 nm in photoresist under water and suggesting exciting possibilities for surface chemistry at the nanoscale. Finally, the monolayer patterning methods we have developed are by no means restricted to near-field lithography; all that is required is a suitable means of confining the optical excitation. For example, SAM photochemistry has been combined with interferometric exposure to facilitate the fabrication of periodic nanostructures over macroscopic areas in fast, simple, inexpensive processes, underlining the versatility of photochemistry as a nanofabrication tool.

2:40pm TF+EM+SS-ThA3 Molecular Layer Deposition (MLD) of Polymer Multiple Quantum Dots on TiO₂, T. Yoshimura, S. Ishii, Tokyo University of Technology, Japan

[Introduction] We previously proposed oxide-semiconductor-based sensitized solar cells, in which polymer multiple quantum dots (MQDs) are utilized for sensitizing layers, and fabricated the polymer MQDs on glass substrates by Molecular Layer Deposition (MLD) [1]. In the present study, we grew polymer MQDs on TiO₂ by MLD. The polymer MQD growth on TiO₂ was confirmed by photoluminescence (PL) spectra.

[Proposed Solar Cells Sensitized by Polymer MQDs] The proposed sensitized solar cell consists of an oxide semiconductor layer and polymer MQDs on the surface. The polymer MQD contains different-length quantum dots (QDs) in the backbone wire, and consequently, a wide absorption band is obtained by superposition of narrow absorption bands of the individual QDs. This spectral division with the narrow bands can reduce the energy loss arising from the heat generation due to excess photon energy in light absorption processes.

[Absorption/Photoluminescence Spectra of Polymer MQDs] Reference samples of poly-azomethine (AM) and polymer MQDs: OTPTPT, OTPT, and OT were grown on glass substrates by connecting terephthalaldehyde (TPA), *p*-phenylenediamine (PPDA), and oxalic dihydrazide (ODH) with designated orders using MLD. The QD lengths in OTPTPT, OTPT and OT

are respectively ~3, ~2 and ~0.8 nm. With decreasing the QD length, while the absorption peak shifts to high-energy side due to the quantum confinement, the PL peak shifts to low-energy side due to the Stokes shift. Namely, in the order of poly-AM to OT, the electrons become highly localized to increase the surrounding atoms' displacement caused by the electron transitions, resulting in the Stokes shift enhancement.

[Growth of Polymer MQDs on TiO₂] We performed MLD to grow poly-AM on ZnO and TiO₂ powder layers. A yellow film of poly-AM was observed on TiO₂. For ZnO, however, no film growth was observed because of weak hydrophilic characteristics of ZnO surfaces. We grew poly-AM and polymer MQDs of TO on the TiO₂ powder layers by MLD, and measured their PL spectra. The PL spectrum of TO was located at lower-energy side than that of poly-AM, which is parallel to the tendency observed in the PL spectra of the reference samples. From this result, it is concluded that polymer MQDs can be grown on TiO₂ by MLD as the sensitizing layers for solar cells.

[1] T. Yoshimura, R. Ebihara, A. Oshima, "Polymer Wires with Quantum Dots Grown by Molecular Layer Deposition of Three Source Molecules for Sensitized Photovoltaics," *J. Vac. Sci. Technol. A*. **29**: 051510-1-6 (2011).

3:00pm **TF+EM+SS-ThA4 Thiol-yne Click Chemistry: Old Concept & New Applications in Surface Science, N.S. Bhairamadgi, H. Zuilhof,** Wageningen University, Netherlands

Click chemistry reactions have opened new horizons in the field of surface chemistry, as these reactions are easy to perform on surfaces. A nice example is the addition of thiol moieties onto C=C bonds, which have been shown to be highly efficient, orthogonal to many other reactions, highly selective, etc. Recently we and others have shown that thiol-yne click reactions can be used efficiently for the modification of semiconductor surfaces and nanoparticles with a wide range of materials. In the current presentation we show an improved procedure involving C≡C bonds, i.e. thiol-yne click reactions.

We modified oxide-free Si(111) surfaces with alkene-terminated and alkyne-terminated monolayers, and these surfaces were further modified with various thiols such as thioglycolic acid, thioacetic acid, thioglycerol, thio-β-D-glucose tetraacetate lactose and 9-fluorenylmethoxy-carbonyl cysteine by using thiol-yne and thiol-yne click reactions. Upon detailed surface analysis it was found that after some optimization the thiol-yne click reaction yielded 20 – 80 % more surface coverage compared to thiol-yne click reactions. Thus surface modification with thiol-yne click reactions promise to be the next step in surface-bound thiol click chemistry.

References:

1. Campos, M. A. C.; Paulusse, J. M. J.; Zuilhof, H., Functional monolayers on oxide-free silicon surfaces via thiol-yne click chemistry. *Chem. Commun.* 2010, 46 (30), 5512-5514.
2. Lowe, A. B.; Hoyle, C. E.; Bowman, C. N., Thiol-yne click chemistry: A powerful and versatile methodology for materials synthesis. *J. Mater. Chem.* 2010, 20 (23), 4745-4750.
3. Ruizendaal, L.; Pujari, S. P.; Gevaerts, V.; Paulusse, J. M. J.; Zuilhof, H., Biofunctional Silicon Nanoparticles by Means of Thiol-Yne Click Chemistry. *Chem. Asian J.* 2011, 6 (10), 2776-2786.
4. Wendeln, C.; Ravoo, B. J., Surface Patterning by Microcontact Chemistry. *Langmuir* 2012, 28 (13), 5527-5538.
5. Wendeln, C.; Rinnen, S.; Schulz, C.; Arlinghaus, H. F.; Ravoo, B. J., Photochemical Microcontact Printing by Thiol-Yne and Thiol-Yne Click Chemistry. *Langmuir* 2010, 26 (20), 15966-15971.

3:40pm **TF+EM+SS-ThA6 Attachment of Conjugated Diruthenium Alkynyl Compounds by Click Chemistry, S. Pookpanratana,** National Institute of Standards and Technology, *S.P. Cummings, T. Ren,* Purdue University, *C.A. Richter, C.A. Hacker,* National Institute of Standards and Technology

Attaching electrochemically-active molecules to a variety of different surfaces is of particular interest for applications in photovoltaic devices, catalysis, and molecular electronics. The family of diruthenium 2-anilinopyridinate (ap) molecules is redox active [1], which makes it an ideal candidate to incorporate on surfaces for molecular catalysis, photoelectrochemical cells for water splitting, and as an active component in molecular electronic devices. Often times, the attachment of a tailored-molecule requires the additional design challenge to incorporate a specific anchoring group (e.g., thiol). Click chemistry has been demonstrated as an effective method to incorporate bulky and complex molecules to a variety of surfaces [2-6]. This route has introduced numerous possibilities of tailoring molecular surfaces.

Here, we have employed a Cu-catalyzed azide-alkyne cycloaddition (CuAAC) click reaction to attach Ru₂(ap)₄-(C≡C-C₆H₄-C≡CH), (henceforth referred to as Ru₂-alkynyl) to Au and SiO₂ surfaces. First, we

form an azide-terminated monolayer on Au and SiO₂ by using azidoundecanethiol and azidoundecyl trimethoxysilane, respectively. Next, the Ru₂-alkynyl is linked to the azide-containing monolayers via a CuAAC reaction (adapted from Ref. 4). The clicked-on Ru₂-alkynyl molecule was physically characterized by X-ray photoelectron spectroscopy (XPS) and infrared (IR) spectroscopy. The formation of the azide monolayer on Au and SiO₂ surfaces is confirmed by IR measurements. After the CuAAC click reaction of the Ru₂-alkynyl to the azide-treated surfaces, there is a reduction of the azide stretch in the IR which indirectly confirms the progress of the click reaction. The incorporation of Ru₂-alkynyl is confirmed by XPS, where we estimate the Ru₂-alkynyl covers about 10% of the azide sites.

The formation of molecular electronic junctions (Au/Ru₂-alkynyl/Si structures) by flip-chip lamination [7] for electrical and backside IR [8] characterizations is currently ongoing. With these results, we are able to obtain a thorough picture linking electrical properties with physical and chemical structure of the diruthenium molecular junctions.

S. P. Cummings et al., *Organometallics* 29, (2010) 2783 – 2788.

R. Chelmoski et al., *Langmuir* 25, (2009) 11480-11485.

G. Qin et al., *J. Am. Chem. Soc.* 132, (2010) 16432-16441.

R. E. Ruther et al., *J. Am. Chem. Soc.* 133, (2011) 5692 – 5694.

A. C. Cardiel et al., *ACS Nano* 6, (2012) 310-318.

P. K. B. Palomaki and P. H. Dinolfo, *Langmuir* 26, (2010) 9677 – 9685.

M. Coll et al., *J. Am. Chem. Soc.* 131, (2009) 12451-12457.

C. A. Richter et al., *J. Phys. Chem. B* 109, (2005) 21836 - 21841.

4:00pm **TF+EM+SS-ThA7 Vapor Phase Surface Functionalization using Hybrid SAMs / ALD Heterostructures, L. Lecordier, M.J. Dalberth, G. Sundaram, J.S. Becker,** Cambridge Nanotech, Inc.

Self-assembled monolayers and atomic layer deposition are two methodologies commonly used to tailor surface properties at the atomic scale and achieve thin films with excellent electrical, chemical, mechanical or optical performances thus leading to a broad portfolio of applications from thin films for flexible electronics to biological surface functionalization.

While ALD film growth is the result of a discretized process where inorganic monolayers are built upon one another through a sequence of reactant exposure/purge cycles until the desired film thickness is achieved (typically 1-100nm), SAMs on the other hand allow the deposition of a single ordered organic monolayer. Both processes are driven by self-limited chemisorbed surface reactions and can be deposited under vacuum conditions at relatively low temperatures, facilitating the integration of these two processes on a single platform.

The current work was implemented on a commercial Cambridge Nanotech hybrid ALD/SAMs platform. The tool is based on a Savannah S200 ALD reactor and integrates a SAMs kit for the accurate delivery of a variety of SAMs reactants. Stable SAMs monolayers are deposited under vacuum conditions using exposure mode (EXPO) characteristic of Cambridge Nanotech ALD tools. Key process metrics such as precursor pulse and exposure times, source and reactor temperatures were investigated for a variety of precursors including non-polar hydrophobic alkylsilanes (DTS), oleophobic fluorinated silanes (FOTS), hydrophilic polyethylene glycol (PEG) and thiols. In all cases, the self-limited surface saturation was achieved within 1 to 15 min minute exposures to the precursor at temperature ranging from 50 to 110°C.

In some instances, oxide ALD films were used to deposit a very thin seed layers (<5Å) to promote the adhesion of a SAM without prior surface cleaning/conditioning. Heterostructures based on oxide ALD (Al₂O₃, ZrO₂, SiO₂) and SAMs were also obtained to develop efficient water moisture barriers to be used for encapsulation. Overall the integration of these processes in a single platform provides a versatile and scalable method to surface functionalization where surface properties such as wettability can be tuned by controlling at the atomic level the structures of these hybrid coatings.

4:20pm **TF+EM+SS-ThA8 Chemically and Mechanically Stable Hydrophobic Thin Films Prepared by Combination of Layer-By-Layer Approach and Thiolen Chemistry, N. Madaan, J.A. Tuscano, N.R. Romriell, M.R. Linford,** Brigham Young University

The current aim of our research is to create robust hydrophobic thin films, for glass/silicon substrates, which can withstand extreme pH conditions and temperatures, have good release properties, and at the same time are mechanically durable. This approach consists of deposition of 3-aminopropyltriethoxy silane (APTES) on a silicon substrate followed by layer-by-layer deposition and cross-linking of alternating layers of poly(acrylic acid) (PAA) and poly(allylamine hydrochloride) (PAH). These

nylon-like cross-linked layers have already been demonstrated to possess stability in extreme pH conditions. Their permeability can be controlled by the extent of crosslinking, which depends on the time and temperature of crosslinking. A careful study using X-ray photoelectron spectroscopy in our lab showed 71% cross-linking when these assemblies were heated at 250 °C for 2 h. We also found that the ratio of ammonium to amine groups in these bilayers is 2:1, and that there is a potential to impart additional properties to the films by utilizing these residual amine groups. This was part of an experimental design over a series of times and temperatures. These substrates can further be modified using a variety of chemistries. One approach is to expose these substrates to basic NaOH solution (pH ~ 10) in order to deprotonate the ammonium groups of the terminal PAH layer followed by treatment with Traut's reagent to convert amine groups into thiol groups. The thiol groups are then reacted with 1,2-polybutadiene and a perfluoroalkanethiol using thiol-ene chemistry. Another approach is to use hydrolyzed poly(maleic anhydride alt 1-octadecene) as a terminal electrostatic anionic layer. A chemical and tribological stability comparison will be performed between the above prepared films and a perfluoroalkane silane film on Si substrates. The effect of the total thickness of cross-linked PAH-PAA bilayers on the stability of prepared films will be studied. The substrates are thoroughly analyzed at each surface modification step using X-ray photoelectron spectroscopy, time-of-flight secondary ion mass spectrometry, ellipsometry, water contact angles, and atomic force microscopy.

4:40pm TF+EM+SS-ThA9 A Detailed Investigation of the Conditions for Monolayer Deposition from Silane Precursors, J. Knauf, Advanced Molecular Films GmbH / RWTH Aachen University, Germany, *L. Reddemann,* Advanced Molecular Films GmbH / Universität zu Köln, Germany, *A. Böker,* RWTH Aachen University, Germany, *K. Reihs,* Advanced Molecular Films GmbH, Germany

We have systematically investigated the process parameters for the vapor-phase deposition of monolayers from fluoroalkylated silane precursors. Our study reveals the influence of many process parameters on the molecular structure of the monolayers. Of particular interest to us are wetting and frictional properties of the monolayer obtained from the variation of process conditions. For reproducibly preparing high quality films particular parameters have to be meticulously controlled in a very narrow range which is not achievable without advanced deposition equipment.

Although the deposition of monolayers from silane precursors has been accomplished by various methods and has been subject to numerous studies, the properties and reproducibility of the resulting films remain unsatisfying for many applications. As an example, fluid wall slippage strongly depends on small changes in monolayer processing conditions which sensitively influence the structure of the monolayer deposited on structured surfaces [1].

Self-assembled monolayers (SAMs) were prepared by controlling a variety of process parameters, such as processing sequence and partial pressures of reactive compounds, deposition temperatures, adsorption/desorption times. These conditions were investigated for linear fluoroalkylated silane precursors of different chain lengths.

SAMs were deposited from fluoroalkylated silane precursors on pre-treated Si-wafers. Samples were examined by dynamic contact angle measurements, x-ray photoelectron spectroscopy (XPS), and static secondary ion mass spectrometry (sSIMS). The precursors applied were linear *1H,1H,2H,2H*-Perfluoroalkyltrichlorosilanes and varying chain lengths of the fluoroalkyl part were used for comparative studies based on detailed investigations using *1H,1H,2H,2H*-Perfluorodecyltrichlorosilane. Short-chain precursors were commercially available in ready-to-use quality whereas longer-chain compounds starting from *1H,1H,2H,2H*-Perfluorododecyltrichlorosilane were synthesized in our labs. While the short-chain compounds could be processed by routine measures special precautions had to be applied for storage and handling of longer-chain compounds due to their higher reactivity.

Results of the study of deposition conditions will be presented and discussed and may serve as a guideline for the reproducible preparation of well-defined monolayers from silane precursors.

[1] L. Reddemann, J. Knauf, A. Böker, K. Reihs, 14th International Conference on Organized Molecular Films (ICOMF14) - LB14, Abstract 146 (2012)

5:00pm TF+EM+SS-ThA10 Self Limiting Behavior in the Directed Self-Assembly of Mounds on Patterned GaAs(001), C.-F. Lin, University of Maryland, *C.J.K. Richardson,* Laboratory for Physical Science, *H.-C. Kan,* University of Maryland, *N.C. Bartelt,* Sandia National Laboratories, *R.J. Phaneuf,* University of Maryland

We present results demonstrating directed self assembly of nm scale mounds during molecular beam epitaxial growth on patterned GaAs(001) surfaces. In the initial stages of growth, a lithographically-defined pattern directs the spontaneous formation of multilayer islands at the centers of bridges between near-neighbor nanopits along [110] crystal orientation, seemingly due to the presence of an Ehrlich-Schwoebel barrier. As growth continues, the heights of mounds at these 2-fold bridge sites "self-limit". Beyond this point mounds at other, 4-fold bridge sites dominate the topography, but these self-limit as well. This behavior suggests the existence of a minimum, 'critical terrace width' for nucleation of islands during growth, and provides a physical mechanism for understanding the transient nature of the observed instability during growth on these patterned surfaces

5:20pm TF+EM+SS-ThA11 Characterization of Fully Functional Spray-on Antibody Thin Film, J.J. Figueroa, S. Magana, D. Lim, R. Schlaf, University of South Florida

Physical adsorption (solid-liquid interface) is known as a simple and rapid option to immobilize biomolecules on various surfaces. Proteins, receptors and antibodies are attached via physisorption to different surfaces by various attachment protocols. However, physical adsorption has been often labeled in the past with disadvantages like variability, reversibility and low surface density of immobilized biomolecules. In contrast, the presented research demonstrates that spray deposition with a pneumatic nebulizer can be used to immobilize fully functional and stable physisorbed antibody coatings on glass surfaces with high reproducibility.

The experiments were performed using a low flow concentric nebulizer (commonly used on mass spectrometry), regular glass slides as a substrate and *E. coli* O157:H7 antibody as prototypical test system. The antibody films were examined for functionality, specificity and shelf life. A series of films with varying thickness and deposition conditions was characterized with respect to functionality, mechanical stability, surface morphology and antibody density. The results demonstrate that the films are comparable to films prepared with the standard covalent attachment protocol (avidin-biotin). They show low denaturation or conformational changes, minimal loss during the rinsing process suggesting good attachment to the surface, and they perform as well with regard to sensitivity, specificity and shelf-life. The morphology studies suggest that the non-oriented attachment of the spray deposited antibodies (compared to the oriented attachment achieved with the covalent attachment scheme) is compensated by a higher antibody density enabled by the non-equilibrium spray deposition process.

Thursday Afternoon Poster Sessions

Thin Film

Room: Central Hall - Session TF-ThP

Thin Film Poster Session

TF-ThP1 Vanadium Oxide Thin Films Grown by ALD using TEMAV and O₃ or H₂O Precursors. A. Premkumar, IMEC, Belgium, M. Toeller, Tokyo Electron Limited, Japan, I. Radu, Katholieke Universiteit, Leuven, Belgium, C. Adelman, M. Schaeckers, J. Meersschaut, T. Conard, J. Malgorzata, S. Van Elshocht, IMEC, Belgium

Vanadium dioxide (VO₂) is a smart material and offers interesting optical and electrical switching applications because of the reversible semiconductor-metal transition (SMT) that is observed at a temperature of about 68°C. Thin film growth of VO₂ has been extensively studied by CVD, PVD and sol-gel techniques. Aggressive scaling and increasing integration complexity have placed greater importance on atomic layer deposition (ALD) for depositing oxides in microelectronics. In this work we have developed an ALD process for VO₂ on 300 mm Si substrates using TEMAV precursor comparing different reactants (O₃ and H₂O) and starting surfaces (SiO₂ or Al₂O₃). We studied the ALD process in a 100-210°C temperature window. The as deposited films (100-150°C) were found to be XRD amorphous. Annealing in N₂/O₂ ambient (425-500°C) resulted in crystalline films. For the O₃ based process, the VO₂ formation conditions were found to be strongly dependent on the substrate investigated with a narrow process window for the preparation of phase pure and continuous VO₂ films. In contrast, highly uniform layers with consistent phase formation pathways were observed for the water based ALD process on all the substrates investigated. Films resulting from the water based process were smoother. Growth/anneal conditions were optimized to yield a resistivity change at the SMT of two orders of magnitude for 8 nm VO_x films.

TF-ThP2 Roles of MoO₃ Layer for Charge Injection and Charge Generation in an Organic Light Emitting Diode. M. Kawamura, S. Yoshida, Y. Abe, Kitami Institute of Technology, Japan

It has been reported that MoO₃ inserted between ITO anode and hole transport layer is useful as a hole injection layer to improve properties of organic light emitting diodes (OLEDs). However, its optimum thickness in the devices varies from sub-nanometer to 30 nm, depending on reports. In addition, as the mechanism of hole injection at the MoO₃ layer and α -NPD layer, it is argued that either charge injection mechanism or charge generation mechanism is dominant. As a fundamental study to investigate the main mechanism, we investigate the influence of MoO₃ thickness on properties of normal OLED device and also a device with a charge generation layer in the present work. First of all, we investigated properties of an OLED consists of ITO/MoO₃/ α -NPD/Alq₃/LiF/Al prepared by vacuum evaporation. As a results, the best device properties were obtained when 1.0 nm thick MoO₃ was inserted. Using atomic force microscopy, we found that the best device properties were obtained when the ITO surface was not completely covered with MoO₃. It is considered that the incomplete coverage was preferable in the view point of energy alignment because HOMO of α -NPD (5.4 eV) is intermediate between work functions of ITO (5.0 eV) and MoO₃ (5.7 eV). Then we confirmed charge generation phenomenon using device consists of ITO/Alq₃/MoO₃/ α -NPD/Al. Current did not flow without MoO₃ layer. When thickness of the MoO₃ layer was above 1.0 nm, a large current flowed and the current-voltage curves were the same even the MoO₃ thickness was increased to 10 nm. As the reason, it is considered that a high charge generation ratio was obtained from continuous MoO₃ layer. Consequently, we propose that MoO₃ work mainly for charge injection when the thickness is thin discontinuous film, and for charge generation when thick continuous film.

TF-ThP4 Effects of Preparation Conditions on the Magnetocaloric Effect of Gd Thin Films. H.F. Kirby, D.D. Belyea, J.T. Willman, University of South Florida, C.G. Hendryx, Newsome High School, C.W. Miller, University of South Florida

The effects of deposition temperature, post-deposition annealing, and chamber gettering were investigated on the magnetocaloric properties in Ta(5nm)/Gd(30nm)/Ta(5nm) grown by magnetron sputtering. The magnetocaloric effect (MCE) in these thin films, as indicated by the magnetic entropy change around the ordering temperature, increases with both growth temperature and post-deposition annealing of samples grown under ambient conditions. The full width at half max of the entropy change peak generally decreased toward the value for bulk Gd with increasing

deposition and annealing temperature. Similarly, the temperature of the maximum entropy change increased toward the bulk Gd ordering temperature. Overall the relative cooling power increased as deposition and annealing temperatures were increased. Gettering proved useful in limiting oxidation of the Gd especially for high temperature growth: ungettered samples grown at 600°C were purely diamagnetic GdO (111), while gettered samples, though still containing some GdO, were ferromagnetic.

TF-ThP5 Advanced Analytical Characterization of Multilayered Thin Films for Corrosion Inhibition. G. Zorn, M. Karadge, GE Global Research, C.C. Pierce, J.I. Melzer, GE Power & Water, M.M. Morra, GE Global Research

Advanced corrosion inhibitors developed by General Electric Power and Water can have complex multilayered structures that incorporate metal, ceramic and polymeric structures. For optimal performance it is important to understand the structure, morphology and composition of different layers. However, characterizing these nano scale films is very challenging, as they can be sensitive to preparation technique and damage. Moreover, surface roughness and homogeneity of the layers should be considered. The challenges in characterizing these multilayered structures will be discussed as an example for thin film characterization in the industrial R&D world. A multi technique approach that provides a detailed view of complex structures and compositions will be presented. Transmission Electron Microscopy (TEM) equipped with EDS was used to define local morphologies, crystalline structures and chemical composition; and Time-of-Flight Secondary Ion Mass Spectrometry (ToF-SIMS) depth profiles were used to determine the molecular distribution within the different layers. TEM provides local information in the range of a few nanometers over Focused Ion Beam (FIB) cross sections while ToF SIMS allows the analysis of larger areas, in the range of hundreds of nanometers, and provides top down views of the layers. The talk will emphasize how these two methods complement each other to achieve a detailed picture of complex structures within thin films.

TF-ThP6 Sputter Deposition of Atomically Smooth ZnO Films with Buffer Layers Crystallized via Nitrogen Mediation. K. Kuwahara, Kyushu University, Japan

Zinc oxide (ZnO) is a promising oxide semiconductor for optoelectronic devices because of its attractive properties such as wide direct band gap (3.3 eV), high exciton binding energy (58 meV), and material abundance. For realizing optoelectronic devices utilizing such attractive properties, a fabrication method of high quality crystalline ZnO films is essential. We have recently demonstrated a novel fabrication method of ZnO films utilizing nitrogen mediated crystallization (NMC), where the crystal nuclei density can be controlled because the nitrogen atoms suppress crystallization of ZnO films [1]. By using NMC-ZnO films as buffer layers, we have succeeded in high-quality epitaxial growth of ZnO films on sapphire substrates by RF magnetron sputtering [2]. However, for device applications such as light emitting diodes (LED), there still remains a need for improvement of properties of ZnO films. Here we apply off-axis sputtering to epitaxial growth of ZnO films on NMC-ZnO buffer layers aiming at reduction of negative-ion bombardment that causes serious damage during oxide deposition. NMC-ZnO buffer layers were fabricated by RF magnetron sputtering. The used gas was N₂-Ar and the total pressure was 0.3 Pa. ZnO ceramic targets were used. The applied RF power was 100 W and the deposition temperature was 700°C. The thickness of the buffer layers was 10 nm. On NMC-ZnO buffer layers, ZnO films were deposited by off-axis RF magnetron sputtering at 700°C. Ar-O₂ was used and the total pressure was 0.67 Pa. The applied RF power was 60 W. The film thickness was 1 μ m. After deposition, the films were annealed in a furnace at 1000°C for 3h in air. The surface of as-deposited ZnO films fabricated by off-axis sputtering on NMC-ZnO buffer layers has subnm scale corrugation and the RMS roughness is 0.28 nm, being significantly small compared with 1.02 nm for the films fabricated by conventional on-axis sputtering. Moreover, the annealed surface has 0.26-nm-high steps corresponding to one molecular layer of ZnO. We have demonstrated fabrication of atomically flat ZnO films by using NMC-ZnO buffer layers together with the off-axis sputtering.

[1] N. Itagaki, K. Kuwahara, K. Nakahara, D. Yamashita, G. Uchida, K. Koga, and M. Shiratani, Appl. Phys. Express 4 (2011) 011101.

[2] K. Kuwahara, N. Itagaki, K. Nakahara, D. Yamashita, G. Uchida, K. Kamataki, K. Koga, and M. Shiratani, Thin Solid Films 520 (2012) 4674.

TF-ThP7 Influence of Substrate Temperature on the Microstructure and Surface Morphology of Pulsed DC Magnetron Sputtered ZrB₂ Films. *C.T. Lee, W.C. Chen*, Instrument Technology Research Center, Taiwan, Republic of China

The ZrB₂ films were prepared on Si(100) substrate by pulsed DC magnetron sputtering with ZrB₂ target. Effects of substrate temperature (from 400 °C to 550 °C) on the microstructure and surface roughness of ZrB₂ films were investigated by X-ray diffraction, field emission scanning electron microscopy and atomic force microscopy. X-ray diffraction analysis reveals that ZrB₂ film was polycrystalline with (001) and (101) orientation when substrate temperature was 450 °C. However, the ZrB₂ film has preferred orientation along (001) when substrate temperature was above 500 °C. An increase in average grain size with increase of substrate temperature was observed. The average grain size of ZrB₂ film was increased from 6.2 nm to 15 nm as substrate temperature increased from 400 °C to 550 °C. In this study, the preferred orientation along (001) of ZrB₂ films on Si(100) substrate can be obtained at substrate temperature above 500 °C by pulsed DC magnetron sputtering.

TF-ThP8 Effect of Fluorine Doping on the Structural, Optical and Electrical Properties of CdS Films Deposited by Chemical Bath Deposition. *K.E. Nieto-Zepeda*, Cinvestav-IPN, Mexico, *E. Mota-Pineda*, ESIME-IPN, Mexico, *M.A. Zapata-Torres*, CICATA-Legaria, IPN, Mexico, *M.A. Melendez-Lira*, Cinvestav-IPN, Mexico

The efficiency of photovoltaic structures based on the CdS/CdTe heterojunction is far from that predicted theoretically. Within the various problems that affect negatively the efficiency of this system is the lack of a methodology to get a controlled doping of the n-type window layer of CdS. The chemical bath deposition methodology generally produces uncontrolled n-type CdS films. This paper proposes the use of fluoride as an electron donor to substituting the atoms of S in CdS. With this objective we deposited CdS films using different molar compositions of thiourea doped with fluorine. The molar compositions used are between 0.025 and 0.25 M with variations of 0.025 M. The samples obtained were characterized by UV-Vis transmission spectroscopy, X-ray diffraction and the electric transport by I vs V measurements. Representative samples were characterized by using Atomic Force Microscopy, Scanning Electron Microscopy, Raman, photoluminescence and photoconductivity spectroscopies. The results are discussed considering the presence of defects associated with the molar concentration of thiourea. The crystallographic quality of the samples increases with fluorine doping. There is a growing trend in the band gap values with thiourea concentrations. Raman spectroscopy results suggest that fluorine is substitutionally incorporated in sulphur sites and photoluminescence spectroscopy indicates that chemical bath deposited samples have a low density of radiative defects. I vs V curves indicated that transport is carried out through a percolation process. Our results indicated that the samples with the best characteristics are those fluorine doped grown with thiourea concentrations between 0.075 y 0.125 M showing that fluorine substitutionally replaces to sulphur and passivates interfacial states.

* This work has been partially supported by CONACYT-Mexico and Instituto de Ciencia y Tecnología-DF

TF-ThP9 Interfacial Properties of Atomic Layer Deposited TiO₂ Films on InAs (100) Surfaces. *L. Ye, T. Gougousi*, UMBC

TiO₂ has been deposited on both native oxide and etched InAs (100) surfaces by thermal atomic layer deposition (ALD) from tetrakis dimethyl amido titanium (TDMAT) and H₂O. X-ray photoelectron spectroscopy (XPS) and high resolution transmission electron microscopy (HRTEM) were utilized to study the interface between the TiO₂ films and the InAs substrate. For depositions at 200°C, the native oxide was thinned and part of the native oxide bubbled to the top of the TiO₂ surface. HRTEM data for a ~4 nm film of TiO₂ on InAs confirmed that the native oxide was completely removed from the interface. When TiO₂ was deposited on HF and NH₄OH etched InAs surfaces, practically sharp interfaces were maintained. To investigate the effect of temperature on the native oxide consumption, two sets of samples with film thickness of 2 and 3 nm were prepared at deposition temperatures ranging from 100 to 325°C. XPS showed that the native oxides were consumed most effectively at 250°C. Deviation of the deposition temperature from 250°C in either direction resulted in a reduction of the native oxide consumption rates.

TF-ThP10 AES and XPS Characterizations in ALD ZnO Films Doped with Al and P. *H. Yuan*, Northwestern Polytechnical University, China, *B. Luo, W.L. Gladfelter, S.A. Campbell*, University of Minnesota

Zinc oxide based films are transparent conductive oxide materials. As part of our research in solar cells, Al- and P-doped ZnO films were prepared at 250 °C in a hot-wall atomic layer deposition (ALD) system. Ozone, diethylzinc, trimethylaluminum or trimethylphosphite were used as the

precursors. We obtained films with different Al or P concentrations by varying the precursor vapor pressures, and characterized their physical, chemical and electrical properties. The Al-doped films were n-type with the lowest resistivity occurring at an Al concentration of 1-2%. The as-deposited P-doped films were n-type, but upon rapid thermal annealing in oxygen, the films changed to p-type. The temperature of the n- to p-type transition decreased as the phosphorus concentration increased.

In this presentation, we will describe details of the Auger electron spectroscopic (AES) and X-ray photoelectron spectroscopic (XPS) measurements. AES depth profiling was used to determine the compositions of all of the films, which confirmed that a layered microstructure for the films prepared by introducing the Zn precursor and Al precursor alternatively, and a homogeneous distribution of the Al in the films prepared by co-injecting the Al and Zn precursors. XPS determined the compositional change of the oxygen species upon sputtering. The oxidation state of the P dopant was determined to be +5 for both the as-deposited and annealed films.

TF-ThP12 Photoluminescence and Life-Time Characterization of Polythiophene Incorporated with Dye Molecules. *H. Kobe, H. Kato, A. Yamada, S. Takemura, T. Hiramatsu, K. Shimada, K. Matsui*, Kanto Gakuin University, Japan

Conducting polymer polythiophene (PT) films incorporated with highly-functional molecules such as copper phthalocyanine (CuPc), fullerene (C60) and rhodamine B (RB), further, tetrathiafulvalene (TTF) which is a donor and tetracyanoquinodimethane (TCNQ) which is an acceptor were synthesized and characterized by photoluminescence measurements (PL), time correlated single photon counting (TCSPC) life time measurements and fourier transform infrared spectroscopy (FTIR) in order to obtain fundamental photoluminescence properties of the polymer complexes. Those molecules were doped in the polymer film by the diffusion method. The solvents used in the doping process were acetonitrile or toluene. In the FTIR measurement, the molecular vibration mode of each molecule was observed in each polymer, and it was observed that each molecule had been doped in PT film. A photoluminescence single emission peak was observed at 610 nm in the case of PT doped sample with CuPc by diffusion method. Adding TCNQ molecules to the CuPc diffused PT sample by the diffusion method made the emission peak position varied and the photoluminescence intensity varied. A photoluminescence double emission peak was observed at 590nm and 738nm in the case of PT doped sample with C60 by diffusion method. Double emission peak was observed at 610nm and 663nm when TTF was added after CuPc doping. When TCNQ was added after CuPc doping, emission peak became a 480nm single peak. A photoluminescence double emission peak was observed at 590-660 nm in the case of PT doped sample with RB by diffusion method. In the case of using acetonitrile as a solvent, emission peaks were 610nm and 660nm. In the case of using toluene as a solvent, emission peaks were 590nm and 660nm. As for intensity, the low wavelength side became stronger. Adding TTF and TCNQ molecules to the RB diffused PT sample by the diffusion method made the emission peak position varied and the photoluminescence intensity varied. In the case of PT doped RB and TTF using toluene as a solvent, emission peak was a 590nm single peak. In the TCSPC measurements, 2 or 3 life time components with several tens of nsec to several hundreds of nsec existed in the case of highly-functional molecules doped PT. Adding TTF or TCNQ caused the life time change in the components. It suggests that the change of the emission states in the polymer complexes causes the shift of the emission peaks and the change in intensity.

This work was aided by MEXT-supported Program for the Strategic Research Foundation at Private Universities.

TF-ThP13 Production of Miniaturized Optical Interference Filters Array for CMOS Sensor. *C.-N. Hsiao, P.-K. Chiou, H.-P. Chen, B.-H. Liao, Y.-W. Lin, F.-Z. Chen*, Instrument Technology Research Center, Taiwan

Optical interference filters designed for use in a space-grade multispectral assembly in a complementary metal-oxide-semiconductor sensor were deposited on fused silica by ion-beam-assisted deposition. The optical parameters of optical interference coatings were optimized using admittance loci analysis. The patterned multispectral assembly containing blue, green, red, near infrared, and panchromatic multilayer high/low alternated dielectric band-pass filter arrays in a single chip was fabricated by photolithography process. The corresponding properties of the films were investigated by *in situ* optical monitoring, ellipsometry, spectrometry, scanning electron microscopy and high resolution scanning transmittance microscopy. It was found that the optical properties were significantly improved by employing ion-beam-assisted deposition. The average transmittances were above 90 % for the multispectral assembly, with a

rejection transmittance of less than 1% in the spectral range 350–1100 nm. To estimate the optical stability of optical coatings for aerospace applications, a space environment assuming a satellite orbiting the Earth at an altitude of near 780 kilometers was simulated by a Co^{60} gamma (γ) radiation test.

TF-ThP14 Analysis of Thin Layers with Low Energy Ion Scattering (LEIS). *B. Hagenhoff, M. Fartmann, D. Breitenstein*, Tascon GmbH, Germany, *T. Grehl, ION-TOF GmbH*, Germany, *H.R.J. ter Veen*, Tascon GmbH, Germany

When growing thin layers – through ALD or other processes – it is important to know how the layer is growing. Low Energy Ion Scattering (LEIS) can play a pivotal role in the study of film growth. It can be used for a quantitative analysis of the outermost atomic layer. This feature is used to determine layer closure or the existence of pinholes.

At the same time, LEIS gives information about the composition below the surface (similar to RBS). This so called "static depth profiling" can be used to monitor and study the evolution of layer thickness.

Examples will be shown for ALD Ta layers on Si, demonstrating the capabilities of LEIS to determine layer closure and the development of the layer thickness in the ALD process, also at low cycle numbers.

A Diamond Like Carbon (DLC) on Si system will be shown to demonstrate the possibilities to combine static depth profiling with dynamic (sputter) depth profiling, combining the advantages of both techniques and overcoming their drawbacks.

TF-ThP15 Reaction Mechanism for the Atomic Layer Deposition of Titanium Dioxide using Titanium Tetrachloride and Titanium Tetraisopropoxide as Precursors, *R.P. Chaukulkar, S. Agarwal*, Colorado School of Mines

Atomic layer deposition (ALD) is a thin film deposition technique widely used to deposit highly conformal thin films of a wide range of materials including metal oxides and nitrides, metals and more recently, polymers. Most ALD processes for the deposition of metal oxides require the use of H_2O , O_2 plasma, O_3 , or H_2O_2 as the oxygen source. ALD processes for depositing metal oxides using metal halides and metal alkoxides as the oxygen source were first reported by Ritala (Science **288**, 319 (2000)) to mitigate the problem of an interfacial oxide formation during deposition on semiconductor surfaces such as Si and Ge. Herein, we report an ALD process to deposit titanium dioxide using TiCl_4 and titanium tetraisopropoxide ($\text{Ti}[(\text{OC}_3\text{H}_7)_3]$, TTIP) as the oxygen source. We have used *in situ* attenuated total reflection Fourier transform infrared spectroscopy to probe the corresponding surface reactions during film growth over a temperature range of 150–250 °C. Depending on the surface temperature, alkyl-transfer and β -hydride elimination have been proposed as two possible reaction pathways for TTIP on a TiCl_3 -terminated surface. However, our infrared data show that alkyl-transfer is the only reaction pathway for this ALD process even at temperatures of up to 250 °C, which is close to the decomposition temperature of TTIP. We also report the growth per cycle, stoichiometry, and the band gap for these TiO_2 films grown over the above temperature range. Finally, we discuss the growth of these TiO_2 films on Cl-terminated Ge nanoparticle surfaces.

TF-ThP16 Nitrogen Doped Zinc Oxide Thin Films Prepared by Reactive RF Magnetron Sputtering of Zinc in Nitrous Oxide Atmosphere and Post-deposition Annealing Structural and Optical Properties, *L.A. Hernández-Hernández*, ESFM-IPN, Mexico, *A. Hernández-Hernández, F. De Moure-Flores, J.G. Quiñones-Galván*, CINVESTAV-IPN, Mexico, *J.J. Araiza-Ibarra, UAF-UAZ*, Mexico, *M. Meléndez-Lira*, CINVESTAV-IPN, Mexico

Nitrogen doped zinc oxide thin films were deposited on glass and silicon substrates by reactive magnetron RF sputtering of zinc in a N_2O -Ar ambient. The deposition conditions were optimized varying the substrate temperature and the $\text{N}_2\text{O}/\text{Ar}$ sputtering gas ratio. Representative films were studied employing structural, optical and spectroscopic techniques. A correlation between the nitrous oxide partial pressure, the chemical composition and the crystalline structure of the films was obtained. Stoichiometric and highly oriented ZnO thin films along the (0 0 2) crystallographic direction were obtained for a nitrous oxide partial pressure of ~33%. Lower temperatures produced samples with higher nitrogen content and slightly higher band-gap energy. Post-deposition annealing treatments in nitrous oxide atmosphere at 500 °C significantly improved the crystallinity of the samples as confirmed by x-ray diffraction.

†: partially funded by CONACyT-Mexico and ICYT-DF.

TF-ThP17 Physical and Electrical Characteristic of Atomic Layer Deposition of $\text{Al}_x\text{Hf}_y\text{O}_z$ on Silicon, *Y. Lin, W. Li, S. Fanz, R. Candler*, UCLA

In order to meet the increasing demand for high frequency electronic devices, the physical dimensions of MOSFETs have been continuously scaled down into nanoscale. However, one of the bottlenecks we encounter during the scaling-down process is the tunneling current leakage at the gates. SiO_2 , the most commonly used traditional gate dielectric experiences an appreciable amount of tunneling current when the gate thickness is below 1–1.2 nm. And leakage greatly degrades the performance of nanoelectronics. Therefore, we propose using high-k dielectrics to replace SiO_2 , which can effectively limit the tunneling leakage without losing the current control at gates. Our research has mainly focus on $\text{Al}_x\text{Hf}_y\text{O}_z$ deposited on silicon via Atomic Layer Deposition (ALD). The Aluminum to Hafnium ratio in the oxide is tuned to maximize the electrical and physical properties of the film. The electrical properties of each oxide will be characterized by fabricating transistors with gate oxide thicknesses of 5, 10, and 15 nm. Other than taking C-V and I-V measurements for capacitors and transistors, the films will be characterized by XPS, AFM, and spectroscopic ellipsometry. Finally, the effects of various annealing and deposition temperatures at the silicon-oxide interface will be studied using TEM.

TF-ThP18 Wetting Properties of Silicon Incorporated DLC Films, *T.G. Kim*, Pusan National University, Korea

Recently, Diamond-like carbon (DLC) films have come to the center stage of developing coatings for moisture resistant lubricant, water repellent and cathode for lithium batteries. Hydrophilic nature of DLC films played an important role in the above applications.

In this study, Silicon incorporated diamond-like carbon films were deposited on aluminum substrate by a radio frequency plasma-enhanced chemical vapor deposition method. The control of hydrophilic of Silicon incorporated diamond-like carbon surfaces has been studied by the use of O_2 plasma etching and heat treatment. The characteristic of DLC films was evaluated by various techniques such as Contact angle, Micro Raman spectroscopy and Nano indentation. Contact angle of Si-DLC film was about 60°. The contact angle was decreased into about 2° by not only by oxygen plasma treatment for 10min but by heat treatment at 700°C, respectively. In addition, increase of heat treatment temperature makes the contact angle of Si-DLC film decrease.

Friday Morning, November 2, 2012

Applied Surface Science

Room: 20 - Session AS+TF+VT-FrM

Surface Analysis using Synchrotron Techniques

Moderator: A. Herrera-Gomez, UAM-Azcapotzalco and CINVESTAV-Queretaro, Mexico, J.C. Woicik, National Institute of Standards and Technology

8:20am **AS+TF+VT-FrM1 Surface and Interface Analyses by X-ray Absorption and Hard X-ray Photoemission Spectroscopies**, *Q. Xiao, X. Cui*, Canadian Light Source, Canada, *H. Piao*, General Electric Global Research Center, *Y.F. Hu*, Canadian Light Source, Canada, *T.K. Sham*, The University of Western Ontario, Canada

Synchrotron-based techniques, such as X-ray absorption spectroscopy (XAS) and variable energy X-ray photoemission spectroscopy (XPS) are increasingly applied to the characterization of surfaces and interfaces of advanced materials. This presentation will introduce the XAS and variable energy XPS capabilities in the study of thin films and nanomaterials at the Canadian Light Source—the third generation synchrotron in Canada. Advantages of these techniques over the conventional techniques (such as lab-based XPS) will be demonstrated using examples in studies of two types of materials: (1) Gate oxide development on SiC and (2) heterogeneous nanocatalysts. In particular, examples using the recently commissioned high energy XPS at the SXRMB beamline (up to 10 KeV) will be highlighted.

8:40am **AS+TF+VT-FrM2 Differences in the Electronic Structure Highly-Oriented Films of H₂, Fe-, Co-, and Cu-Phthalocyanines Revealed by NEXAFS Spectroscopy**, *T.M. Willey, M. Bagge-Hansen, J.R.I. Lee, R. Call, L. Landt, T. van Buuren*, Lawrence Livermore National Laboratory, *C. Colesniuc, C.M. Monton, I. Schuller*, University of California, San Diego

Phthalocyanines are extensively studied as molecular semiconductor materials for chemical sensors, dye-sensitized solar cells, and other applications. Phthalocyanines offer high tunability through the choice of metal center atom; nearly all transition metals and many other heavier elements can reside at the relatively stable square planar center of the phthalocyanines. H₂, Fe-, Co-, and Cu-phthalocyanine molecules in films deposited on gold substrates show prostrate orientation, as opposed sapphire substrates, where phthalocyanines stand in a more upright conformation under deposition conditions used. Angular dependence in NEXAFS, commonly attributable to π^* and σ^* resonances, in both carbon and nitrogen K-edges, quantify the orientational order. H₂-phthalocyanine shows the cleanest angular dependence, with nearly no intensity in the π^* regime with normal beam incidence. Metal L-edges in prostrate films, on the other hand, have dramatic variation in angular dependence of resonances into empty states. Fe- and Co- resemble the K-edges; StoBe DFT shows that the lowest-energy allowed resonances are indeed molecular π^* states, with a high degree of mixing with the d_{xz} and d_{yz} orbitals of the metals. In contrast, the intense, in-plane resonance of the Cu-PC L-edge LUMO resembles a molecular σ^* state. Confirmed by StoBe, the $d_{x^2-y^2}$ character at the Cu center is responsible for this intense in-plane resonance. NEXAFS thus directly probes the electronic structure, illuminating the uniqueness of Cu-compared to H₂, Fe-, and Co- phthalocyanines.

9:00am **AS+TF+VT-FrM3 Hard X-ray Photoelectron Study of Graphene/ h-BN Layer Structures Grown on Polycrystalline Cu Substrates**, *L. Kövér*, MTA ATOMKI, Hungary, *L. Tapasztó*, Inst. Tech. Physics and Materials Sci. & Korea-Hungary Joint Lab for Nanosciences, Hungary, *C. Hwang*, KRISS & Korea-Hungary Joint Lab for Nanosciences, Republic of Korea, *L.P. Biró*, Inst. Tech. Physics and Materials Sci. & Korea-Hungary Joint Lab for Nanosciences, Hungary, *I. Cserny, J. Tóth, A. Csik*, MTA ATOMKI, Hungary, *W. Drube, S. Thiess*, Deutsches Elektronen-Synchrotron DESY, Germany

INVITED

Graphene-hexagonal BN layer structures are recently in the focus of interest having a great potential importance as promising candidates to be utilized in many electronic and spintronic ultrathin device applications. Hard X-ray photoelectron spectroscopy (HAXPES) based on application of synchrotron radiation for excitation is a useful tool for revealing multilayer structures nondestructively providing information on the chemical state of the components at the surface and (even in the case of deeply embedded) interface layers. The aim of the present study is to test the applicability of the HAXPES method for characterizing graphene-hexagonal BN layer systems. h-BN and single layer graphene/multilayer h-BN structures were grown on polycrystalline Cu substrates using the Chemical Vapor Deposition technique [1]. HAXPES measurements were performed at the

BW2 beamline of the DORIS III synchrotron at DESY using the Tunable High Energy XPS facility [2] and monochromatic photons of 3000 eV energy. The surface layer structure of the same samples were also studied with conventional XPS in ATOMKI using non-monochromated Al K α radiation [3]. For obtaining information on the order and relative depth of the particular layers the dependence of the XPS and HAXPES spectra on the angle of emission of photoelectrons was also studied. Our results demonstrate the advantage of the combination of XPS and HAXPES measurements, the use of the Auger parameter for identifying the chemical state of the components at the interface between the layer structure and the substrate, the removal of the overlap between the Auger spectra from the substrate and the photoelectron spectra of the overlayer structure in the HAXPES spectra. In addition, HAXPES, due to the high energy resolution and sensitivity applied, makes possible the separation and identification of the contributions from atoms in different chemical states to photoelectron peaks of the components of the layer structure, and the quantitative estimation of their relative intensity, even at near grazing photon beam incidence (high surface sensitivity).

The research leading to these results has received funding from the European Community's Seventh Framework Programme (FP7/2007-2013) under grant agreement n° 312284, by OTKA grants PD 84244, K 101599 and in the framework of the Korea- Hungary Joint Laboratory for Nanosciences.

[1] C. Hwang, K. Yoo, S.J. Kim, E.K. Seo, H. Yu, L.P. Biro, J. Phys. Chem. C 115, 22369 (2011)

[2] W. Drube, T. M. Grehk, R. Treusch and G. Materlik, J. Electron Spectrosc. Relat. Phenom. **88-91**, 683 (1998).

[3] L. Kövér, D. Varga, I. Cserny, J. Tóth, K. Tökési, Surf. Interface Anal. **19**, 9 (1992).

9:40am **AS+TF+VT-FrM5 Beyond Hard X-ray Photoelectron Spectroscopy: Simultaneous Combination with X-ray Diffraction**, *G.R. Castro, J. Rubio-Zuazo*, SpLine at the European Synchrotron Radiation Facility, France

Nowadays, the great challenge in materials science is the incorporation of complex systems in the area of the nano-technologies. A fundamental aspect is the production of materials with specific and controlled properties. Many of these materials are aggregates of different components, frequently multilayer thin films where the interface and the surface play a key role. Therefore, it is very important to develop an experimental set-up capable to investigate different aspects under identical experimental conditions, in particular to differentiate between surface and bulk properties.

Hard X-ray photoelectron spectroscopy (HAXPES) is a powerful novel emerging technique for bulk compositional, chemical and electronic properties determination in a non-destructive way. It benefits from the exceptionally large escape depth of high kinetic energy photoelectrons enabling the study of bulk and buried interfaces up to several tens of nanometres depth. At SpLine, the Spanish CRG beamline at the European Synchrotron Radiation Facility (ESRF), we have developed a novel and exceptional set-up that combine HAXPES and X-ray diffraction (X-ray Reflectivity, Surface X-ray Diffraction, Grazing Incidence X-ray Diffraction and reciprocal space maps). Both techniques can be operated simultaneously on the same sample and using the same excitation source. The set-up includes a robust 2S+3D diffractometer with its main axis vertical hosting an UHV chamber equipped with a unique photoelectron spectrometer (few eV < E_{kin} < 15keV), X-ray tube (Mg/Ti), 15 keV electron gun and auxiliary standard surface facilities: MBE, ion gun, LEED, sample heating/cooling system, leak valves, load-lock port, etc.. The photon energy ranges between 7 and 45 keV. The HAXPES analyzer is an electrostatic cylinder-sector (FOCUS HV CSA), with a compact geometry and high transmission due to second order focusing. The analyzer is capable to handle kinetic energies both up to 15 keV and down to a few eV with the same analyzer setup and power supply. The SpLine station offers a unique opportunity to obtain, on a same sample and under identical experimental conditions, simultaneous information about the electronic properties, chemical composition and geometric/crystalline structure of bulk, buried interfaces and surfaces. This *novel tool* for non-destructive characterization of bulk and buried interfaces is available to the *scientific community*.

In this contribution, we will present a general view of HAXPES-XRD station available at SpLine. Three aspects will be specially addressed: physical background, experimental set-up and selected examples.

10:00am **AS+TF+VT-FrM6 Spectroscopic Imaging using Vector Potential Photoelectron Microscopy**, *R. Browning*, R. Browning Consultants

A new class of electron microscope, vector potential photoelectron microscopy (VPPEM) has been developed. This microscope will enable the chemical microanalysis of a wide range of samples using photoelectron spectroscopy (PES). The microscope is a full field spectroscopic imaging technique with a very large equivalent depth of focus. The unique imaging properties of this method opens up many experimental opportunities including the chemical microanalysis of a wide range of real world samples. Highly structured, three dimensional samples, such as fiber mats and fracture surfaces can be imaged, as well as insulators, and magnetic materials. The new microscope uses the vector potential field from a solenoid magnet as a spatial reference for imaging. A prototype instrument has demonstrated imaging of Au grids, uncoated silk, magnetic steel wool, and micron sized single strand tungsten wires.

10:20am **AS+TF+VT-FrM7 Trends in Synchrotron-based Photoemission; High Energy and High Pressure**, *H.J. Bergersen, J. Åhlund, R. Moberg*, VG Scienta, Sweden

The fields of Hard X-ray Photoelectron Spectroscopy (HAXPES) and High Pressure Photoemission (HiPP) are growing fast. In this contribution we present instrument development and results within HAXPES and HiPP as well as the merged field of HiPP-HAXPES.

Photoelectron spectroscopy (PES) is an excellent tool in surface science due to the possibility to probe electronic and geometric structure. During the past decade Angle Resolved Photoelectron Spectroscopy (ARPES) has had a remarkable upswing, due to the development of parallel angular detector analyzers, and is today used routinely for band mapping, depth profiling and X-ray diffraction (XPD) in the Ultra Violet (UV) and soft X-ray regime. With higher energies (hard X-rays), in combination with improvements in PES detection techniques, this tool can be extended to the HAXPES regime, enabling studies of bulk materials. Here we demonstrate new development of analysers capable of measuring angular resolved spectra in the High Energy regime as well as results obtained using such analyzers.

Experiments done under normal surface science conditions (Ultra High Vacuum) are of limited use in some applications, e.g catalysis, due to the pressure gap problem. This motivates the study of systems at ambient pressures. Here we present a HiPP instrument developed in collaboration with Advanced Light Source (ALS). This instrument allows standard PES measurements as well as spatial and angle resolved spectra at HiPP conditions. Some recent results include spatially resolved investigations of solid oxide electrochemical cells (SOC:s) and electrochemical properties of junctions.

Finally, we report on recent advances in constructing a new generation of instrumentation combining HiPP and HAXPES. A novel electron analyser, designed for optimal transmission in combination with very efficient differential pumping, will be presented together with preliminary results.

Authors Index

Bold page numbers indicate the presenter

— A —

Abdallah, L.S.: EL+TF+AS+EM+SS-TuP2, 29;
EL+TF+BI+AS+EM+SS-MoA9, 12
Abdulagatov, A.: TF+EN-MoA3, 19
Abe, Y.: TF-ThP2, 57
Abell, J.L.: TF+SE+NS-WeM12, **34**
Adam, T.N.: EL+TF+AS+EM+SS+PS+EN+NM-
MoM9, 3
Adamiv, V.T.: AC+TF+SS+MI-MoA7, 11
Adams, D.: TF+EM+SE+NS-ThM5, **46**
Addou, R.: GR+EM+NS+SS+TF-ThA7, **51**
Adelmann, C.: TF-ThP1, 57
Adusumilli, S.P.: EN+TF-WeA12, 39
Agarwal, S.: TF-ThP15, 59
Ahlgren, M.: TF+NS+EM-ThM11, 48
Åhlund, J.: AS+TF+VT-FrM7, 61
Ahn, J.R.: GR+EM+NS+PS+SS+TF-MoM11, 6;
GR+EM+NS+PS+SS+TF-MoM4, 5
Aihara, T.: EN+TF-TuA11, **25**; EN+TF-TuA12, 25
Ajayan, P.: GR+EM+NS+SS+TF-ThA3, 51
Ajayi, O.: TF-MoM8, **8**
Akyildiz, H.: TF2-TuA10, **28**
Alian, A.: EM+TF+OX+GR-MoA1, 12
Almer, J.: TF+NS+EM-ThM11, 48
Altman, E.I.: OX+SS+TF+MI-MoA2, **17**
Alves, E.: AC+TF+SS+MI-MoA9, 11
Ancona, M.G.: TF+AS-TuA3, 26
Anderson, T.J.: EN+TF-TuM10, 21;
GR+EM+ET+NS+TF-MoA1, 15
Ando, T.: EM+TF+OX+GR-MoA7, **13**
Anwar, S.R.M.: EM+TF+OX+GR-MoA4, **13**
Araiza-Ibarra, J.J.: TF-ThP16, 59
Armstrong, I.: SP+AS+BI+ET+MI+TF-WeA8, **40**
Arnold, M.S.: EN+TF-TuA3, **24**
Aryal, P.: EL+TF+AS+EM+SS+PS+EN+NM-
MoM1, 2
Atalay, R.: EM+TF+AS-ThA11, 50; EM+TF+AS-
ThA9, 50
Attygalle, D.: EL+TF+AS+EM+SS+PS+EN+NM-
MoM1, 2
Atwater, H.A.: EN+TF-TuA1, **24**
Auer, M.: TF+EM+SE+NS-ThM6, 46
Aydi, E.S.: EN+TF-MoA8, 15; EN+TF-MoA9,
15; EN+TF-TuM9, 21

— B —

Baba, A.: TF+AS-WeA8, 41
Baby, A.: TF+NS+EM-ThM10, 48
Bagge-Hansen, M.: AS+TF+VT-FrM2, **60**
Bakhr, H.: EM+TF+OX+GR-MoM3, 3
Barlam, D.: OX+EM+MI+NS+TF-MoM11, 7
Barnes, T.: TF+AS-WeA10, 42
Bartels, L.: SP+AS+BI+ET+MI+NM+NS+SS+TF-
WeM5, 31
Bartelt, N.C.: TF+EM+SS-ThA10, 56
Barton, D.: EL+TF+AS+EM+SS+PS+EN+NM-
MoM10, 3
Bartynski, R.A.: OX+SS+TF+MI-MoA6, 17
Baruth, A.: EN+TF-MoA9, 15
Baski, A.A.: EM+TF+AS-ThA4, 49
Batzill, M.: GR+EM+NS+SS+TF-ThA7, 51
Beaudry, A.L.: TF+SE+NS-WeM9, **34**
Beck, D.: SP+AS+BI+ET+MI+TF-WeA11, 40
Becker, J.S.: TF+EM+SS-ThA7, 55; TF-WeM1, 35
Belyea, D.D.: TF-ThP4, 57
Bemis, J.: SP+AS+BI+ET+MI+TF-WeA11, 40
Benavidez, T.: EL+TF+BI+AS+EM+SS-MoA3, 11
Benedek, G.: EM+TF-WeM12, 31
Bennett, B.: EM+TF+OX+GR-MoA10, 14
Bera, K.: TF+AS-TuA11, **27**
Berdova, M.: TF+NS+EM-ThM10, **48**
Bergersen, H.J.: AS+TF+VT-FrM7, **61**
Bernal Ramos, K.: TF+NS+EM-ThM2, **46**;
TF+NS+EM-ThM9, 47
Bernasconi, M.: EM+TF-WeM12, 31
Berry, N.: TF+AS-WeA2, 41

Besnier, J.-F.: EL+TF+AS+EM+SS+PS+EN+NM-
MoM3, 2
Bezares, F.J.: GR+EM+ET+NS+TF-MoA1, 15
Bhairamaj, N.S.: TF+EM+SS-ThA4, **55**
Bielefeld, J.: GR+EM+NS+SS+TF-ThA1, 51
Bindl, D.J.: EN+TF-TuA3, 24
Bingham, N.: OX+EM+MI+NS+TF-MoM1, 6
Biró, L.P.: AS+TF+VT-FrM3, 60
Blomfield, C.J.: AS+NS+SS+TF-WeA8, 37
Bockowski, M.: AC+TF+SS+MI-MoA9, 11
Böker, A.: TF+EM+SS-ThA9, 56
Bol, A.: TF+EN-MoA4, 19
Bolotin, K.I.: GR+EM+ET+NS+TF-MoA3, **16**
Bonnell, D.A.: SP+AS+BI+ET+MI+TF-WeA3, 39;
SP+AS+BI+ET+MI+TF-WeA4, 39
Boos, J.B.: EM+TF+OX+GR-MoA10, 14
Borchers, J.: OX+EM+MI+NS+TF-MoM10, 7
Borner, K.: EM+TF-WeM5, 30
Borsa, D.: TC+EM+AS+TF+EN-ThM2, 44
Bosch, R.: TC+EM+AS+TF+EN-ThM2, 44
Bose, S.: OX+EM+MI+NS+TF-MoM10, 7
Bostwick, A.: GR+EM+ET+NS+TF-MoA8, 16
Boutwell, C.: TF+AS-WeA9, **42**
Boutwell, R.C.: TF+AS-WeA7, 41
Bowman, S.R.: EM+TF+AS-ThA6, 49
Boyce, M.C.: EM+TF-WeM11, 31
Brant, A.T.: AC+TF+SS+MI-MoA7, 11
Braunstein, P.: GR+EM+ET+NS+TF-MoA7, 16
Breitenstein, D.: TF-ThP14, 59
Breitung, E.: TF-MoM3, 8
Brennan, B.: EM+TF+OX+GR-MoM5, 4
Brenner, D.W.: TF+AS-TuA12, 27; TF+AS-TuA7,
26
Brett, M.J.: TF+SE+NS-WeM11, 34; TF+SE+NS-
WeM5, 33; TF+SE+NS-WeM9, 34
Brewer, J.R.: EL+TF+AS+EM+SS-TuP1, 29
Broitman, E.: TF+NS+EM-ThM12, 48
Brown, R.D.: EM+TF-WeM12, 31
Browning, R.: AS+TF+VT-FrM6, **61**
Bruhn, T.: GR+EM+NS+SS+TF-ThA6, 51
Brukman, M.: SP+AS+BI+ET+MI+TF-WeA4, **39**
Brumbach, M.T.: OX+SS+TF+MI-MoA9, **18**
Buchanan, D.A.: AC+TF+SS+MI-MoA7, 11
Buchholz, M.: OX+SS+TF+MI-MoA10, **18**
Buecheler, S.: TF+AS-WeA3, 41
Buie, C.: EM+TF+OX+GR-MoA4, 13
Burak, Ya.V.: AC+TF+SS+MI-MoA7, 11
Burst, J.: TF+AS-WeA10, 42
Butorin, S.M.: AC+MI+SS+TF-MoM5, 1

— C —

Cabrera, W.: EM+TF+OX+GR-MoA6, **13**;
TF+NS+EM-ThM9, 47
Caillard, L.: EL+TF+BI+AS+EM+SS-MoA2, 11
Caldwell, J.D.: GR+EM+ET+NS+TF-MoA1, 15
Call, R.: AS+TF+VT-FrM2, 60
Callahan, C.: SP+AS+BI+ET+MI+TF-WeA11, 40
Campbell, C.: EN+TF-TuM10, 21
Campbell, S.A.: EN+TF-TuM9, 21; TF-ThP10, 58
Campi, D.: EM+TF-WeM12, 31
Candler, R.: TF-ThP17, 59
Cantor, M.: EM+TF+OX+GR-MoA1, 12
Cao, Y.: TF+AS-WeA1, 41
Carcia, P.F.: TF-MoM10, 9; TF-WeM3, **35**
Cartier, E.A.: EM+TF+OX+GR-MoA7, 13
Caspar, J.: TF+AS-WeA1, 41
Castro, G.R.: AS+TF+VT-FrM5, **60**
Cavanagh, A.: TF+EN-MoA3, 19
Caymax, M.: EM+TF+OX+GR-MoA1, 12
Ceballos-Sanchez, O.: EM+TF+OX+GR-MoA9,
13
Chabal, Y.J.: EL+TF+BI+AS+EM+SS-MoA2, 11;
EM+TF+OX+GR-MoA6, 13; EM+TF-WeM4,
30; EN+TF-WeA7, 38; TF+AS+SS-ThA3, 53;
TF+NS+EM-ThM2, 46; TF+NS+EM-ThM9,
47
Chae, J.: GR+EM+ET+NS+TF-MoA10, **16**
Chagarov, E.:
SP+AS+BI+ET+MI+NM+NS+SS+TF-WeM6,
32
Champlain, J.: EM+TF+OX+GR-MoA10, 14
Chan, C.: TF+AS-WeA1, 41
Chang, C.S.: GR+EM+ET+NS+TF-MoA6, 16
Chang, J.P.: EM+TF+AS-ThA3, 49; EN+TF-
WeA9, 38; TF+NS+EM-ThM6, 47
Chapman, R.: EM+TF-WeM4, 30
Chase, B.: SP+AS+BI+ET+MI+TF-WeA9, 40
Chaukulkar, R.P.: TF-ThP15, **59**
Chen, F.-Z.: TF-ThP13, 58
Chen, H.-P.: TF-ThP13, 58
Chen, J.: EL+TF+AS+EM+SS+PS+EN+NM-
MoM4, 2
Chen, L.: TF+SE+NS-WeM4, 33
Chen, W.C.: TF-ThP7, 58
Chen, X.: TF+EN-MoA6, **19**
Chien, D.: EM+TF+AS-ThA3, **49**
Chiou, P.-K.: TF-ThP13, 58
Chirita, V.: TF+AS-TuA4, **26**; TF+AS-TuA9, 26
Chitre, K.: OX+SS+TF+MI-MoA6, 17
Cho, H.K.: OX+EM+MI+NS+TF-MoM2, 7
Cho, J.: EN+TF-WeA9, **38**
Cho, T.S.: TC+EM+AS+TF+EN-ThM12, 45
Choi, J.: GR+EM+ET+NS+TF-MoA7, 16
Choi, J.Y.: GR+EM+NS+PS+SS+TF-MoM11, 6
Choi, K.: EM+TF+OX+GR-MoA7, 13
Christiani, G.: TF+AS-TuA10, 27
Chumbuni-Torres, K.: EL+TF+BI+AS+EM+SS-
MoA3, 11
Chun, S.H.: OX+EM+MI+NS+TF-MoM2, 7
Chung, B.W.: AC+MI+SS+TF-MoM9, 1
Clark, B.D.: TF+MI-WeA3, 43
Clark, K.: GR+EM+NS+PS+SS+TF-MoM2, 5
Clark, M.D.: EN+TF-TuA7, 24
Clavel, G.: TF+NS+EM-ThM9, 47
Clavero, C.: TF+AS+SS-ThA8, 53
Cleveland, E.: EM+TF+OX+GR-MoA10, **14**
Cleveland, J.: SP+AS+BI+ET+MI+TF-WeA11, 40
Coclite, A.M.: TF-WeM5, **35**
Coh, S.: OX+SS+TF+MI-MoA6, 17
Cohen, K.D.:
SP+AS+BI+ET+MI+NM+NS+SS+TF-WeM5,
31
Cohen, S.R.: OX+EM+MI+NS+TF-MoM11, 7
Colby, R.: AS+NS+SS+TF-WeA3, 37;
AS+NS+SS+TF-WeA4, 37
Colesniuc, C.: AS+TF+VT-FrM2, 60
Collazo, R.: EM+TF+AS-ThA1, 49
Collins, R.W.: EL+TF+AS+EM+SS+PS+EN+NM-
MoM1, 2; EL+TF+AS+EM+SS+PS+EN+NM-
MoM4, 2
Colón Santana, J.: GR+EM+ET+NS+TF-MoA7,
16
Comes, R.B.: TF+MI-WeA4, 43
Conard, T.: TF-ThP1, 57
Condon, N.J.: EM+TF+AS-ThA6, 49
Cook, K.: EL+TF+BI+AS+EM+SS-MoA10, **12**
Copel, M.W.: GR+EM+NS+PS+SS+TF-MoM8, 6
Corso, M.: SP+AS+BI+ET+MI+NM+NS+SS+TF-
WeM4, 31
Cortes, R.: GR+EM+NS+SS+TF-ThA2, **51**
Coultas, S.J.: AS+NS+SS+TF-WeA8, 37
Coutu, R.: TF-WeM1, 35
Craft, S.: EM+TF+AS-ThA1, 49
Creatore, M.: EL+TF+AS+EM+SS+PS+EN+NM-
MoM6, 2; TC+EM+AS+TF+EN-ThM2, 44
Cserny, I.: AS+TF+VT-FrM3, 60
Csik, A.: AS+TF+VT-FrM3, 60
Cui, X.: AS+TF+VT-FrM1, 60
Culbertson, J.C.: GR+EM+NS+PS+SS+TF-
MoM3, 5
Cummings, P.T.: TF+AS-TuA1, **25**
Cummings, S.P.: TF+EM+SS-ThA6, 55

Cumpson, P.J.: SP+AS+BI+ET+MI+NM+NS+SS+TF-WeM10, 32
 Curtiss, L.: TF+EN-MoA1, 19
 Cyganik, P.: TF+AS+SS-ThA2, 52

— **D** —

Dadson, A.E.: TF2-TuA2, 27
 Dahal, A.: GR+EM+NS+SS+TF-ThA7, 51
 Dähne, M.: EM+TF+AS-ThA10, 50
 Dalberth, M.J.: TF+EM+SS-ThA7, 55; TF-WeM1, 35
 Dalmau, R.: EM+TF+AS-ThA1, 49
 Darakchieva, V.: AC+TF+SS+MI-MoA9, 11
 Davis, R.C.: TF2-TuA2, 27
 De Luca, F.: TF-WeM5, 35
 De Moure-Flores, F.: TF-ThP16, 59
 De Padova, P.: GR+EM+NS+SS+TF-ThA6, 51
 Dean, C.: GR+EM+ET+NS+TF-MoA10, 16
 Dekoster, J.: EM+TF+OX+GR-MoA1, 12
 Deng, R.: TF+SE+NS-WeM6, 34
 Desplats, O.: EM+TF+OX+GR-MoA9, 13
 Detchprohm, T.: EM+TF+AS-ThA7, 49
 Devaraj, A.: AS+NS+SS+TF-WeA3, 37; AS+NS+SS+TF-WeA4, 37
 Dezelah, C.L.: EN+TF-WeA10, 38
 Dhakal, T.: EN+TF-WeA12, 39
 Dhere, N.: EN+TF-TuM11, 22; TF+AS-WeA11, 42
 Diebold, A.C.: EL+TF+AS+EM+SS+PS+EN+NM-MoM9, 3
 Dietz, N.: EM+TF+AS-ThA11, 50; EM+TF+AS-ThA9, 50
 DiLabio, G.: SP+AS+BI+ET+MI+NM+NS+SS+TF-WeM2, 31
 Dillon, E.: SP+AS+BI+ET+MI+TF-WeA9, 40
 Diwan, A.: TF-WeM6, 36
 Dong, H.: EM+TF+OX+GR-MoM5, 4
 Dongare, A.D.: TF+AS-TuA7, 26
 Doris, B.: EL+TF+AS+EM+SS+PS+EN+NM-MoM9, 3
 Dormstetter, J.-C.: EL+TF+AS+EM+SS+PS+EN+NM-MoM3, 2
 Douidin, B.: GR+EM+ET+NS+TF-MoA7, 16
 Dowben, P.A.: AC+TF+SS+MI-MoA1, 10; AC+TF+SS+MI-MoA7, 11; GR+EM+ET+NS+TF-MoA7, 16
 Drayman-Weisser, T.: TF-MoM3, 8
 Driskell, J.D.: TF+SE+NS-WeM12, 34
 Drube, W.: AS+TF+VT-FrM3, 60
 Dudley, N.: EN+TF-WeA1, 38
 Duenow, J.: TF+AS-WeA10, 42
 Dunn, B.: EN+TF-WeA9, 38
 Durakiewicz, T.: AC+MI+SS+TF-MoM8, 1
 Dutta, P.: EN+TF-TuA8, 24

— **E** —

Ealet, B.: GR+EM+NS+SS+TF-ThA6, 51
 Eastman, P.Y.: AS+NS+SS+TF-WeA9, 38
 Ebert, P.: EM+TF+AS-ThA10, 50
 Eddy, Jr., C.R.: EM+TF+AS-ThA6, 49; EM+TF+OX+GR-MoM9, 4; GR+EM+ET+NS+TF-MoA1, 15; GR+EM+NS+PS+SS+TF-MoM1, 5; GR+EM+NS+PS+SS+TF-MoM3, 5; TF+NS+EM-ThM1, 46
 Edgar, J.H.: EM+TF+OX+GR-MoM9, 4
 Edmonds, M.: SP+AS+BI+ET+MI+NM+NS+SS+TF-WeM6, 32
 Edwards, P.R.: AC+TF+SS+MI-MoA9, 11
 Eggenspiele, D.: EM+TF-WeM11, 31
 Eisele, H.: EM+TF+AS-ThA10, 50
 Elam, J.W.: TC+EM+AS+TF+EN-ThM6, 44; TF+EN-MoA1, 19
 El-Khatib, S.: OX+EM+MI+NS+TF-MoM10, 7
 Elliott, S.: TF-TuM3, 22
 Engelhard, M.: TF+AS+SS-ThA11, 54
 Enta, Y.: GR+EM+NS+PS+SS+TF-MoM10, 6

Erkens, I.J.M.: TF-TuM11, 23
 Everitt, H.O.: TF2-TuA1, 27

— **F** —

Fager, H.: TF+NS+EM-ThM12, 48
 Fahey, A.J.: AS+NS+SS+TF-WeA7, 37
 Fanz, S.: TF-ThP17, 59
 Fartmann, M.: TF+AS+SS-ThA4, 53; TF-ThP14, 59
 Felhofer, J.L.: EL+TF+BI+AS+EM+SS-MoA3, 11
 Feng, G.: TF+AS-TuA1, 25
 Ferekides, C.S.: EN+TF-TuM1, 21
 Ferguson, G.S.: EL+TF+BI+AS+EM+SS-MoA10, 12
 Ferguson, I.: EM+TF+AS-ThA11, 50; EM+TF+AS-ThA9, 50
 Figueroa, J.J.: TF+EM+SS-ThA11, 56
 Firrincelli, A.: EM+TF+OX+GR-MoA1, 12
 Fitz-Gerald, J.M.: TF+MI-WeA4, 43
 Fitzmorris, B.C.: TF+SE+NS-WeM3, 33
 Fleischauer, M.D.: TF+SE+NS-WeM11, 34
 Fleurence, A.: TF+AS-WeA8, 41
 Floro, J.A.: TF+MI-WeA4, 43
 Foussekis, M.: EM+TF+AS-ThA4, 49
 Fowlkes, J.D.: TF+EM+SE+NS-ThM3, 45
 Frank, M.M.: EM+TF+OX+GR-MoA7, 13
 Franke, K.J.: SP+AS+BI+ET+MI+NM+NS+SS+TF-WeM4, 31
 Franssila, S.: TF+NS+EM-ThM10, 48
 Freitas, Jr., J.A.: EM+TF+AS-ThA6, 49
 French, B.: GR+EM+NS+SS+TF-ThA1, 51
 French, M.: GR+EM+NS+SS+TF-ThA1, 51
 Fromm, F.: GR+EM+NS+PS+SS+TF-MoM10, 6
 Fuentes-Cabrera, M.: TF+EM+SE+NS-ThM3, 45
 Fukidome, H.: GR+EM+NS+PS+SS+TF-MoM10, 6
 Fukuyama, A.: EN+TF-TuA12, 25

— **G** —

Gaddy, B.: EM+TF+AS-ThA1, 49
 Gall, D.: TF+SE+NS-WeM6, 34
 Galoppini, E.: OX+SS+TF+MI-MoA6, 17
 Galtsyan, E.: EN+TF-TuA8, 24
 Gamage, S.D.: EM+TF+AS-ThA11, 50; EM+TF+AS-ThA9, 50
 Gao, Y.: EN+TF-TuA8, 24; GR+EM+ET+NS+TF-MoA10, 16
 Garces, N.Y.: EM+TF+OX+GR-MoM9, 4; GR+EM+NS+PS+SS+TF-MoM1, 5; GR+EM+NS+PS+SS+TF-MoM3, 5
 Garcia, C.D.: EL+TF+BI+AS+EM+SS-MoA3, 11
 Garren, J.M.: TF+SE+NS-WeM12, 34
 Gartstein, Yu.N.: EL+TF+BI+AS+EM+SS-MoA2, 11; EN+TF-WeA7, 38
 Gaskill, D.K.: GR+EM+ET+NS+TF-MoA1, 15; GR+EM+NS+PS+SS+TF-MoM1, 5; GR+EM+NS+PS+SS+TF-MoM3, 5
 Gates, G.: TF-MoM3, 8
 Gaub, H.E.: SP+AS+BI+ET+MI+NM+NS+SS+TF-WeM11, 32
 Gazquez, J.: OX+EM+MI+NS+TF-MoM10, 7
 Geisse, N.: SP+AS+BI+ET+MI+TF-WeA11, 40
 George, S.M.: TF+EN-MoA3, 19; TF2-TuA8, 28; TF-MoM10, 9
 Gessert, T.A.: EN+TF-MoA1, 14; TF+AS-WeA10, 42
 Ghafoor, N.: TF+NS+EM-ThM11, 48; TF+NS+EM-ThM12, 48
 Giessibl, F.J.: SP+AS+BI+ET+MI+TF-WeA12, 40
 Giner, I.: OX+SS+TF+MI-MoA11, 18
 Girshevitz, O.: OX+EM+MI+NS+TF-MoM11, 7
 Gladfelter, W.L.: TF-ThP10, 58
 Gleason, K.K.: EM+TF-WeM11, 31; TF-WeM5, 35
 Goertz, M.P.: TF-TuM9, 23
 Goldoni, A.: AC+TF+SS+MI-MoA3, 10
 Goldstein, C.: TF+AS-TuA12, 27
 Gonçalves, A.: AC+TF+SS+MI-MoA6, 10

Gonon, P.: TF+AS-WeA12, 42
 Gorovikov, S.: AC+TF+SS+MI-MoA3, 10
 Gotlib-Vainshtein, K.: OX+EM+MI+NS+TF-MoM11, 7
 Gougousi, T.: TF-ThP9, 58
 Grampeix, H.: EM+TF+OX+GR-MoA9, 13; TF+AS-WeA12, 42
 Granados, B.: TF-TuM6, 22
 Grant, J.T.: TF+AS+SS-ThA10, 54
 Greeley, J.: TF+EN-MoA1, 19
 Greene, A.: EM+TF+OX+GR-MoM3, 3
 Greene, J.E.: TF+AS-TuA4, 26; TF+NS+EM-ThM12, 48
 Greer, F.: TF-MoM5, 8
 Grehl, T.: TF+AS+SS-ThA4, 53; TF-ThP14, 59
 Greiner, M.T.: OX+SS+TF+MI-MoA7, 18
 Gretener, C.: TF+AS-WeA3, 41
 Grigoros, K.: TF+NS+EM-ThM10, 48
 Grundmeier, G.: OX+SS+TF+MI-MoA11, 18; TF+AS+SS-ThA1, 52
 Guerrero, J.: EM+TF+OX+GR-MoA9, 13
 Guo, J.H.: GR+EM+ET+NS+TF-MoA11, 17
 Gupta, S.: TF+EM+SE+NS-ThM4, 45; TF+MI-WeA3, 43; TF+SE+NS-WeM10, 34
 Gupta, V.: TF-MoM4, 8
 Gwo, S.: EM+TF+AS-ThA10, 50

— **H** —

Haasch, R.T.: TC+EM+AS+TF+EN-ThM6, 44
 Hacker, C.A.: TF+EM+SS-ThA6, 55
 Haehner, G.: SP+AS+BI+ET+MI+NM+NS+SS+TF-WeM9, 32
 Hagenhoff, B.: TF+AS+SS-ThA4, 53; TF-ThP14, 59
 Hager, G.: AS+NS+SS+TF-WeA7, 37
 Hähner, G.: SP+AS+BI+ET+MI+TF-WeA7, 40
 Halbur, J.C.: TF2-TuA1, 27; TF-MoM9, 9
 Halls, M.D.: TF+NS+EM-ThM2, 46
 Handa, H.: GR+EM+NS+PS+SS+TF-MoM10, 6
 Hannon, J.B.: GR+EM+NS+PS+SS+TF-MoM8, 6
 Hashimoto, N.: EM+TF+AS-ThA12, 50
 Havela, L.: AC+TF+SS+MI-MoA6, 10
 He, C.: OX+EM+MI+NS+TF-MoM10, 7
 Hemminger, J.C.: TF+AS-WeA2, 41
 Henderson, C.: EL+TF+BI+AS+EM+SS-MoA6, 11
 Hendryx, C.G.: TF-ThP4, 57
 Herdiech, M.W.: OX+SS+TF+MI-MoA2, 17
 Herman, G.S.: TC+EM+AS+TF+EN-ThM5, 44
 Hermkens, P.M.: TF-TuM5, 22
 Hernández, S.C.: GR+EM+NS+PS+SS+TF-MoM1, 5
 Hernandez, S.H.: TF+MI-WeA1, 43
 Hernández-Hernández, A.: TF-ThP16, 59
 Hernández-Hernández, L.A.: TF-ThP16, 59
 Herrera-Gomez, A.: EM+TF+OX+GR-MoA9, 13
 Heyns, M.: EM+TF+OX+GR-MoA1, 12
 Hikita, Y.: OX+EM+MI+NS+TF-MoM3, 7
 Hillhouse, H.W.: EN+TF-MoA3, 14
 Hinkle, C.L.: EM+TF+OX+GR-MoA4, 13
 Hinkov, V.: TF+AS-TuA10, 27
 Hiramatsu, T.: TF-ThP12, 58
 Hite, J.K.: EM+TF+AS-ThA6, 49; TF+NS+EM-ThM1, 46
 Hohlbauch, S.: SP+AS+BI+ET+MI+TF-WeA11, 40
 Holloway, P.H.: EM+TF-WeM9, 30
 Holzke, C.: SP+AS+BI+ET+MI+NM+NS+SS+TF-WeM5, 31
 Hone, J.C.: GR+EM+ET+NS+TF-MoA10, 16
 Hong, J.: TC+EM+AS+TF+EN-ThM12, 45
 Hong, Y.-L.: EM+TF+AS-ThA10, 50
 Hordagoda, M.: OX+EM+MI+NS+TF-MoM1, 6
 Horn, K.: GR+EM+ET+NS+TF-MoA8, 16
 Horsfall, A.B.: GR+EM+NS+PS+SS+TF-MoM1, 5
 Hosono, H.: TC+EM+AS+TF+EN-ThM3, 44
 Hossain, T.: EM+TF+OX+GR-MoM9, 4
 Howe, B.M.: TF+NS+EM-ThM12, 48
 Howe, J.: GR+EM+NS+PS+SS+TF-MoM3, 5

- Hsiao, C.-N.: TF-ThP13, **58**
 Hu, L.: TF+EN-MoA6, 19
 Hu, Q.: SP+AS+BI+ET+MI+TF-WeA9, 40
 Hu, X.: TF+EN-MoA7, 19
 Hu, Y.: SP+AS+BI+ET+MI+TF-WeA8, 40
 Hu, Y.F.: AS+TF+VT-FrM1, **60**
 Huang, J.: TF2-TuA9, **28**
 Huang, L.W.: GR+EM+ET+NS+TF-MoA6, **16**
 Hubault, C.: TF+AS-WeA8, **41**
 Hultman, L.: TF+AS-TuA4, 26; TF+AS-TuA9, 26;
 TF+NS+EM-ThM11, 48; TF+NS+EM-ThM12,
 48
 Hund, Z.M.: EM+TF-WeM12, **31**
 Hussey, L.: EM+TF+AS-ThA1, 49
 Hutton, S.J.: AS+NS+SS+TF-WeA8, 37
 Hwang, C.: AS+TF+VT-FrM3, 60
 Hyde, R.H.: OX+EM+MI+NS+TF-MoM1, 6
— I —
 Iacobucci, S.: AC+TF+SS+MI-MoA3, 10
 Ianno, N.J.: EL+TF+AS+EM+SS-TuP1, 29
 Ide, T.: GR+EM+NS+PS+SS+TF-MoM10, 6
 Ikari, T.: EN+TF-TuA12, **25**
 Ingram, G.: TF+SE+NS-WeM5, 33
 Irving, D.: EM+TF+AS-ThA1, 49; TF+AS-TuA12,
 27
 Ishigami, M.: GR+EM+ET+NS+TF-MoA2, 16
 Ishii, S.: TF+EM+SS-ThA3, 54
 Ismail-Beigi, S.: OX+SS+TF+MI-MoA2, 17
 Itoi, T.: EM+TF+AS-ThA12, 50
 Ivanova, L.: EM+TF+AS-ThA10, 50
— J —
 Jaehnig, M.: GR+EM+NS+SS+TF-ThA1, 51
 Jain, R.: EM+TF-WeM6, 30
 Jakubiak, R.: TF+AS+SS-ThA10, 54
 Jen, S.H.: TF-MoM10, 9
 Jensen, D.S.: TF2-TuA2, 27
 Jernigan, G.G.: TF+AS-TuA3, **26**
 Jerspersen, M.L.: EN+TF-TuA7, 24
 Jesse, S.: SP+AS+BI+ET+MI+TF-WeA1, **39**
 Ji, S.-H.: GR+EM+NS+PS+SS+TF-MoM8, 6
 Jiang, S.: EM+TF+OX+GR-MoA1, 12
 Johansson, M.P.: TF+NS+EM-ThM11, 48
 Johnson, M.: EN+TF-MoA8, **15**; EN+TF-MoA9,
 15
 Jones, J.G.: TF+AS+SS-ThA10, 54
 Jousseau, V.: TF+AS-WeA12, 42
 Joy, R.: TC+EM+AS+TF+EN-ThM2, 44
 Jung, S.: GR+EM+ET+NS+TF-MoA10, 16
 Jur, J.S.: TF+NS+EM-ThM5, 47; TF2-TuA1, **27**;
 TF2-TuA10, 28; TF-MoM9, 9; TF-TuM9, 23
— K —
 Kakekkhani, A.: OX+SS+TF+MI-MoA2, 17
 Kalanyan, B.: TF+EN-MoA8, 19
 Kalfon-Cohen, E.: OX+EM+MI+NS+TF-MoM11,
 7
 Kan, H.-C.: TF+EM+SS-ThA10, 56
 Kanjolia, R.K.: TF+NS+EM-ThM2, 46
 Kanyal, S.: TF2-TuA2, 27
 Karadge, M.: TF-ThP5, 57
 Kasouit, S.: EL+TF+AS+EM+SS+PS+EN+NM-
 MoM3, 2
 Kato, H.: TF-ThP12, 58
 Katoch, J.: GR+EM+ET+NS+TF-MoA2, **16**
 Kaufman-Osborn, T.: EM+TF+OX+GR-MoA3, **12**
 Kaul, A.: EN+TF-TuM11, **22**; TF+AS-WeA11, 42
 Kawai, Y.: GR+EM+NS+PS+SS+TF-MoM10, 6
 Kawamura, M.: TF-ThP2, **57**
 Keimer, B.: TF+AS-TuA10, 27
 Kelkar, U.: TF+AS-TuA11, 27
 Kelly, T.D.: AC+TF+SS+MI-MoA7, **11**
 Kent, T.J.: SP+AS+BI+ET+MI+NM+NS+SS+TF-
 WeM6, **32**
 Kessels, W.M.M.:
 EL+TF+AS+EM+SS+PS+EN+NM-MoM6, 2;
 TC+EM+AS+TF+EN-ThM2, 44; TF+EN-
 MoA4, 19; TF-TuM10, 23; TF-TuM11, 23; TF-
 TuM5, 22
 Kiantaj, K.: EM+TF+OX+GR-MoA3, 12
 Kilpi, L.: TF+NS+EM-ThM10, 48
 Kim, D.H.: TF+EN-MoA8, **19**
 Kim, J.: EM+TF+OX+GR-MoM6, 4; TF2-TuA9,
 28
 Kim, M.J.: EM+TF+OX+GR-MoA4, 13
 Kim, P.: GR+EM+ET+NS+TF-MoA10, 16
 Kim, S.H.: EN+TF-TuM12, 22
 Kim, T.G.: TF-ThP18, **59**
 Kim, W.K.: EN+TF-TuM10, 21
 Kim-Ngan, N.-T.: AC+TF+SS+MI-MoA6, 10
 King, S.: GR+EM+NS+SS+TF-ThA1, **51**
 Kinoshita, T.: GR+EM+NS+PS+SS+TF-MoM10,
 6
 Kirby, H.F.: TF-ThP4, **57**
 Kis, A.: GR+EM+NS+SS+TF-ThA10, **52**
 Kjoller, K.: SP+AS+BI+ET+MI+TF-WeA9, 40
 Knauf, J.: TF+EM+SS-ThA9, **56**
 Knoops, H.C.M.:
 EL+TF+AS+EM+SS+PS+EN+NM-MoM6, **2**;
 TC+EM+AS+TF+EN-ThM2, 44; TF-TuM5, 22
 Kobe, H.: TF-ThP12, **58**
 Koiraal, P.: EL+TF+AS+EM+SS+PS+EN+NM-
 MoM4, **2**
 Kong, L.: GR+EM+ET+NS+TF-MoA7, **16**
 Kornegay, S.M.: TF+EM+SE+NS-ThM4, 45
 Koskinen, J.: TF+NS+EM-ThM10, 48
 Kotru, S.: EN+TF-WeA11, **39**
 Kotsugi, M.: GR+EM+NS+PS+SS+TF-MoM10, 6
 Kövér, L.: AS+TF+VT-FrM3, **60**
 Kranz, L.: TF+AS-WeA3, 41
 Krishnan, R.: EN+TF-TuM10, 21
 Krommenhoek, P.J.: TF2-TuA1, 27
 Krueger, B.: TC+EM+AS+TF+EN-ThM11, 45
 Kub, F.J.: EM+TF+AS-ThA6, 49
 Kucukgok, B.: EM+TF+AS-ThA9, 50
 Kuhn, M.: GR+EM+NS+SS+TF-ThA1, 51
 Kumar, A.: EL+TF+BI+AS+EM+SS-MoA8, 12
 Kumar, S.: EL+TF+BI+AS+EM+SS-MoA8, 12
 Kummel, A.C.: EM+TF+OX+GR-MoA3, 12;
 SP+AS+BI+ET+MI+NM+NS+SS+TF-WeM6,
 32
 Kung, M.: TF+EN-MoA1, 19
 Kungas, R.: SP+AS+BI+ET+MI+TF-WeA3, 39
 Kusakabe, K.: EM+TF+AS-ThA12, 50
 Kuwahara, K.: TF-ThP6, **57**
 Kwon, J.: TF+NS+EM-ThM2, 46
 Kwon, Y.H.: OX+EM+MI+NS+TF-MoM2, 7
 Kwon, Y.J.: TF+AS-WeA2, **41**
— L —
 LaForge, J.M.: TF+SE+NS-WeM5, **33**;
 TF+SE+NS-WeM9, 34
 Lahiri, J.: GR+EM+NS+SS+TF-ThA2, 51
 Lalany, A.: TF+SE+NS-WeM11, **34**
 Landt, L.: AS+TF+VT-FrM2, 60
 Larsen, G.K.: TF+SE+NS-WeM3, **33**
 Latu-Romain, L.: TF+AS-WeA12, 42
 Laver, M.: OX+EM+MI+NS+TF-MoM10, 7
 Law, M.: EN+TF-MoA6, **15**; TF+AS-WeA2, 41
 Le Lay, G.: GR+EM+NS+SS+TF-ThA6, 51
 Le, D.: GR+EM+ET+NS+TF-MoA2, 16
 LeBeau, J.: EM+TF+AS-ThA1, 49
 Lecordier, L.: TF+EM+SS-ThA7, **55**; TF-WeM1,
 35
 Lee, B.H.: TF-MoM10, 9
 Lee, C.-M.: GR+EM+ET+NS+TF-MoA7, 16
 Lee, C.T.: TF-ThP7, **58**
 Lee, J.H.: EN+TF-TuM12, **22**;
 OX+EM+MI+NS+TF-MoM2, 7
 Lee, J.R.I.: AS+TF+VT-FrM2, 60
 Lee, J.S.: EM+TF+OX+GR-MoA3, 12
 Lee, J.Y.: OX+EM+MI+NS+TF-MoM2, 7
 Lee, K.M.: TF+EN-MoA8, 19
 Lee, M.: TF2-TuA9, 28
 Lee, Y.: TF2-TuA8, **28**
 Lee, Y.H.: EN+TF-TuM12, 22
 Leever, B.J.: EN+TF-TuA7, **24**
 Leggett, G.J.: TF+EM+SS-ThA1, **54**
 Leick, N.: EL+TF+AS+EM+SS+PS+EN+NM-
 MoM6, 2; TF-TuM10, 23
- Leick-Marius, N.: TF+EN-MoA4, 19
 Leighton, C.: EN+TF-MoA8, 15; EN+TF-MoA9,
 15; OX+EM+MI+NS+TF-MoM10, 7
 Lenz, A.: EM+TF+AS-ThA10, 50
 Lewis, N.S.: EM+TF-WeM12, 31
 Li, A.-P.: GR+EM+NS+PS+SS+TF-MoM2, 5
 Li, S.: TF+AS-TuA1, 25
 Li, W.: TF-ThP17, 59
 Liang, T.: OX+SS+TF+MI-MoA1, 17
 Liao, B.-H.: TF-ThP13, 58
 Libera, J.A.: TC+EM+AS+TF+EN-ThM6, 44
 Lim, D.: TF+EM+SS-ThA11, 56
 Lin, C.-F.: TF+EM+SS-ThA10, **56**
 lin, Y.: TF-ThP17, **59**
 Lin, Y.-W.: TF-ThP13, 58
 Linder, B.P.: EM+TF+OX+GR-MoA7, 13
 Linford, M.R.: TF+EM+SS-ThA8, 55; TF2-TuA2,
27; TF-MoM4, 8; TF-WeM6, 36
 Liu, Z.: GR+EM+NS+SS+TF-ThA3, 51
 Livadaru, L.:
 SP+AS+BI+ET+MI+NM+NS+SS+TF-WeM2,
 31
 Lo, M.: SP+AS+BI+ET+MI+TF-WeA9, 40
 Logvenov, G.: TF+AS-TuA10, 27
 Longo, C.: TF+SE+NS-WeM3, 33
 Lorenz, K.: AC+TF+SS+MI-MoA9, 11
 Losovyj, Ya.B.: AC+TF+SS+MI-MoA1, 10;
 AC+TF+SS+MI-MoA7, 11
 Lotze, C.: SP+AS+BI+ET+MI+NM+NS+SS+TF-
 WeM4, **31**
 Lou, J.: GR+EM+NS+SS+TF-ThA3, **51**
 Lu, M.: TF+AS-WeA1, 41
 Lu, N.: EM+TF+OX+GR-MoA4, 13
 Lu, T.-M.: TF+SE+NS-WeM4, 33
 Lu, Z.-H.: OX+SS+TF+MI-MoA7, **18**
 Lucero, A.T.: EM+TF+OX+GR-MoM6, **4**; TF2-
 TuA9, 28
 Lukaszew, R.A.: TF+AS+SS-ThA8, 53
 Luo, B.: TF-ThP10, **58**
 Luo, H.: EL+TF+BI+AS+EM+SS-MoA9, 12
 Lyytinen, J.: TF+NS+EM-ThM10, 48
— M —
 Ma, Q.: SP+AS+BI+ET+MI+NM+NS+SS+TF-
 WeM5, 31
 Macak, E.: AS+NS+SS+TF-WeA8, 37
 Macak, K.: AS+NS+SS+TF-WeA8, **37**
 Macke, S.: TF+AS-TuA10, **27**
 Mackus, A.J.M.: TF+EN-MoA4, 19; TF-TuM10,
23
 Madaan, N.: TF+EM+SS-ThA8, **55**
 Madisetti, S.: EM+TF+OX+GR-MoM3, 3
 Magana, S.: TF+EM+SS-ThA11, 56
 Magnone, K.:
 SP+AS+BI+ET+MI+NM+NS+SS+TF-WeM5,
 31
 Mahadik, N.: TF+NS+EM-ThM1, 46
 Maidecchi, G.: EL+TF+BI+AS+EM+SS-MoA8,
 12
 Majkic, G.: EN+TF-TuA8, 24
 Malgorzata, J.: TF-ThP1, 57
 Malko, A.V.: EL+TF+BI+AS+EM+SS-MoA2, 11;
 EN+TF-WeA7, 38
 Mann, H.S.: TF+EN-MoA7, 19
 Mannequin, C.: TF+AS-WeA12, 42
 Manno, M.: EN+TF-MoA8, 15; EN+TF-MoA9, 15
 Marcott, C.: SP+AS+BI+ET+MI+TF-WeA9, 40
 Maria, J.-P.: TF+AS-TuA12, 27
 Marichy, C.: TF+NS+EM-ThM9, **47**
 Marquardt, A.E.: TF-MoM3, **8**
 Marquis, E.A.: AS+NS+SS+TF-WeA1, **37**
 Marshall, C.: TF+EN-MoA1, 19
 Marsillac, S.: EL+TF+AS+EM+SS+PS+EN+NM-
 MoM1, 2; EL+TF+AS+EM+SS+PS+EN+NM-
 MoM4, 2
 Martin, F.: EM+TF+OX+GR-MoA9, 13
 Martin, R.L.: AC+MI+SS+TF-MoM3, **1**
 Martin, R.W.: AC+TF+SS+MI-MoA9, 11
 Martinez, E.: EM+TF+OX+GR-MoA9, **13**
 Masters, A.E.: TF+EN-MoA7, 19

- Mastro, M.A.: EM+TF+AS-ThA6, 49;
TF+NS+EM-ThM1, 46
- Matsui, K.: TF-ThP12, 58
- Maxisch, M.: OX+SS+TF+MI-MoA11, 18
- McClory, J.W.: AC+TF+SS+MI-MoA1, 10;
AC+TF+SS+MI-MoA7, 11
- McHale, S.R.: AC+TF+SS+MI-MoA1, 10
- McLean, R.S.: TF-MoM10, 9
- McNamara, J.D.: EM+TF+AS-ThA4, 49
- Medikonda, M.:
EL+TF+AS+EM+SS+PS+EN+NM-MoM9, 3
- Medina, A.A.: EL+TF+AS+EM+SS-TuP2, 29
- Meersschant, J.: TF-ThP1, 57
- Mehr, T.: SP+AS+BI+ET+MI+TF-WeA11, 40
- Mei, A.R.B.: TF+NS+EM-ThM12, 48
- Mei, W.N.: AC+TF+SS+MI-MoA1, 10
- Meléndez-Lira, M.: TF-ThP16, 59
- Melendez-Lira, M.A.: TF-ThP8, 58
- Melese, Y.G.: EL+TF+AS+EM+SS+PS+EN+NM-MoM6, 2
- Melton, A.G.: EM+TF+AS-ThA11, 50;
EM+TF+AS-ThA9, 50
- Melzer, J.I.: TF-ThP5, 57
- Membreno, D.: EN+TF-WeA9, 38
- Merckling, C.: EM+TF+OX+GR-MoA1, 12
- Meyer III, H.M.: EM+TF+OX+GR-MoM9, 4
- Meyer, J.R.: EM+TF+AS-ThA6, 49
- Michely, T.W.: GR+EM+NS+PS+SS+TF-MoM5, 6
- Miller, C.W.: TF-ThP4, 57
- Mily, E.: TF+AS-TuA12, 27
- Minne, S.C.: SP+AS+BI+ET+MI+TF-WeA8, 40
- Mirmelstein, A.: AC+MI+SS+TF-MoM9, 1
- Mita, S.: EM+TF+AS-ThA1, 49
- Miyashita, H.: GR+EM+NS+PS+SS+TF-MoM10, 6
- Moberg, R.: AS+TF+VT-FrM7, 61
- Montgomery, A.M.: TF+EM+SE+NS-ThM4, 45
- Monton, C.M.: AS+TF+VT-FrM2, 60
- Moody, B.: EM+TF+AS-ThA1, 49
- Moon, J.S.: GR+EM+NS+PS+SS+TF-MoM1, 5
- Moore, R.: EM+TF+OX+GR-MoM3, 3
- Morra, M.M.: TF-ThP5, 57
- Morrish, R.: EN+TF-MoA10, 15
- Moshar, A.: SP+AS+BI+ET+MI+TF-WeA11, 40
- Mota-Pineda, E.: TF-ThP8, 58
- Mowll, T.: GR+EM+NS+PS+SS+TF-MoM2, 5
- Mukherjee, D.: OX+EM+MI+NS+TF-MoM1, 6
- Mukherjee, P.: OX+EM+MI+NS+TF-MoM1, 6
- Mumcu, G.: TF-MoM8, 8
- Murphy, N.R.: TF+AS+SS-ThA10, 54
- Muscat, A.J.: EM+TF-WeM6, 30; TF-TuM6, 22
- Muthinti, G.R.:
EL+TF+AS+EM+SS+PS+EN+NM-MoM9, 3
- Muzzillo, C.: EN+TF-TuM10, 21
- Myers-Ward, R.L.: GR+EM+ET+NS+TF-MoA1, 15;
GR+EM+NS+PS+SS+TF-MoM1, 5;
GR+EM+NS+PS+SS+TF-MoM3, 5
- N —
- Nachimuthu, P.: TC+EM+AS+TF+EN-ThM5, 44
- Naes, B.E.: AS+NS+SS+TF-WeA7, 37
- Nagaiah, P.: EM+TF+OX+GR-MoM3, 3
- Nagareddy, V.K.: GR+EM+NS+PS+SS+TF-MoM1, 5
- Najmaei, S.: GR+EM+NS+SS+TF-ThA3, 51
- Nakano, Y.: EN+TF-TuA12, 25
- Nampoori, V.: EN+TF-WeA11, 39
- Nanayakkara, S.: SP+AS+BI+ET+MI+TF-WeA4, 39
- Narayanan, V.: EM+TF+OX+GR-MoA7, 13
- Natarajathinam, A.: TF+MI-WeA3, 43;
TF+SE+NS-WeM10, 34
- Nath, A.: GR+EM+ET+NS+TF-MoA1, 15;
GR+EM+NS+PS+SS+TF-MoM1, 5;
GR+EM+NS+PS+SS+TF-MoM3, 5
- Nefedov, A.: OX+SS+TF+MI-MoA10, 18
- Nelson, C.M.: EL+TF+BI+AS+EM+SS-MoA9, 12
- Nepal, N.: EM+TF+OX+GR-MoM9, 4;
GR+EM+ET+NS+TF-MoA1, 15; TF+NS+EM-ThM1, 46
- Ng, A.: EM+TF-WeM6, 30
- Nguyen, H.M.: EL+TF+BI+AS+EM+SS-MoA2, 11;
EN+TF-WeA7, 38
- Nguyen, S.: TF+EN-MoA1, 19
- Nieto-Zepeda, K.E.: TF-ThP8, 58
- Noei, H.: OX+SS+TF+MI-MoA10, 18
- Nonnenmann, S.S.: SP+AS+BI+ET+MI+TF-WeA3, 39
- Notestein, J.: TF+EN-MoA1, 19
- Novak, S.: EM+TF+OX+GR-MoM3, 3
- Novikova, I.: TF+AS+SS-ThA8, 53
- Nyakiti, L.O.: GR+EM+ET+NS+TF-MoA1, 15;
GR+EM+NS+PS+SS+TF-MoM1, 5;
GR+EM+NS+PS+SS+TF-MoM3, 5
- O —
- O'Brien, C.J.: TF+AS-TuA7, 26
- O'Connor, S.: EM+TF+AS-ThA6, 49
- Oden, M.: TF+NS+EM-ThM12, 48
- Odén, M.: TF+NS+EM-ThM11, 48
- O'Donnell, K.P.: AC+TF+SS+MI-MoA9, 11
- Oezkaya, B.: TF+AS+SS-ThA1, 52
- Offi, F.: AC+TF+SS+MI-MoA3, 10
- Ohkouchi, T.: GR+EM+NS+PS+SS+TF-MoM10, 6
- Ohuchi, F.S.: TC+EM+AS+TF+EN-ThM11, 45
- Oktyabrysky, S.: EM+TF+OX+GR-MoM3, 3
- Okuda, T.: EM+TF+AS-ThA12, 50
- Oldham, C.J.: TF2-TuA7, 28
- O'Leary, L.E.: EM+TF-WeM12, 31
- Olmstead, M.A.: TC+EM+AS+TF+EN-ThM11, 45
- Oppen, F.V.:
SP+AS+BI+ET+MI+NM+NS+SS+TF-WeM4, 31
- Ossowski, J.: TF+AS+SS-ThA2, 52
- Ostrikov, K.: TF+EM+SE+NS-ThM1, 45
- Owen, A.G.: TF+EM+SE+NS-ThM4, 45
- P —
- Pacholski, M.L.: AS+NS+SS+TF-WeA9, 38
- Padbury, R.P.: TF+NS+EM-ThM5, 47; TF2-TuA10, 28; TF-TuM9, 23
- Page, S.J.: AS+NS+SS+TF-WeA8, 37
- Palai, R.: AC+TF+SS+MI-MoA1, 10
- Palmer, J.A.: TF-TuM9, 23
- Panaccione, G.: AC+TF+SS+MI-MoA3, 10
- Pandey, A.: TC+EM+AS+TF+EN-ThM5, 44
- Park, C.-Y.: GR+EM+NS+PS+SS+TF-MoM4, 5
- Park, J.-H.: GR+EM+NS+PS+SS+TF-MoM11, 6
- Parkin, J.D.:
SP+AS+BI+ET+MI+NM+NS+SS+TF-WeM9, 32;
SP+AS+BI+ET+MI+TF-WeA7, 40
- Parsons, G.N.: TF+EN-MoA8, 19; TF2-TuA1, 27;
TF2-TuA7, 28
- Pascual, J.I.:
SP+AS+BI+ET+MI+NM+NS+SS+TF-WeM4, 31
- Payzant, E.A.: EN+TF-TuM10, 21
- Peixoto, T.: TF+AS+SS-ThA3, 53
- Peng, W.: EM+TF-WeM4, 30; EN+TF-WeA7, 38
- Perea, D.E.: AS+NS+SS+TF-WeA3, 37;
AS+NS+SS+TF-WeA4, 37
- Pereira, L.: AC+TF+SS+MI-MoA6, 10
- Perera, A.G.U.: EM+TF+AS-ThA9, 50
- Perez Medina, G.J.: GR+EM+ET+NS+TF-MoA7, 16
- Perkins, F.K.: TF+AS-TuA3, 26
- Perng, Y.-C.: EM+TF+AS-ThA3, 49
- Perrenoud, J.: TF+AS-WeA3, 41
- Petaccia, L.: AC+TF+SS+MI-MoA3, 10
- Pethe, S.: EN+TF-TuM11, 22; TF+AS-WeA11, 42
- Petrosky, J.C.: AC+TF+SS+MI-MoA1, 10;
AC+TF+SS+MI-MoA7, 11
- Petrov, I.: TF+AS-TuA4, 26; TF+NS+EM-ThM12, 48
- Pettit, C.: EN+TF-TuM9, 21
- Pham, C.D.: TF+NS+EM-ThM6, 47
- Pham, H.: TC+EM+AS+TF+EN-ThM11, 45
- Phaneuf, R.J.: TF+EM+SS-ThA10, 56; TF-MoM3, 8
- Phillpot, S.R.: OX+SS+TF+MI-MoA1, 17
- Piao, H.: AS+TF+VT-FrM1, 60
- Pierce, C.C.: TF-ThP5, 57
- Pinna, N.: TF+NS+EM-ThM9, 47
- Pittenger, B.: SP+AS+BI+ET+MI+TF-WeA8, 40
- Pitters, J.: SP+AS+BI+ET+MI+NM+NS+SS+TF-WeM2, 31
- Piva, P.: SP+AS+BI+ET+MI+NM+NS+SS+TF-WeM2, 31
- Podraza, N.J.: EL+TF+AS+EM+SS+PS+EN+NM-MoM1, 2; EL+TF+AS+EM+SS+PS+EN+NM-MoM4, 2
- Poepplmeier, K.: TF+EN-MoA1, 19
- Ponomarev, M.V.:
EL+TF+AS+EM+SS+PS+EN+NM-MoM6, 2;
TC+EM+AS+TF+EN-ThM2, 44
- Pookpanratana, S.: TF+EM+SS-ThA6, 55
- Portoles, J.F.:
SP+AS+BI+ET+MI+NM+NS+SS+TF-WeM10, 32
- Povey, I.M.: EM+TF+OX+GR-MoA6, 13
- Pradhan, P.: EL+TF+AS+EM+SS+PS+EN+NM-MoM1, 2
- Prater, C.B.: SP+AS+BI+ET+MI+TF-WeA9, 40
- Premkumar, A.: TF-ThP1, 57
- Prokes, S.M.: EM+TF+OX+GR-MoA10, 14
- Proksch, R.: SP+AS+BI+ET+MI+TF-WeA11, 40
- Provo, J.L.: AC+TF+SS+MI-MoA4, 10
- Q —
- Qin, X.: EM+TF+OX+GR-MoM5, 4
- Qu, T.: TF+MI-WeA1, 43
- Quiñones-Galván, J.G.: TF-ThP16, 59
- R —
- Rack, P.D.: TF+EM+SE+NS-ThM3, 45
- Radi, A.: TF+AS-TuA10, 27
- Radja, A.: EL+TF+BI+AS+EM+SS-MoA2, 11
- Radu, I.: TF-ThP1, 57
- Radue, E.: TF+AS+SS-ThA8, 53
- Rahman, T.S.: GR+EM+ET+NS+TF-MoA2, 16
- Raj, R.: TF+EM-MoA3, 19
- Rajachidambaram, M.S.: TC+EM+AS+TF+EN-ThM5, 44
- Ramana, C.V.: TF+AS+SS-ThA11, 54;
TF+AS+SS-ThA9, 54
- Rangan, S.: OX+SS+TF+MI-MoA6, 17
- Ranish, J.: TF+AS-TuA11, 27
- Ranjan, V.: EL+TF+AS+EM+SS+PS+EN+NM-MoM1, 2
- Rao, M.V.: GR+EM+NS+PS+SS+TF-MoM1, 5
- Raso, R.: AS+NS+SS+TF-WeA8, 37
- Raynaud, P.: TF+NS+EM-ThM3, 47
- Reddemann, L.: TF+EM+SS-ThA9, 56
- Reeves, R.: TF+EM+SE+NS-ThM5, 46
- Reihs, K.: TF+EM+SS-ThA9, 56
- Ren, T.: TF+EM+SS-ThA6, 55
- Reshchikov, M.A.: EM+TF+AS-ThA4, 49
- Resta, A.: GR+EM+NS+SS+TF-ThA6, 51
- Revenko, I.: SP+AS+BI+ET+MI+TF-WeA11, 40
- Reznicek, A.: EL+TF+AS+EM+SS+PS+EN+NM-MoM9, 3
- Ribeiro, F.: TF+EN-MoA1, 19
- Rice, T.: EM+TF+AS-ThA1, 49
- Richardson, C.J.K.: TF+EM+SS-ThA10, 56
- Richter, C.A.: TF+EM+SS-ThA6, 55
- Rieth, L.W.: TF-WeM2, 35
- Ritz, E.: TC+EM+AS+TF+EN-ThM12, 45
- Rizzo, A.: AC+TF+SS+MI-MoA3, 10
- Roberts, A.J.: AS+NS+SS+TF-WeA8, 37
- Roberts, N.A.: TF+EM+SE+NS-ThM3, 45
- Robertson, J.: EM+TF+OX+GR-MoM10, 4
- Robinson, Z.R.: GR+EM+NS+PS+SS+TF-MoM2, 5
- Roca i Cabarrocas, P.:
EL+TF+AS+EM+SS+PS+EN+NM-MoM3, 2
- Rockett, A.: TF+NS+EM-ThM12, 48

Rodenhausen, K.B.: EL+TF+BI+AS+EM+SS-MoA1, 11
 Rogström, L.: TF+NS+EM-ThM11, 48
 Romriell, N.R.: TF+EM+SS-ThA8, 55
 Ronkainen, H.: TF+NS+EM-ThM10, 48
 Roodenko, K.: EL+TF+BI+AS+EM+SS-MoA2, 11
 Roozeboom, F.: TF-TuM11, 23; TF-TuM5, 22
 Rosa, L.: GR+EM+ET+NS+TF-MoA7, 16
 Rosenfeld, D.H.: TF+AS-WeA1, 41
 Ross, F.M.: GR+EM+NS+PS+SS+TF-MoM8, 6
 Rotenberg, E.: GR+EM+ET+NS+TF-MoA8, 16
 Routaboul, L.: GR+EM+ET+NS+TF-MoA7, 16
 Rozen, J.: EM+TF+OX+GR-MoA7, 13
 Rubio-Zuazo, J.: AS+TF+VT-FrM5, 60
 Rubloff, G.W.: TF+EN-MoA6, 19; TF-MoM3, 8
 Ruffo, M.: TF-WeM1, 35
 Ruggieri, C.: OX+SS+TF+MI-MoA6, 17
 Ruocco, A.: AC+TF+SS+MI-MoA3, 10
 Ruppalt, L.: EM+TF+OX+GR-MoA10, 14
 Ruzic, D.N.: TC+EM+AS+TF+EN-ThM12, 45
 Rysz, J.: TF+AS+SS-ThA2, 52
 Ryzhkov, M.V.: AC+MI+SS+TF-MoM9, 1

— S —
 Sabitova, A.: EM+TF+AS-ThA10, 50
 Sabnis, V.A.: EN+TF-TuA9, 25
 Salatin, A.: TF+AS-WeA12, 42
 Salib, D.: SP+AS+BI+ET+MI+NM+NS+SS+TF-WeM5, 31
 Saly, M.J.: TF+NS+EM-ThM2, 46
 Samala, S.K.: TF+AS+SS-ThA9, 54
 Samaraweera, R.L.: EM+TF+AS-ThA11, 50; EM+TF+AS-ThA9, 50
 Sangiovanni, D.G.: TF+AS-TuA4, 26; TF+AS-TuA9, 26
 Sardela, M.: TF+NS+EM-ThM12, 48
 Sarkar, A.: EL+TF+AS+EM+SS-TuP1, 29
 Sawatzky, G.: TF+AS-TuM10, 27
 Scarel, G.: TF+EN-MoA7, 19
 Schaafhausen, S.: EM+TF+AS-ThA10, 50
 Schaeckers, M.: TF-ThP1, 57
 Schlaf, R.: TF+EM+SS-ThA11, 56
 Schlessler, R.: EM+TF+AS-ThA1, 49
 Schmidt, D.: EL+TF+BI+AS+EM+SS-MoA1, 11
 Schmitt, J.: OX+EM+MI+NS+TF-MoM10, 7
 Schnell, E.: EN+TF-TuM11, 22
 Schoenfeld, W.V.: TF+AS-WeA7, 41; TF+AS-WeA9, 42
 Schubert, E.: EL+TF+BI+AS+EM+SS-MoA1, 11
 Schubert, E.F.: TF+SE+NS-WeM1, 33
 Schubert, M.: EL+TF+BI+AS+EM+SS-MoA1, 11
 Schuller, I.: AS+TF+VT-FrM2, 60
 Schwab, Y.: TF+EN-MoA7, 19
 Scott, T.B.: AC+TF+SS+MI-MoA6, 10
 Seitz, O.: EL+TF+BI+AS+EM+SS-MoA2, 11; EM+TF-WeM4, 30; EN+TF-WeA7, 38
 Selvamaniackam, V.: EN+TF-TuA8, 24
 Senevirathna, M.K.I.: EM+TF+AS-ThA11, 50; EM+TF+AS-ThA9, 50
 Sershen, M.J.: TF-WeM1, 35
 Seyller, Th.: GR+EM+ET+NS+TF-MoA8, 16; GR+EM+NS+PS+SS+TF-MoM10, 6
 Shafarman, W.N.: EN+TF-TuM3, 21
 Sham, T.K.: AS+TF+VT-FrM1, 60
 Sharma, K.: TC+EM+AS+TF+EN-ThM2, 44
 Sharma, M.: OX+EM+MI+NS+TF-MoM10, 7
 Shea, M.J.: EN+TF-TuA3, 24
 Shen, J.: EN+TF-TuM10, 21
 Shepard, K.L.: GR+EM+ET+NS+TF-MoA10, 16
 Shetty, R.: SP+AS+BI+ET+MI+TF-WeA9, 40
 Shi, Z.: EM+TF-WeM5, 30
 Shimada, K.: TF-ThP12, 58
 Shin, H.: GR+EM+NS+PS+SS+TF-MoM4, 5
 Shin, H.-J.: GR+EM+NS+PS+SS+TF-MoM11, 6
 Shiradkar, N.: EN+TF-TuM11, 22
 Shirazi, M.: TF-TuM3, 22
 Shutthanandan, V.: AS+NS+SS+TF-WeA4, 37
 Sibener, S.J.: EM+TF-WeM12, 31
 Siebentritt, S.: EN+TF-TuM5, 21
 Silverstein, R.: EN+TF-MoA10, 15

Simons, M.T.: TF+AS+SS-ThA8, 53
 Singh, A.: TF+MI-WeA3, 43
 Sinnott, S.B.: OX+SS+TF+MI-MoA1, 17
 Siringhaus, H.: TC+EM+AS+TF+EN-ThM9, 44
 Sitar, Z.: EM+TF+AS-ThA1, 49
 Snow, A.W.: TF+AS-TuA3, 26
 Soffa, W.A.: TF+MI-WeA4, 43
 Sohn, Y.H.: EN+TF-TuM10, 21
 Solzbacher, F.: TF-WeM2, 35
 Song, I.: GR+EM+NS+PS+SS+TF-MoM4, 5
 Spies, M.: EL+TF+BI+AS+EM+SS-MoA9, 12
 Srikanth, H.: OX+EM+MI+NS+TF-MoM1, 6
 Stach, E.: TF+EN-MoA1, 19
 Stair, P.C.: OX+SS+TF+MI-MoA3, 17; TF+EN-MoA1, 19
 Stefani, G.: AC+TF+SS+MI-MoA3, 10
 Steiner, M.A.: TF+MI-WeA4, 43
 Strocio, J.A.: GR+EM+ET+NS+TF-MoA10, 16
 Su, C.: SP+AS+BI+ET+MI+TF-WeA8, 40
 Su, H.: TF+EM+SE+NS-ThM4, 45; TF+SE+NS-WeM10, 34
 Subramanian, V.: AS+NS+SS+TF-WeA4, 37
 Suemitsu, M.: GR+EM+NS+PS+SS+TF-MoM10, 6
 Sugiyama, M.: EN+TF-TuA12, 25
 Sukenik, C.N.: OX+EM+MI+NS+TF-MoM11, 7
 Sun, D.Z.: SP+AS+BI+ET+MI+NM+NS+SS+TF-WeM5, 31
 Sun, L.: TF+AS+SS-ThA10, 54
 Sun, Y.: TF-TuM9, 23
 Sundaram, G.: TF+EM+SS-ThA7, 55; TF-WeM1, 35
 Sutarto, R.: TF+AS-TuA10, 27
 Sutter, E.: GR+EM+NS+SS+TF-ThA2, 51
 Sutter, P.W.: GR+EM+NS+SS+TF-ThA2, 51
 Sweet, W.J.: TF2-TuA7, 28
 Synowicki, R.A.: EL+TF+AS+EM+SS+PS+EN+NM-MoM5, 2

— T —
 Takemura, S.: TF-ThP12, 58
 Tan, X.: EL+TF+AS+EM+SS+PS+EN+NM-MoM4, 2
 Tao, F.: TF+AS+SS-ThA6, 53
 Tapasztó, L.: AS+TF+VT-FrM3, 60
 Taschuk, M.T.: TF+SE+NS-WeM11, 34; TF+SE+NS-WeM5, 33; TF+SE+NS-WeM9, 34
 Taucer, M.: SP+AS+BI+ET+MI+NM+NS+SS+TF-WeM2, 31
 ten Elshof, A.: EL+TF+BI+AS+EM+SS-MoA8, 12
 ter Veen, H.R.J.: TF+AS+SS-ThA4, 53; TF-ThP14, 59
 Terauds, K.: TF+EN-MoA3, 19
 Terfort, A.: TF+AS+SS-ThA2, 52
 Thevuthasan, S.: AS+NS+SS+TF-WeA3, 37; AS+NS+SS+TF-WeA4, 37; TC+EM+AS+TF+EN-ThM5, 44; TF+AS+SS-ThA11, 54
 Thiess, S.: AS+TF+VT-FrM3, 60
 Thissen, P.: TF+AS+SS-ThA3, 53
 Tiwald, T.E.: EL+TF+BI+AS+EM+SS-MoA1, 11
 Tiwari, A.N.: TF+AS-WeA3, 41
 Tkach, I.: AC+TF+SS+MI-MoA6, 10
 Tobin, J.G.: AC+MI+SS+TF-MoM9, 1
 Toeller, M.: TF-ThP1, 57
 Toivola, M.: EN+TF-WeA10, 38
 Tokranov, V.: EM+TF+OX+GR-MoM3, 3
 Tompkins, H.G.: EL+TF+AS+EM+SS+PS+EN+NM-MoM8, 3
 Torija, M.: OX+EM+MI+NS+TF-MoM10, 7
 Torun, B.: TF+AS+SS-ThA1, 52
 Tosun, B.S.: EN+TF-TuM9, 21
 Tóth, J.: AS+TF+VT-FrM3, 60
 Tracy, J.B.: TF2-TuA1, 27
 Travis, J.: TF+EN-MoA3, 19
 Trioni, M.I.: AC+TF+SS+MI-MoA3, 10
 Tripp, R.A.: TF+SE+NS-WeM12, 34
 Tromp, R.M.: GR+EM+NS+PS+SS+TF-MoM8, 6

Tucker, R.T.: TF+SE+NS-WeM11, 34; TF+SE+NS-WeM9, 34
 Tuscano, J.A.: TF+EM+SS-ThA8, 55
 Tweedy, J.: EM+TF+AS-ThA1, 49
 Twigg, M.E.: EM+TF+AS-ThA6, 49
 Tyagi, P.: GR+EM+NS+PS+SS+TF-MoM2, 5

— U —
 Urban, F.K.: EL+TF+AS+EM+SS+PS+EN+NM-MoM10, 3

— V —
 Vail, M.A.: TF2-TuA2, 27
 Vallee, C.: TF+AS-WeA12, 42
 van Buuren, T.: AS+TF+VT-FrM2, 60
 van de Loo, B.W.H.: EL+TF+AS+EM+SS+PS+EN+NM-MoM6, 2; TF-TuM5, 22
 Van Elshocht, S.: TF-ThP1, 57
 VanDerslice, J.: EL+TF+BI+AS+EM+SS-MoA1, 11
 Vanhart, D.: EN+TF-WeA12, 39
 VanSant, K.: TF+AS-WeA10, 42
 Varela, M.: OX+EM+MI+NS+TF-MoM10, 7
 Vasekar, P.S.: EN+TF-WeA12, 39
 Vega, A.: TF+AS+SS-ThA3, 53
 Velden, M.: TC+EM+AS+TF+EN-ThM2, 44
 Vemuri, R.S.: TF+AS+SS-ThA11, 54
 Ventrice, Jr., C.A.: GR+EM+NS+PS+SS+TF-MoM2, 5
 Verheijen, M.A.: TF+EN-MoA4, 19; TF-TuM10, 23; TF-TuM11, 23
 Victoria, R.H.: TF+MI-WeA1, 43
 Vilayurganapathy, S.: TC+EM+AS+TF+EN-ThM5, 44
 Vilmercati, P.: AC+TF+SS+MI-MoA3, 10
 Vincent-Johnson, A.J.: TF+EN-MoA7, 19
 Vogel, E.M.: EM+TF-WeM4, 30
 Vogt, P.: GR+EM+NS+SS+TF-ThA6, 51
 Vohs, J.M.: SP+AS+BI+ET+MI+TF-WeA3, 39
 Vurgafman, I.: EM+TF+AS-ThA6, 49

— W —
 Waerenbogh, J.-C.: AC+TF+SS+MI-MoA6, 10
 Walker, A.V.: EM+TF-WeM5, 30
 Wallace, R.M.: EM+TF+OX+GR-MoM1, 3; EM+TF+OX+GR-MoM5, 4
 Walter, A.: GR+EM+ET+NS+TF-MoA8, 16
 Walters, D.: SP+AS+BI+ET+MI+TF-WeA11, 40
 Walton, S.G.: GR+EM+NS+PS+SS+TF-MoM1, 5
 Wang, G.-C.: TF+SE+NS-WeM4, 33
 Wang, J.: TF-MoM8, 8
 Wang, L.: AC+TF+SS+MI-MoA1, 10; GR+EM+ET+NS+TF-MoA10, 16; TF+AS+SS-ThA8, 53
 Wang, R.: EN+TF-TuA8, 24
 Wang, Y.: EN+TF-TuA12, 25; OX+SS+TF+MI-MoA10, 18
 Weber, J.W.: EL+TF+AS+EM+SS+PS+EN+NM-MoM6, 2
 Weber, M.J.: TF+EN-MoA4, 19
 Wei, D.: EM+TF+OX+GR-MoM9, 4
 Wei, M.: TF+AS-WeA7, 41; TF+AS-WeA9, 42
 Wetzel, C.: EM+TF+AS-ThA7, 49
 Wheeler, V.D.: GR+EM+ET+NS+TF-MoA1, 15; GR+EM+NS+PS+SS+TF-MoM1, 5; GR+EM+NS+PS+SS+TF-MoM3, 5
 White, E.: EM+TF-WeM6, 30
 Wiemer, M.: EN+TF-TuA9, 25
 Wilcock, J.: TF-WeM6, 36
 Willey, T.M.: AS+TF+VT-FrM2, 60
 Willman, J.T.: TF-ThP4, 57
 Winans, L.: TF+EM+MI, 19
 Witanachchi, S.: OX+EM+MI+NS+TF-MoM1, 6
 Woicik, J.C.: OX+SS+TF+MI-MoA9, 18
 Wolden, C.A.: EN+TF-MoA10, 15
 Wolkow, R.A.: SP+AS+BI+ET+MI+NM+NS+SS+TF-WeM2, 31
 Wöll, Ch.: OX+SS+TF+MI-MoA10, 18
 Won, S.-O.: EN+TF-TuM12, 22

- Woodroof, M.: TF+EN-MoA8, 19
 Wormeester, H.: EL+TF+BI+AS+EM+SS-MoA8, **12**
 Wu, J.: AC+TF+SS+MI-MoA1, 10
 Wu, M.-Y.: EN+TF-TuA3, 24
 Wu, Y.: TF+EM+SE+NS-ThM3, **45**; TF-TuM5, **22**
 Wu, Y.L.: TC+EM+AS+TF+EN-ThM12, **45**
 Wyrick, J.: SP+AS+BI+ET+MI+NM+NS+SS+TF-WeM5, 31
- **X** —
- Xiao, Q.: AS+TF+VT-FrM1, 60
 Xie, J.: EM+TF+AS-ThA1, 49
 Xie, X.: TF-WeM2, 35
 Xu, Y.: EL+TF+BI+AS+EM+SS-MoA9, 12
 Xue, J.: EM+TF-WeM9, **30**
- **Y** —
- Yague, J.L.: EM+TF-WeM11, **31**
 Yakimov, M.: EM+TF+OX+GR-MoM3, 3
 Yakobson: GR+EM+NS+SS+TF-ThA8, **52**
 Yamada, A.: TF-ThP12, 58
 Yamada-Takamura, Y.: TF+AS-WeA8, 41
 Yang, J.: EM+TF-WeM5, 30
- Yang, K.: TF+AS+SS-ThA8, 53
 Yang, M.: EN+TF-TuA8, 24
 Yanguas-Gil, A.: TC+EM+AS+TF+EN-ThM6, **44**
 Yao, B.: EN+TF-TuM10, 21
 Yckache, K.: EM+TF+OX+GR-MoA9, 13
 Ye, D.: TF+EM+SE+NS-ThM6, **46**
 Ye, L.: TF-ThP9, **58**
 Yilmaz, D.E.: OX+SS+TF+MI-MoA1, **17**
 Yin, J.: EM+TF-WeM11, 31
 Yokus, M.: TF2-TuA10, 28
 Yoon, J.-H.: EN+TF-TuM12, 22
 Yoshida, S.: TF-ThP2, 57
 Yoshikawa, A.: EM+TF+AS-ThA12, **50**
 Yoshimura, T.: TF+EM+SS-ThA3, **54**
 Young, A.: GR+EM+ET+NS+TF-MoA10, 16
 Yu, S.W.: AC+MI+SS+TF-MoM9, 1
 Yuan, H.: TF-ThP10, 58
 Yuen, H.B.: EN+TF-TuA9, 25
- **Z** —
- Zandvliet, H.J.W.: EL+TF+BI+AS+EM+SS-MoA8, 12
 Zapata-Torres, M.A.: TF-ThP8, 58
- Zhan, Y.: GR+EM+NS+SS+TF-ThA3, 51
 Zhang, J.Z.: TF+SE+NS-WeM3, 33
 Zhang, L.: GR+EM+ET+NS+TF-MoA11, **17**;
 TF+AS-WeA1, **41**
 Zhang, X.: EN+TF-MoA8, 15; EN+TF-MoA9, **15**
 Zhao, Y.: GR+EM+ET+NS+TF-MoA10, 16
 Zhao, Y.-P.: TF+SE+NS-WeM12, 34; TF+SE+NS-WeM3, 33
 Zharnikov, M.: EM+TF-WeM1, **30**
 Zheng, X.: TC+EM+AS+TF+EN-ThM11, 45
 Zhitenev, N.B.: GR+EM+ET+NS+TF-MoA10, 16
 Zhou, R.: EM+TF-WeM9, 30
 Zhu, H.: TF+EN-MoA6, 19
 Zhu, J.F.: GR+EM+ET+NS+TF-MoA11, 17
 Zhu, Y.: SP+AS+BI+ET+MI+NM+NS+SS+TF-WeM5, **31**
 Zollner, S.: EL+TF+AS+EM+SS-TuP2, 29;
 EL+TF+BI+AS+EM+SS-MoA9, **12**
 Zorn, G.: TF-ThP5, **57**
 Zuilhof, H.: EM+TF-WeM3, **30**; TF+EM+SS-ThA4, 55